Fault Classification and Fault Location Schemes in Power Transmission and Distribution Systems

Thesis submitted by

Monideepa Paul

Doctor of Philosophy in Engineering

Department of Electrical Engineering

Faculty Council of Engineering & Technology

Jadavpur University

Kolkata, India

INDEX NO. 66/16/E

Fault Classification and Fault Location Schemes in Power Transmission and Distribution Systems

Under the guidance of

Dr. Sudipta Debnath

Professor

Department of Electrical Engineering

Jadavpur University

Kolkata 700032

India

List of publications:

Journal:

1. Monideepa Paul and Sudipta Debnath, “Fault Detection and Classification Scheme for Transmission Lines Connecting Windfarm Using Single end Impedance,” *IETE Journal of Research*, doi.org/10.1080/03772063.2020.1754934.

2. Monideepa Paul, Sudipta Debnath and Biswapriya Chatterjee, “Fault Detection and Classification Scheme for Smart Grids considering High Impedance Evolving and Cross Country faults,” *Electrical Engineering*, Springer, https://doi.org/10.1007/s00202-022-01490-y.

3. Monideepa Paul and Sudipta Debnath, “Back-up Protection Scheme for Series Compensated Transmission Line Connected to Wind farm, ” *IETE Journal of Research*, DOI: 10.1080/03772063.2022.2071772.

Conference:

1. Monideepa Paul and Sudipta Debnath, “ANFIS based single line to ground fault location estimation for transmission lines,” Michael Faraday IET International Summit-2020, October 3-4, 2020, Proceedings of MFIIS-2020.

2. Monideepa Paul and Sudipta Debnath, “Wavelet Based Single Ended Scheme for High Impedance Fault Classification in Transmission Lines,” IEEE-ICSTCEE 2020, REVA University Bengaluru, October 09th -10th, 2020.

Statement of Originality

I, Monideep Paul registered on 21.12.2016, do hereby declare that this thesis entitled "**Fault Classification and Fault Location Schemes in Power Transmission and Distribution Systems**" contains literature survey and original research work done by the undersigned candidate as part of Doctoral studies.

All information in this thesis have been obtained and presented in accordance with existing academic rules and ethical conduct. I declare that, as required by these rules and conduct, I have fully cited and referred all materials and results that are not original to this work.

I also declare that I have checked this thesis as per the "Policy on Anti Plagiarism, Jadavpur University, 2019", and the level of similarity as checked by iThenticate software is 5%.

Signature of the Candidate:

Date:

Certified by Supervisor:
(Signature with date, seal)

CERTIFICATE FROM THE SUPERVISOR

*This is to certify that the thesis entitled "**Fault Classification and Fault Location Schemes in Power Transmission and Distribution Systems**" submitted by **Ms. Monideepa Paul**, who got her name registered on December 21, 2016 for the award of Ph. D. (Engineering) degree of Jadavpur University is absolutely based upon her own work under the supervision of Prof. Sudipta Debnath, Professor, Department of Electrical Engineering and that neither her thesis nor any part of the thesis has been submitted for any degree/ diploma or any other academic award anywhere before.*

_____

(*Prof. Sudipta Debnath*)

Acknowledgement

First and foremost, praises and thanks to the God, the Almighty, for His showers of blessings throughout my research work to complete the research successfully.

I would like to express my deep and sincere gratitude to my research supervisor, Prof. Sudipta Debnath, for giving me the opportunity to do research and providing invaluable advice, continuous support, and patience during my Ph.D study. Her immense knowledge and experience have encouraged me all the time in my research.

I am extremely grateful to my parents, Mr. Kuchil Chandra Paul and Mrs. Ahuti Paul for their love, prayers, caring and sacrifices for educating and preparing me for my future. I consider myself notihing without them. They gave me enough moral support, inspiration, and helped me to reach my own objectives. I am very much thankful to my husband Mr. Sanatnu Kumar his love, understanding, prayers and continuing support to complete this research work.

I would also like to thank the members of my thesis committee for their informative suggestions, which helped me to improve my research. I am also grateful to Dr. Subhra De and Dr. Biswapriya Chatterjee for their unwavering support, encouragement, and advice. They have helped me to improve my research abilities. Their constant counsel has stayed with me throughout research tenure.

I would also want to thank the Head of the Department and renowned academic members of the Electrical Engineering Department of Jadavpur University for their unconditional support.

Dedicated to

My Parents

and

My Husband

CONTENTS

CHAPTER 1

Introduction

1.1. Introduction

Electricity is so crucial to the global economy that specialized indices are used to reflect the country's economic position (electricity output or consumption per capita) and people's living standards, such as electricity consumption per capita in the domestic/ residential sector. Furthermore, power supply has certain qualities /characteristics that distinguish power industry from of industries. Except for electric batteries, the final product i.e. electricity must be supplied instantly and automatically in response to the consumer's demand. People rely on energy in almost every facet of their daily life, from charging their phones to powering public transportation. It is difficult to imagine how life might be without adequate electricity. Furthermore, advancements in technology in the health sector are attributed towards making human existence safer and more comfortable. Hence, rapid technological progress necessitates an uninterrupted power supply and continuous expansion of power system networks.

To fulfill this uninterrupted power demand requirement, it may appear that simply expanding the capacity of current generation units or establishing new power plants will solve the problem. The majority of the electrical energy comes from conventional sources such as coal, hydro, and nuclear. Furthermore, building a new unit or power plant is a complex process nowadays due to environmental and land problems. As a result, power generation from non-conventional energy sources is exploding in many regions of the globe. Wind, solar, tidal, and ocean energies are the commonly used non-conventional sources of energy.

There is no technology that can store the electric power in significant/ bulk quantities, but increased generation will increase the power flow in transmission lines, eventually leading to overload and higher transmission losses putting the power system in an unstable condition. A rational transmission line expansion plan is necessary to transmit additional electric power, which implies that new transmission lines would be constructed to provide a reliable and cost-effective operation. Further, compensated transmission lines (MOV, UPFC, TCSC, SVC, STATCOM) are also utilized in power supply systems to preserve voltage profile, enhance system stability (both steady-state and transient), and improve power transmission capability. To increase the reliability of the power network, significant penetration of distributed generation (DG), particularly wind power and solar power, into the grid is a usual practice.

In a power system network, transmission lines are the most vulnerable component and are frequently subjected to faults. Faults in the transmission lines are inevitable, hence reliable and fast identification and classification of faults in transmission lines and quick restoration of power

supply are of prime importance in power system protection schemes. The system architecture becomes larger and more intricate as technology progresses (usage of flexible alternating current transmission system (FACTs) devices). As a result, the development of power system protection schemes become complicated. Because of the stochastic nature of wind energy, wind power system faces significant hurdles. The addition of DG units changes the behaviour of protective devices. In these circumstances, developing an accurate, efficient, and quick response protection mechanism is a challenge. In normal cases, faults can be detected by relays. However, in some extraordinary situations, relays may fail to perform, causing serious problems and, in some cases, put human lives in danger. High impedance fault (HIF) detection is difficult because the fault current in case of HIF is within the normal range, making conventional methods difficult to detect.The protection systems are further impacted by week-in feed conditions, close-in fault conditions, swing, load encroachment, current transformer (CT) saturation, and capacitive voltage transformer (CVT) transients.

1.2. Research Objectives

The aim of this thesis is to understand and overcome the main difficulties and challenges for effective operation of power system networks and protection systems. In this research work, reliable power system protection schemes for various network topologies (compensated and uncompensated transmission lines) have been developed to protect transmission lines during various types of faults (shunt fault, cross country fault, evolving fault) under various stressed and dynamic circumstances. First, a wavelet-based method has been developed for classifying high and low impedance faults in transmission lines. Then, fault identification and classification for a single-circuit transmission line in presence of DG have been addressed. Following that, an adaptive-neuro-fuzzy inference system (ANFIS)-based fault location estimation technique for single line to ground fault has been implemented on a single-circuit transmission line. Subsequently, a fault (cross-country and evolving fault) detection and classification scheme for metal-oxide varistor (MOV)-compensated transmission lines has been formulated. A protection technique for series compensated transmission lines has been developed that uses the positive sequence current component to distinguish internal and external faults. Finally, a fault zone and fault location scheme based on power spectral density have been developed for MOV compensated transmission lines for protection against ground faults. All these techniques have been discussed in the following chapters.

1.3. Literature Survey

An electrical power system is a complex and sophisticated system comprised of several interconnected electrical and electronic equipment. Generation, transmission, and distribution are the three basic stages of every electrical power system. All power systems must strive to ensure a high standard of service continuity to fulfill consistent customer demand and minimize

outage times in the event of unexpected situations. Power outages and voltage dips in electrical system are virtually unavoidable due to catastrophic occurrences, equipment breakdown, or improper operation of equipment. To deal with such situations, power system professionals concentrated their efforts on developing quick, reliable, and effective power system protection mechanisms. These protection techniques can quickly identify the fault, fault zone/ location, minimizing the amount of damage, downtime time, and other detrimental issues.

Transmission line protection systems are either based on sequence components or transform-based. Compared to transform-based protection techniques, sequence component-based protection has a lower computational complexity. On the contrary, sequence component-based protection systems may cause relays to fail to operate due to a change in fault path impedance. Wavelet Transform (WT) is well known as an effective tool for analyzing transient voltage and current signals that occur during faults. Shaik et. al. proposed a transmission line protection scheme combining WT with artificial neural network (ANN) in [1]. This system makes use of synchronized data of voltage and current signals from both transmission line terminals. Detail coefficients (cDs) of current signals are used to detect and classify faults whereas approximation coefficients (cAs) of voltage and current signals are used to locate the fault by applying ANN. Two distinct ANNs have been created for ground and non-ground faults in the localization process. Reddy et al. proposed WT based protection scheme for transmission lines in [2-5]. A fault location technique for a smart grid based on remote telemetry unit (RTU) and computational intelligence techniques has been described in [2]. This method used cDs of current signals acquired from two ends of the line and fed to the ANN and ANFIS to estimate the fault location. The results of ANFIS justify its superiority over ANN. A protection technique for multi-generator-connected transmission lines using wavelet multi resolution analysis has been reported in [3]. RTUs and global positioning system (GPS) have been used to collect synchronized currents in this fault classification method. The developed algorithm has been tested in real-time smart grid operation, but the influence of synchronization delay has not been discussed. A real-time wavelet-fuzzy combined scheme for transmission lines to classify and locate faults has been described in [4]. This method employs 3rd level cDs of post-fault (one-cycle) current signals for fault classification and localization.A frequency-domain-based digital relaying algorithm for transmission lines has been proposed in [5]. The dynamic parameters of fault signals are derived using WT. The key characteristics are extracted from wavelet multi resolution analysis (MRA) and fed to fuzzy inference system (FIS) and ANFIS to get exact information about the fault location. Yadav et al. proposed a combined WT and ANN-based protection scheme for double circuit transmission lines (DCTL) [6] using single end three-phase voltage and current signals. In this research, cAs have been extracted using discrete wavelet transform (DWT) to determine the faulty section and assess the location of faults. Li et. al. [7] developed a combined WT-MRA and ANN technique for detecting and classifying faults in a medium-voltage DC system. Using WT-MRA and Parseval's theorem, the energy variation of fault signal is derived, and these features are supplied as input to ANN, to classify fault types automatically. Furthermore, this system has been evaluated on a real-time platform. Rathore et al. introduced a two-terminal [8] and multi-terminal [9] transmission line protection scheme based on wavelet-alienation approach. Alienation coefficients are estimated utilizing cAs of post-fault current signals (quarter-cycle) from both ends of the transmission line to identify and

classify faults in both the scenarios. In addition, to estimate the fault location, cAs of one end voltage and current samples are fed to ANN.

In [10], Usama et al. demonstrated the real-time implementation of WT-based fault detection and identification scheme on a low-end embedded system. High frequency (5 kHz –10 kHz) cDs of current signals are used to identify and classify faults in this scheme. Moreover, the analysis of hardware implementation validates the efficacy of this algorithm. Zarbita et al. [11] developed an accurate real-time approach for HVB-systems based on the Detail-Spectrum-Energy of current signals, which distinguishes faults from other disturbances. This method was then tested on a real-time system to demonstrate its effectiveness. Continuous efforts are being made by the researchers for the implementation of a real-time hybrid model based on WT and ANN. In [12], the authors proposed a microcontroller-based low-cost, rapid, and reliable transmission line protection mechanism that uses WT in conjunction with ANN. This technique employs the fundamental component of the current signal for fault detection, classification, and faulty zone/ section identification, whereas fault location is determined using the standard deviation (SD) of cAs of both voltage and current samples. This method is also effective in real-time applications.

A modern algorithm based on maximum wavelet singular value (MWSV) which follows the principle of singular value decomposition and has sufficient information to detect and classify all types of faults has been discussed in [13]. The high-frequency components of current signals are derived using DWT to construct a wavelet matrix, from which MWSV is computed. Dubey et al. described an out-of-step blocking protection technique for transmission lines based on wavelet singular entropy (WSE) in [14]. At first, the WSE (Shannon entropy) of current signals was retrieved using DWT to discriminate stable power swings from unstable ones. Finally, a WSE-based indicator is employed to differentiate between faults and power swings. Costa et al. formulated an algorithm to identify fault-induced transients in transmission lines to make the WT-based protection system independent of the mother wavelet [15]. The boundary effects of the sliding windows are taken into consideration in this approach when calculating the wavelet coefficient energy of faulty signals. As a result, the choice of the mother wavelet does not affect the performance of the proposed energy analysis, resulting in no time delay in real-time fault identification. In [16], Ekici et al. demonstrated a transmission line protection system based on DWT and support vector machine (SVM). To reduce the data set for SVM, wavelet entropy criteria are applied to the 3^{rd} level cDs of voltage and current signals. Faults are classified and located using SVMs. In [17] Dasgupta et al. developed a technique for identifying and locating faults in transmission lines based on wavelet packet decomposition and ANN. In this algorithm entropy values of 3^{rd} level cAs and 1^{st} level and 3^{rd} level cDs of voltage signals are fed to the PNN to identify the faults and faulty phase/s, whereas Elman back-propagation architecture is used to locate the occurrence of faults in transmission lines. A WT–ANN-based new approach to classify the faults in extra-high voltage transmission line (EHV) is described in [18]. To classify the faults ten separate Rough Membership Neural Network classifiers have been used. Ten numbers of time-frequency-domain features and three numbers of time-domain features of post fault quarter cycle current signal are fed to ten separate Rough Membership Neural Network classifiers to classify the faults. In this process, rough neurons are used as input

layers whereas hidden layers use fuzzy neurons to reduce the training time of the neural network. Zhang et al. proposed an ANFIS-based fault classification scheme for a neutral non-effectively grounded distribution system in [19]. At first, WT acquires transient information from current and voltage samples to detect and classify faults by computing statistical variables known as fault index (FI). To get the final result, the FIs are fed into three ANFISs.

Fault inception angle, fault resistance, and fault distance all have an impact on time-domain analysis for fault detection. In [20-21], the authors proposed a transmission line protection scheme to address these concerns. Reddy et al. established a frequency domain-based relaying approach using digital signal processing (DSP) and MRA to analyze transmission line faults [20]. MRA is used in this study to retrieve important properties from a faulty current signal. Ananthan et al. established a fault detection and classification technique in a laboratory hybrid model of an EHV line using frequency-domain investigation of current waveforms [21]. In this real-time transmission line fault analysis approach, three-phase one-end line currents are captured and digitalized using an NI 9227 and sent to the PC through NI CDAQ and USB.

Wavelet is a time-localized wave-like oscillation with two main coefficients: dilation or scale and translation. The major drawback of WT is that scale and translation coefficients do not represent any physical features. Hence, many researchers have also used other transform-based techniques. Stockwell transform is a transform that represents a signal in the time and frequency domain. It is also known as a variable window of short-time Fourier transform or an extension of WT. The main feature of this transform is that it can monitor the frequency change of a signal over time. As a result, it has a wide range of applications. Hence, Stockwell transform and its updated/ modified variants are now widely utilized in various power system protection methods [22-24] despite its certain drawbacks.

A digital relaying method for the protection of hybrid transmission lines has been designed in [22]. In this work, to derive the features from one end three-phase current waveforms, the entropy concept was combined with the fast discrete orthogonal S-transform (FDOST). The faults were classified and localized using the support vector regression (SVR) and SVM classifier. Based on the DOST and the SVM, Reddy et al. presented a smart transmission line protection technique in [23]. In this approach, the energy coefficients of both end current signals are extracted using discrete orthogonal stockwell transform (DOST), and these coefficients are then utilized for fault detection and classification, as well as sent to the SVM locator to locate the fault. Samantaray et al. [24] established a Fast-S-transform-based effective protective relaying method for transmission line. In this scheme, Fast-S-transform is used to estimate the voltage and current phasors (magnitude and phase) that are used to compute impedance and assess the faulty state in the transmission line.

The power spectral density (PSD) of a signal analyses the power distribution over the full frequency range. The primary objective of utilizing this approach is to estimate the spectral density from the available dataset/ signal to identify any abnormalities in the system network. Unlike the Fourier transform, the WT may save the time information of signals. Hence, many researchers have successfully incorporated PSD into the relaying schemes [25-27].

Due to the increasing use of power electronics devices, different types of harmonics are developed in the network which create problems in the proper operation of relays. In [25], Yilmaza et al. introduced four distinct parametric spectral estimating techniques viz. Yule-Walker, Burg, Covariance and Modified Covariance techniques for the identification of harmonics. In [26], Guillen et al. utilized the PSD technique for fault classification and detection in transmission lines. To obtain PSD in the frequency and time domain, this study analyzes the transient information of half-cycle current samples under fault conditions. Though this scheme is tested in the New England power grid, the performance of this scheme has not been investigated under varying source strength, power transfer angle, and in presence of a series compensator. In [27] Roy et al. discussed another protection scheme combined with DWT and PSD for a multi-feeder radial distribution system. The three-phase currents are analyzed using the DWT algorithm to extract the time and frequency information for HIF detection, faulty feeder, and faulty phase/s identification. The impacts of DG and nonlinear load are investigated with wide range of variations.

In addition to the wavelet theory, discrete fourier transform (DFT) is used to estimate fundamental phasors from the signals and has been successfully employed in a variety of relaying methods [28-37]. The presence of a decaying dc component leads to incorrect assessment of the fundamental phasor. In [28], Zadeh et al. presented a DFT-based phasor estimation approach. The main concern of this approach is to nullify the adverse effect of ddc offset of fault currents. This approach shows good results during severe distortion of signals and also in the presence of the subsynchronous frequency component. Gu et al. proposed a Fourier filter-based technique for estimating the DC offset from faulty signals in [29]. Gabr et al. [30] introduced an impedance-based fault location technique in a radial distribution system. The mutual impedance problem is solved using the modal transformation of current and voltage data. In this research, DFT is used to extract phasors from voltage and current data. As it only employs a single formula to calculate the fault distance, this system is non-iterative. Farshad et al. proposed a k-nearest neighbour (k-NN)-based technique for estimating the location of an single line to ground (SLG) fault in a transmission line using the harmonic spectrum of one end voltage signal [31]. The harmonic components are extracted using DFT, and the amplitude of the harmonic components is used to locate faults using k-NN. Gopakumar et al. described an SVM-based power grid protection technique [32]. Using fast fourier transform (FFT) analysis equivalent voltage and current phasor angles are determined, which are then used to determine faulty buses and branches, as well as estimate fault distance in those branches. The theory was validated using extensive case studies on the IEEE 14-bus and WSCC-9 systems. An analytical approach for determining the fundamental frequency components of faulty signals was proposed by Nam et al. [33]. The suggested approach contains four stages: a sine filter, a linear filter, Prony's technique, and measurement. Harmonic components are eliminated by sine filter whereas linear filter eliminates the fundamental frequency component signals. The dc-offset and distinctive frequency component are determined by Prony's approach. Finally, the fundamental frequency component is calculated by modifying the sine-filtered signal with the expected values. But this approach was solely used for SLG faults.

To decrease the computational burden and increase the speed of convergence, Jafarpisheh et al. proposed a DFT-based phasor estimation scheme in [34]. First, a new auxiliary signal based on basic high-frequency modulation is used to modulate the fault current. For each one-cycle-data set, the DFT of the fault current sample and summation of both the fault current and the auxiliary signal are computed. Following that, the ddc-induced DFT estimate error is computed. Finally, an accurate fundamental phasor is achieved by eliminating this inaccuracy. Capacitor-coupled voltage transformer (CCVT) is used to monitor the system voltage in a high voltage transmission line. Because of the transitory nature of CCVT, improper relaying occurs. Reis et al. conducted research using full and half-cycle DFT to examine the effects of CCVT on power system protection and fault position estimate approaches in [35].

Swetapadma et al. [36] proposed a DFT-decision tree (DT)-based technique for identifying and classifying faults in double circuit transmission line during power swing using one terminal three-phase current and voltage data as well as zero-sequence components of current signals. The DFT approach was employed in this work to compute the fundamental component of voltage and current signals, which were then fed into DT for fault classification. To ensure its efficacy, this DT-based approach was tested on an IEEE 9-Bus system. In [37], DFT has been utilized to identify and classify faults in transmission lines. In this paper, positive sequence components of the voltage sample and FIS have been used to determine the position of faults. Eight separate FISs have been utilized for estimating the fault location. Hence, huge storage space is required for this purpose.

Apart from the techniques described above, sequence component analysis has recently gained popularity due to its easy usability and low computational complexity. Ghorbani et al. [38] developed a scheme for fault location in multi-terminal double circuit transmission line that makes use of the negative sequence component of current signals. Signals have been recorded at the relay point in this proposed approach. Ma et al. reported SLG fault detection method based on voltage phase comparison in [39]. The angular difference between fault voltages and measured currents is derived after computing the phase relationship between the negative-sequence current at the fault and the measurement point. Finally, the phase angle difference of fault voltage at the relay point is computed using the measured voltage as a reference to detect out-of-zone and in-zone faults. This method is then verified on Real-Time Digital Simulator (RTDS) platform to prove its usefulness. Under week-infeed situations, faulty phase selection is a challenging assignment in transmission lines. Huang et al. [40] proposed a ground fault phase identification technique based on relative phase-angle relationship between different sequence components of voltage signals for high voltage and EHV transmission lines. This technique was successfully implemented on the IEEE 39-bus test system. Yadav et al. [41] developed a transmission line protection approach for identifying, classifying, and determining the direction of faults in a power network. In this analysis, three distinct FISs are used. The first FIS uses the phase angle of the positive sequence current components to determine whether faults are in the forward or reverse direction. Fundamental components of voltage and current signals are utilized as input to the second FIS for classifying faults. The third FIS receives positive sequence current and voltage data to estimate the fault location. Although the Monte Carlo simulation methodology was used to evaluate the fault localization method, the use of three FISs increases

the processing burden of this method. A fault localization algorithm for single-circuit un-transposed overhead transmission lines has been presented in [42]. This approach locates fault on both short and long transmission lines by using synchronized measurement of positive and negative sequence voltage and current signals. Even though the algorithm delivers good results, the influence of measurement error owing to synchronization delay has not been explored in this study. Didehvar et al. [43] developed a fault location estimation technique to reduce errors caused by synchronized measurement. In this study, the pre-fault remote end Thevenin equivalent impedance of transmission line is used to calculate the remote end fault current, which is then utilized to locate the fault point. Apostolopoulos et al. introduced a fault location estimation methodology in [44] for both transposed and un-transposed double circuit transmission lines. Positive sequence current phasors of two-end unsynchronized current signals were utilized to locate the fault position in this methodology. However, the impacts of non-linear HIF and mutual coupling between two parallel lines have remained unexplored.

To mitigate the drawbacks of conventional directional relay schemes Swetapadma et al. proposed a transmission line fault protection technique based on finite state automata theory (FSM) [45]. In this study, the phase angle of positive sequence components of current is applied as input to FSM to determine the fault direction in the transmission line. In [46], Seyedi et al. presented a zero sequence compensation algorithm that compensates for the effect of mutual coupling on conventional distance relays for double circuit transmission lines. The compensation part is derived using a zero-sequence equivalent circuit in this approach. The calculated impedance is then adjusted using a recursive technique, and the fault resistance effect is eventually nullified. Zhong et al. in [47] describe a distance protection algorithm that uses a linear differential equation for the RL lumped transmission line model. The Clark phase-modal transformation matrix is adopted in this research to establish only the ground fault location. To avoid coupling interference in the transmission line, system networks are transformed into sequence system networks. As the authors used lumped transmission line model, this approach also addressed the capacitance impact of the long transmission line. This approach considers both fundamental and ddc components in this scenario. Mahamedi et al. [48] described a novel fault location methodology for double circuit transmission lines based on the negative-sequence component of voltage signals. The ratio between the magnitudes of both end negative-sequence components is used in this fault location approach, which eliminates the need for synchronization. Additionally, as only the voltage data is required, errors caused by CTs are avoided.

Detection of HIF is challenging because, in the case of HIF, high impedance is introduced in the fault path, and therefore the fault current is within the normal range. Due to this reason, it is very difficult to detect the HIF by conventional methods. HIF causes a risk of fire because it produces arcing; therefore, quick detection of HIF is very important. Due to HIF and its associated electric arc, the wave propagation becomes complicated in transmission lines because of the non-linear characteristics of arcing phenomenon. The authors in [49-65] presented several HIF detection methodologies.

Adly et al. [49] proposed a method to detect low impedance fault (LIF) and HIF and at the same time classify the LIF using three-phase current signals by applying WT without using any classifier. The advantage of this scheme is that only cDs and cAs of one end current signal is sufficient to identify LIFs and HIFs which reduces the cost of protecting devices. Paul et al. [50] presented a method for distinguishing HIFs and LIFs and classifying both types of faults using the same algorithm. The energy spectrum of cDs and cAs of one end current signal is utilized in this study to differentiate HIFs from LIFs. As the technique only utilizes one end current signal, synchronization between two end signals is not necessary. Baqui et al. [51] developed a HIF detection mechanism for distribution feeders based on WT combined with ANN. This method distinguishes HIF from LIF and typical transient switching occurrences using current waveforms. Unique features of distinct harmonic components are extracted from current data using DWT technique and used to train ANNs. The Levenberg-Marquardt back-propagation algorithm and multilayer perceptron network are utilized in this scheme. Soheili et al. developed an evidential reasoning-based HIF detection technique for distribution systems [52]. This HIF detection system uses five key features to separate HIFs from other switching events viz. ratio ground, mathematical morphology, odd and even harmonics, WT and combinational attempt of harmonic behaviour. The efficacy of this scheme is demonstrated by its application on IEEE 13-Node standard distribution system and real-world data from the southwest Tehran Distribution Company. Lai et al. [53] developed a pattern recognition based HIF detection scheme for distribution systems. The Nearest Neighbor rule is used for fault classification in this study, where the conversion of wavelet scale coefficients to RMS values has been done directly by computing the signal energies. Hence, a proper distribution pattern of RMS value (voltage and current signals) has been obtained from wavelet and scale coefficients. Santos et al. developed a transient-based technique for distribution systems in [54] to identify HIFs from other switching events e.g. capacitor bank switching, and feeder energization. Low and high-frequency voltage components generated during HIFs are used in this approach to distinguish HIFs from other disturbances. Energy spectrums of cAs and cDs are calculated to locate faults. To confirm its efficacy, this method was tested on a 13.8 kV Brazilian distribution grid system. Hubana et. al. [55] compared two techniques for identifying and classifying HIFs in medium-voltage power distribution systems. The first technique is based on the voltage phase difference (VPD) method, while the second one is based on the DWT-ANN technique. In this work, the VPD is computed as the difference between two instantaneous phases of a voltage signal using the Hilbert transform. The authenticity of this algorithm is verified on the distribution system in Bosnia and Herzegovina. A detailed evaluation of fuzzy concepts along with WT for HIF detection and classification in distribution systems has been introduced in [56]. Arcing detection is another challenging task in a power system network. In [57], a DWT-based scheme has been proposed to detect the series arc faults in low voltage residential networks. To detect a series arc fault, the energy level of line current signals with and without arc faults was calculated. This study reveals that the performance of arc fault detection is significantly affected by the sampling frequency, decomposition levels, and conditions of load. An algorithm has been reported in [58], to locate the faulted section in a 11 kV underground distribution system. This proposed algorithm utilizes the difference between the average of absolute coefficients of voltage signals and the reference database. This technique has been tested on a 38-node 11 kV distribution

system in Malaysia.The proposed algorithm utilizes the historical database, which increases the computational burden.

Michalik et al. [59] demonstrated HIF detection and faulted feeder identification scheme using the transient features of zero-sequence current and voltage data in the CWT domain. This scheme responds during HIFs and does not respond during other switching operations such as capacitor bank switching as well as energizing and de-energizing of feeders. However, this algorithm has been tested only under medium voltage distribution systems. Soheili et al. presented a modified FFT-based technique to detect and distinguish the HIFs and other switching events considering linear and non-linear loads in [60]. This technique makes use of the relation between the 3^{rd}, 5^{th}, & 7^{th} harmonic components of three-phase current signals. This approach operates well in IEEE 13-Node distribution system and "Palash" distribution grid in Tehran, Iran. Torres et al. developed an algorithm for detecting HIF in distribution feeders from other transient events in distribution system in [61]. This algorithm examines the harmonic content of the feeder current to detect HIF. DFT tool was used to determine the harmonic content of current waveforms. Gaur et al. [62] proposed an algorithm based on time-synchronized measurement of current and voltage samples from all three terminals of the transmission line to detect fault and identify the faulty section and finally compute the fault location during HIF. Modified-DFT was used to compute the phasors of voltage and current samples in this study. Afterward, these phasors are converted to sequence phasors using sequence component analysis.

In addition to the aforementioned techniques, Mathematical Morphology based algorithms have been applied in several HIF protection schemes [63-65]. A threshold-based method that employs Mathematical Morphology to identify and classify HIFs in distribution systems has been presented by Kavi et al. [63]. This approach uses the randomness, arc extinction, and re-ignition aspects of HIFs to detect and classify HIF. Furthermore, the effectiveness of this algorithm is evaluated in the presence of noise and other sorts of disruptions. Throughout this study, the IEEE 13-bus system is used. Gautam et al. presented a distribution system protection scheme based on Mathematical Morphology methodology in [64]. HIF was identified and distinguished from other disturbances in this study using voltage waveforms collected at the substation. To demonstrate the effectiveness of this scheme, the IEEE 13-node, and IEEE 34-node test systems were employed. This method makes use of the fact that all mathematical morphology-based tools have a low computational burden, making them ideal for real-time applications. In [65], Sarlak et. al. established a multi-resolution morphological gradient-based algorithm to discriminate HIF from other switching events *viz*. capacitor bank switching, load switching and no-load transformer switching. This approach derives time-based features from the post-disturbance current signal (1/2 cycle) using multi-resolution morphological gradient algorithm. These attributes are fed into three multi-layer perceptron neural networks to achieve the final result.

Series compensated transmission lines are used in power supply systems to maintain voltage profiles, improve system stability, and also enhance power transmission capability. Four new methods have been suggested in [66] only for the detection of the fault zone in series

compensated transmission lines based on the dc component of current and voltage samples, instantaneous current, and instantaneous power waveform behaviour. Unified power flow controller (UPFC) is one of the modern FACTs devices that are extensively utilized nowadays. In [67], a fuzzy-based protection method for identifying faults and estimating fault location in a double circuit transmission line has been developed by Goli et al. This approach is suitable for both UPFC compensated and uncompensated transmission lines. However, the impacts of changes in line parameters owing to loading, aging, and environmental conditions were not discussed. Pradhan et al. developed a DWT integrated FIS for fault detection and classification scheme of series compensated transmission lines [68]. FIS receives suitable features (1^{st} level, 2^{nd} level cDs, and 2^{nd} level cAs) from three-phase current signals which accurately classify the faults. For faulty phase selection and fault section detection, two separate FISs have been constructed. Eristi developed a unique fault analysis technique combining WT and ANFIS for a series compensated transmission line in [69]. From each phase of faulty current and voltage signals, the norm entropy of fundamental, harmonic, and transient frequency components was computed. The ANFIS was then used to determine the fault type, faulty section, and fault location using the norm entropy. The primary disadvantage of this method is that it employs three ANFIS for fault detection, classification, and fault location determination, which increases the computation time and burden.

Swetapadma et al. presented a DWT-ANN-based protective relaying concept for finding the fault position of multi-location faults in series compensated transmission lines based on standard deviation in [70-71]. In [70], to estimate the fault location of a single circuit thyristor controlled series compensated (TCSC) transmission line, the standard deviation of 3^{rd} level cAs of one pre-fault and two post-fault current and voltage cycle data are fed to an ANN for training the fault locator. Although this approach does not require fault classification to estimate fault distance, it requires a considerable amount of data, increasing the computational burden and execution time. Multi-location fault position estimation for series compensated double circuit transmission lines have been developed by Swetapadma et al. in [71]. In this research, DWT is used to obtain up to the 3^{rd} level of cAs from one pre-fault and one post fault current and voltage cycle data. The standard deviation of cAs of voltage and current data are supplied as input to ANN to estimate the fault distance. Vyas et al. presented a new technique based on undecimated discrete wavelet transform (UDWT) and Chebyshev neural network (ChNN) to identify the fault zone for series compensated transmission lines [72]. Only 1^{st} level cDs of the current signal are utilized in this work. In comparison to the DWT approach, this research shows that the UDWT technique produces reliable results.

More computationally intensive tools are necessary as the complexities of the interactions between the input and output features of the protection techniques increase. Deep Neural networks (DNN) have an intelligent architecture that outperforms traditional neural networks when it comes to dealing with complex input-output relationships. Mirzaei et al. developed DWT and DNN-based protection algorithms for compensated transmission lines in [73-74]. In [73], effective features from both ends of current signals are used to locate the fault position in TCSC compensated transmission lines, whereas in [74], faulty section and fault location of shunt compensated transmission lines in the presence of STATCOM are determined using the features

of three-terminal voltage signals. In these two articles, the characteristics of the signals were obtained using DWT. Furthermore, the minimum set of attributes is identified utilizing norm entropy, standard deviation, and the maximum and minimum values of cDs. As this approach necessitates a large number of hidden DNN layers, the execution time is considerably high.

In [75], Biswal et al. proposed an online protection technique for shunt compensated transmssion lines. The Intrinsic Mode Function of synchronized current signals is first calculated. The Hilbert-Huang Transform is then used to calculate the discrete teager energy (DTE) of that signal. Finally, the fault index, which is used to classify the faults, is derived using the differential DTE of both ends. To address the limitations of standard fault location schemes Swetapadma et al. [76] developed a fault location estimation approach for series compensated lines utilizing DWT and decision tree regression (DTR). The major focus of this work is on locating faults without the use of complex calculations. DTR is used to determine faults because of its capacity to work with enormous data sets with great precision. By generating suitable features, DWT makes the DTR analysis process simple.

Tripathy et al. proposed a novel differential relaying technique for UPFC compensated transmission lines in [77-78]. The Fast Discrete S-Transform (FDST) in [77] is used to calculate the spectrum energy of the current signals of UPFC linked double circuit transmission line. In this protection technique, three-phase current signals are first measured from both ends of transmission lines to determine the differential spectral energy used for detection, classification, and faulty section recognition. A cross-differential protection mechanism for UPFC compensated parallel transmission lines was reported in [78]. The UPFC is linked only in one line in this work. The FDST is used to calculate the spectral energy of three-phase current signals to detect the faulty phase. The proposed method is validated using an RTDS platform to further verify its resilience. For STATCOM connected power systems signal analysis, Krishnanand et al. introduced a cross-differential protection scheme based on the FDST in [79]. This approach employs a cross-differential mechanism to lower the computational burden of the processor during the execution of the S-Transform in online mode (TMS320C6713 digital signal processor). To circumvent the limits of distance relay operations, Moravej et al. [80] provided a pattern-recognition-based approach for fault type identification, fault loop status supervision, and fault zone detection in the presence of UPFC in transmission line. At first, relevant features are extracted from one-end signal using the FDOST. After that, the Gram-Schmidt approach determines the high-ranking features, which are then delivered to eleven SVM classifiers to perform the above three tasks. A fault classification technique based on DT and FDOST for series compensated transmission lines has been described in [81]. FDOST coefficients were derived from both voltage and current signals and then sent to DT for fault classification. To validate its efficacy, this approach is evaluated on a three-machine, nine-bus WSCC test system. In [82], a fault position estimation technique for UPFC compensated long transmission lines using FDOST and Gaussian Process Regression algorithm has been proposed. In this study, one end $3/4^{th}$ cycle of the voltage signal is divided into four divisions, each of which is subjected to FDOST to extract the features. The fault location is found using Gaussian process regression using the first ten principal components of these characteristics.

Voltage inversion and current inversion are the two main problems in the directional relaying technique for series compensated transmission lines. Jena et al. in [83] proposed a positive-sequence-based technique to overcome these two problems. This proposed approach uses a phase change in positive-sequence current and a magnitude change in positive-sequence voltage to eliminate current and voltage inversion problems. In [84] positive sequence complex power has been utilized to separate the internal faults from external ones in UPFC compensated transmission lines. To find the location of faults, the authors used both the sequence components (positive and negative) of current and voltage signals from both local and remote end buses, therefore, symmetrical faults cannot be detected by this technique. The fundamental issue with double circuit transmission lines is the effect of mutual coupling between neighbouring circuits of the line. To mitigate this issue, Nemati et al. proposed fault location schemes for series compensated double circuit transmission lines based on negative sequence components of signals in [85- 86]. In [85], the proposed fault location formula is developed by applying KVL to the parallel circuits and shunt capacitance loops, but in [86], the KVL is used in the negative sequence circuit of series compensated double circuit transmission lines to circumvent the drawbacks of impedance-based systems. Even though this method uses voltage components, its efficiency has not been examined during close-in fault conditions and it only considered LIF. A communication-aided technique for detecting and locating faults in TCSC-compensated transmission lines has been developed in [87]. This algorithm is accomplished by using the sequence component of the current signal. Although this method employed synchronized measurements of the current signal, it did not address the issue of CT saturation. Series capacitor banks (SCBs) are used in transmission lines for line compensation because of their long life, low cost, and ease of maintenance. Elmitwally et al. introduced a fault location estimation technique for SCB compensated transmission lines in [88–89]. In this study, current data at the relay point is sufficient for detecting, classifying, and locating the fault point in series compensated transmission lines. In [88], the reverse synchronous reference frame approach was used to classify faults, whereas the fault location was determined using symmetrical components of current signals. The authors in [89] introduced a fault location approach for single circuit series compensated transmission lines and series compensated double circuit transmission lines based on sequence network modeling. Nayak et al. [90] developed a negative-sequence current-based relaying method that detects faults under power swing condition. This scheme utilizes the cumulative sum of the magnitude of the negative-sequence current for fault detection purpose. This scheme performs well both for unbalanced and balanced faults in series-compensated lines. In [91], Makwana et al. introduced an impedance-based adaptive relaying technique. This method uses local end sequence components of three-phase current and voltage phasors to identify different inter-circuit faults on series compensated transmission lines. The proposed approach was tested under various dynamic conditions, including reverse fault and mutual coupling, remote infeed/outfeed, loading effect*, etc.* Using positive-sequence current and voltage from both terminals of long transmission lines, Chatterjee et al. proposed a protection scheme for power networks [92]. Positive sequence admittance was employed to identify the fault while the location of the fault was determined using positive sequence voltage and current phasors. This technique has been tested in both series-compensated and double circuit transmission lines. In series compensated transmission lines, due to the change in positive sequence impedance, distance relays cannot operate accurately. To overcome this issue, a mutual impedance-based

protection scheme for the protection of series compensated transmission lines has been proposed in [93]. Since this approach employs positive-sequence impedance, the designed system solely provides protection against ground faults. As a result, this protection mechanism is ineffective in non-ground fault situations. Taheri et al. proposed a threshold-based fault detection and faulty phase selection technique for series compensated transmission lines [94]. The proposed approach uses DFT to calculate the differential phase angle superimposed current signal (DPASC). After that, DPASC is fed into the DT model to produce thresholds for fault analysis. The authors of [95] proposed a series compensated transmission line protection system that uses a sequence-spaced-aided SVM to differentiate between fault and power swing in the power network. In this technique, the current phasor is estimated using a modified full-cycle DFT, which is then fed to a SVM classifier to identify the fault situation. In [96], Kundu et al. developed fault detection and localization approach for UPFC compensated double circuit transmission lines. The phase angles of negative sequence currents are utilized to distinguish between internal and external faults in this study, while the ratio of negative sequence currents is employed to determine the fault position.

In addition to the methods listed above, travelling wave theory [97-99] has gained a lot of attention due to its ease of usage. The main disadvantage of the approaches mentioned above is that they will necessitate more mathematical calculations than the travelling wave theory. Furthermore, when combined with certain AI approaches (ANN, SVM, ANFIS, FIS, DT), these methodologies require substantial training to obtain optimal accuracy.

Deng et al. developed a single-ended travelling wave-based transmission line protection method [97] to address the synchronization issue and communication difficulties between the two end signals of transmission lines. To develop this transmission line protection method, first propagation characteristics are calculated using continuous wavelet transform (CWT) at different scales, then the correlation and difference of the complete waveform for internal and external faults are computed. This scheme has been evaluated on an IEEE 30-bus standard test system to ensure its reliability. Based on travelling wave theory, Akmaz et al. [98] developed a fault location estimation approach for series compensated transmission lines. The transient properties of current and voltage signals are used in this method. The fault signal is translated to the frequency domain using FFT, and the final location of the fault is estimated by examining the frequencies in the transient spectrum. The performance of the differential protection scheme is affected by distributed capacitance current and CT saturation [99]. A differential protection system based on a combination of WT and equivalent travelling wave theory is employed in transmission lines to identify internal and external faults. The goal of this research is to create a sensitive and effective differential protection scheme based on travelling wave theory with the least amount of communication traffic. To enhance sensitivity during faults with low fault inception angle and high fault resistance, the current energy ratio is computed and employed as an operational criterion.

A differential power-based directional relaying algorithm to detect and classify faults in transmission lines is well discussed in [100-101]. The authors in [100] dealt with the detection and classification of faults in transmission lines based on the magnitude of differential power

(MODP), which is the difference between real power and the product of calculated current and voltage phasors. MODP of all phases is given to DT to define robust thresholds for identifying the faulty phase. The main advantage of this technique is that it is unaffected by the distributed capacitive current. In [101], Kumar et al. proposed a differential power-based backup protection theory for UPFC compensated transmission lines. This algorithm can distinguish internal faults from other dynamic situations.

In the case of HIF, healthy phase current and faulty phase current are in the same order, so the moving sum approach-based fault detection and classification scheme are not trustworthy. In [102], Biswal et al. proposed a novel scheme based on an integrated moving sum to solve this problem. This method classifies the fault using the half-cycle period of the current signal. This technique is tested in a variety of dynamic conditions, including close-in faults, CT saturation, weak in-feed conditions, as well as series compensated transmission lines. Another new scheme for identifying and classifying faults in transmission lines during power swings was developed by Musa et al. in [103]. In this technique, the covariance index is derived from synchronized current signals and compared to a threshold value to identify and classify faults. The method was further tested on an IEEE 9-bus system to ensure its authenticity.

It is well known that phasor measuring units (PMUs) significantly improve smart grid monitoring capabilities and have positive effects on power network management. In [104], Das et al. proposed a new fault location determination method based on the network bus admittance matrix and wide area measurement system (WAMS). Variations in the bus injected current is utilized to detect and diagnose faults in transmission line in this study. This technique has been deployed to validate its authenticity on the IEEE 14-bus and New England 39-bus systems. A PMU-based transmission line protection method that uses the minimum number of PMUs for the detection and localization of faults has been developed by Barman et al. in [105]. This method turns the transfer impedance matrix into a linear least square estimation problem to estimate the fault location. The validity of this method was confirmed by testing on IEEE 14, 30, 39 and 118-bus systems. Yu et al. [106] introduced a PMU based backup protection technique that only handles voltage magnitudes as input. This protection approach identifies faults, faulty feeders, and also analyzes the protection performance of the circuit breakers. Though the performance of this scheme has been validated on the IEEE 14-bus system, it does not address close-in faults as it used only the voltage signals. In [107], Pignati et al. proposed PMU-based real-time fault detection and localization solution for active distribution systems. At first parallel state estimator is computed in this approach, and then fault and faulty lines have been detected by comparing the weighted measurement residuals of all the state estimators. In [108], Fathabadi et al. described a method for detecting, classifying, and estimating the location of short-circuit faults in short transmission lines. A hybrid framework consisting of a two-stage finite impulse filter and ANN is used in this work. Four SVMs are utilized to detect and classify short circuit faults, while eleven SVRs are used to locate faults in short transmission lines.

After a thorough study of different protection schemes, it has been seen that with the continuous development of power system networks and also due to their complex nature, conventional protection systems are not capable of detecting cross-country faults, complex

cross-country faults, and evolving faults. Therefore, to supply uninterrupted power to the consumers, reliable and high-speed protection for transmission lines is an utmost requirement, which reduces maintenance time as well as improves the system's stability and reliability. Very few researchers [109-116] have focused on these critical types of faults. Ashok et al. [109] developed a Maximal-Overlap-DWT-based scheme to identify and classify cross-country and evolving faults in transmission lines. The energy level variation in three-phase instantaneous currents is used in this methodology. This design works effectively on the dual-circuit transmission line in Chhattisgarh State Power Transmission Network. In [110], an adaptive CWT-based differential protection method has been developed to define the fault zone and faulty phase/s during cross-country faults in the transmission line in the presence of CT saturation. This technique employs three-phase both end current signals. A protection technique based on DWT and ANN has been presented to estimate the location of shunt faults along with evolving and cross-country faults without classifying the faults in [111]. The standard deviations of cAs of voltage and current signals were determined after the cAs were computed using DWT. Furthermore, utilizing the values received from DWT, ANN is used to find the location of the fault. A first zone distance relaying algorithm for cross-country grounded faults has been described in [112] and non-grounded faults has been described in [113]. In the case of grounded faults [112], fault distance is estimated by computing the fault impedance using the symmetrical component of one-end voltage and current signals; however, in the case of non-grounded faults [113], fault zone distance can be calculated by analyzing the relationship between phase currents and sequence component of currents of parallel lines. Mutual coupling between the lines can be mitigated by expressing the sequence currents of the neighbouring parallel lines at the relay position by the zero-sequence current of the concerned line. In [114] Govar et al. described a unique transmission line and distribution line protection technique based on wavelet packet transform (WPT) and extreme learning machine (ELM) for high impedance evolving faults and cross-country faults. Wavelet packet transform is utilized in this work to extract high frequency data from three-phase both end current signals. During the last cycle, the remote and local end wavelet packet transform coefficients (absolute values) of each phase are combined via a high-speed communication channel. The remote and local end WPT coefficients (absolute values) of each phase are added during last cycle through a high speed communication link. Finally, the data from each phase is compared to other phases to identify HIF and faulty phase/s. A fault position determination scheme for multi-terminal multiple-circuit transmission lines has been introduced in [115]. The proposed method is based on the Taylor series expansion of distributed-parameter transmission line model. This technique employs synchronized current and voltage signals to determine the fault location as well as identify the faulty section. Jena et al. introduced a fuzzy-logic-based directional relaying technique for double-circuit transmission lines with and without series compensation in [116]. Four separate aspects of positive sequence voltage and current phasors are supplied to FIS in this study to detect the direction of the fault. In the presence of balanced and unbalanced faults, HIF, far-end faults, cross-country faults, close-in faults, and single-pole tripping, this relaying system functions effectively.

Significant penetration of DG, especially wind power, into the grid is a common practice to improve the reliability of the power network. Power system is facing serious challenges due to the stochastic behaviour of wind energy. The incorporation of DG units changes the behaviour

of protective devices. In this context, an accurate, efficient, and fast response protection scheme [117-121] is necessary to detect any abnormal or faulty condition in the power networks. Sahoo et al. reported [117] a travelling wave theory-based fault detection and location estimation technique for TCSC compensated transmission lines integrated with DG. FDST was applied to both end current signals to measure the arrival time to estimate the location of the fault. Though the results obtained from the RTDS platform demonstrate the reliability of this methodology, the precision of this method is dependent on a high sample frequency (f_s) (200 kHz). The authors in [118] described a new scheme for identifying and classifying, faults in distribution lines in presence of DGs. In this study, cDs of positive sequence components of currents signals, singular value matrices, and Shannon entropy are utilized to extract effective features which are fed into a FIS to identify and classify faults. In [119], Ma et al. proposed a wind farm collector line protection system. This approach makes the use of the angular difference between the fault current phasor and the zero-sequence current phasor at the relay point. Only low fault resistance up to 30Ω is suitable for this technique. In [120], ElNozahy et al. presented a WT-ANN-based approach for detecting single phasing in the transmission line coupled to the wind farm. DWT is used to extract the characteristics identifying the individual property for each frequency band from the modal signal of the transient current signals. Finally, ANN is employed to detect and identify the single-phasing. A differential relaying scheme combined with WT and DFT has been introduced in [121] for tapped transmission lines integrated with UPFC and wind farms. But this algorithm did not address the effect of CT saturation though the proposed scheme utilized current signals.

1. 4. Materials and Method used in this Thesis

Different mathematical tools and artificial intelligent techniques have been used to formulate the power system protection schemes. The subsequent sections provide a detailed discussion of them.

1.4.1. Discrete Wavelet Transform

In power system engineering, WT has been extensively used in fault analysis. WT is a powerful tool as it has strong analysis capability of non-stationary signals in both time and frequency domain [27]. In DWT, the original signal is decomposed into approximation and detail coefficients after passing through the low pass and high pass filter respectively. cAs contain low-frequency components, and cDs contain high frequency components of the processed signal. In case of multilevel decomposition, approximation coefficients are decomposed further into the next levels of approximation and detail coefficients. Down sampling is done after each decomposition level as the volume of data becomes double after each level of decomposition. Therefore, DWT acts as filter banks and extracts the features of a

signal at different frequency bands. To obtain the distinctive features of the fault signals, DWT technique is implemented using MRA. The DWT of a signal *s(n)* is defined as [26]

$$DWT(j,k) = \frac{1}{2^{j/2}} \sum_{n} s(n) \varphi\left(2^{-j} n - k\right) \tag{1.1}$$

where, φ is the mother wavelet, n is the number of samples which depend on sampling frequency and j and k represent dilation and translation (time shift) parameters respectively.
The cAs and cDs can be expressed as

$$d_i = \sum_{j=1}^{N} X[j] g[2i - j] \tag{1.2}$$

$$a_i = \sum_{j=1}^{N} X[j] h[2i - j] \tag{1.3}$$

where, X represents the signal, i represents the wavelet decomposition level and j is the detail and approximation coefficients at each decomposition level. The total number of detail and approximation coefficients at each decomposition level varies from 1 to N. d_i is detail coefficient i.e. output of HP filter and a_i is approximation coefficient i.e. output of LP filter.

1.4.2. Fuzzy Inference System

The fuzzy system is based on knowledge in the form of fuzzy if-then rules to map the crisp input data set to the crisp output data. Fuzzification, rule base, inference, and defuzzification are the four components of a FIS. Fuzzifier and defuzzifier allow the user to work with real values of input and output variables. The classical logic system gives an approximate answer based on stored knowledge which is not totally reliable. On the other hand, the fuzzy-based logic system is flexible, allows imprecise data and it uses very simple mathematical concept with fuzzy reasoning. Hence, it gives results which are accurate to validate the rules.

1.4.3. Adaptive Neuro-Fuzzy Inference System

ANFIS is a widely used ANN that has been successfully used to estimate the location of faults in transmission lines [2, 5, 20 and 69]. In this proposed method ANFIS is used to estimate the SLG fault location in the transmission line. ANFIS is an intelligent data learning technique which is based on the Takagi–Sugeno fuzzy inference system. Since it consists of both ANN and fuzzy logic principles, it can utilize the benefits of both in a single framework. Sugeno-Fuzzy model considered IF-THEN rules to model any system from its input-output data. ANFIS

architecture consists of five layers - i) input layer, ii) rule layer, iii) normalization layer, iv) consequent layer and v) output layer. Input layer is also known as the fuzzification layer which takes the input data and adjusts the membership functions associated with them automatically.

1.4.4. Discrete Fourier Transform

The fundamental component of the signals is extracted by applying DFT. DFT is the most powerful and efficient tool in the field of signal analysis and signal processing systems. From DFT analysis, one can get the spectrum of a finite-duration signal using a periodic sequence. Fault signals are the combination of exponentially ddc and sinusoidal components. Sinusoidal components are harmonically related to each other. Hence, any fault signal may be represented by [34]

$$s(t) = S_0 . e^{t/\tau} + \sum_{k=1}^{p} |S_k| cos(k \varpi_1 t + \theta_k) \tag{1.4}$$

where, S_0 and τ are the magnitude and time constant of the ddc, p is the maximum order of harmonic and k is the harmonic order. θ_k is the phase angle and $|S_k|$ is the magnitude of k-th harmonic. Therefore, discretization representation of the faulted signal is expressed as

$$s[n] = s_{ddc}[n] + s_{ac}[n] \tag{1.5}$$

where

$$s_{ddc}[n] = S_0 . e^{n\Delta t/\tau} \tag{1.6}$$

$$s_{ac}[n] = \sum_{k=1}^{\frac{N}{2}-1} |S_k| cos\left(\frac{2\pi}{N} n + \theta_k\right) \tag{1.7}$$

where, N indicates the number of samples per cycle and Δt is the sampling interval. The first term of Eq. (1.5) represents the *ddc* component of the given signal and the second term represents the sinusoidal components which consist of the fundamental and harmonically related components. Hence, the evaluated phasor of fundamental frequency component obtained from DFT ($\hat{s}_1$) is expressed as

$$\hat{S}_1 = \frac{2}{N} \sum_{n=0}^{N-1} s[n] e^{-j\frac{2\pi}{N} n} \tag{1.8}$$

1.4.5. Power Spectral Density

Spectral analysis is widely used in different fields of engineering to reveal different latent features in signals. A power spectrum is the frequency-domain energy distribution of a time series. It is a real quantity, so it cannot give any phase-related information. PSD estimation methods are broadly classified into two categories: Parametric and Non-Parametric methods. Periodogram, Modified Periodogram, Welch, Bartlett, and Blackman-Tukey methods are examples of non-parametric methods based on DFT. In FFT-based analysis, the square of the absolute values of the FFT coefficients are used to determine the power of a signal. The limitations of these non-parametric methods are windowing of the autocorrelation sequence, spectral leakage, and lack of process information into the estimation procedure. Burg's method, Yule-Walker method, Covariance, and Modified Covariance techniques are examples of parametric methods. The main advantage of parametric technique is that it gives more accurate results with less computational complexity.

The added advantage of the covariance matrix method over other parametric methods is that it does not require any zeroing of data. It uses all the data points for power estimation and prediction error calculation. Autoregressive method is usually used for the estimation of autoregressive parameter by solving the linear equation of the network. It can be expressed as [25]

$$\begin{bmatrix} c(1,0) \\ - - \\ c(p,0) \end{bmatrix} + \begin{bmatrix} c(1,1) & - - & c(1,p) \\ - - & - - & - - \\ c(p,1) & - - & c(p,p) \end{bmatrix} \begin{bmatrix} \hat{a}(1) \\ - \\ \hat{a}(p) \end{bmatrix} = \begin{bmatrix} 0 \\ - \\ 0 \end{bmatrix} \tag{1.9}$$

where

$$c(j,k) = \frac{1}{N-p} \sum_{n=p}^{N-1} x^*(n-j)x(n-k) \tag{1.10}$$

Autoregressive parameter estimate can be expressed as

$$\hat{a} = -C_p^{-1} C_p \tag{1.11}$$

In the covariance matrix, output vectors contain a normalized estimate of the autoregressive system parameters and the PSD can be defined as

$$\hat{P}_{cov}(f) = \frac{\hat{\sigma}^2}{\left| 1 + \sum_{k=1}^{p} \hat{a}(k) e^{-j2\pi fk} \right|^2} \tag{1.12}$$

where, $\hat{\sigma}^2$ is white noise variance and it can be expressed as

$$\hat{\sigma}^2 = c[0,0] + \sum_{k=1}^{p} \hat{a}[k]c[0,k] \tag{1.13}$$

The WT-based power distribution function has been proved to be the optimal method for calculation of the PSD of non-stationary signals [27]. In case of WT based PSD estimation method, the sum of the square of the wavelet coefficients i.e. detail and approximation has been used to find out the PSD. Finally, the wavelet covariance matrix has been used to compute the PSD of the fault signal. Wavelet matrix contains detail and approximation coefficients to store the transient information of the non-stationary signals. If the signal is decomposed up to L level, then the wavelet matrix can be represented as $W(L+1,n)$, where n is the number of samples. Therefore, covariance matrices become

$$C^t_{(n,n)} = W^t W \tag{1.14}$$

$$C^f_{(L+1,L+1)} = W W^t \tag{1.15}$$

where, C_t and C_f represent the time and frequency domain covariance matrix of the signal respectively. Diagonal elements of the covariance matrix represent the PSD. Therefore, it can be expressed as

$$PSD^t = diag\left[C^t_{(n,n)} \right] \tag{1.16}$$

$$PSD^f = diag\left[C^f_{(L+1,L+1)} \right] \tag{1.17}$$

PSD^t and PSD^f represent the time and frequency domain PSD of the signal respectively. PSD of a signal is related to its energy, and wavelet-based PSD can be used to extract the transient information from a signal during fault. Unlike previously published works in the literature, the PSD-based approach can preserve high-frequency components in time-frequency during a fault. As the frequency information is decoupled from the time information, it is easier to classify various types of faults because additional information can be acquired from high-frequency components. PSD^t defines the spectral density at each moment, allowing for a faster detection time when a transmission line fault occurs [26].

1.5. Outcome of the Reported Research

As a consequence of this research, which aims to develop innovative relaying techniques for transmission networks, the following outcomes have been obtained:

* An algorithm to identify all types of faults in transmission lines along with the phases/s involved has been developed. The developed technique is robust to fault type, fault distance, fault resistance and fault inception angle. An integrated approach has been made to classify both high and low impedance faults by the same algorithm.
* Based on wavelet transform and fuzzy inference system, a novel approach for detecting and classifying faults in transmission lines in the presence of distributed generation has been developed. To classify faults, the fuzzy inference system uses the line impedance determined from the ratio of the approximation coefficients of voltage and current signals.
* A line impedance based protection scheme for transmission lines has been developed to estimate the location of faults. DWT is utilized to extract the approximation coefficients from the voltage and current signals to compute the line impedance, which are then fed to the ANFIS-based fault locator to estimate the fault location.
* An admittance-based transmission line protection scheme has been proposed to discriminate the internal fault from the external ones and also to identify the faulty phase/s under evolving and cross-country fault conditions. In this algorithm, the fundamental components of voltage and current signals from both ends of the transmission lines have been considered to evaluate the admittance-based fault index.
* Positive sequence current component based algorithm has been developed for the protection of series-compensated transmission line integrated with wind farms. The phase difference between the positive sequence currents at the two ends of the line is used to discriminate internal and external faults whereas differential apparent power is used to classify the faults.
* Using power spectral density, a novel approach for protection against single line to ground and double line to ground faults in series compensated transmission lines has been developed. PSDs for all three phases were computed using the wavelet covariance matrix to classify ground faults and identify faulty sections, as well to locate faults using ANN.

1.6. Outline of the Thesis

The first chapter provides the introduction to the research work. The importance of electricity in the global economy as well as the relevance of power system protection systems, which are very essential for providing uninterrupted power flow to the consumers, are discussed in the first portion of this chapter. The second section presented a concise review of the relevant literature. Mathematical tools which are used throughout this research work are reported thereafter. The research outcomes are stated at the end of Chapter 1.

Chapter 2 presents a WT-based technique for classifying high and low impedance faults in transmission lines. The ten distinct types of faults have been classified using the energy spectrum of first-level current signals from both detail coefficients and approximation coefficients. Furthermore, no data synchronization is required as only one end current signal is required for fault classification. The results demonstrate that the developed technique is

unaffected by fault type, fault distance, fault resistance, and fault inception angles.

The impedance-based fault detection and classification technique for DG-linked transmission lines is described in Chapter 3. The line impedance is derived using the ratio of the voltage and current approximation coefficients and fed to the FIS to classify faults in this study. The proposed algorithm has been tested successfully in a real-time digital simulator for non-linear HIFs in the presence of wind farm, considering the effects of CT saturation. All types of faults with the variation of pre-fault loading condition, line parameters, line length and source impedance can be correctly classified using the proposed algorithm.

As the most commonly occurring fault in the transmission line is single line to ground fault, hence in Chapter 4, a single line to ground fault location technique based on WT and ANFIS has been developed. In this proposed method 1st level approximation coefficients are used to determine the line impedance which is the input of the ANFIS structure. The computational burden is reduced as single level decomposition is used. Simulation results reveal that this method is unaltered by fault resistance and fault inception angle.

Chapter 5 addresses, a new threshold-based fault detection along with fault classification and faulty phase/s identification algorithm for power networks. The fundamental components of faulted signals are needed to formulate the line admittance-based proposed algorithm. This technique makes a substantial contribution by reliably detecting and classifying non-linear HIF in transmission networks, including evolving, cross-country and complex cross-country faults.

In chapter 6, a new and reliable backup protection algorithm has been developed for series-compensated transmission lines connected to wind farms. To detect the fault and distinguish the internal and external faults, phase angle differences of the positive sequence current signals from both ends of the line segment have been used. In the case of internal fault, the faulty phase/s is identified from the differential apparent power obtained from the two ends of the line segment.

Chapter 7 describes a PSD based unique scheme for protection against single line to ground and double line to ground faults in series compensate transmission lines. This approach use DWT to extract transient information from current signals, which is then stored in a wavelet covariance matrix to calculate the PSD value. PSD value is then used to classify ground faults and identify faulty sections, as well as provided to ANN to locate faults.The reliability of this scheme is demonstrated by simulation results.

Chapter 8 contains the concluding observations, a comparative evaluation of the methods and tools employed in this study, and a discussion on the future scope of this research.

CHAPTER 2

Wavelet Based Single Ended Scheme for High Impedance Fault Classification in Transmission Lines

2.1. Introduction

Fast technological growth and continuous development in the urban area demand uninterrupted power supply. Due to this reason high speed fault clearance is very much necessary as well as development of high quality, better performance transmission line protection system is essential. For transmission line protection, variety of fault classification and location methods are now available.

It is well established that WT is an efficient tool for analyzing transient voltage and current signals which occur during faults. A modern algorithm based on maximum wavelet singular value to detect and classify all types of faults has been well discussed in [13]. A high speed transmission line protection scheme based on the wavelet-alienation technique to detect, classify and locate different types of faults in the transmission line within a quarter cycle has been presented in [8]. The authors in [19] studied the nature of transient fault signals and proposed an ANFIS-based LIF fault classification scheme. Sustained efforts are being made by the researchers for the implementation of real-time hybrid model based using WT and ANN. The authors in [12] addressed a microcontroller-based low cost, fast and reliable transmission line protection scheme using WT in combination with ANN, which is effective in real time. For real time monitoring and detecting faults, Ananthan et al. [21] developed a wavelet MRA-based technique using LabVIEW in a laboratory hybrid model. Detection of HIF is very challenging because, during HIF, high impedance is introduced in the fault path and therefore, fault current is within the normal range. Due to this reason, it is very difficult to detect HIF by conventional methods. HIF causes risk of fire because it produces arcing; therefore, quick detection of HIF is very important. In a transmission line with HIF and its associated electric arc, the wave propagation becomes complicated because of the non-linear characteristics of the arcing phenomenon. Adly et al. [49] developed a method to detect LIF and HIF and at the same time classify LIF using three-phase current signals by applying WT without using any classifier. HIF detection methodology based on WT combined with ANN has been proposed in [51] to distinguish HIF from LIF and normal transient switching events by using current waveforms obtained from the simulation of a real distribution network. A general purpose HIF model has been proposed in [61]. In this study, the authors developed an algorithm for HIF detection in distribution feeders from other transient phenomena existing in EDS. DWT has been used extensively for HIF identification and location in [53, 58]. CWT-based method for detecting HIF in medium-voltage distribution networks has been described in [59]. This method uses zero-sequence currents and voltages in the wavelet domain to accurately detect HIF and also localize

the faulted feeder. The authors in [56] provided a detailed evaluation of the fuzzy concept along with WT for HIF detection and classification in a distribution network.

Various methods have been used to distinguish HIF from other non-fault transient phenomena, such as different switching events and arc furnace loads. Mathematical morphology [64], Fast Fourier Transform [60], and multi-resolution morphological gradient [65] are some of the popular HIF detection methods.

This chapter proposes a method for detection and classification of LIF and HIF based on DWT technique. The advantages of our proposed scheme are as follows:

- The scheme requires only three phase current signals and does not require voltage signals. Hence the method is simple and cost effective from the viewpoint of real time implementation with respect to any current and voltage-based method.
- The inputs to the system are one terminal three-phase current signal. Hence synchronization of signals from two terminals of the line is not required, which reduces the impacts on the environmental and external phenomena.
- Only single level wavelet decomposition is employed. Hence, this scheme has reduced the computational burden compared to most of the wavelet-based existing techniques which used multilevel decomposition.
- The proposed scheme does not employ any artificial intelligence techniques e.g. fuzzy logic, ANN, support vector machine, etc., and hence does not require huge amount of data for training purposes.
- One important characteristic of the proposed method is that the logic is deterministic which makes it system independent and avoids collection of data that may not be readily available.

2.2. Features of High Impedance Faults

The idea of detection of fault occurring in transmission lines by WT analysis is not new and many publications are there related to this research. Basically, the transmission line faults are classified into two categories, LIF which occurs due to short circuit between the phase conductors or phase conductors and ground and HIF which occurs when energized phase conductors come in contact with a poor conductive surface or high resistive surface limiting the fault current within the normal value.

Low values of fault currents and arcing phenomenon are the two main characteristics of HIF. The magnitude of fault currents in HIF increases gradually and also they have different maximum and minimum values during the positive and negative half cycle and this build-up automatically stops after a few cycles. Again due to arcing phenomenon, V-I characteristic curve is non-linear. Arcing also generates heat that may reduce moisture on ground surfaces and sometimes causes chemical reactions that change the conductivity of the surfaces. These dynamic characteristics of HIF make the detection of fault more complicated. HIF detection is

also influenced by some other factors such as conditions of weather, duration of fault occurrence, conductor type, short-circuit rate, and fault conditions.

2.3. Feature Extraction by Wavelet Transform

The energy spectrum of cDs (ξd) and energy spectrum of cAs (ξa) have been considered in this chapter for fault classification. The wavelet energy coefficient can be expressed as follows:

$$\xi d_i = \sum_{j=1}^{N} \left| d_{ij} \right|^2 \quad i = 1,.....l \tag{2.1}$$

$$\xi a_i = \sum_{j=1}^{N} \left| a_{ij} \right|^2 \tag{2.2}$$

where, ξd_i is the energy of the detail coefficients at decomposition level i and ξa_i is the energy of the approximate coefficients at decomposition level i. In this analysis only first level (i.e i=1) of decomposition (d_1 and a_1) is considered.

The cDs contain transient information embedded in the fault signals. Though the magnitude variations of fault currents in HIF is not significant to detect the HIFs, energy spectrum of cD (ξd) and energy spectrum of cA (ξa) are used to distinguish the HIF and LIF and also classify the different types of grounded and non-grounded faults.

2.4. HIF Model

In this work, a 2-diode HIF model which is based on arcing in sandy soil [49] is used. Fig. 2.1(a) shows the HIF model, which consists of two DC voltage sources V_p and V_n, connected in anti-parallel by two diodes. These two voltage sources represent the arcing voltage of air in soil and/ or between trees and the transmission line and the values vary from 2 kV to 8 kV. R_p and R_n whose values vary from 100 Ω to 1500 Ω represent the FR.

Asymmetrical fault currents are being simulated by using unequal values of the two FR R_p and R_n. The fault current starts flowing towards the ground when positive DC voltage V_p is less than the line voltage and when the line voltage is less than negative DC voltage V_n, then the fault current reverses back from the ground. Moreover, if the line voltage lies between V_p and V_n then the line voltage is counter balanced by V_p or V_n, therefore no fault current flows. Fig. 2.1(b) illustrates the LIF model which is used in this work. LIF consists of a fixed value of fault resistance R_f, which is present at the fault location in the transmission line.

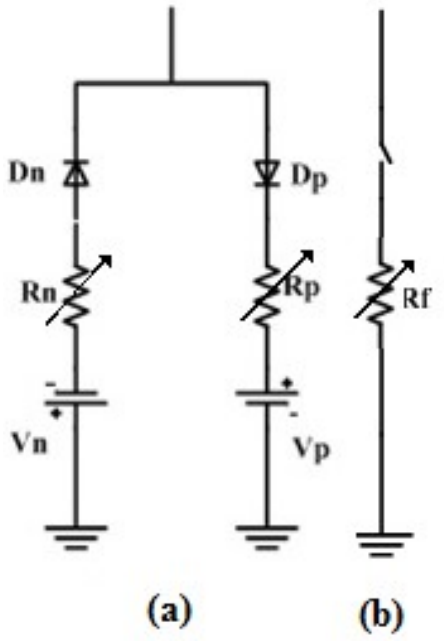

Fig. 2.1. HIF and LIF models
(a) 2- diode HIF model (b) LIF model

2.5. Fault Detection and Classification Scheme

In this chapter, an algorithm is proposed to detect and classify the HIF and LIF. DWT technique is applied to obtain the cAs (Ia_1A, Ia_1B and Ia_1C) from the three phase current signals. Current signals are measured from one end of the transmission line for one cycle after the fault. In the proposed method, cDs are used to detect faults. If the summation of the first level absolute values of cDs is greater than zero, then fault is detected. Fig. 2.2. describes the proposed fault classification methodology. If the sum of the summation of cAs (ΣIa_1A + ΣIa_1B + ΣIa_1C) of three-phase current is nearly equal to zero, then it indicates non-ground fault i.e. LL or LLL fault. The fault is said to be ground fault i.e. SLG or LLG fault if this value is larger than zero.

For classifying the ten different types of faults, the energy spectrum of first level approximation coefficients (ξa_1) and the energy spectrum of first level detail coefficients (ξd_1) of all the three phase currents are computed. Then a fault index (Fg) is calculated for detecting the SLG fault and LLG fault. Fault index (Fg) is the ratio of energy difference between the approximation energy (ξIa_1) of the lower two values to the highest approximation energy (ξIa_1) among all three phases. For ground fault classification, if Fg is less than 0.1, then it is SLG fault otherwise it is LLG fault. In the case of the SLG fault, the faulty phase has the highest value of approximation energy (ξa_1) compared to the other two phases. In the LLG fault, the healthy phase has the lowest value of approximation energy (ξa_1) and the other two faulty phases has larger approximation energy (ξa_1) compared to the healthy one.

To classify the non-ground faults, the fault approximation ratio (F_r) is computed. F_r is obtained by dividing the summation of the absolute values of approximation coefficients ($\Sigma|Ia_1|$) under fault condition to $\Sigma|Ia_1|$ under normal condition. Fault approximation ratio (F_r) is expressed as follows:

$$F_r = \frac{\Sigma \left|I_{a1}\right|(fault)}{\Sigma \left|I_{a1}\right|(normal)} \tag{2.3}$$

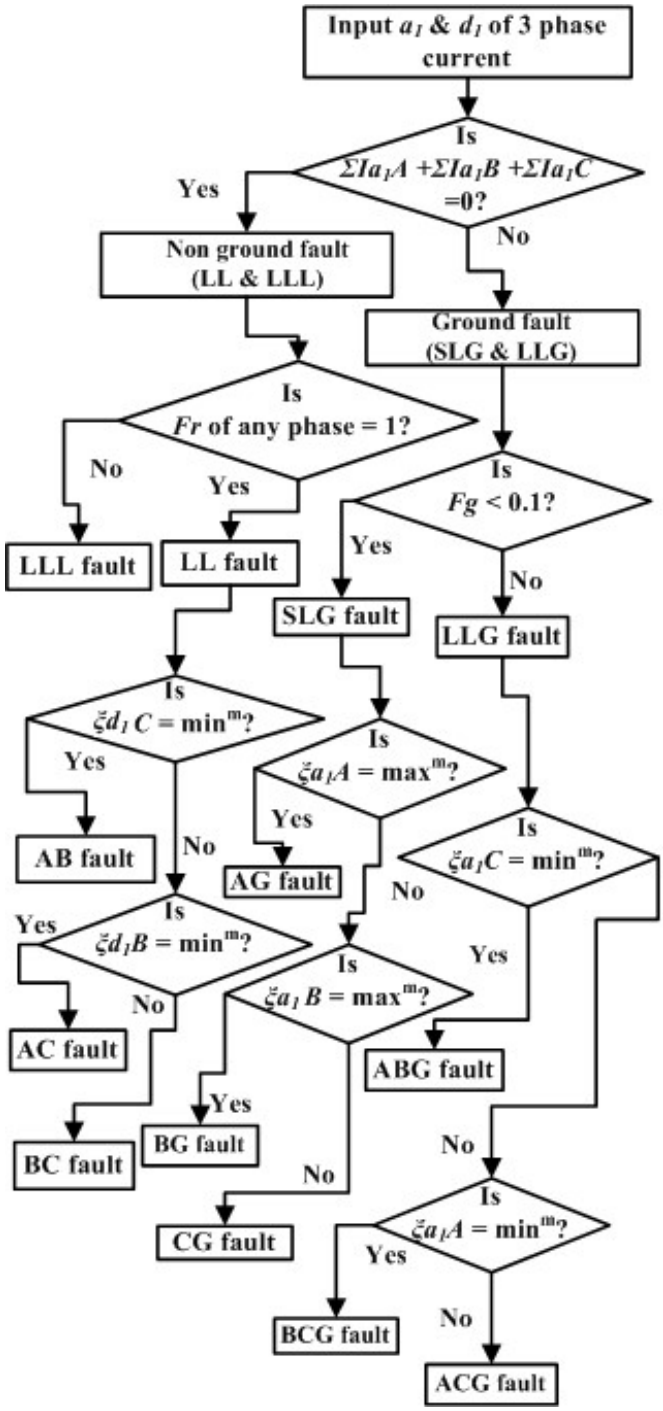

Fig. 2.2. Flowchart for fault classification

If F_r of any one phase is 1, then it indicates LL fault, else it is LLL fault. For LL fault, faulty phases can be identified by calculating the detail energy (ξd_1). In case of the LL fault, the phase with the minimum ξd_1 value is the healthy phase and other two are the faulty phases.

2. 6. Simulation Results of the Proposed Scheme

2.6.1. Test System

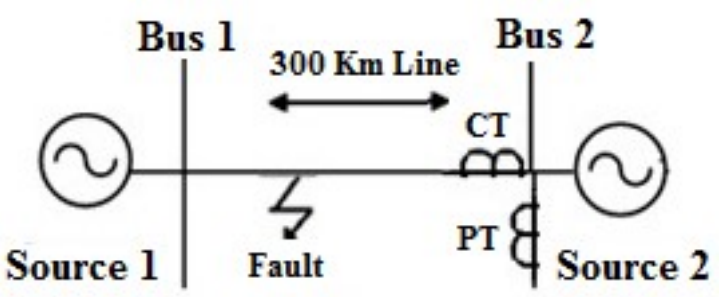

Fig. 2.3. Single line diagram of test power system model

In order to investigate the performance of the proposed fault diagnosis algorithm, a 400 kV, 50Hz transmission line of 300 km length, fed at both ends is simulated in Matlab. The configuration of the model is shown in Fig. 2.3. A sampling frequency of 12.5 kHz (i.e 250 samples/cycle) at 50Hz is chosen for fault simulation. Transmission line parameters such as positive sequence impedance and zero sequence impedance are 40.736+j91.04Ω and 123.648+j41.48 Ω respectively. 4.077nF/km and 2.48nF/km are the positive-sequence capacitance and zero-sequence capacitance respectively, of the system under test. The source impedance of both sources are 0.5333+j 5.333Ω. The load angle of source 1 is 0° and that of source 2 is 20°. Different behavior of HIF is obtained by varying the parameters of the model shown in Fig. 2.1 (a). In this study, we have investigated three HIF scenarios by modulating the HIF model parameter. The voltage sources V_p and V_n were 3588 V and 3847 V, respectively, and the resistances R_p and R_n were 208 Ω and 212 Ω respectively, in condition 1, whereas in condition 2, both resistances R_p and R_n were 245 Ω, and the voltage sources V_p and V_n were 6180 V and 6155 V respectively. In condition 3, R_p and R_n are 270 Ω and 290 Ω respectively and two dc voltage sources, V_p and V_n, are 8092 V and 9358 V respectively.

2.6.2. Performance of the Proposed Algorithm

In order to investigate the performance and efficiency of the proposed algorithm, a database was created by simulating the model for different values of FIA and fault impedances

at various fault distances. The proposed algorithm consists of three stages, namely data collection, feature extraction, and data analysis.

In this chapter, all ten types of faults (AG, BG, CG, ABG, BCG, ACG, AB, BC, AC, and ABC) have been considered for three different FIA (0°, 45°, and 90°), three different RF at regular intervals of 30 km in the transmission line both for LIF (0 Ω, 10 Ω and 20 Ω) and HIF (cond.1, cond.2 and cond.3). In the first stage i.e. data collection stage, the samples of the three phase fault currents during one cycle immediately after the fault inception are collected from bus 2 at a sampling frequency of 12.5 kHz. In the second stage, features of the sample data are extracted using DWT. In DWT choice of mother wavelet is important because different types of mother wavelets show different properties. According to the requirement, the order of the daubechis wavelet can be controlled easily compared to other wavelet functions. In this thesis db4 wavelet is chosen as the mother wavelet due to its good performance in the field of power systems. In this chapter, single level wavelet decomposition has been used to reduce the computational burden.

Table 2.1. Results of fault classification for SLG & LLG (LIF); FR 0 Ω, 120 km

Fault types	FIA (°)	Approximation energy($\xi a_1 x10^8$)			*Fg*	Result
		Phase A	Phase B	Phase C		
AG	0	60.9	1.45	1.67	0.00	AG
AG	45	50.7	1.44	1.67	0.04	AG
AG	90	38.1	1.16	1.65	0.01	AG
BG	0	1.67	44.7	1.45	0.00	BG
BG	45	1.65	38.98	1.47	0.00	BG
BG	90	1.65	54.02	1.47	0.00	BG
CG	0	1.47	1.65	42.8	0.00	CG
CG	45	1.46	1.66	58.5	0.00	CG
CG	90	1.44	1.68	56.4	0.00	CG
ABG	0	91.5	32.1	1.59	0.33	ABG
ABG	45	66.7	11.8	1.59	0.15	ABG
ABG	90	75.7	31.7	1.59	0.40	ABG
BCG	0	1.59	65.01	14.5	0.20	BCG
BCG	45	1.58	85.5	42.1	0.47	BCG
BCG	90	1.58	102.6	50.1	0.47	BCG
CAG	0	49.8	1.58	94.9	0.51	CAG
CAG	45	42.6	1.58	99.3	0.41	CAG
CAG	90	14.8	1.59	73.1	0.18	CAG

Table 2.2. Results of fault classification for SLG & LLG (HIF); FR cond. 3, 210 km

Fault types	FIA (°)	Approximation energy($\xi a_1 x10^8$)			*Fg*	Result
		Phase A	Phase B	Phase C		
AG	0	1.99	1.54	1.60	0.01	AG
AG	45	4.25	1.57	1.54	0.01	AG
AG	90	4.24	1.57	1.54	0.01	AG
BG	0	1.51	4.25	1.57	0.01	BG
BG	45	1.54	4.26	1.57	0.01	BG
BG	90	1.54	4.30	1.56	0.01	BG
CG	0	1.56	1.54	4.27	0.00	CG
CG	45	1.56	1.54	4.30	0.01	CG
CG	90	1.57	1.54	4.28	0.01	CG
ABG	0	4.36	4.27	1.55	0.62	ABG
ABG	45	4.31	4.27	1.55	0.63	ABG
ABG	90	4.30	4.32	1.55	0.64	ABG
BCG	0	1.54	4.31	4.28	0.64	BCG
BCG	45	1.55	4.32	4.32	0.64	BCG
BCG	90	1.55	4.36	4.30	0.63	BCG
CAG	0	4.32	1.55	4.33	0.63	CAG
CAG	45	4.27	1.55	4.37	0.62	CAG
CAG	90	4.25	1.55	4.34	0.62	CAG

The performance of the proposed method to classify the different types of faults is validated through several case studies by creating different types of faults at various distances considering different FIA and different FR (both for LIFs and HIFs). These results have been tabulated in Tables 2.1-2.4. From Table 2.1 and Table 2.2 it is seen that if the fault index *Fg* is less than 0.1 then it indicates SLG, else LLG. In case of ground fault, to identify the faulty phase, the energy spectrum of approximation coefficients (ξa_1) of all the phases are computed which are shown in Tables 2.1 and 2.2. From these two tables, it is seen that faulty phase/ phases has/ have the highest/ higher approximation energy. For an example, considering AG (LIF) fault in Table 2.1 when FIA is 90°, $\xi a_1 A$ is 38.1×10^8 which is greater than $\xi a_1 B$ (1.16×10^8) and $\xi a_1 C$ (1.65×10^8). Similarly, in case of LLG fault (BCG at FIA 45^0), $\xi a_1 B$ (85.5×10^8) and $\xi a_1 C$ (42.1×10^8) are larger than $\xi a_1 A$ (1.58×10^8).

From Table 2.3 and Table 2.4 it is seen that, if the fault approximation ratio (F_r) of any one phase is equal to 1, it indicates double line fault (LL), else triple line fault (LLL). The computed values of energy spectrum of detail coefficients (ξd_1) for different types of double line faults are also tabulated in Table 2.3 and Table 2.4. From these tables, it is clearly seen that the phase which has detail energy (ξd_1) near to zero is the healthy one. For example, in Table 2.4,

Table 2.3. Results of fault classification for LL & LLL (LIF); FR 0 Ω, 210 km

Fault types	FIA (°)	F_r			Detail energy (ξd_1)			Result
		Phase A	Phase B	Phase C	Phase A (ξd_1Ax10^4)	Phase B (ξd_1Bx10^4)	Phase C (ξd_1Cx10^4)	
AB	0	9.93	9.12	1.00	59.3	59.4	0.000262	AB
AB	45	8.22	7.23	1.00	122	122	0.000507	AB
AB	90	9.28	8.50	1.00	64.2	64.2	0.000254	AB
BC	0	1.00	8.25	7.29	0.00047	115	115	BC
BC	45	1.00	10.1	9.44	0.000125	32.6	32.7	BC
BC	90	1.00	11.0	10.6	0.000036	6.68	6.68	BC
CA	0	10.3	1.00	10.8	9.06	0.000033	9.05	CA
CA	45	9.98	1.00	10.7	28.5	0.000132	28.4	CA
CA	90	7.59	1.00	8.58	112	0.000474	112	CA
ABC	0	12.5	9.31	10.3	-	-	-	ABC
ABC	45	10.1	9.45	12.6	-	-	-	ABC
ABC	90	8.96	12.1	11.04	-	-	-	ABC

Table 2.4. Results of fault classification for LL & LLL (HIF); FR condition 3, 270 km

Fault types	FIA (°)	F_r			Detail energy(ξd_1)			Result
		Phase A	Phase B	Phase C	Phase A ($\xi d_1 Ax10^4$)	Phase B ($\xi d_1 Bx10^4$)	Phase C ($\xi d_1 Cx10^4$)	
AB	0	1.67	1.68	1.00	1.95	1.92	0.000257	AB
AB	45	1.67	1.68	1.00	3.57	3.53	0.000507	AB
AB	90	1.68	1.68	1.00	1.64	1.62	0.000256	AB
BC	0	1.00	1.67	1.67	0.000471	3.24	3.2	BC
BC	45	1.00	1.68	1.68	0.000127	0.767	0.758	BC
BC	90	1.00	1.69	1.68	0.000032	0.288	0.285	BC
CA	0	1.69	1.00	1.68	0.124	0.000032	0.0126	CA
CA	45	1.68	1.00	1.68	0.996	0.000127	1.01	CA
CA	90	1.68	1.00	1.68	3.36	0.000471	3.40	CA
ABC	0	1.86	1.85	1.86	-	-	-	ABC
ABC	45	1.85	1.85	1.86	-	-	-	ABC
ABC	90	1.85	1.86	1.85	-	-	-	ABC

considering AC fault at 90^0, it is seen that $\xi d_1 A$ and $\xi d_1 C$ are 3.36x10^4 and 3.40x10^4 respectively whereas $\xi d_1 B$ is 0.000471 which is near to zero, therefore it indicates LL (AC) fault. The

accuracy of this proposed method for detection and fault classification of HIF and LIF in the transmission line is 100% and uses 1st level of decomposition of current signals which reduces the computational burden. Therefore, this method shows fast and accurate fault classification which is very important for quick maintenance and power supply restoration.

2.7. Conclusion

The main objective of the proposed scheme is to develop an adaptive fault detection and classification scheme and discriminate between HIF and LIF. In this scheme, the input parameters for fault detection and classification are the three phase current signals under various fault conditions. DWT analysis has been performed on the current signals for feature extraction which are used for the detection of HIF and LIF and also to classify them. The same algorithm has been used for the classification of both HIF and LIF. The proposed scheme does not require information about the line parameters and loads. As current signals are measured from one end of the transmission line, it does not need synchronization of the monitoring devices. Moreover, single level wavelet decomposition reduces the computational burden and computing time.

CHAPTER 3

Fault Detection and Classification Scheme for Transmission Lines Connecting Wind farm using Single End Impedance

3.1. Introduction

The continuous expansion of the power system networks has drawn attention towards developing a highly reliable and accurate protection scheme that should have a quick response to detect, classify and clear faults in transmission lines as soon as possible and also have immunity against different dynamic situations.

Faults in the transmission lines are inevitable, hence reliable and fast detection and classification of faults in transmission lines are of great importance. Among the existing techniques, wavelet-based fault detection technique has been widely used due to its outstanding ability to analyze non-stationary signals, reveal discontinuities and necessary frequency spectrum. Wavelet analysis-based real-time implementation of fault detection and identification module on a low-end embedded system has been demonstrated in [10]. DWT-based detail energy spectrum [11] and singular value decomposition [13] can efficiently detect and classify faults in transmission lines. Synchronized measurement of voltage and current signals from the remote end of the transmission line can provide reliable transmission line protection schemes. Shaik et. al. proposed a transmission line protection scheme combining WT with ANN in [1]. This system makes use of synchronized data of voltage and current signals from both transmission line terminals. cDs of current signals are used to detect and classify the faults whereas cAs of voltage and current signals are used to locate the fault by applying ANN. Rathore et al. introduced a two-terminal [8] transmission line protection scheme based on wavelet-alienation approach. Alienation coefficients are estimated utilizing cAs of post-fault current signals (quarter-cycle) from both ends of the transmission line to identify and classify faults. Wavelet transform, in conjunction with ANFIS, can provide a classification scheme that is adaptable to neutral non-effectively grounded distribution system (DS) [19]. Flexible ac transmission systems are nowadays used to fully utilize the existing transmission system. Fault classification in series compensated transmission line (SCTL) has been carried out in [69] combining WT with ANFIS. In [67], Goli et al. developed a fuzzy-based protection method for identifying faults and estimating the location of the fault in a double circuit UPFC compensated transmission line. Wavelet singular entropy, in combination with fuzzy logic, can also detect and accurately classify faults in the presence of DGs [118].

HIF detection is a challenging task as a feeder operating with HIF does not show any abnormal behaviour or interruption in electric power supply owing to low magnitudes of fault currents. The efficacy of WT in detecting HIF has been presented in [49, 54, 55, 56, and 58].

The non-linear characteristics of mathematical morphology have been exploited to detect and classify HIF in [63, 64]. Evidential reasoning-based and FFT-based approaches have been applied in [52] and [60] respectively, to detect and distinguish between HIF and other switching events such as capacitor and load switching. Magnitude of differential power evaluated from current and voltage signals, at the local and remote terminal of the transmission line, can classify all types of faults, including HIF under different dynamic situations [100, 101].

In the time–frequency domain, a full waveform of the travelling wave can represent panoramic fault information. Faults in compensated transmission lines connected to wind farms can be localized using travelling wave phenomenon [117]. A new travelling-wave-based protection algorithm has been presented in [97] to address the synchronization issue and communication difficulties between the two end signals of transmission lines. At first propagation characteristics are calculated using CWT at different scales, then the correlation and difference of the complete waveform for internal and external faults are computed. Fundamental components of three-phase voltage and current signals and zero-sequence current signals have been used as inputs for fault classification in [41, 36]. The authors in [102] presented an integrated moving sum approach-based fault classification scheme and a novel filter-based ANN approach for fault classification has been presented in [108]. An impedance-based fault location scheme for overhead unbalanced radial distribution networks has been proposed in [30]. Discrimination between high and low impedance faults and classification of both types of faults using the same algorithm has been presented in [50].

3.2. Problem Statement

Transmission lines are integral part of the electrical power system network. Accurate fault detection and classification in transmission lines are very much essential for restoring the power supply taking minimal clearance time. HIF specially poses serious challenge as it is difficult to detect due to low magnitudes of fault currents. Moreover, in the modern era, the share of electricity from renewable energy sources is increasing significantly due to on-going effort towards prospective low carbon energy system. In recent years, distributed generation has extensively penetrated into the power system network. After the connection of DG, the system no longer remains radial and protective equipment loses coordination. Extracting features from faulty signals is a challenging task in the presence of DG as the behaviour of signals during fault changes. Faulty phase identification becomes a challenging job as the back-feed current from the DG masks the faulty phase. This chapter presents a new fault detection and classification scheme in the presence of wind farms as wind power generation nowadays forms a major part of electric power generation. Integration of wind farms to the grid through transmission line enhances the stability and reliability of the power system. The main problem of the wind farm is the non-linear relationship between power output and the wind speed. Therefore, when these farms are connected to the electric power system network, voltage and power transmitted to the system continually fluctuate at the relay end, which greatly affects the relaying scheme. Hence, this

problem needs to be addressed under various stressed and dynamic conditions and the reliability of the developed schemes needs to be verified under diversified situations.

In this chapter, all types of faults have been classified with and without the presence of wind farms under both LIF and HIF conditions. The current and voltage signals are recorded from one end of the transmission line. These signals are analyzed using the db4 mother wavelet and single level decomposition has been performed to obtain the cAs and cDs. The summation of the absolute values of first-level cDs of current signal of each phase is calculated over one full cycle to detect fault. If the summation of the absolute values of cDs of any phase is greater than the threshold value, then fault is detected, that is, each of $\Sigma|IAd_1|$, $\Sigma|IBd_1|$, and $\Sigma|ICd_1|$ is below the threshold under no-fault condition. However, when fault occurs, at least one of these values is much above the threshold value. After fault detection, fault classification is carried out by calculating the line impedance considering one cycle data from the inception of fault. The impedance is calculated from the ratio of the summation of the absolute values of cAs of voltage and current signals. The impedance of all three phases has been fed to the fuzzy-based classifier to classify faults. Therefore, the proposed method does not require synchronization of signals from the remote end. The proposed methodology gives accurate results under various conditions which normally affect fault detection and classification process in long transmission lines viz. power angle variation, transmission line parameter variation, transmission line length variation, source impedance variation, presence of nonlinear HIF, and CT saturation.

3.3. Materials and Method

Formulation of the proposed protection scheme for fault classification has been performed in two stages: feature extraction using the MRA and fault classification using FIS. In this chapter, the db4 mother wavelet has been chosen due to its satisfactory performance in detecting the quick changes in signals and it also takes less computational time with good localization efficiency. In this work, only single level decomposition of the signal is applied to reduce the computational burden.

The ratio of the summation of absolute values of cAs of voltage and current signals, obtained from single level decomposition by WT has been fed to the fuzzy-based classifier to classify the faults. Mamdani-type FIS has been designed which has three inputs and one output. Max–Min composition and the centroid of area method for defuzzification have been used in this FIS.

3.4. Test System

The continuous expansion of the transmission network demands integration of renewable energy sources with the main power system grid. For this reason, the authors have developed

two test systems in Matlab environment to evaluate the performance and feasibility of the proposed fault classification method.

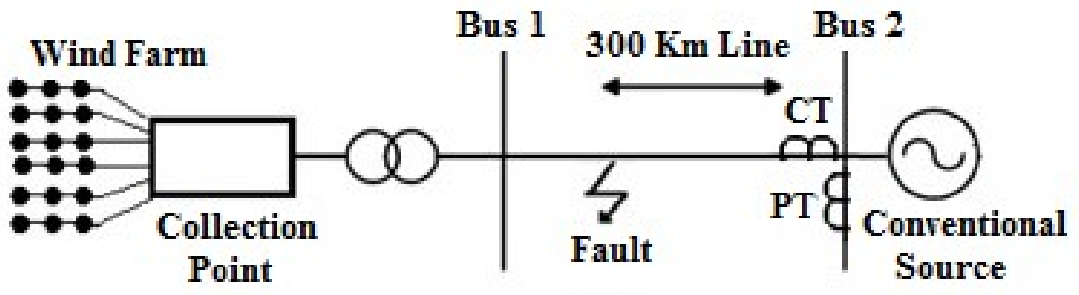

Fig. 3.1. Single line diagram of Test System 2

The test system 1 consists of a 300 km transmission line fed at both ends by conventional sources similar to the test system considered in [50]. Fig. 3.1 shows the test system 2 which is fed by wind farm at one end and a conventional source at the other end. The faults have been classified by calculating the line impedance obtained from the wavelet decomposition of voltage and current signals at the measuring point. The simulation is executed with a 12.5 kHz sampling frequency (i.e. 250 samples /cycle) at 50 Hz as most of the commercial devices are available at this sampling frequency.

One cycle data length i.e. 250 samples or 0.02s data window has been used to calculate the cDs and cAs. Single level wavelet decomposition has been carried out and first-level cDs and cAs have been utilized to detect and classify faults. First-level cDs capture frequency ranges from 3.125 kHz to 6.25 kHz and first-level cAs capture frequency ranges from 0 to 3.125 kHz.

In our study, we have considered two conventional sources in test system 1. The source impedance of both the conventional sources is 0.5333 + j5.33 Ω and the load angle of source 2 is 20° and that of source 1 is 0°. In the second system i.e. test system 2 shown in Fig. 3.1, one source is replaced by a wind farm. The wind farm consists of 40 numbers of 1.5 MW wind turbines with rated speed of 5 m/s. Wound rotor type double fed induction generator and an AC/DC/AC IGBT-based PWM converter are used in the wind farm and connected with a 70 MVA, 575 V/400 kV, /Yn transformer.

The transmission line parameters, such as positive-sequence capacitance and zero-sequence capacitance, are 4.077 nF/km and 2.48 nF/km, respectively, whereas positive-sequence and zero-sequence impedances are 0.136 + j0.30347 Ω/km and 0.4122 + j 0.1395 Ω/km, respectively. All types of faults have been simulated at different FIA, different FR and also at different locations of the transmission line. The main parameters of the source, transmission line, transformer, and doubly fed induction generator used in wind farm are represented in Table 3.1.

Table 3.1. System parameters

	Parameters	Value
Source	Nominal voltage	400 kV
	Frequency	50 Hz
	Source impedance	0.5333+j 5.33 Ω
	Internal connection	Yg
	Load Flow (Generator type)	Swing
Transmission line	Length	300 km
	Positive-sequence impedance	0.136+ j 0.0347Ω/km
	Zero-sequence impedance	0.4122 +
	Positive-sequence capacitance	4.077nF/km
	Zero-sequence capacitance	2.48nF/km
Double fed induction generator in wind farm	Rated Power	1.5 MW
	Rated frequency	50Hz
	Number of wind farm	40
	Stator rated voltage	575 V
	Stator resistance	0.023 pu
	Stator leakage inductance	0.18 pu
	Rotor resistance	0.016 pu
	Rotor leakage inductance	0.16 pu
	Magnetizing inductance	2.9 pu
Transformer	Rated capacity	70MVA
	Rated voltage	575V/400kV

3.5. Simulation Results

In order to validate the proposed transmission line protection scheme and observe the efficiency of this algorithm, the voltage and current signals for one cycle after the inception of fault have been acquired from one end of the transmission line. Single level decomposition of the signals has been performed in the wavelet domain and the first-level cAs and cDs have been obtained. In this chapter, all ten types of faults (AG, BG, CG, ABG, BCG, ACG, AB, BC, AC, and ABC) have been simulated under different FIA (0-90°), different resistances (0-300Ω) and at different locations in the transmission line. Fault detection algorithm is based on first-level cDs (d_1) of the current signal. If the summation of the absolute values of cDs of any phase is greater than the threshold value, then fault is detected. It has been observed that the summation of the absolute values of cDs of all the phases is always less than 6 for test system 1 and less than 18 for test system 2 under no-fault condition. During fault the summation of the absolute values of cDs of at least one phase is much above these values. Hence, the threshold value has

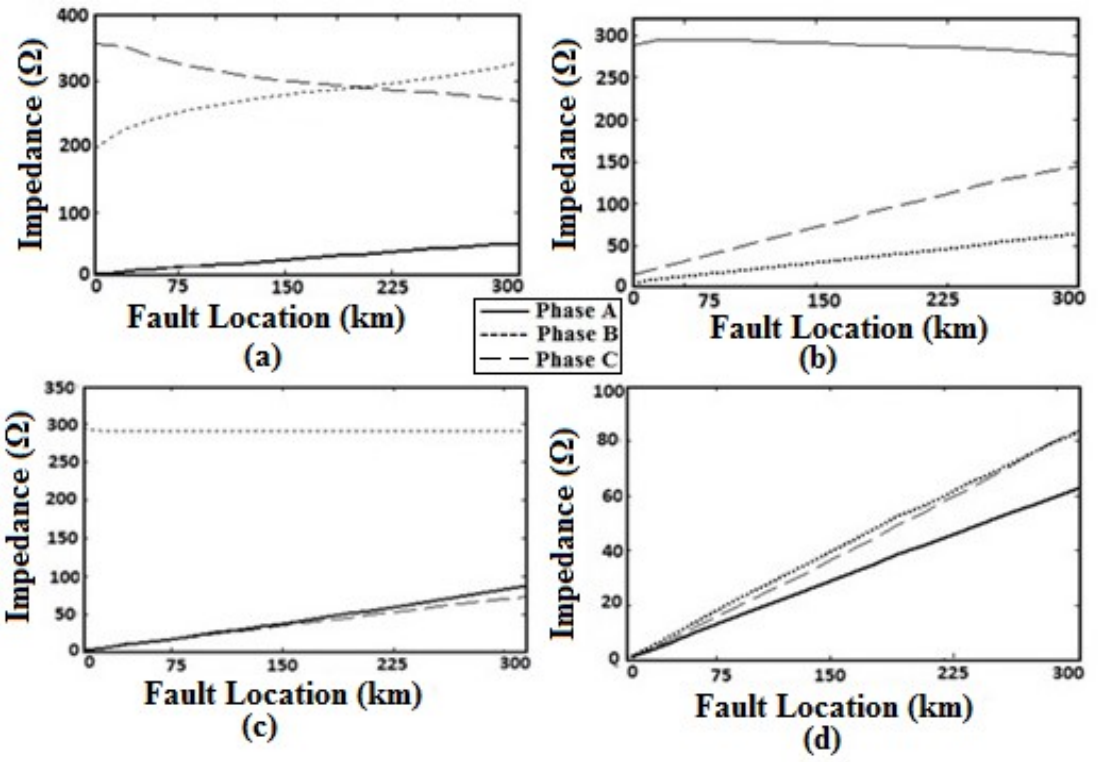

Fig. 3.2. Line impedance vs. location of fault at 0 Ω FR and 0° FIA for Test System 1 (a) AG (b) BCG (c) AC (d) ABC

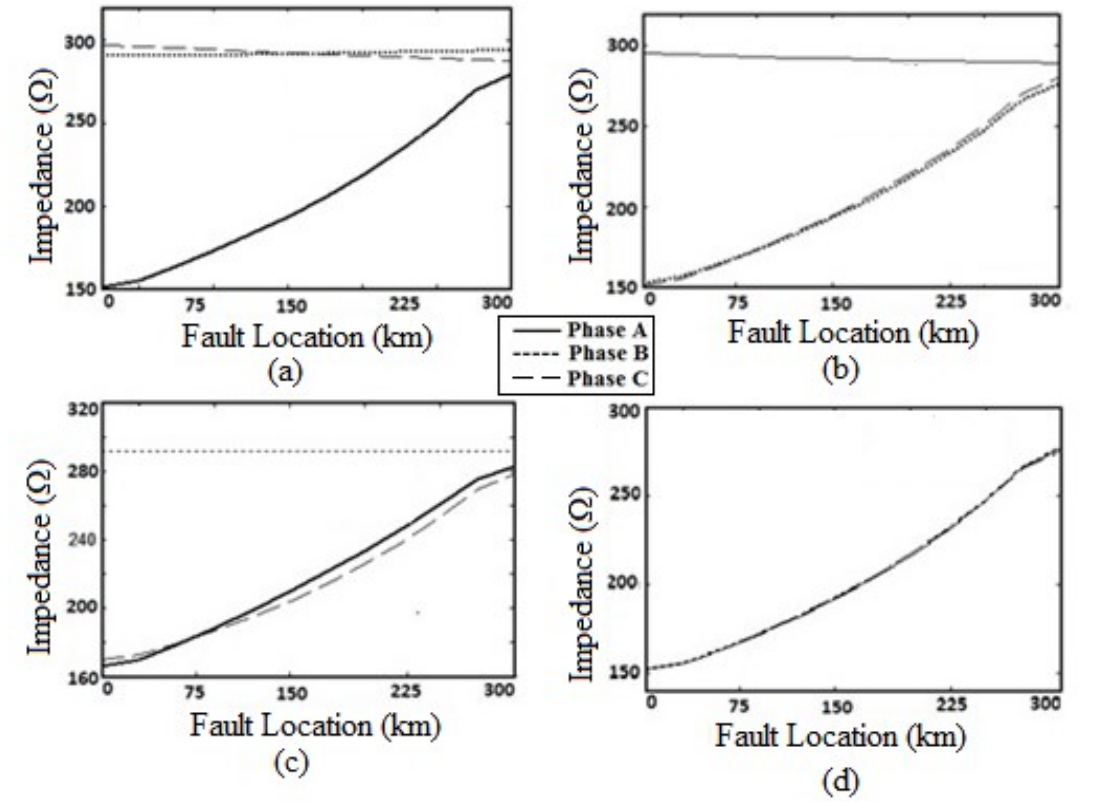

Fig. 3.3. Line impedance vs. location of fault at 300 Ω FR and 0° FIA for Test System 1: (a) AG (b) BCG (c) AC (d) ABC

been considered as 20 for both test systems. The fuzzy-based fault classifier is used to classify the faults. In the fault classification stage, the impedance of the line, calculated from the ratio of the summation of the absolute values of cAs of voltage and current signals of one cycle after the inception of fault, acts as the input to the FIS.

Fig. 3.2 and Fig. 3.3 show the line impedance at different locations of fault in the transmission line. It is seen that faulty phase/s have lower impedances than the healthy phase/s and the line impedance of the faulty phase increases with the increase of the distance of fault from the measuring point. In Fig. 3.3 it is observed that for HIFs the impedance of the healthy phases does not change appreciably.

Fig. 3.4 and Fig. 3.5 show the line impedance vs. fault location when one end of the line is fed by wind farm in test system 2. It is seen that in this case, the line impedance of the faulty phase is much less than that of the healthy phase for 0 Ω and 300 Ω fault resistance throughout the whole length of the line.

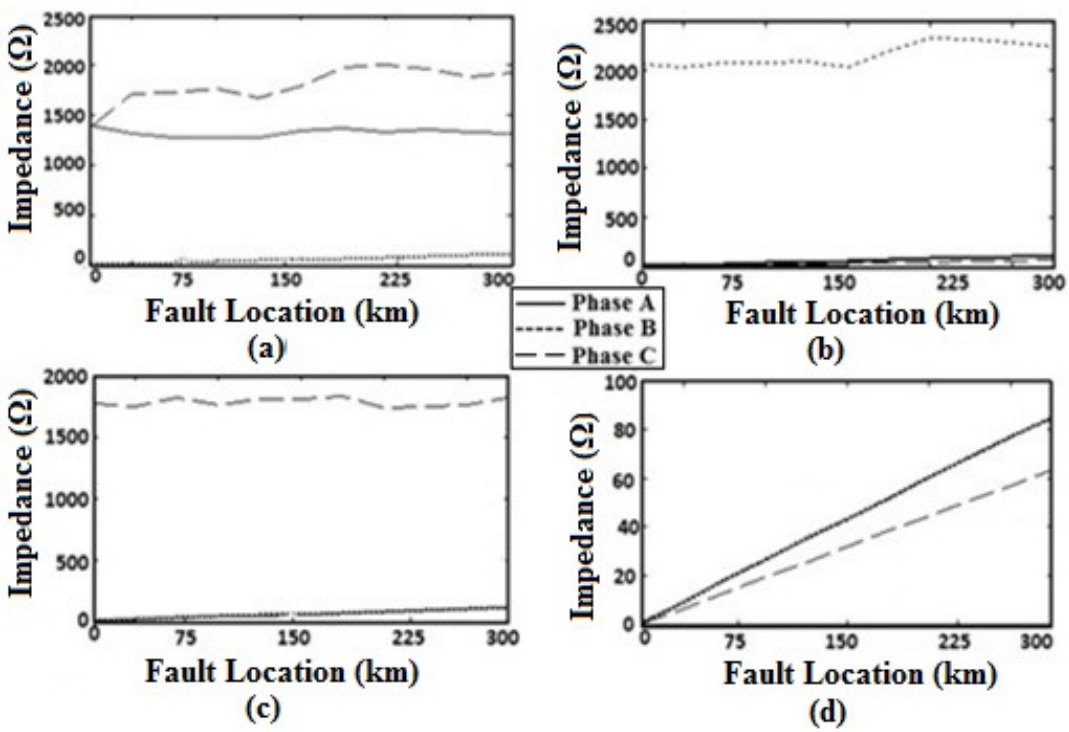

Fig. 3.4. Line impedance vs. location of fault at 0 Ω At 45° FIA for Test System 2: (a) BG (b) ACG (c) AB (d) ABC

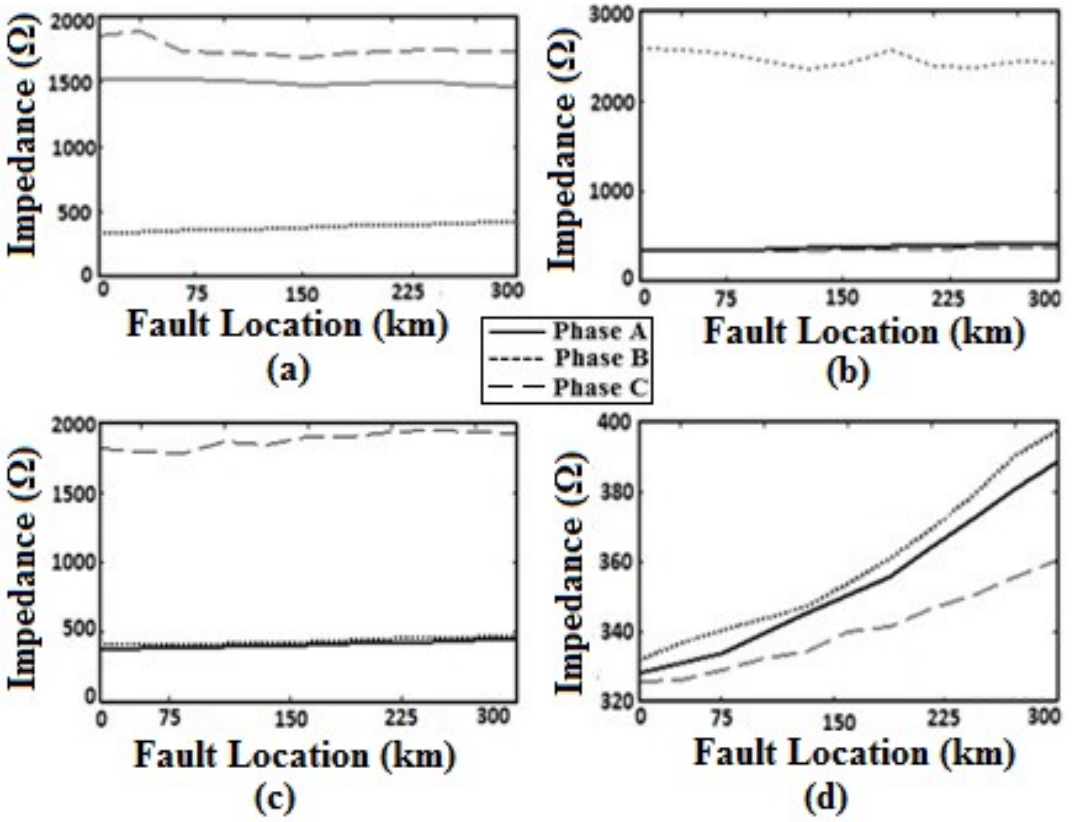

Fig. 3.5. Line impedance vs. location of fault at 300 Ω at 45° FIA for Test System 2 (a) BG (b) ACG (c) AB (d) ABC

3.6. Classification of Fault using FIS

This section explains the classification process of different types of ground and non-ground faults based on the fuzzy logic approach. In this chapter, to perform the fault classification process for both systems, Mamdani type FIS has been designed which has three inputs and one output. The fault type is single-valued and represents an amalgamation of the three impedances Z_a, Z_b, and Z_c of three phases A, B, and C., respectively. Triangular membership functions (MF) have been used for three input variables. All these three inputs have seven MFs for test system 1 and only two MFs for each of the three inputs in test sytem 2 are sufficient to classify all types of faults. Therefore, it can be concluded that this fuzzy-based fault classification scheme is fast, accurate, and also reliable in the presence of renewable energy sources.

For output, seven linguistic variables are used and all the output variables have triangular MFs. Each type of fault is identified by a number or range of numbers. To distinguish between double line to ground fault and double line fault, the summation of the cAs of the current signal of all the phases has been used. If this summation is zero, then it indicates that the fault is a non-ground fault (LL), else ground fault (LLG). The accuracy of the proposed fuzzy-based protection scheme has been found to be 100%.

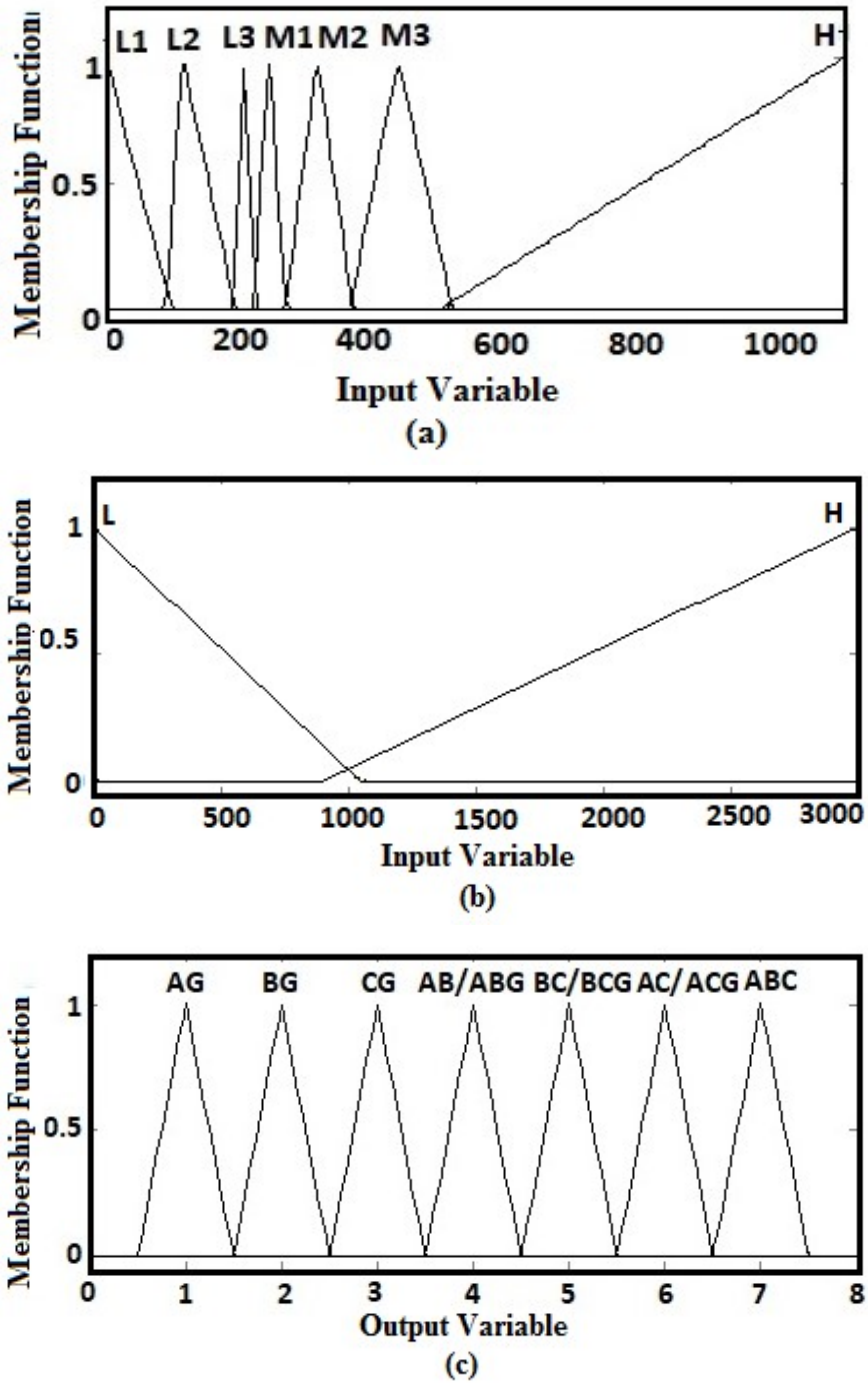

Fig. 3.6. Membership functions of Fuzzy based classifier
(a) Input Membership functions for System 1
(b) Input Membership functions for System 2
(c) Output Membership functions

Fig. 3.6 shows the input and output MFs for both test systems. A total of 187 rules are designed in the FIS for test system 1 some of which are as follows:

- If (Z_a is L1) and (Z_b is M1) and (Z_c is M2) then (output is AG)
- If (Z_a is L2) and (Z_b is M3) and (Z_c is M1) then (output is AG)
- If (Z_a is L1) and (Z_b is M1) and ($Z_c$is M1) then (output is AG)
- If (Z_a is L1) and (Z_b is M1) and (Z_c is M3) then (output is AG)
- If (Z_a is L3) and (Z_b is M2) and (Z_c is M2) then (output is AG)
- If (Z_a is L1) and (Z_b is H) and (Z_c is H) then (output is AG)
- If (Z_a is L1) and (Z_b is L2) and ($Z_c$is M2) then (output is AB/ABG)
- If (Z_a is L1) and ($Z_b$is L1) and (Z_c is M2) then (output is AB/ABG)
- If (Z_a is L1) and (Z_b is L1) and (Z_c is H) then (output is AB/ABG)
- If (Z_a is L2) and (Z_b is L2) and (Z_c is H) then (output is AB/ABG)
- If (Z_a is L1) and (Z_b is L2) and (Z_c is H) then (output is AB/ABG)
- If (Z_a is M1) and (Z_b is M2) and (Z_c is H) then (output is AB/ABG)
- If (Z_a is L1) and (Z_b is L1) and (Z_c is L2) then (output is ABC)
- If (Z_a is L1) and (Z_b is L2) and (Z_c is L1) then (output is ABC)
- If (Z_a is L2) and (Z_b is L1) and (Z_c is L1) then (output is ABC)

For test system 2 seven rules have been developed to classify faults which are as follows:

- If (Z_a is L) and (Z_b is H) and (Z_c is H) then (output is AG)
- If (Z_a is H) and (Z_b is L) and (Z_c is H) then (output is BG)
- If (Z_a is H) and (Z_b is H) and (Z_c is L) then (output is CG)
- If (Z_a is L) and (Z_b is L) and (Z_c is H) then (output is AB/ABG)
- If (Z_a is H) and (Z_b is L) and (Z_c is L) then (output is BC/BCG)
- If (Z_a is L) and (Z_b is H) and (Z_c is L) then (output is AC/ACG)
- If (Z_a is L) and (Z_b is L) and (Z_c is L) then (output is ABC)

3.7. Case Studies and Discussion

To assess the efficiency of the proposed method, both test systems have been modelled in Opal-RT real-time simulator. Different fault cases, such as different types of faults with varying FR, fault location, FIA and system parameters, have been created in both the systems to create the test data set. Also, the performance of the proposed scheme has been studied under different dynamic conditions. In the following subsections, results of different case studies have been discussed.

3.7.1. Effect of Fault Type, Fault Location, FR and FIA

Operation of traditional line protection schemes is affected by change in fault location, variation of FR and FIA. To evaluate the reliability of the proposed protection scheme, all types of ground and non-ground faults have been simulated in the 300 km transmission line with varying FR (0-300Ω) and FIA (0-90°). The fault location has been varied from 15 km to 285 km at intervals of 15 km. The impedance values for test systems 1 and 2 have been shown in Table 3.2 for single line to ground fault at FIA of 0° and at a distance of 90 km from the measuring point. This impedance-based fault classification method accurately classifies all types of faults and is immune to variations of FR, FIA and fault location.

Table 3.2. Line impedances for SLGA fault at different FR

	Test System 1			Test System 2		
FR (Ω)	Z_a	Z_b	Z_c	Z_a	Z_b	Z_c
0	25.72	276.93	301.74	23.48	2977.48	1814.46
10	34.94	280.80	302.27	30.94	2696.38	1855.24
100	109.6	289.69	295.31	120.4	2631.78	1962.38
300	182.9	291.15	293.13	343.0	2767.57	1918.49

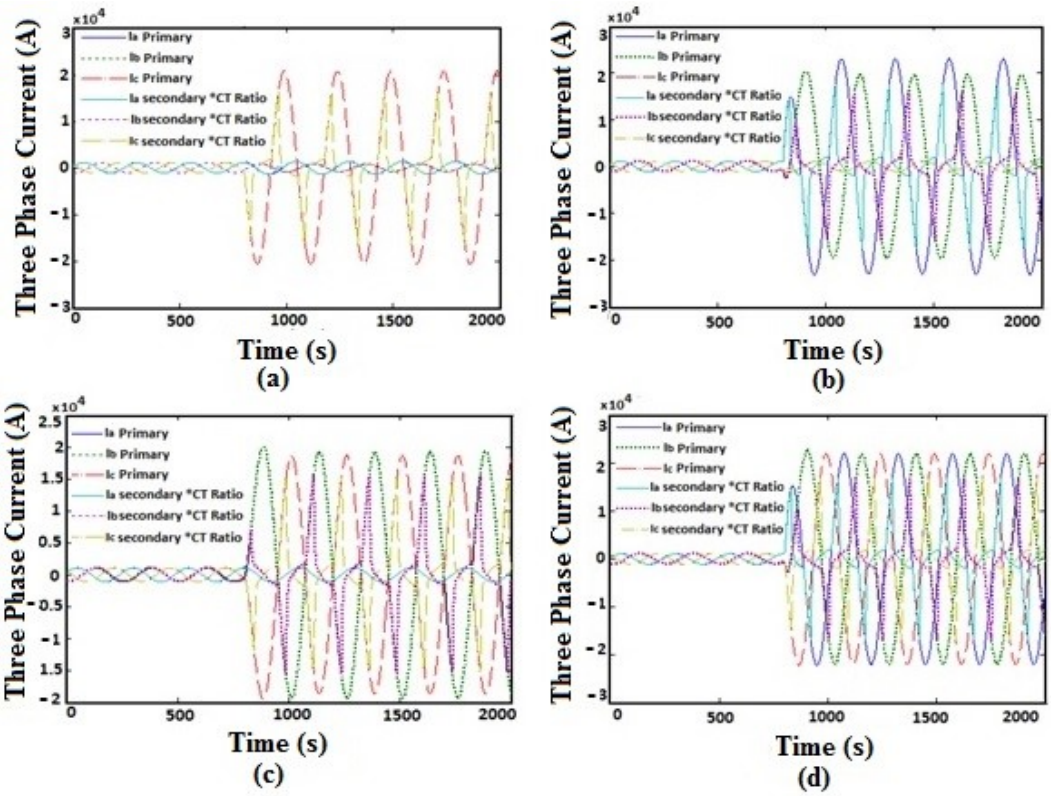

Fig. 3.7. Three phase current waveform with CT Saturation 15 Km from Bus 2 of Test System 1 at FR 10 Ω and FIA 75° : (a) CG (b) ABG (c) BC (d) ABC

3.7.2. Effect of CT Saturation

CT saturation causes an increase in the magnetizing current; therefore, CT secondary current decreases. To consider the effect of CT saturation one CT rated 2000 A/ 5A, 30 VA, is used to measure the current on bus 2. The primary and secondary resistances and inductances are the same as in [101]. Fig. 3.7 shows the three-phase current waveform with CT saturation in test system 1 and Fig. 3.8 shows the three-phase current waveform with CT saturation for test system 2. The efficiency of the proposed scheme is not affected by the presence of CT saturation for both test systems.

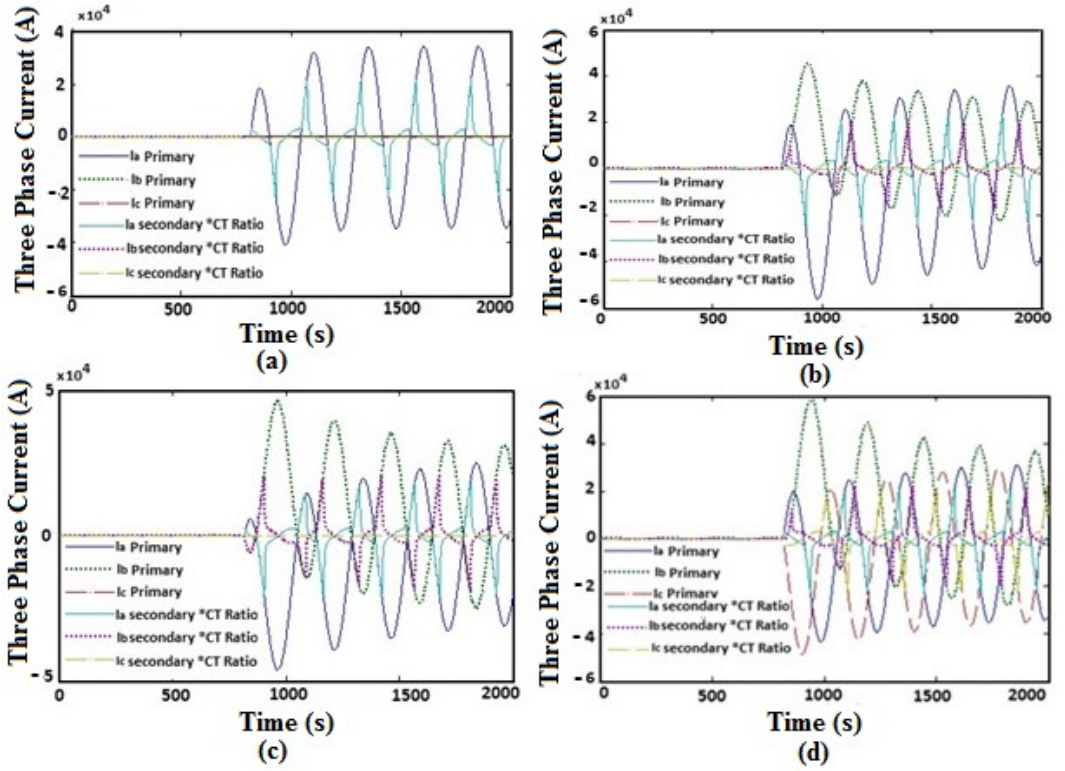

Fig. 3.8. Three phase current waveform with CT Saturation 15 Km from Bus 2 for Test System 2 at FR 0 Ω and FIA 90° : (a) AG (b) ABG (c) AB (d) ABC

3.7.3. Effect of Variations of Line Parameters

Transmission lines are exposed to the atmospheric conditions. Therefore, due to changes in weather conditions and due to the aging effect, the parameters of the transmission line conductors get changed which causes the change in impedance of the line. The proposed method is tested by changing the preset impedance values of the line conductors in the range of ±5% to ±10%. Extensive simulations have been conducted to ascertain that the proposed scheme is independent of variations of line parameters.

3.7.4. Effect of Variations of Transmission Line Length

The operation of the transmission line protection scheme may be affected by the change in the length of the line. In this chapter, the authors have considered a transmission line length of 300 km. To investigate the effect of change in line length, the proposed scheme has been tested for 250 km and 400 km of the transmission line. The results indicated that the proposed scheme is robust to the change in line length.

Table 3.3. Line impedances for SLGA fault at different FR and different conditions for system 1

	Initial			Variation of line parameter			Variation of line length			Variation of pre fault power transfer angle		
FR (Ω)	Z_a	Z_b	Z_c	Z_a	Z_b	Z_c	Z_a	Z_b	Z_c	Z_a	Z_b	Z_c
0	18.61	263.2	314.6	20.49	289.1	340.2	50.35	381.0	371.1	19.33	476.2	650.6
10	27.37	272.2	314.9	29.17	297.5	341.0	60.98	379.4	372.5	28.97	504.9	664.3
100	99.14	288.6	298.1	102.5	314.3	324.8	150.6	277.6	376.9	118.8	564.9	602.9
300	173.0	290.8	294.1	181.8	316.7	320.4	241.9	377.8	377.8	244.7	574.2	587.2

Table 3.4. Line impedances for SLGA fault at different FR and different conditions for system 2

Impedance		FR(Ω)			
		0	10	100	300
Initial	Z_a	22.12	30.32	121.71	343.35
	Z_b	1831.43	2029.51	2287.39	2537.01
	Z_c	1356.57	1405.25	1767.48	2537.01
Variation of line parameter	Z_a	29.56	38.57	131.35	360.87
	Z_b	2437.94	2355.19	2272.28	2430.34
	Z_c	1620.89	1667.15	2272.28	1982.84
Variation of line length	Z_a	22.15	30.33	121.42	343.27
	Z_b	1733.64	1751.03	2069.40	2007.93
	Z_c	1220.84	1200.99	1419.38	1397.56
Variation of pre fault power transfer angle	Z_a	21.08	1847.57	121.87	347.75
	Z_b	1847.57	1960.11	2082.27	2258.54
	Z_c	1497.2	1582.20	1877.95	2005.55

3.7.5. Effect of Variations of Pre-fault Power Transfer Angle

The line impedance depends on the line current which is directly related to the line loading or pre-fault power transfer angle. The operation of conventional relays may be affected by the change of load transfer in the transmission line. To investigate the dependency of the proposed method on line loading, different simulations have been performed by changing the load angle. In this work, a load angle of 20° is chosen initially. The proposed scheme has been tested for a load angle of 10° to verify its performance and reliability of this proposed scheme. Table 3.3 and Table 3.4 show the line impedances when SLGA fault occurs at 75 km from the measuring point at different FR under different conditions for test systems 1 and 2, respectively.

3.7.6. Effect of Non-linear High Impedance Fault

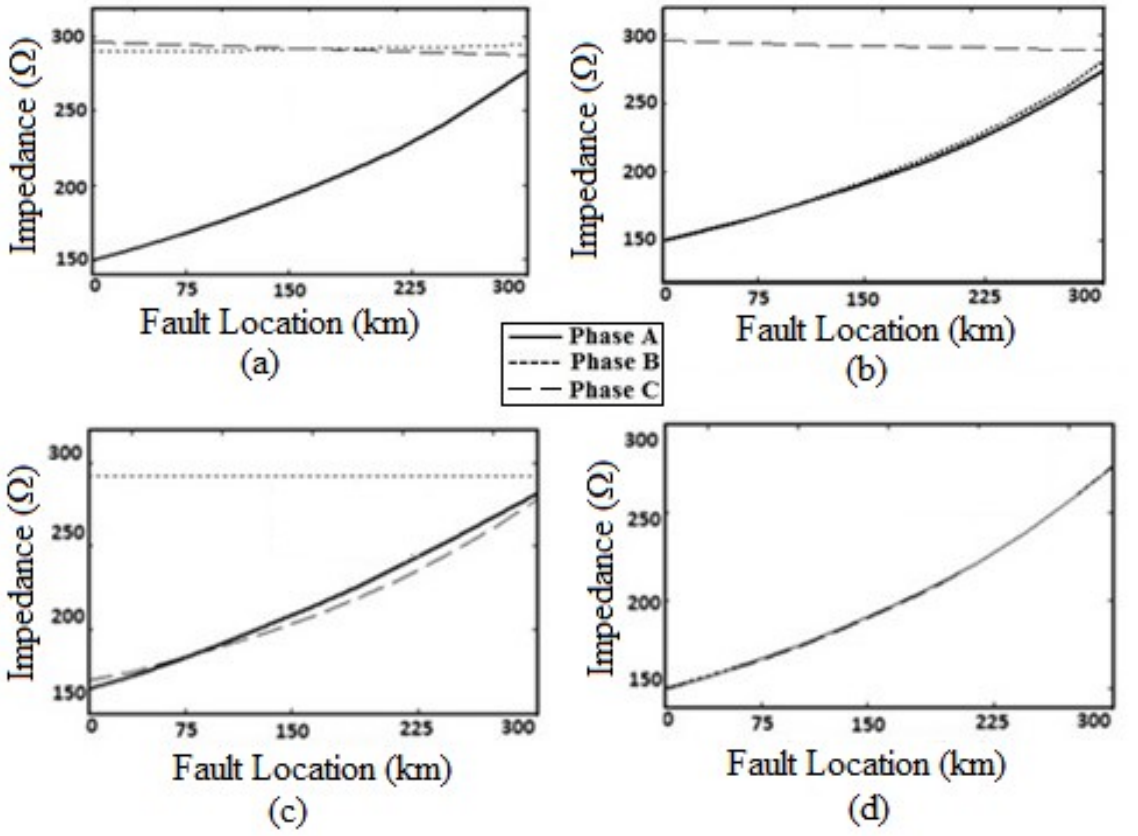

Fig. 3.9. Line impedance vs. location under HIF at Condition 3, 45° FIA for Test System 1 : (a) AG (b) ABG (c) AC (d) ABC

HIF is often associated with electric arc which introduces non-linearity and asymmetry to the fault currents. To account this nature of HIF, a 2-diode HIF model is used for HIF simulation [50]. The 2-diode HIF model comprises of two diodes connected in antiparallel with two DC

voltage sources V_p and V_n. The fault resistances R_p and R_n connected to V_p and V_n respectively, vary from 100 Ω to 1500 Ω, unequal values of these fault resistances allow asymmetrical fault current modeling. Fault condition 1 is created by considering V_P and R_P to be 3588 V and 208 Ω respectively and V_n and R_n as 3847 V and 212 Ω respectively [50]. Fault condition 2 is simulated by considering V_P and V_n to be 6180 V and 6155 V respectively and both the fault resistances to be 245 Ω. When V_P and R_p are 8092 V and 270 Ω respectively and V_n and R_n are 9358 V and 290 Ω respectively then fault condition 3 is considered.

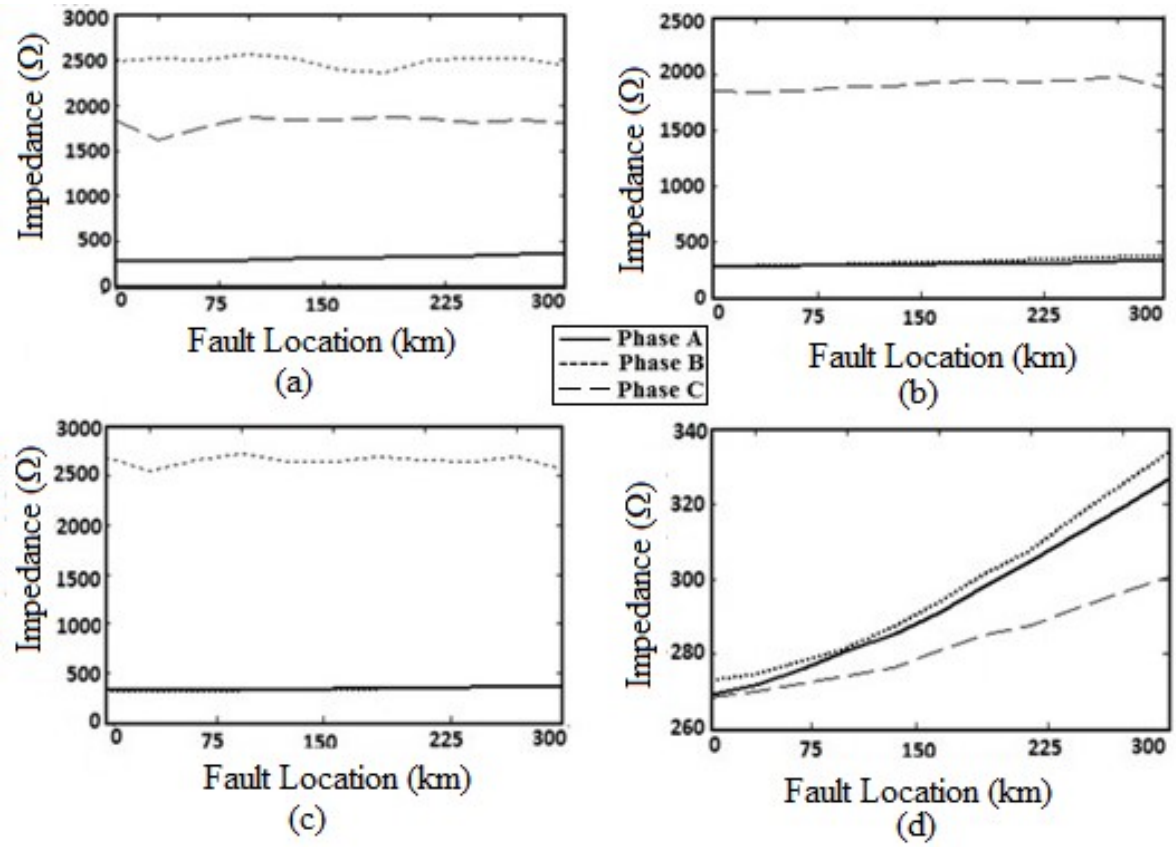

Fig. 3.10. Line impedance vs. location under HIF at Condition 2, 45° FIA for Test System 2: (a) AG (b) ABG (c) AC (d) ABC

HIF detection is very difficult due to its non-linear V-I characteristics which cause different maximum and minimum values during positive and negative half cycle. Fig. 3.9 shows the line impedance *vs*. fault location graph for different types of faults for test system 1 and Fig. 3.10 represents the same for test system 2. Analyzing the results obtained from the simulation of the non-linear HIF model in both system 1 and 2, it is seen that the performance results of the proposed method are accurate under HIF.

3.7.7. Effect of Wind-Speed Variation

In wind farm generation, the main problem is uncontrollable and continually changing wind speed throughout the day. Therefore, when these farms are connected to the power system network, the performance of the distance protection system becomes complicated. The proposed fuzzy-based fault detection and classification scheme is highly efficient to classify accurately all ten types of faults at different FR and FIA with the variation of the speed of wind farms. Wind speed has been varied from 1 m/s to 5 m/s to ascertain the efficacy of the proposed method. Table 3.5 shows the line impedances when SLGA fault occurs at 105 km from the measuring point at FR of 0 Ω and FIA of 0° for two different wind speeds.

Table 3.5. Line impedances for SLGA fault at different wind speed for system 2

	Wind speed 1m/sec			Wind speed 5m/sec		
FR (Ω)	Z_a	Zb	Zc	Za	Zb	Zc
0	34.83	2485.54	1636.64	27.43	2575.72	1638.63
10	34.86	2485.54	1636.64	34.83	2485.55	1636.64
100	123.76	2502.78	1895.81	123.76	2502.79	1895.81
300	345.56	2649.36	1956.89	345.56	2649.37	1956.89

3.7.8. Influence of Sampling Frequency

In transient-based fault detection and classification scheme rate of samples per second plays an important role because sampling frequency of voltage and current signals are used to convert these analog signals into digital form. To evaluate the effect of sampling frequency on the proposed fault classification method, the signals were analyzed at different sampling frequencies: 4 kHz, 51.2 kHz and 89.6 kHz. All ten types of faults at different FIA, FR and at different locations on the transmission line were carried out and it has been seen that the accuracy of the proposed method is same at different sampling frequencies.

3.7.9. Influence of Noise

In real-time system the voltage and current signals are always contaminated with noise. Hence the effect of noise is also taken into consideration. In the power system noise is present throughout the whole recorded signal irrespective of the presence or absence of any disturbance. Noise is represented by signal to noise power ratio (SNR).

$$SNR_{dB} = 20 \log_{10} (A_{signal}/A_{noise}) \quad (3.1)$$

where, A is the root mean square of the signal. In this chapter, the authors have validated the proposed method under two different noise levels: 20 dB SNR and 40 dB SNR. Both the noise levels give accurate and reliable results.

3.7.10. Change of Source Strength

In this work, the performance of the proposed method, under the effect of source strength variation at different FR, FIA and at different fault locations, has been studied. The proposed scheme has accurate performance when the source strength is doubled and made 0.8 times the considered source strength for both test systems. However, for test system 2, the scheme also shows accurate performance when the source strength is halved.

3.7.11. Fault Zone Identification

Once the fault has been detected, the next phase of transmission line protection system is to detect the fault zone. The transmission line in test system 2 is divided into two zones. Bus 1 is placed at a distance of 200 km from bus 2. Any fault between bus 1 and bus 2 is considered as internal fault and the fault between bus 1 and the wind farm is considered as external fault. The fault zone identification technique uses current signals from both buses. One cycle of current signal after fault is considered and the standard deviation of the first-level cAs of both bus currents is calculated. The ratio of the standard deviation (F_Z) of the first-level cAs of current signals of faulty phase at bus 2 to that at bus 1 determines the faulty zone. If the value of *Fz* is greater than 1, then the fault is confirmed as internal fault and if this value is equal to 1, then it is external fault.

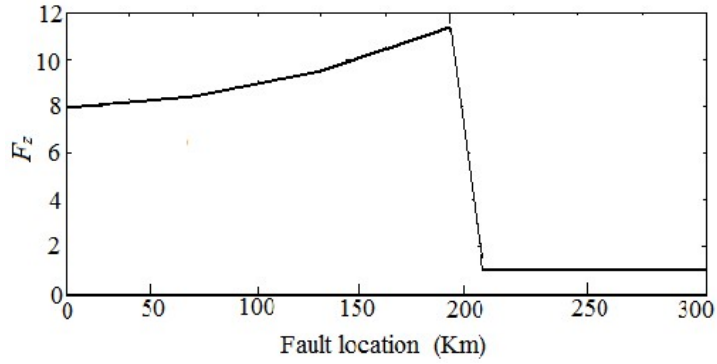

Fig. 3.11. F_Z vs fault location for internal and external fault

$$F_Z = \frac{I_{2sd}}{I_{1sd}} \tag{3.2}$$

where, I_{2sd} and I_{1sd} are the standard deviations of the first-level cAs of current signals of faulty phase at bus 2 and bus 1, respectively.

Fig. 3.11 shows the variation of *Fz* with the variation of fault location during AG fault at fault resistance of 300 Ω and fault inception angle of 0°. It is observed that for internal fault i.e. for fault location between 0 and 200 km, the value of *Fz* of faulty phase i.e. phase A is greater than 1 and the value of *Fz* is equal to 1 when fault location exceeds 200 km i.e. for external fault.

3.8. Comparative Assessment

The proposed method is compared with other methods presented in [118] and [117] since they have considered DG for fault detection in transmission lines. Paper [118] is based on WT and fuzzy logic. Although the fault detection and classification time are within half cycle from the inception of fault, they have considered fault resistance of 1 mΩ only. Moreover, they have used 10 levels of decomposition increasing the computational burden and considered short transmission lines of lengths 5 km and 25 km. S-transform-based fault detection technique has been used in [117]. A much higher sampling frequency of 200 kHz has been used compared to 12.5 kHz in our method. The different dynamic situations, viz. change of pre-fault line loads, CT saturation, change of line parameters or line length, were not considered in these studies. Also, the effect of the presence of noise, change of sampling frequency, and source strength variation were not studied.

Table 3.6 presents a comparative study report of some other techniques with the proposed one. The fault detection and classification algorithm in [11, 13, 1, 8, 69, 67, 49] is based on wavelet transform. A differential power-based algorithm is presented in [100] and [101]. Fundamental and zero sequence components of three-phase currents have been selectedin [41] and [102] and considered integrated moving sum approach for fault classification. The authors in [108] used a finite impulsive response filter along with support vector machine for fault classification. Although it is found that some techniques take only half-cycle compared to one cycle in the proposed algorithm, the proposed algorithm has been verified under diversified conditions most of which have not been considered in other papers. The accuracy and reliability are the main concerns of the proposed method. Moreover, most of the techniques with less operating time consider signals from both ends of the line.

Table 3.6. Proposed scheme compared with other schemes

References Criterion	[11]	[13]	[1]	[8]	[69]	[67]	[49]	[100]	[101	[41]	[102]	[108]	Proposed scheme
Data collection	Both end	One end	Both end	Both end	One end	Both end	One end	Both end	Both end	One end	One end	One end	One end
Fault resistance (Ω)	-	40	-	15	50	15	100	100	600	100	150	-	300
Distributed generation	x	x	x	x	x	x	x	x	x	x	x	x	√
Line length (km)	59.6	100	320	230	320	200	350	300	80	100	300	50	300
Line parameter and length variation	x	x	x	x	x	x	x	x	√	x	x	x	√
Prefault power transfer angle	x	x	x	x	x	x	x	√	√	x	√	x	√
CT saturation	x	x	x	x	x	x	x	√	√	x	√	x	√
Source strength variation	x	x	x	x	x	x	x	√	x	x	√	x	√
Sampling frequency variation	x	x	x	x	x	x	x	x	x	x	x	x	√
Effect of noise	x	x	x	x	x	x	x	x	x	x	x	x	√
Operating time (cycle)	1/2	1/2	1/2	1/4	1	1/2	1	1/2	1	1/2	1/2	1	1
HIF modeling	x	x	x	x	x	x	√	x	x	x	x	x	√

3.9. Conclusion

This chapter presents a new impedance-based fault classification technique in long transmission lines using fuzzy logic. The proposed method uses voltage and current signals from one end of the trnsmission line only. The line impedance calculated from the ratio of the cAs of voltage and current signals has been used as inputs to the fuzzy-based fault classifier. Results obtained from the simulation data analysis ascertain that the proposed scheme is capable of detecting and classifying faults accurately under wide variations in operating conditions. The important features of the proposed scheme are listed below:

- The scheme is reliable in the presence of DG.
- Synchronization of signals from remote terminals is not required as this scheme uses signals at one end of the line.
- The scheme has reduced computational burden as it uses single level wavelet decomposition compared to multi-level decomposition in other wavelet-based techniques.
- The proposed scheme does not use any training-based technique such as artificial neural network and support vector machine; hence computational burden is much less.
- The scheme is not affected by non-linear HIF.
- CT saturation does not affect the fault classification scheme.
- The system is immune to changes in transmission line length and parameters, pre-fault power transfer angle, source strength, wind speed, sampling frequency, and presence of noise in the signals.

CHAPTER 4

ANFIS Based Single Line to Ground Fault Location Estimation for Transmission Lines

4.1. Introduction

The performance of the power system is influenced by faults in the transmission lines. These faults lead to the economic loss of the system and at the same time, it makes the system unstable. Quick detection and identification of faults help in faster maintenance and power supply restoration. It also reduces operating costs and improves power system stability. Therefore, to limit the impact of the fault in power system, accurate fault detection and estimation of fault location are necessary. Nowadays differential relaying protection scheme is commonly used for the transmission line. The authors in [100] dealt with the detection and classification of faults in transmission lines based on the magnitude of differential power, where differential power is the difference between real power and the multiplication of calculated current and voltage phasors. Another scheme has been proposed in [101] to detect and classify faults in UPFC compensated transmission lines, where zero-sequence current at the local end and the apparent power differential feature are used to identify the presence of faults and the type of faults. Mutual impedance between the phases is considered in [93] for protection against SLG and LLG faults. SVM is an important tool in the field of fault classification in transmission lines. In [95] sequence-space-aided SVM has been utilized to detect and classify faults and at the same time, to discriminate the fault condition from the power swing disturbances in SCTL utilizing the absolute component of sequence components of current signals. DT is another imperative technique that is used to classify and detect faults in the transmission line due to its capacity to handle large amounts of data set with minimum processing time. A DT-based method that uses one terminal current and voltage data along with zero-sequence components of current signals for detection and classification of fault in double circuit line during power swing has been proposed in [36]. In the case of high resistance fault, healthy phase current and faulty phase current are in the same order, so the moving sum approach based fault detection and classification scheme is not trustworthy. To overcome this problem a method based on an integrated moving sum has been proposed in [102]. This method can classify faults using the half-cycle period of the current signal. The authors in [104] proposed a new fault location determination method based on the network bus admittance matrix and Wide Area Measurement System (WAMS). In this method, the voltage signal is obtained by WAMS. A technique for short-circuit fault detection, classification, and estimation of fault location is presented in [108]. This technique uses a hybrid framework consisting of a two-stage finite impulse filter and ANN for this purpose. Four SVMs are used for short circuit fault detection and classification purpose while eleven support vector regressions are used for locating faults in short transmission lines.

WT is an efficient tool for fault detection in power systems. Many researchers have used this tool in their work in the field of the transmission line protection. A new approach to classify the faults in an extra high voltage transmission line is described in [18]. In this method, ten separate Rough Membership Neural Network classifiers have been used to classify faults by using the ten time-frequency domain features and three time-domain features of the post-fault quarter cycle current signal. In this process, rough neurons are used as input layers whereas hidden layers use fuzzy neurons to reduce the training time of the neural network. The Maximum wavelet singular value technique for classifying faults in transmission lines has been described in [13]. This method shows highly satisfactory results and does not require any training process. This method utilizes the post-fault quarter cycle current signal data to classify faults. The authors in [8] presented a scheme based on a wavelet-alienation technique to detect, classify and locate faults in transmission lines. The cAs of both end current and voltage signals of a quarter cycle are used in this approach. The authors in [1] presented a transmission line protection scheme combining WT with ANN. This scheme utilizes the synchronized data of voltage and current signals from both terminals of transmission lines. cDs of current signals are used to detect and classify faults whereas cAs of voltage and current signals are used to locate faults by applying ANN. A fault location technique for a smart grid based on Remote Telemetry Unit and computational intelligence techniques has been described in [2]. By using GPS, synchronized current signals are measured from RTUs and features have been extracted by using WT which are fed to the ANN and ANFIS to estimate the fault location. The results of ANFIS justify its superiority over ANN. This system uses both end cAs of a quarter-cycle current and voltage signal. The authors in [12], described a cost-effective real-time implementation scheme that can perform all the protective relaying functions (fault detection, classification, fault zone identification, and fault location) in DCTLs. This technique utilizes the absolute value of the fundamental frequency component of post fault current signals for detection, classification and zone identification of faults in the transmission line. For determining the location of fault, this technique utilizes the standard deviation of wavelet cAs of voltage and current signals. To overcome the problems of malfunctioning of conventional relay near the tap point during high resistance ground fault to identify the faulty section and estimate the fault location in three-terminal transmission line, the authors in [62] presented a technique utilizing the time-synchronized voltage and current signals. SLG fault is the most common type of fault in the transmission line. The authors in [31] described a method based on k-NN to estimate the location of SLG fault in the transmission line utilizing the harmonic spectrum of one end voltage signal. An impedance-based fault location estimation method has been presented in [30] which used modal transformation of voltage and current signals to eliminate the mutual impedance effect.

The most common fault in the transmission line is the SLG fault. Its probability of occurrence is quite high compared to the LLG fault. In this chapter, an attempt is made to propose an impedance-based SLG fault location scheme in transmission lines. This proposed method uses the wavelet cAs of one terminal current and voltage signals to estimate the location of fault in transmission lines. The line impedances of the three phases are the input features of the ANFIS based fault locator. In this chapter, only 1st level wavelet decomposition is considered for calculating the line impedance. Therefore, it reduces the computational burden. Most of the fault location methods use pre-fault and post-fault data or both end data for locating faults, but

this method utilizes only one cycle and one terminal post fault data of voltage and current signals which eliminates the time synchronizing problem. This proposed SLG fault location scheme is independent of fault inception angle and fault resistance.

4.2. Preliminaries

The electric power system is divided into three sections: generation, transmission, and distribution. Electric power is transmitted via transmission lines from power station. The faults occurring in transmission lines cause damages to equipment and interruption to power flows in the network system. To understand the faulty and healthy condition of the transmission line, relevant data extraction from voltage and current signals is very essential. This proposed method uses multi-resolution analysis of voltage and current signals to extract reasonable features, which are then used as input to the ANFIS to estimate the location of the SLG fault.

4.3. Estimation of Fault Location by DWT and ANFIS

In the pre-processing stage voltage and current signals have been acquired from one end of the transmission line. The samples are taken one cycle after the fault inception at a sampling frequency of 12.5 kHz (250 samples/ cycle). The features of these one-cycle fault samples are extracted by using the DWT technique. In this proposed method 1st level MRA decomposition is done to get the 1st level approximation value of voltage and current signals. Db4 mother wavelet shows good performance results in the field of power system fault analysis. Therefore, in this proposed fault location method db4 mother wavelet is used in the MRA process. Here only single level decomposition has been considered to reduce the computational burden.

The proposed method is based on the impedance of the transmission line. 1st level cAs (a_1) of voltage and current signals are used to determine the impedance of the transmission line. Line impedance is the ratio of the summation of the absolute values of cAs (a_1) of the voltage and current signals,

$$Z_x = \frac{\Sigma \left| a_{1V} \right|}{\Sigma \left| a_{1C} \right|} \tag{4.1}$$

where, Z represents the impedance of the line, x is the phase (A, B, C) and V and C denotes the voltage and current respectively.

The proposed ANFIS-based SLG fault location model consists of three inputs (Z_A, Z_B, and Z_C) and one output (fault location L in km). Three types of SLG faults (AG, BG, and CG) have been simulated at different fault inception angles (FIA) (0° to 90°), different FR (0Ω to 50Ω) at different locations on a 300 km transmission line to generate input-output data set for ANFIS

network. For each input variable four linguistic variables with Gaussian MFs are generated such as MF1, MF2, MF3, and MF4, as shown in Fig. 4.1. The ranges of the ANFIS input variables are based on the maximum and minimum values from the database. In this proposed method, the range of the input variables of the ANFIS model is given below:

Input variable1 (Faulty phase) ranging from 3.81to 310.3,
Input variable 2 (Healthy phase 1) ranging from 48.13 to 541.3
Input variable 3 (Healthy phase 2) ranging from 47.41 to 393.4.

The output variable is fault distance (L) in kilometre and it has a constant valued MF as Takagi–Sugeno type ANFIS model is considered for the proposed fault location scheme.

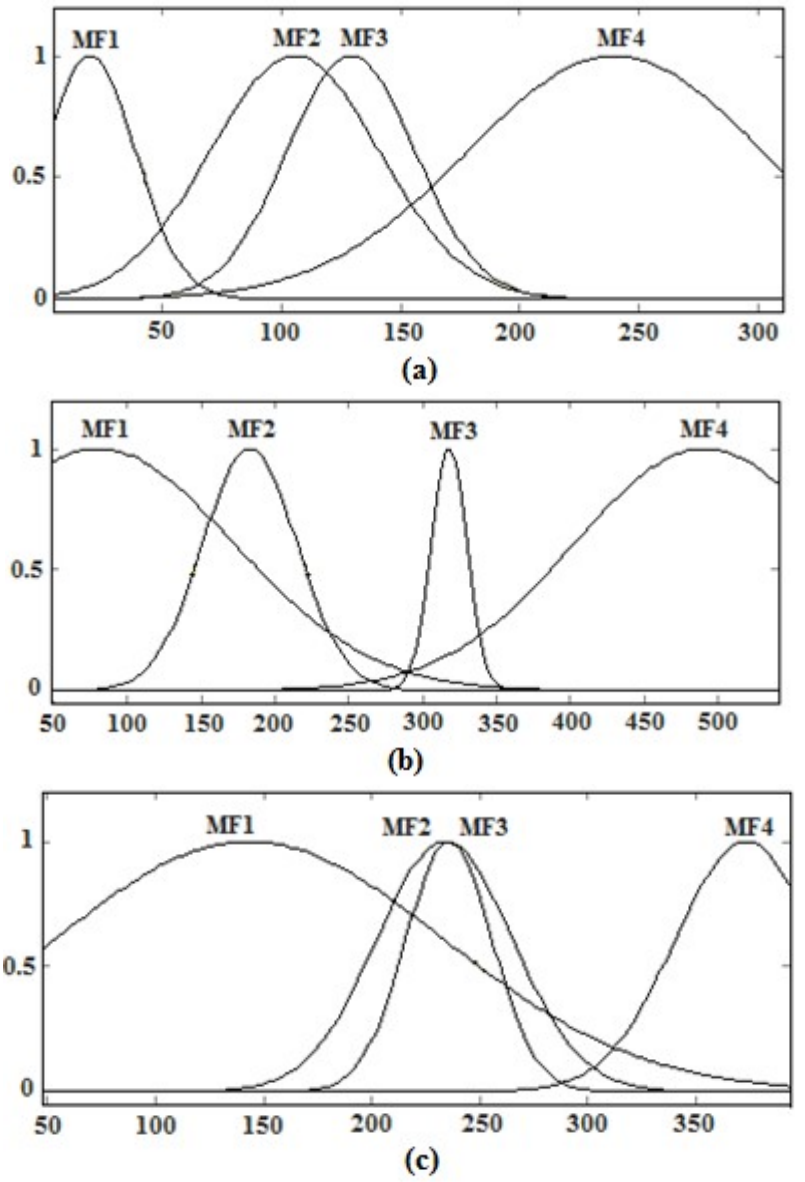

Fig. 4.1. Gaussian MFs used for three inputs
(a) ANFIS Input-1 (Z_A) (b) ANFIS Input-2 (Z_B) (c) ANFIS Input-3 (Z_C)

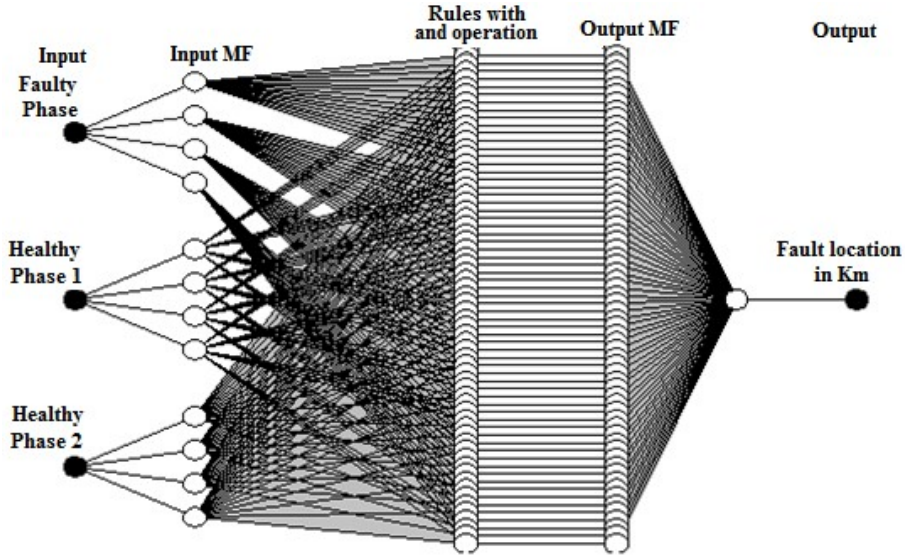

Fig. 4.2. ANFIS Architecture

The hybrid learning algorithm is used as an optimization tool for the effective search. The ANFIS network is trained in the Matlab environment. The trained ANFIS model generated 64 rules from the input-output data set. These 64 rules produce 64 output MFs. These 64 output MFs are connected to a common output node known as fault location (L) in km. Once the ANFIS training is completed, the ANFIS model is ready to estimate the fault location within 300 km of transmission line. Fig. 4.1 shows the four MFs of three inputs, and Fig. 4.2 shows the ANFIS architecture which is developed for the proposed scheme to estimate the fault location.

4.4. Transmission System Model and Specification

To test the feasibility of the proposed method, a 300 km long overhead transmission line connecting two sources (E_1 and E_2) has been considered. The voltage rating of the transmission line is 400 kV and operates at a power frequency of 50 Hz. Fig. 4.3 shows the single line diagram of the power system model. Matlab environment is used to simulate the power system model to generate the input-output data set for estimating the location of SLG fault. Three-phase voltage and current signals are sampled at 12.5 kHz from bus-2. The internal impedance of both the sources is 0.5333 + j 5.333Ω, whereas the load angle of the source connected to bus-1 (E_1) is 0° and the source connected to bus-2 (E_2) is 20°. Table 4.1 shows the line parameters considered in this study.

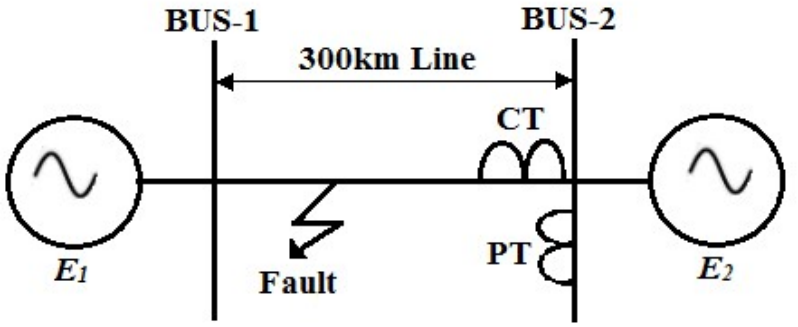

Fig. 4.3. Single line diagram of the power system model

Table 4.1. Transmission line parameter

Transmission line parameters	Value
Positive-sequence impedance (Z_1)	4.0736+j91.04 Ω
Zero-sequence impedance (Z_0)	123.648+j41.48 Ω
Positive-sequence capacitance (C_1)	40.77 nF/km
Zero-sequence capacitance (C_0)	2.48 nF/km

4.5. Simulation Results and Performance of the Proposed Method

To test the validity and accuracy of the proposed SLG fault location method all types of SLG faults are simulated with varying FR, FIA and at different fault locations at an interval of 10 km on a 300 km transmission line. The block diagram of the proposed fault location method is shown in Fig. 4.4.

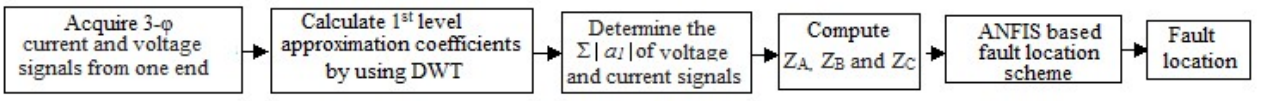

Fig. 4.4. Block diagram of proposed SLG fault location scheme

Three-phase remote end current and voltage signals are decomposed with db4 mother wavelet and applying Eq. (4.1) line impedance is calculated. Three line impedances for three different phases are fed as the input vector to the ANFIS to determine the fault location. As one end data is sufficient to estimate the location of faults, the computational burden is less and the synchronization problem can be neglected. In this ANFIS architecture, to get the best set of

output 100 epochs and 0.01 tolerance level with hybrid structure have been chosen. The % error of the estimated fault location determines the performance of the proposed method and this % error is expressed as

$$\%\ Error = \frac{\left(Actual\ \ fault\ location - Estimated\ \ fault\ location\right)}{Total\ length\ of\ \ the\ transmissi\ on\ line} \times 100 \tag{4.2}$$

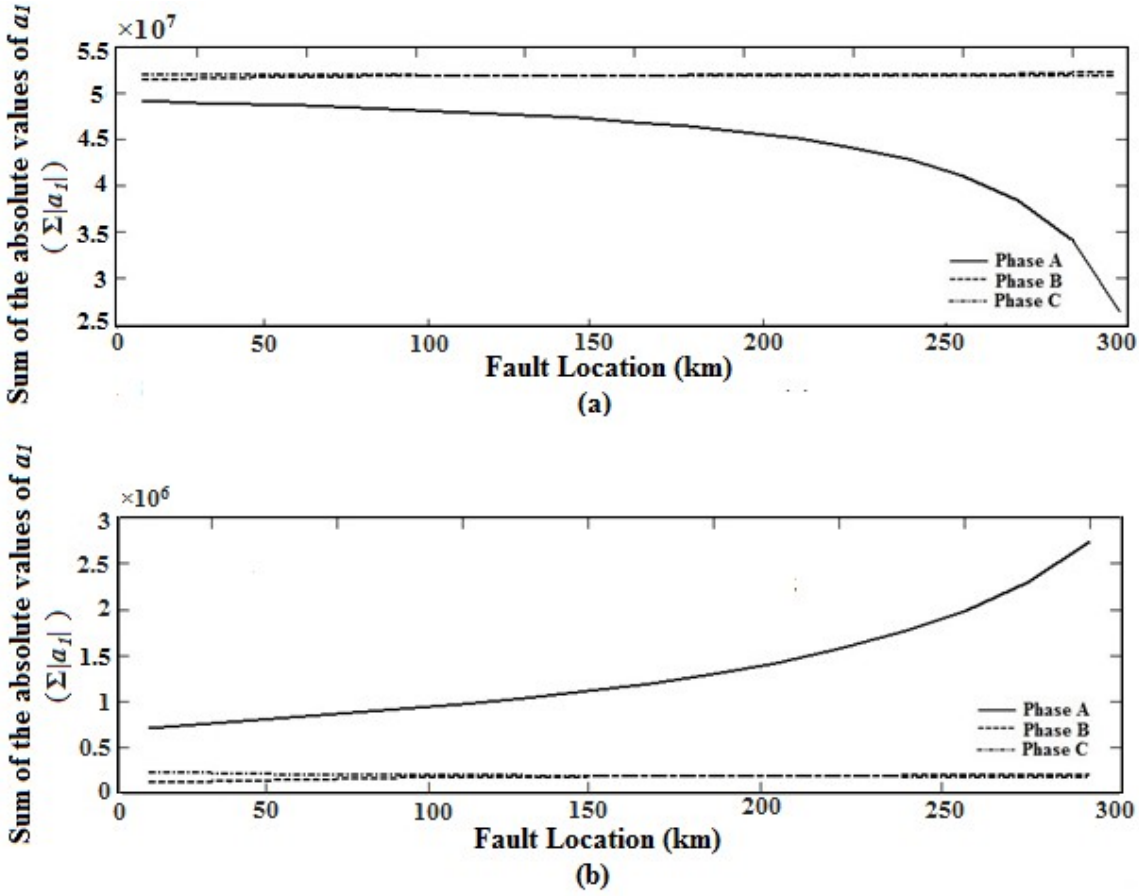

Fig. 4.5. Variation of $\sum |A_1|$ for different fault location during AG fault with FR 0Ω and FIA 0°

(a) Three phase voltage signals (b) Three phase current signals

Fig. 4.5 illustrates the variation of summation of the absolute values of a_1 of the three-phase voltage and current signals for different locations of AG fault with FR = 0 Ω and FIA= 0°. The summation of the absolute values of a_1 ($\sum| a_1 |$) is used to determine the line impedances. These line impedances are the inputs to the ANFIS-based fault locator. From Fig. 4.5 it is observed that for fault near the measuring point, $\sum| a_1 |$ of the faulty phase voltage signal is low in magnitude and gradually increases with the fault distance from the measuring point. In case of the faulty phase current signal the value of $\sum| a_1 |$ is large near the measuring point and decreases when the fault occurs far away from the measuring point. The value of $\sum| a_1 |$ of healthy phases remain unchanged throughout the transmission line during fault condition both for voltage and

Table 4. 2. % Error for SLG fault at different FR and FIA

Fault Type	FR (Ω)	FIA (°)	Fault location (km)	ANFIS location (km)	% error
AG	50	45	15	14.1	0.3
	10	0	45	44.4	0.2
	5	75	190	189	0.33
	0	90	270	268.5	0.5
BG	0	0	15	15	0
	10	45	105	106.8	0.6
	50	90	240	240	0
	15	75	280	278.4	0.53
CG	0	90	30	28.5	0.5
	15	75	130	129	0.33
	10	45	210	210.3	0.1
	50	0	285	285	0

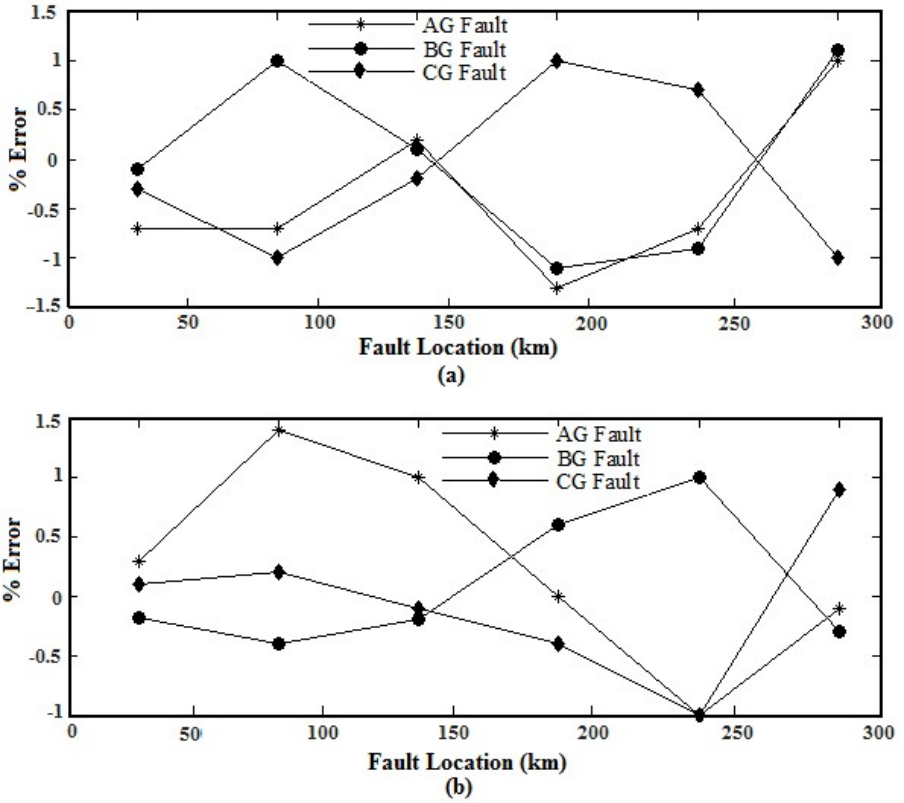

Fig. 4. 6. % Error for different fault location
(a) SLG fault at FR 0 Ω and FIA 0° (b) SLG fault at FR 50 Ω and FIA 90°

current signals. Therefore, from Fig. 4.5 it is concluded that, the impedance of the faulty phase increases when the fault distance increases from the measuring point and at the same time, line impedances of the healthy phases remain invariable throughout the line under the fault conditions. Table 4.2 shows the errors obtained for SLG fault at different locations with varying FR and FIA.

In this study, the authors have been considered different FR varying from 0 Ω to 50 Ω and FIA varying from 0° to 90°. Fig. 4.6 depicts the % error for different locations at varying FR and FIA. It can be seen that the ANFIS based proposed method gives good results and most of the cases have error maximum up to 1.5%.

4.6. Conclusion

An SLG fault location scheme based on WT and ANFIS has been proposed in this chapter. One-cycle samples of three-phase voltage and current signals after the occurrence of the fault are used to estimate the location of the fault. In this proposed method 1st level cAs are used to determine the line impedance which is the input of the ANFIS structure. The computational burden is reduced as single level decomposition is used. This SLG fault location method is unaffected by variations of FR and FIA. Unlike other fault location schemes, this method does not require any pre-fault data and as only one terminal data is sufficient to estimate the fault location, this method is unaffected by the time synchronization problem. Extensive simulation has been performed at different fault conditions to evaluate the performance of the proposed method and it has been observed that the ANFIS-based fault locator can estimate the fault location accurately for single line to ground fault in transmission lines.

CHAPTER 5

Fault Detection and Classification Scheme for Smart Grids considering High Impedance Evolving and Cross Country Faults

5.1. Introduction

5.1.1. Motivation

In power system network the transmission lines are the most vulnerable component and are frequently subjected to faults. For quick restoration of power supply, quick detection of faults in transmission lines along with faulty phase identification is of prime importance in power system protection schemes. The commonly used transmission line protection schemes are conventional distance, differential and over current protection schemes. Also, many protection schemes are based on a combination of sequence component and transform based methods. The computational complexity of sequence component-based protection schemes is low compared to the transform-based protection schemes. On the other hand, sequence component-based protection techniques may lead to improper functioning of relays due to the change in impedance in the fault path. In long transmission lines, improper operation of differential relay may occur due to the line charging current. Also, some faults such as evolving and cross country faults are more complex and they deteriorate the performance of the distance protection schemes. Hence, it is indispensable to develop a fast and reliable protection scheme under these challenging conditions.

5.1.2. Literature Survey

Rapid advancements of economic and technological growth in different sectors have imposed high requirement of energy. Expansion of power system networks is necessary to address the increasing power demand. The scarcity of land and many other environmental and socio-economic problems create difficulties for expanding the electricity sectors and power networks. Advancements in technology are trying to defeat all the issues related to increasing power demand. Transform-based techniques have been comprehensively implemented in transmission line fault analysis. Nowadays, WT has been successfully applied in transmission line protection schemes. WT can correctly analyze the transient frequency components of faulty signals. A wavelet-alienation-based protection technique for a two-terminal transmission lines has been developed in [9]. In this work, cAs of current samples have been utilized for detection and classification of faults. Also, cAs of both voltage and current samples have been fed to ANN

to determine the location of fault. However, utilization of ANN increases the computational burden of this technique. A new fault analysis technique using WT and ANFIS for a SCTL has been presented in [69]. The main drawback of this technique is that it uses three ANFIS for fault identification, classification, and determination of fault position which increases the computational time and also computational burden. The authors in [67] have described a WT-based fault classification and fault location estimation technique for DCTL system. This method is reliable when one line of the system is compensated with UPFC. But, higher values of fault resistance have not been considered in this technique. A protection scheme using PSD has been discussed in [26]. For fault detection and classification, DWT has been used to derive transient information from faulted current signals to evaluate the PSD value in the time and frequency domain. A fault classification technique based on WT and ANFIS for a neutral non-effectively grounded distribution system has been described in [19]. This scheme utilized current and zero-sequence voltage signals for classifying the faults. This scheme shows good results in the neutral compensated grounding DS and also at high resistance. The drawback of this technique is that it uses three different ANFIS for fault classification purpose.

Mal-operation of protective relays may occur during HIFs as fault currents are in the range of rated value during HIF. To overcome this problem, methods such as evidential-reasoning-based fault detection scheme [52], DWT and ANN-based algorithm [51] and DWT-based algorithm [61] have been used in DS to detect and classify HIFs. HIF detection and faulted feeder identification in DSs have been presented in [59] utilizing the transient features of zero-sequence current and voltage signals in the wavelet domain. This scheme responds during HIFs and does not respond during other switching operations such as capacitor bank switching as well as energizing and de-energizing of feeders. However, this algorithm has been tested only under medium voltage DSs. An algorithm has been reported in [58], to locate the faulted section in 11 kV underground DS. This proposed algorithm utilizes the difference between the average of the absolute coefficients of voltage signals and the reference database. The proposed algorithm utilizes the historical database, which increases the computational burden.

Arcing detection is another challenging task in power system network. In [57], a DWT-based scheme has been proposed to detect the arc faults in low voltage residential networks. This study reveals that the performance of arc fault detection is significantly affected by the sampling frequency, decomposition levels, and conditions of load. The advantage of the scheme presented in [49] for HIF identification in transmission lines is that only one end current signal is sufficient to identify the LIFs and HIFs which reduce the cost of protecting devices. The main drawback of this algorithm is that this algorithm classifies only LIFs and not HIFs. A differential relaying scheme combined with WT and DFT has been introduced in [121] for tapped transmission lines integrated with UPFC and wind farms. But this algorithm did not address the effect of CT saturation though the proposed scheme utilized current signals.

The main drawback of WT is that wavelet and scale coefficients do not exhibit any physical characteristics. To overcome this difficulty a new scheme has been developed in [53] where the conversion of wavelet scale coefficients to RMS values has been done directly by computing the signal energies. Hence, a proper distribution pattern of RMS value (voltage and

current signals) has been obtained from wavelet and scale coefficients. The authors in [60] presented a modified FFT-based technique to detect and distinguish the HIFs and other switching events considering linear and nonlinear loads. In [37], DFT has been utilized to identify and classify faults in transmission lines. Positive-sequence components of the voltage sample and the FIS have been used to determine the position of faults. Eight separate FISs have been utilized for estimating the fault location. Hence, huge storage space is required for this purpose. Nam et al. [33] proposed an analytical method to determine the fundamental frequency components of faulty signals. This method only investigated SLG fault. The DFT-based phasor estimation technique has been described in [28]. The main focus of this approach is to nullify the adverse effect of ddc offset of fault currents. This approach shows good results during the severe distortion of signals and also in the presence of the subsynchronous frequency component. However, the main drawback of this algorithm is that it suffers from heavy logarithmic computations which increase the computational burden. Hence, to decrease the computational burden and increase the speed of convergence, Jafarpisheh et al. proposed a DFT-based phasor estimation scheme in [34]. This algorithm eliminated the error due to ddc in the fundamental component. Another fault position estimation method has been developed in [82] using FDOST and Gaussian process regression for UPFC compensated long transmission line. Here Gaussian process regression has been used to reduce the dimension of the features of voltage signal extracted by FDOST. A digital relaying scheme for hybrid transmission line protection scheme has been designed in [22]. This technique is based on FDOST and SVM. Performance of this scheme under dynamic situations such as swing, load fluctuation and source strength has not been discussed.

Due to the low computational burden, sequence-based algorithms nowadays are extensively applied in the field of transmission line fault analysis. Inverse components of voltage and current are the two main problems in the directional relaying technique for SCTLs. Authors in [83] proposed a positive-sequence-based technique to overcome these two problems. This proposed approach uses the phase change in positive-sequence current and magnitude change in positive-sequence voltage to eliminate current and voltage inversion problems. In SCTLs, malfunction of distance relay is caused by the change in positive-sequence impedance in the fault path. In [93] a novel backup distance protection technique has been reported to overcome this difficulty. The main disadvantage of this protection scheme is that this scheme is applicable for ground faults only. Improper functioning of protective elements also occurs due to the power swing in the power network. Authors in [95] proposed a scheme based on sequence-spaced-aided SVM for SCTL to differentiate between power swing and fault situations in the power network. Though the accuracy of this scheme is high, this scheme has not considered varying source strength. In [85], positive-sequence complex power has been utilized to separate the internal faults from the external ones. To find the location of faults, authors used both the sequence components (positive and negative) of current and voltage signals, therefore, symmetrical faults cannot be detected by this technique. Using positive-sequence current and voltage from both terminals of long transmission line, authors in [92] proposed a protection scheme for power networks. This protection scheme addresses all the dynamic conditions, but classification and fault location accuracy under multi-location fault conditions have not been discussed. A power differential backup protection theory for UPFC compensated transmission

line has been reported in [101]. This algorithm can distinguish the internal faults from other dynamic situations. However, the impact of source impedance fluctuation has not been examined in this study. In high voltage transmission line, CCVTs are used to measure the system voltage. Improper relaying operation occurs due to the transient characteristics of CCVT. In [35] a study has been done using full and half-cycle DFT to observe the consequences of CCVT on power system protection and fault position estimation techniques.

After a thorough study of different protection schemes, it has been seen that with the continuous development of power system networks and also due to their complex nature, conventional protection systems are not capable of detecting cross-country faults, complex cross-country faults, and evolving faults. Therefore, to supply uninterrupted power to the consumers, reliable and high-speed protection for transmission line is an utmost requirement, which reduces maintenance time as well as improves the system stability and reliability. Very few researches have been focused on these critical types of faults. MODWT has been used to identify and classify faults in transmission lines in cross-country and evolving fault situations in [109]. In [110], a CWT-based method has been developed to identify the fault zone and faulty phase/s during cross-country faults in the transmission line in the presence of CT saturation. A protection technique based on DWT and ANN has been presented to estimate the location of shunt faults along with evolving and cross-country faults, but without classifying the faults in [111]. A first zone distance relaying algorithm for cross-country grounded faults has been described in [112] and the algorithm for cross-country non-grounded faults has been described in [113]. Multi-location fault position estimation for series compensated DCTLs has been described in [71]. The combination of WT and ANN has been used in this fault position estimation scheme. The authors in [114] described a novel transmission line and distribution line protection technique based on WPT and ELM for high impedance evolving faults and cross-country faults. A fault position determination scheme for multi-terminal multiple-circuit transmission lines has been introduced in [115]. The proposed method is based on the Taylor series expansion of distributed-parameter transmission line model. DFT has been widely used to estimate the fundamental phasor of fault signals in transmission line [29].

5.1.3. Contributions

Due to the environmental and electric stresses, transmission lines not only experience single fault at a particular location, but at the same time also experience cross-country, complex cross-country, and evolving faults. Since cross-country and evolving faults are complex types of faults, they have a significant impact on transmission line protection systems. In the event of an evolving fault, a fault first occurs in a particular phase of the transmission line. Another fault occurs at the same location in a different phase on the transmission line, after a short delay. Hence, in evolving fault, SLG fault is converted to LLG fault after a short time delay. According to the fault inception time, evolving faults can be considered to be consisted of two types of faults; primary fault and secondary fault. This dual nature may confuse the protection scheme about the fault type and faulty phase.

In this chapter, another type of fault, known as cross-country fault, has also been addressed. Cross-country faults are similar to evolving faults but they are more alarming. The difference between them is that cross-country fault occurs at two distinct positions at the same time or at a different time, usually at a time interval of less than one cycle [112]. Due to this complex nature, faulty phase identification is a very complicated job if fault occurs in different phases. Complex cross-country fault is another type of complex fault that has also been addressed in this chapter. In complex cross-country fault, one fault occurs in the internal zone or the protection zone and the second fault occurs outside the protection zone.

This chapter addresses a new threshold-based fault detection along with fault classification and faulty phase/s identification algorithm for power networks considering cross-country, evolving, and complex cross-country LIFs and HIFs. The fundamental components of faulted signals are needed to formulate the line admittance-based proposed algorithm. For this algorithm, three-phase synchronized voltage and current samples are acquired from both the transmision line terminals. The merit of this proposed algorithm is that a single threshold-based value of fault index (*FI*) is sufficient to distinguish the faults in the main protection zone from external fault zone and at the same time it can detect the faulty phase/s. To ensure its efficacy, the proposed algorithm has been tested under diversified fault situations. This algorithm is robust and efficient as it accurately classifies and identifies the faults in the protection zone under different dynamic situations like power swing, week-infeed, load angle and source strength variation, and in the presence of series compensator.

5.2. Mathematical Modeling of Admittance based Protection Scheme

This section describes the mathematical modelling of the proposed technique. This algorithm is used to identify the faults in the protective zone and distinguish the internal fault from the external ones. Moreover, the designed algorithm has the capability to classify the faults and to find the faulty phase/s during evolving and cross-country faults. To compute the line admittance, the proposed algorithm uses synchronized voltage and current samples of all the phases from both sides of transmission line. The fundamental component of the signals is extracted by applying DFT.

5.2.1. Fault Index Formulation under No-Fault Condition

A threshold value (FI_{Th}) of *FI* has been derived to segregate the fault in the protective zone from no-fault condition. Fig. 5.1 depicts the equivalent network configuration when there is no-fault in the protective zone.

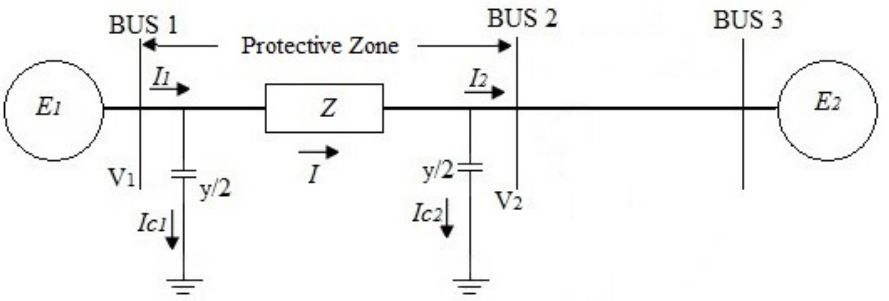

Fig. 5.1. Transmission line model under no-fault condition

Applying Kirchhoff's current law (KCL) at bus 1, we get

$$\tilde{I}_{1m} = \tilde{I}_{m} + \tilde{I}_{c1m} \tag{5.1}$$

$$\tilde{I}_{m} = \frac{\tilde{V}_{1m} - \tilde{V}_{2m}}{Z} \tag{5.2}$$

and

$$\tilde{I}_{c1m} = \left(\tilde{V}_{1m}\right) \cdot \left(\frac{y}{2}\right) \tag{5.3}$$

where, m represents the phase. Hence, the line admittance (Y_{1m}) at bus 1 can be calculated as

$$Y_{1m} = \frac{\tilde{I}_{1m}}{\tilde{V}_{1m}} = \left(\frac{1}{Z} + \frac{y}{2}\right) - \left(\frac{1}{Z}\right) \cdot \left(\frac{\tilde{V}_{2m}}{\tilde{V}_{1m}}\right) \tag{5.4}$$

Applying KCL at bus 2, we get

$$\tilde{I}_{2m} = \tilde{I}_{m} - \tilde{I}_{c2m} \tag{5.5}$$

and

$$\tilde{I}_{cm} = \left(\tilde{V}_{2m}\right) \cdot \left(\frac{y}{2}\right) \tag{5.6}$$

Hence, the bus 2 line admittance (Y_{2m}) can be calculated as

$$Y_{2m} = \frac{\tilde{I}_{2m}}{\tilde{V}_{2m}} = \left(\frac{1}{Z}\right) \cdot \left(\frac{\tilde{V}_{1m}}{\tilde{V}_{2m}}\right) - \left(\frac{1}{Z} + \frac{y}{2}\right) \tag{5.7}$$

From Eq. (5.4) and (5.7) we get,

$$Y_{1m}+Y_{2m}=\left(\frac{1}{Z}\right)\cdot\left(\frac{\tilde{V}_{1m}}{\tilde{V}_{2m}}-\frac{\tilde{V}_{2m}}{\tilde{V}_{1m}}\right) \tag{5.8}$$

$$Y_{1m}-Y_{2m}=2\cdot\left(\frac{1}{Z}+\frac{y}{2}\right)-\left(\frac{1}{Z}\right)\cdot\left(\frac{\tilde{V}_{1m}}{\tilde{V}_{2m}}+\frac{\tilde{V}_{2m}}{\tilde{V}_{1m}}\right) \tag{5.9}$$

Solving Eq. (5.8) and (5.9) Fault index, *FI* can be formulated as

$$F_{1m}=\frac{|Y_{1m}-Y_{2m}|}{|Y_{1m}+Y_{2m}|}=\frac{\left|2\cdot\left(1+k-\left(\frac{\tilde{V}_{1m}}{\tilde{V}_{2m}}+\frac{\tilde{V}_{2m}}{\tilde{V}_{1m}}\right)\right)\right|}{\left|\left(\frac{\tilde{V}_{1m}}{\tilde{V}_{2m}}-\frac{\tilde{V}_{2m}}{\tilde{V}_{1m}}\right)\right|} \tag{5.10}$$

where, $k=\frac{yZ}{2}$

5.2.2. Fault Index Formulation under Fault Condition

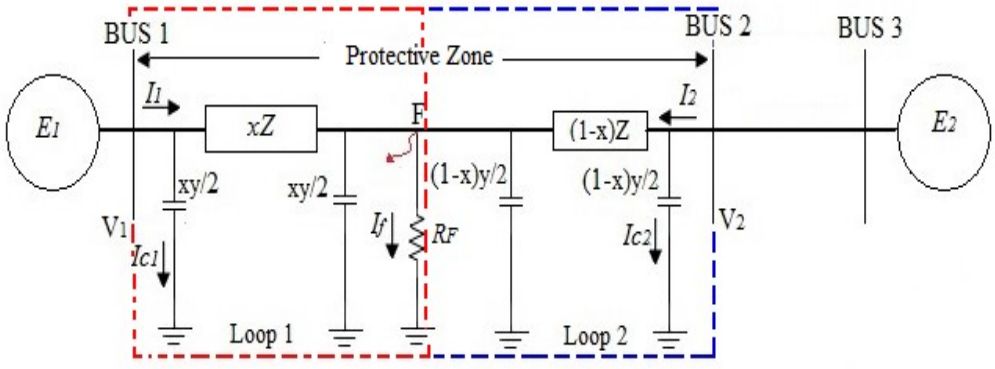

Fig. 5.2. Transmission line model for fault in the Protective Zone

Fig. 5.2 shows the equivalent network configuration during fault in the protective zone, when fault occurs between bus 1 and bus 2.

Applying Kirchhoff's voltage law (KVL) in Loop 1, we get

$$\tilde{V}_{1m}-(xZ)\cdot(\tilde{I}_{1m}-\tilde{I}_{c1m})-(\tilde{I}_{fm})\cdot(R_F)=0 \tag{5.11}$$

$$(1+x^2k)\cdot(\tilde{V}_{1m})-(xZ)\cdot(\tilde{I}_{1m})-(\tilde{I}_{fm})\cdot(R_F)=0 \tag{5.12}$$

From Eq. (5.12)

$$Y_{1m} = \frac{\tilde{I}_{1m}}{\tilde{V}_{1m}} = \left(\frac{1}{xZ}\right)\cdot\left(1 + x^2 k\right) - \left(\frac{1}{xZ}\right)\cdot\left(\frac{\tilde{I}_{fm} R_F}{\tilde{V}_{1m}}\right) \tag{5.13}$$

Following the same procedure in loop 2, we get,

$$\tilde{V}_{2m} - \left(\overline{1-x}\right)Z\cdot\left(\tilde{I}_{2m} - \tilde{I}_{c2m}\right) - \left(\tilde{I}_{fm}\right)\cdot\left(R_F\right) = 0 \tag{5.14}$$

$$1 + (1-x)^2 k\cdot\left(\tilde{V}_{2m}\right) - \overline{(1-x)}Z\cdot\left(\tilde{I}_{2m}\right) - \left(\tilde{I}_{fm}\right)\cdot\left(R_F\right) = 0 \tag{5.15}$$

From Eq. (5.15) we get

$$Y_{2m} = \frac{\tilde{I}_{2m}}{\tilde{V}_{2m}} = \left(\frac{1}{\overline{(1-x)}Z}\right)\cdot\overline{1 + (1-x)^2 k} - \left(\frac{1}{\overline{(1-x)}Z}\right)\cdot\left(\frac{\tilde{I}_f R_F}{\tilde{V}_{2m}}\right) \tag{5.16}$$

Solving Eq. (5.13) and Eq. (5.16) we get

$$\text{Fault index } FI_m = \frac{\left|Y_{1m} - Y_{2m}\right|}{\left|Y_{1m} + Y_{2m}\right|} \tag{5.17}$$

From the above discussion and from Eq. (5.10) and Eq. (5.17), it is noticed that during fault in the protective zone, the value of FI_m of faulty phase/s is larger than no-fault condition. Therefore, to detect the fault in the protective zone, a threshold value of FI has been considered.

5.3. System Description

The test system depicted in Fig. 5.3 has been designed in the MATLAB/ Simulink platform to apply the proposed algorithm. Table 5.1 summarises the parameters of this test system. The system comprises of a 400 kV, 50 Hz, doubly-fed 300 km long transmission line. Faults have been simulated in the 200 km line between bus 1 and bus 2 and are considered as internal faults. External faults are created in the 100 km line between bus 2 and bus 3. The voltage and current signals are collected from both ends of the 200 km transmission line and the internal fault in that line along with the faulty phase has been detected. The simulation is carried out with 12.5 kHz of sampling frequency.

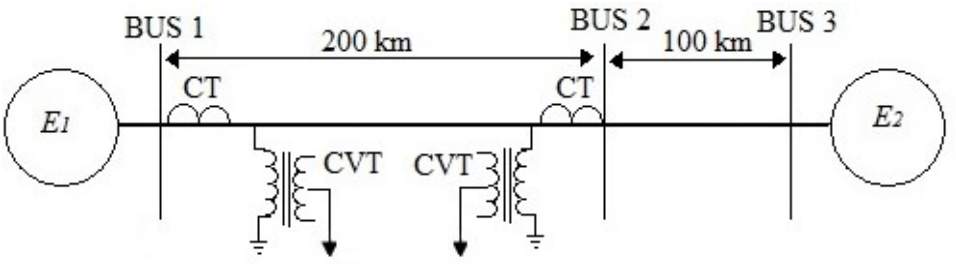

Fig. 5.3. Test system

Table 5.1. Source and Transmission line parameters

	Operating parameters	Values
Source	-	400 kV, 50 Hz, 1000 MVA
Trasmission line	Positive-sequence impedance	0.02979 + j 0.3318 Ω/km
	Zero-sequence impedance	0.16192 + j 0.6113 Ω/km
	Positive-sequence capacitance	12.74 nF/km
	Zero-sequence capacitance	7.75 nF/km

5.4. Simulation Results and Discussion

In this study, segregation of internal fault, no-fault and external fault has been performed using the appropriate threshold value (FI_{Th}). If the *FI* of any phase exceeds FI_{Th}, then it indicates fault in the protective zone. After the detection of fault, identification of faulty phase/s is carried out using the same FI_{Th}. For faulty phase, the *FI* value is above FI_{Th}, while the *FI* value of the healthy phase is significantly lower than the FI_{Th}. Therefore, it is worth mentioning here that, the selection of the accurate threshold value (FI_{Th}) is quite important to segregate the faults in the main protective zone from no-fault condition and also for fault classification. A detailed description of FI_{Th} selection has been illustrated in the next sub-section.

5.4.1. Selection of Threshold Value of Fault Index (FI_{Th})

To compute the *FI*, synchronized data of voltage and current samples have been obtained from bus 1 and bus 2. From Eq. (5.10) and Eq. (5.17) it is seen that the *FI* value of faulty phase/s is higher when fault occurs in the protective zone compared to the no-fault condition. Under no-fault condition, *FI* value is 0.47 which is obtained from Eq. (5.10). In the proposed algorithm authors have selected an appropriate threshold value FI_{Th}, which is two times the *FI* value at no-fault condition and it is set as 0.94. Extensive simulations have been performed to test the reliability of the threshold value FI_{Th}. The following criterion has been used to distinguish the fault from no-fault condition:

$$\begin{cases} If\ FI\ of\ any\ Phase > FI_{Th,}\ then\ fault\ in\ the\ protective\ zone \\ If\ FI\ of all\ phases < FI_{Th,} then\ no-fault\ in\ the\ protective\ zone \end{cases}$$

It has been observed that *FI* values under some dynamic and stressed situations other than fault in the protective zone and under some external fault conditions, exceed the calculated *FI*

under normal condition, but always remain below twice the calculated *FI*. The *FI* value is always above twice the no-fault *FI*, when fault occurs in the protective zone.

5.4.2. Fault Classification using Proposed Algorithm

The criterion of faulty phase identification using line admittance is based on the *FI* value. During fault, the faulty phase admittance is much higher compared to the healthy one. Moreover, under faulty condition, line admittances of all three phases are different from the no-fault condition. Hence, the faulty phase can be identified by comparing the *FI* value to FI_{Th}. Faulty phase *FI* value is always higher than $FI_{Th,,}$ *w*hereas, the *FI* value of the healthy phase is lower than FI_{Th}.

Table 5.2 presents some of the fault classification results obtained from simulation. As observed in Table 5.2, the *FI* value of one phase (faulty phase) is greater than the FI_{Th} for SLG fault. In case of LL and LLG fault, two phases have higher values of *FI* compared to the FI_{Th}. During LLL fault all three phases have fault indices higher than FI_{Th}. As a result, the fault classification algorithm based on line admittance correctly distinguishes all types of faults in the transmission line.

Table 5.2. **Classification results of internal faults**

Fault Location	Types of faults		FR (Ω)	FIA (°)	FI_{Th}	FI_A	FI_B	FI_C
10	SLGA		0	0		**1.11**	0.38	0.46
50	SLGB	S	50	90		0.50	**3.73**	0.42
100	SLGA	L	0	0		**17.71**	0.42	0.37
150	SLGA	G	300	45		**1.81**	0.47	0.47
190	SLGC		100	45		0.47	0.47	**11.19**
10	LLGAB	L	100	45		**1.9**	**1.52**	0.45
100	LLGBC	L	0	0		0.42	**20.96**	**13.62**
150	LLGAC	G	50	45	**0.94**	**22.17**	0.46	**12.67**
190	LLGAB		300	90		**1.75**	**2.17**	0.46
10	LLAC		50	45		**6.01**	0.46	**1.19**
50	LLAB	L	0	0		**2.57**	**14.16**	0.46
150	LLAB	L	100	45		**2.82**	**3.11**	0.48
190	LLBC		300	90		0.46	**1.84**	**1.65**
10	ABC	L	50	45		**1.9**	**1.64**	**1.92**
100	ABC	L	0	0		**58.72**	**20.01**	**14.64**
150	ABC	L	100	45		**5.34**	**4.01**	**4.88**
190	ABC		300	45		**2.06**	**1.92**	**2.13**

5.4.3. Evaluation of Proposed Algorithm

To assess the reliability of this algorithm, rigorous simulation has been performed under different dynamic conditions such as variation of FR (0-300 Ω), FIA (0-90°), types of fault (cross-country fault, evolving fault, and normal shunt faults), fault location (at an interval of 10 km), source strength (strong/ weak), load angle and also at different compensation levels (30%, 50%, and 70%).

5.4.3.1. Effect of Evolving and Cross-Country Faults

The applicability and reliability of the proposed algorithm have been verified by simulating the evolving and cross-country faults under different conditions. To study the evolving faults, SLGA fault has been simulated at 10 km from bus 1 at t = 0.02s and then a second fault has been generated at t = 0.025s in phase B (SLGB) at the same location. To investigate the effect of cross-country fault, SLGA fault has been generated at 10 km from bus 1 at t = 0.02s, and then the second fault has been generated at t = 0.025s in phase B (SLGB) at 50 km from bus 1. Figs. 5.4(a) and (b) show evolving faults, whereas Fig. 5.4(c) and (d) depict the cross-country faults with FR = 0 Ω and 300 Ω respectively. As seen in Fig. 5.4, *FI* of phase A crosses FI_{Th} first, and then, after a short interval of time, *FI* of phase B crosses FI_{Th}. As a result, it is clear that the proposed threshold-based algorithm can accurately detect faults and identify the faulty phases under cross-country and evolving faults.

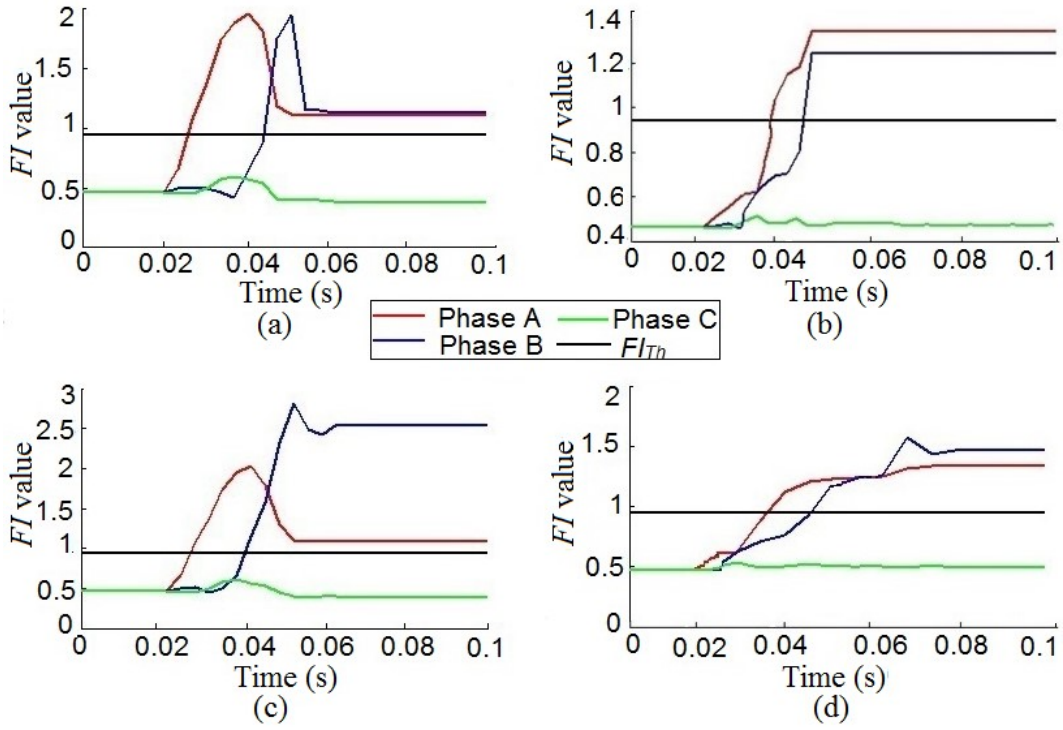

Fig. 5.4. Effect of Evolving and Cross-country faults
Evolving fault: (a) With FR = 0 Ω (b) With FR = 300 Ω
Cross-country fault: (c) With FR = 0 Ω (d) With FR = 300 Ω

In Figs. 5.4(a), 5.4(b), 5.4(c) and 5.4(d) SLGA fault occurs at 0.02s while the SLGB fault occurs at 0.025s. *FI* of phase A crosses FI_{Th} line at 0.026s and the same in phase B crosses FI_{Th} at 0.043s in Fig. 5.4(a). The *FI* of phase A crosses the FI_{Th} line at 0.038s, and the same for phase B crosses FI_{Th} at 0.0435s in Fig. 5.4(b). *FI* of phase A and phase B crosses FI_{Th} at 0.026s and 0.039s, respectively, as shown in Fig.5.4(c), and *FI* value of phase A and phase B crosses FI_{Th} at 0.037s and 0.042s, respectively, as shown in Fig. 5.4(d).

5.4.3.2. Effect of Complex Cross-Country Faults

The primary goal of this algorithm is to detect faults in the protection zone properly. Hence, it is quite important to segregate the internal faults from the external ones. However, in the case of a cross-country fault, there is some possibility that one fault occurs in the protective zone while another occurs in the external fault zone. These types of fault conditions are known as complex cross-country faults. To investigate the efficiency of this algorithm during complex cross-country fault, SLGA has been generated at 20 km from bus 1 at 0.0225s in the protective zone while SLGB has been generated at 250 km from bus 1 at 0.025s. Figs. 5.5(a) and (b) depict the response of the proposed threshold-based algorithm with FR 0 Ω and 300 Ω respectively. It is seen that the proposed methodology can accurately identify the internal fault along with the faulty phase.

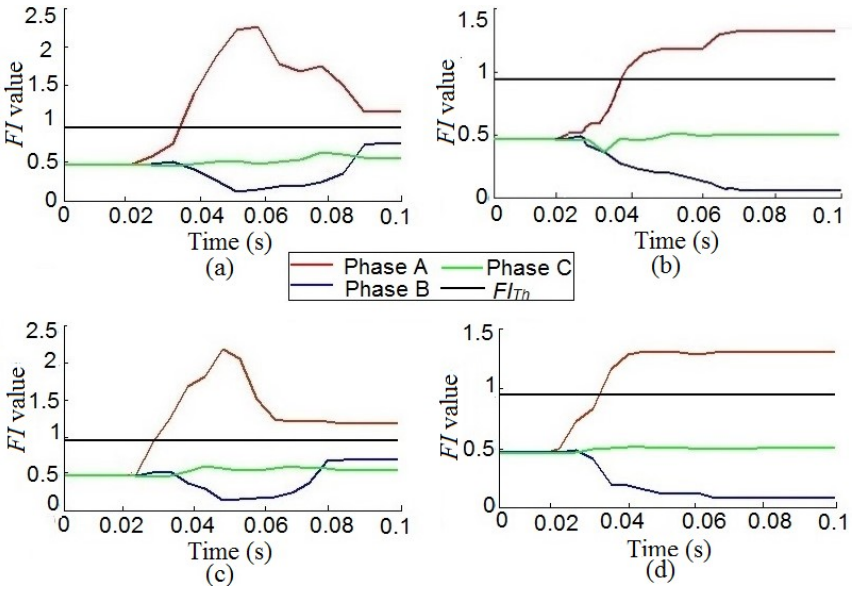

Fig. 5.5. Effect of Complex Cross-Country faults:
(a) With FR = 0 Ω at 0.0225s (b) With FR = 300 Ω at 0.0225s
(c) With FR = 0 Ω at 0.02s (d) With FR= 300 Ω at 0.02s

In Fig. 5.5(a) and Fig. 5.5(b) SLGA fault occurs at 0.0225s while in Fig. 5.5(c) and Fig. 5.5(d) SLGA fault occurs at 0.02s in the protective zone and for both the cases SLGB fault

occurs at 0.025s beyond the protective zone. *FI* of phase A crosses the FI_{Th} line at 0.035s in Fig. 5.5(a) and at 0.038s in Fig. 5.5(b). *FI* of phase A crosses FI_{Th} at about 0.028s and 0.035s in Fig. 5.5(c) and 5.5(d) respectively.

5.4.3.3. Evaluation of the Proposed Algorithm with Varying FR

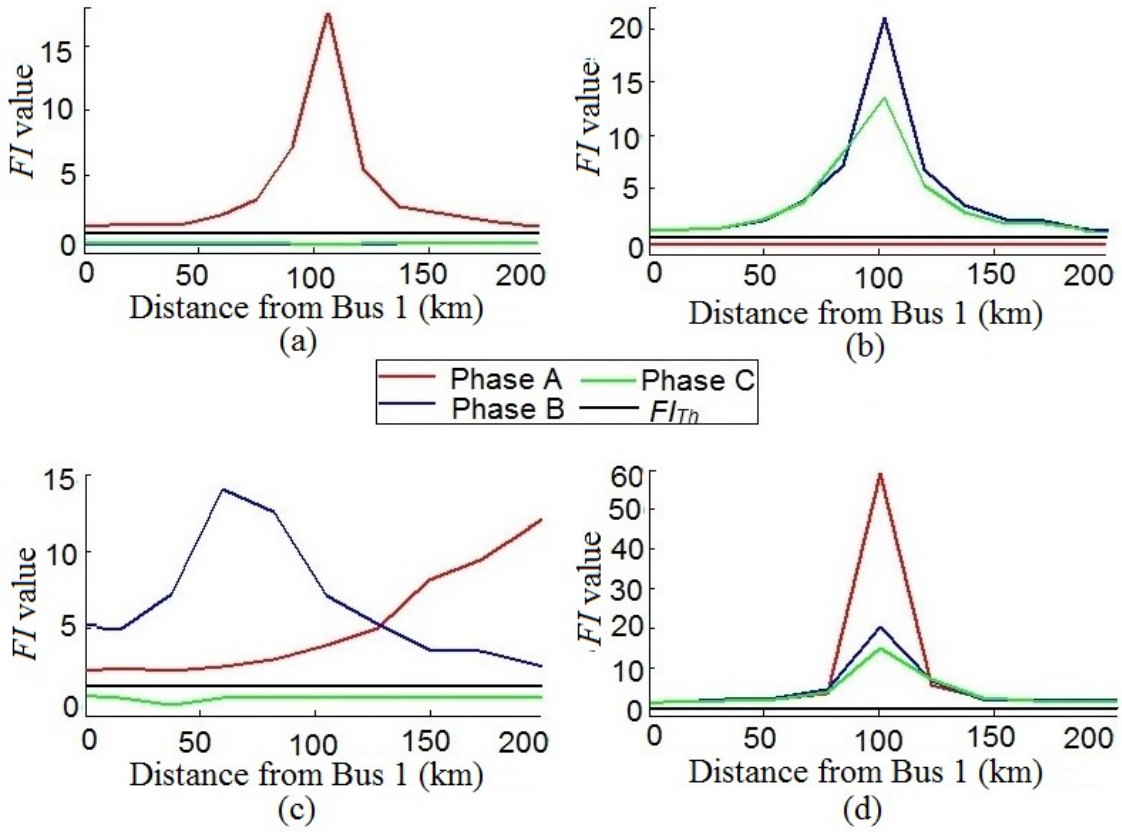

Fig. 5.6. *FI* value at different fault location during internal fault with FR = 0 Ω and FIA 0°: (a) SLGA (b) LLGBC (c) LLAB (d) LLL

The network shown in Fig. 5.3 has been subjected to different types of faults at various FR (0-300 Ω) to test the performance of this scheme. Fig. 5.6 and Fig. 5.7 show the changes of *FI* value with the variation of fault location when fault occurs in the protection zone with FR = 0 Ω and 300 Ω respectively. From Fig. 5.6 & Fig. 5.7, it has been noticed that the trajectory of *FI* of faulty phase/s is well above the FI_{Th} value. Similarly, from Fig. 5.8 and Fig. 5.9 it is seen that the trajectory of *FI* is less than the pre-determined FI_{Th} with FR of 0 Ω and 300 Ω respectively for external faults. As a result, it is worth noting that FR variation has no impact on this fault detection and fault zone identification scheme.

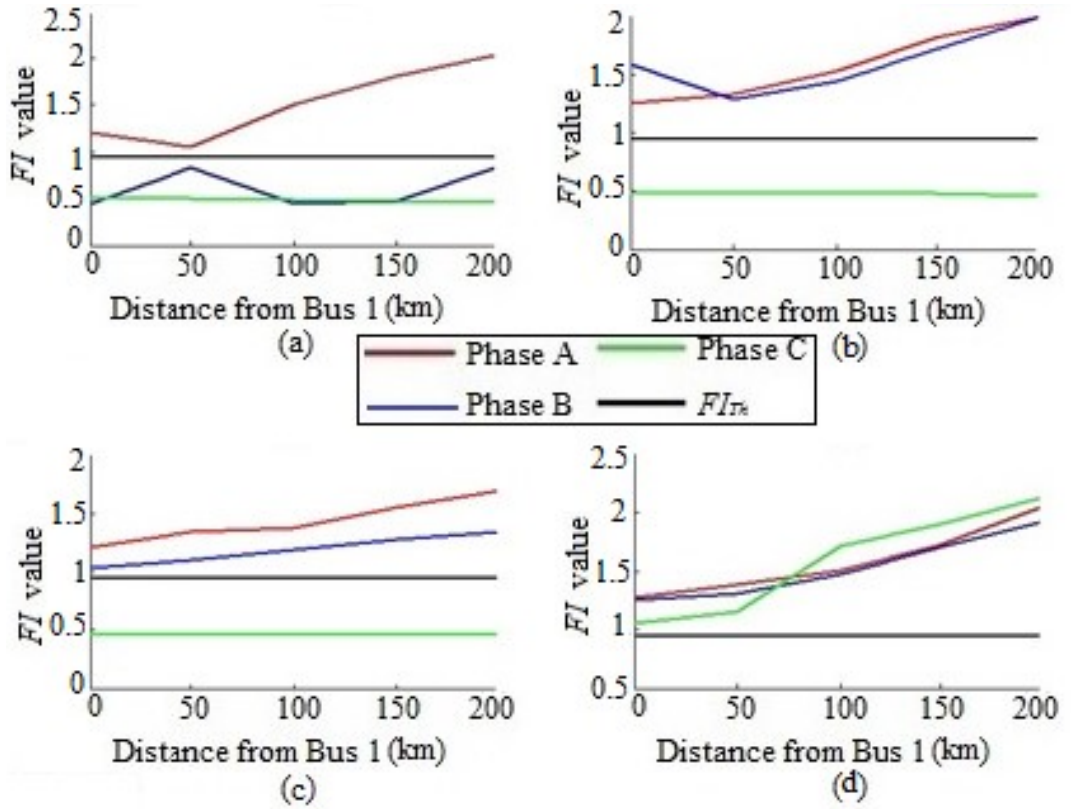

Fig. 5.7. *FI* value at different fault location during internal fault with FR = 300 Ω at 45° : (a) SLGA (b) LLGAB (c) LLAB (d) LLL

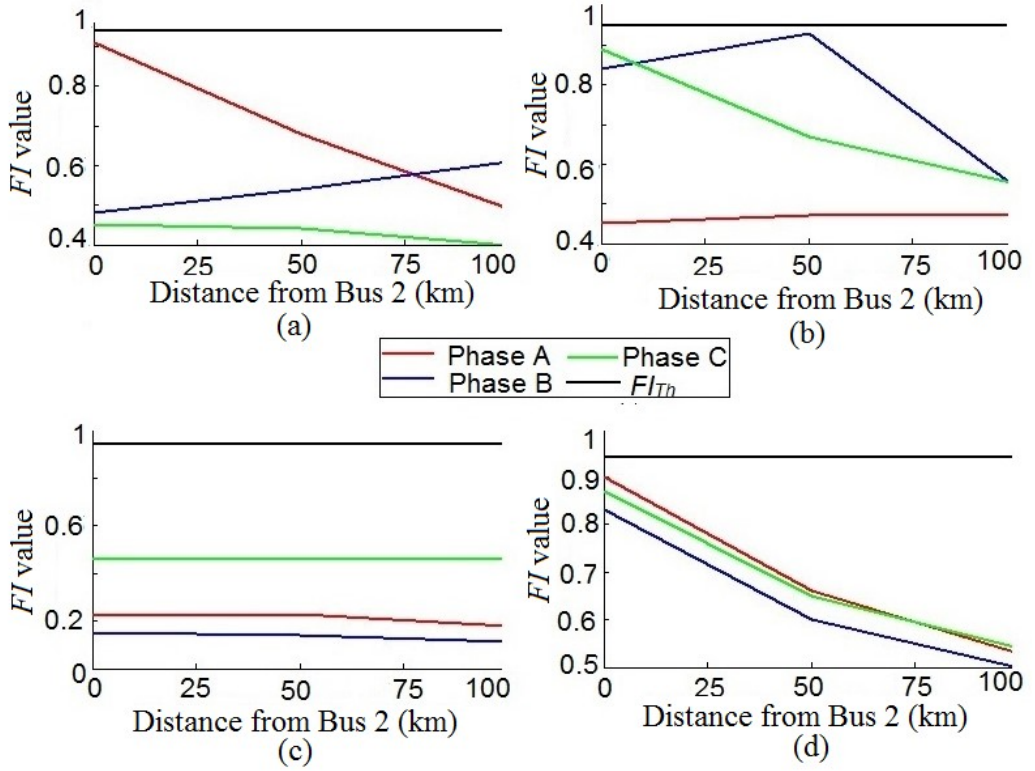

Fig. 5.8. *FI* value at different fault location during external fault with FR = 0 Ω and FIA 0°: (a) SLGA (b) LLGBC (c) LLAB (d) LLL

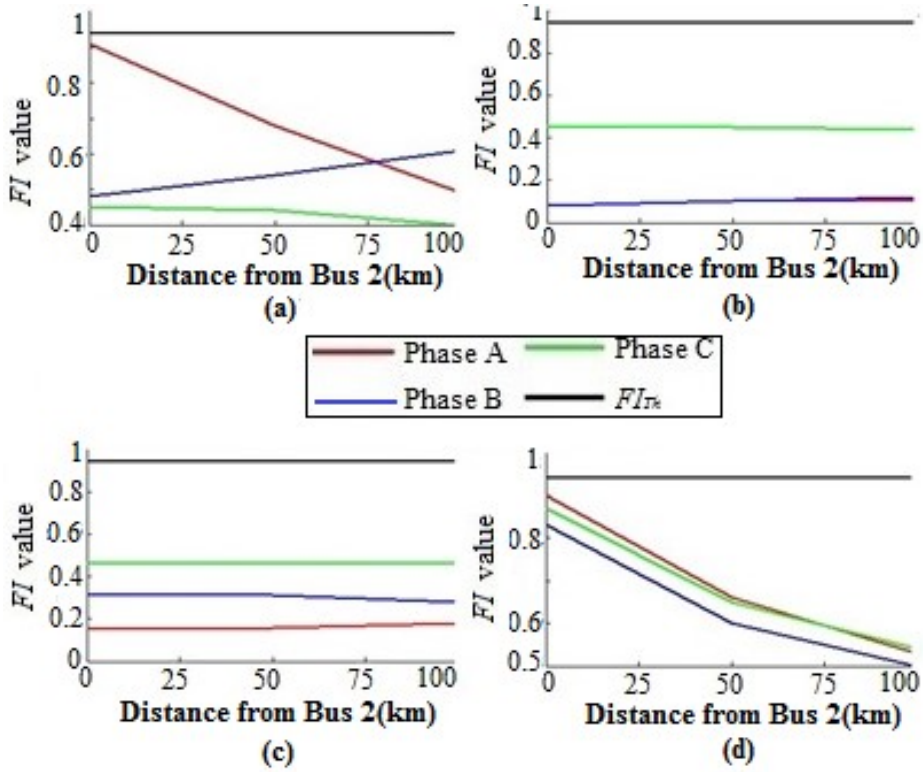

Fig. 5.9. *FI* value at different fault location during external fault with FR = 300 Ω at 45°: (a) SLGA (b) LLGBC (c) LLAB (d) LLL

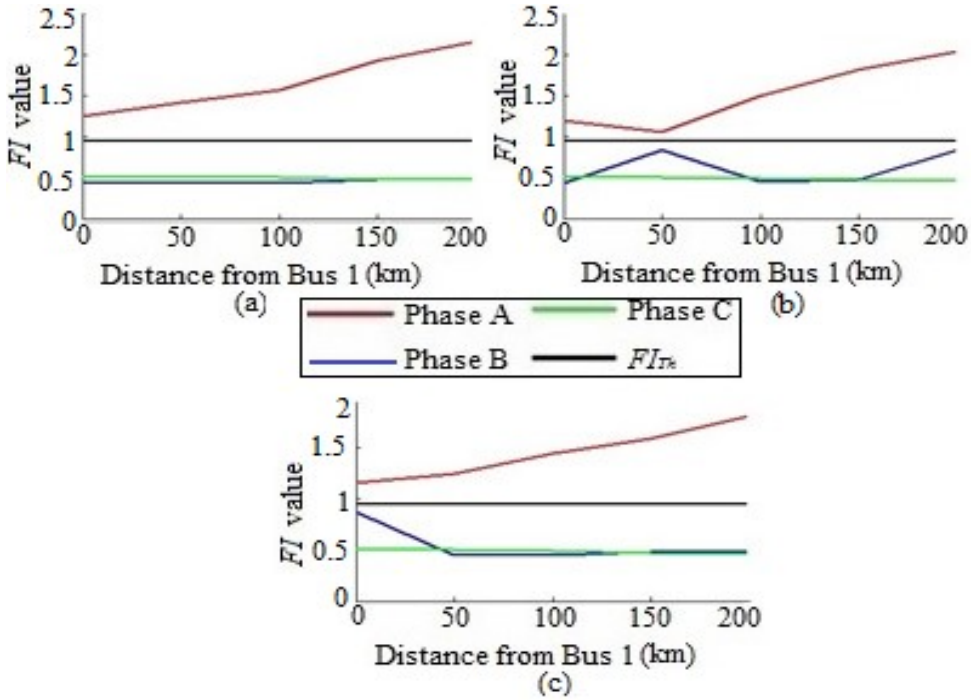

Fig. 5.10. *FI* value at different fault location in the Protection Zone with FR = 300 Ω: (a) SLGA at 0° (b) SLGA at 45° (c) SLGA at 90°

5.4.3.4. Effect of Change in FIA

As faults may occur any time, it is necessary to verify the proposed approach with faults at different FIAs. In this research work, the impact of FIA ranging from 0° to 90° has been investigated by simulating faults in the test system as illustrated in Fig. 5.3. Fig. 5.10 depicts the simulation results of SLGA fault in the protection zone with varying FIA. It has been noticed that the proposed fault detection algorithm based on line admittance is capable to correctly detect internal faults and faulty phase/s.

5.4.3.5. Effect of Change in Source Strength

Weak-infeed condition may cause mal-operation of relays. Weak-infeed happens when the source impedance is quite high and the current needed to actuate the relays is not sufficient. As a result, the relays do not operate during abnormal conditions in transmission lines. So, to study the sensitivity of the proposed approach with the change of source strength, the transmission line has been simulated at different source strengths of 800 MVA, 1000 MVA, and 1200 MVA. *FI* value at no-fault condition depends on the source strength of the system. Therefore, threshold values should be different at different source strengths.

Table 5.3 represents the different FI_{Th} values for different source impedances. LLL fault has been simulated with FR = 300 Ω and source strength of 800 MVA at various locations on the transmission line to validate the effectiveness of this proposed technique. Fig. 5.11(a) illustrates that *FI* values of all the phases are well above FI_{Th} for LLL fault in the protective zone while it falls below the threshold value when a fault occurs beyond the protective zone, which is shown in Fig. 5.11(b). This proves that the proposed algorithm can detect faults accurately with the variation of source strengths.

Table 5.3. Threshold value of Fault Index (FI_{Th}) at different condition

		FI at no-fault condition	FI_{Th}
Source strength (MVA)	800	0.57	1.14
	1000	0.47	0.94
	1200	0.4	0.80
Level of Compensation	30%	0.457	0.91
	50%	0.427	0.854
	70%	0.426	0.852
Power transfer angle	10°&-10°	0.89	0.89
	20°&-20°	0.47	0.94
	30°&-30°	0.31	0.93

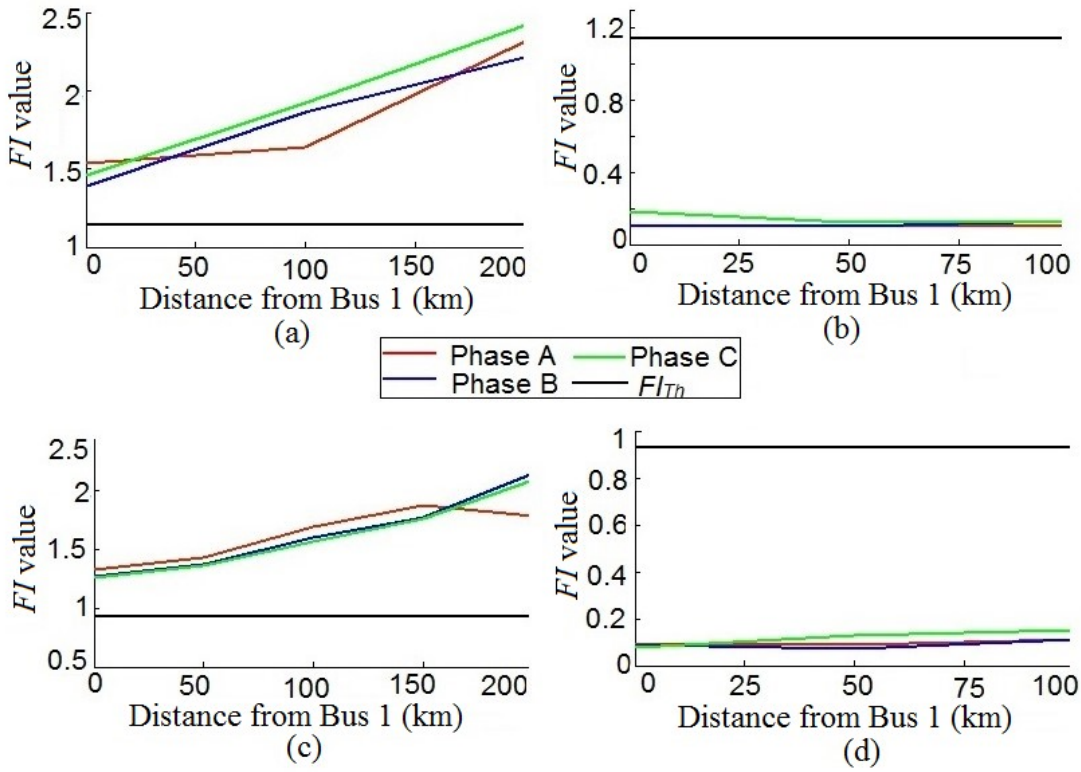

Fig. 5.11. Effect of source strength variation and CVT transient and CT saturation
Source strength variation: (a) Internal fault (b) External fault.
CVT transient and CT saturation: (c) Internal fault (d) External fault.

5.4.3.6. Effect of CT and CVT Transient

As shown in Fig. 5.3, six CTs and six CVTs (capacitive voltage transformers) are installed at bus 1 and bus 2 to measure current and voltage samples. CVT and CT produce transients in transmission lines and these transients create problems to the proper functioning of relays. Hence, it is quite important to analyze the influence of CTs and CVTs on the developed algorithm. To design the CTs and CVTs the necessary parameters are taken from Ref. [101] and [35] respectively. To test the reliability of this algorithm, LLL fault has been generated at various locations on the transmission line with FR 300 Ω and the results of this algorithm have been presented in Fig. 5.11(c) and Fig. 5.11(d). It is noticed that the values of *FI* rise above the FI_{Th} after the occurrence of fault during an internal fault. During an external fault, *FI* of all the phases are well below the FI_{Th} line. This proves the robustness of this algorithm in presence of CT saturation and CVT transients.

5.4.3.7. Effect of Synchronization Delay

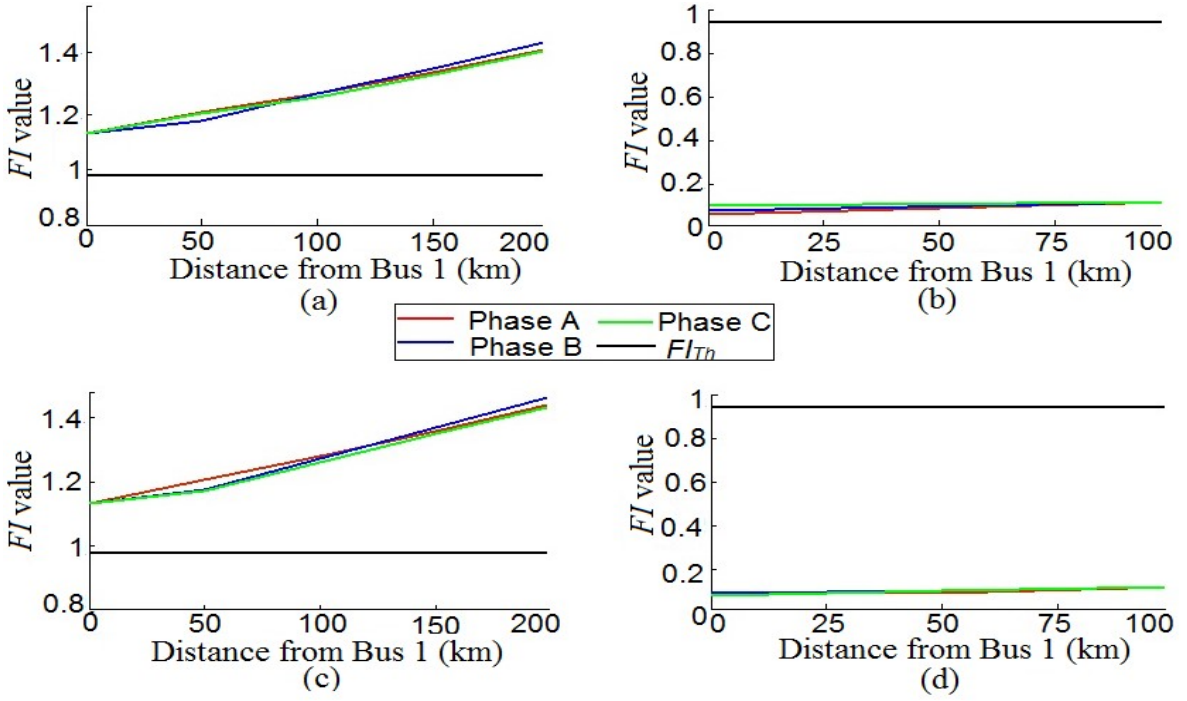

Fig. 5.12. Effect of Synchronization delay
Delay 7.5 ms with FR 0Ω: (a) Internal fault (b) External fault
Delay10 ms with FR 300 Ω: (c) Internal fault (d) External fault

Voltage and current samples from buses 1 and 2 have been used to compute the *FI* in the proposed algorithm. Any time delay in collecting the data samples (voltage and current) from bus 1 and bus 2 can affect the performance of this algorithm. Hence, synchronization delays of 2.5 ms, 5 ms, 7.5 ms, and 10 ms have been considered to determine the robustness of this algorithm. To investigate the effect of synchronizing delays, all types of faults have been simulated with FR varying from 0 Ω to 300 Ω at various locations in the transmission lines. Voltage and current samples are collected from bus 2 considering delay times of 2.5 ms, 5 ms, 7.5 ms, and 10 ms. Fig. 5.12(a) and Fig. 5.12(b) show the trajectories of *FI* during LLL fault with a delay time of 7.5 ms and FR 0 Ω and Fig. 5.12(c) and Fig. 5.12(d) show the trajectories of *FI* during LLL fault with a delay time of 10 ms and FR 300 Ω. Fig. 5.12 reveals that the synchronization delay has no impact on the proposed algorithm.

5.4.3.8. Effect of Close-in Fault

The faults that occur close to the relay points are known as close-in faults. Close-in fault causes serious issues in the event of three-phase fault condition. The main problem of close-in fault is the unavailability of the voltage signal during LLL fault, as voltages in all the phases collapse. Hence, an investigation has been done on close-in fault cases to test the efficiency of

the proposed technique. All ten categories of faults have been generated near the relay points (from bus 1 and bus 2 in steps of 1 km from 0.1 km to 9 km) with varying FR from 0 Ω to 300 Ω to validate the authenticity of the developed scheme in the event of close-in faults. It has been noticed that for internal fault *FI* values of faulty phases are greater than FI_{Th} and for external faults, the same are less than FI_{Th}. Fig. 5.13 presents the performance of the proposed algorithm for close-in fault.

5.4.3.9. Effect of Series Compensation

Series compensators are widely used in long transmission lines to enhance the system stability, decrease transmission losses, and maximize power transfer capability. But at the same time, these devices create problems in actuating relays. The presence of series compensator changes the line impedance which adversely affects the operation of the relays. Hence, the performance of the proposed logic has been assessed in the presence of a series compensator. The test model has been shown in Fig. 5.14 and simulated for evaluating the proposed algorithm under three different series compensation levels (30%, 50% and 70%). In this study, a MOV type series compensator is positioned at the middle point of the line between bus 1 and bus 2 which is 200 km long. Threshold values of *FI* with varying compensation levels are tabulated in Table 5.3. Fig. 5.15(a) and Fig. 5.15(b) show the test results of the proposed algorithm with FR = 300 Ω and compensation level is 30% whereas Fig. 5.15(c) and Fig. 5.15(d) illustrate the *FI* values of all the phases with FR=0 Ω and compensation level is 70%. It has been noticed that *FI* of faulty phase/s for internal faults are greater than FI_{Th} and the same for external fault cases are less than FI_{Th}. Thus the proposed algorithm can be successfully applied in SCTLs.

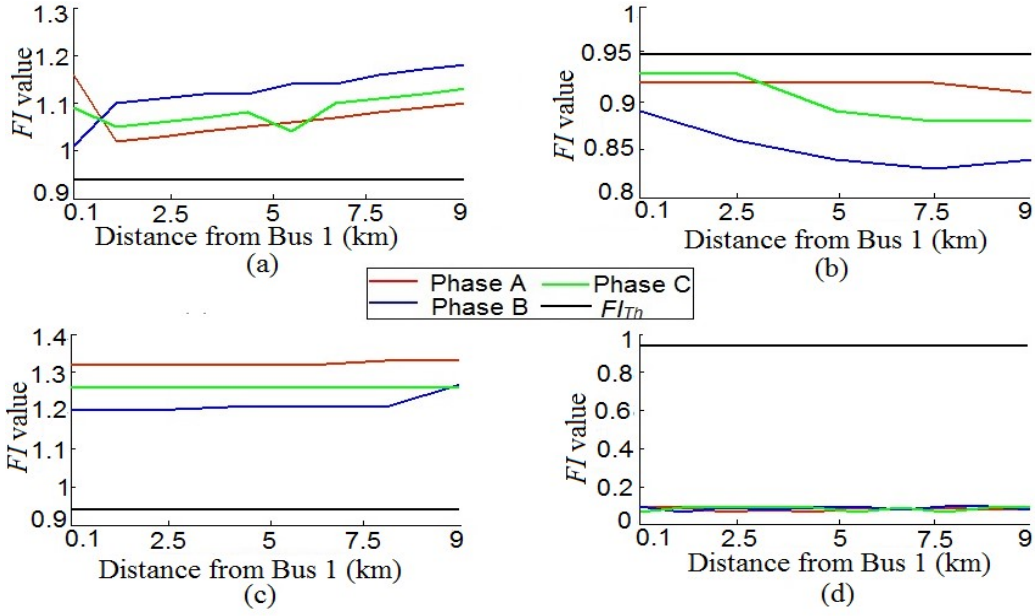

Fig. 5.13. Effect of Close in fault
(a) Internal fault with FR 0 Ω (b) External fault with FR 0 Ω
(c) Internal fault with FR 300 Ω (d) External fault with FR 300 Ω

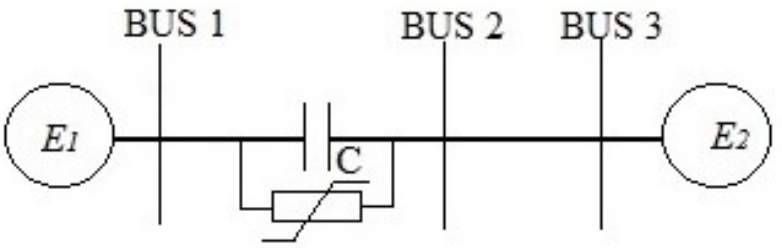

Fig. 5. 14. Test system for Series Compensation.

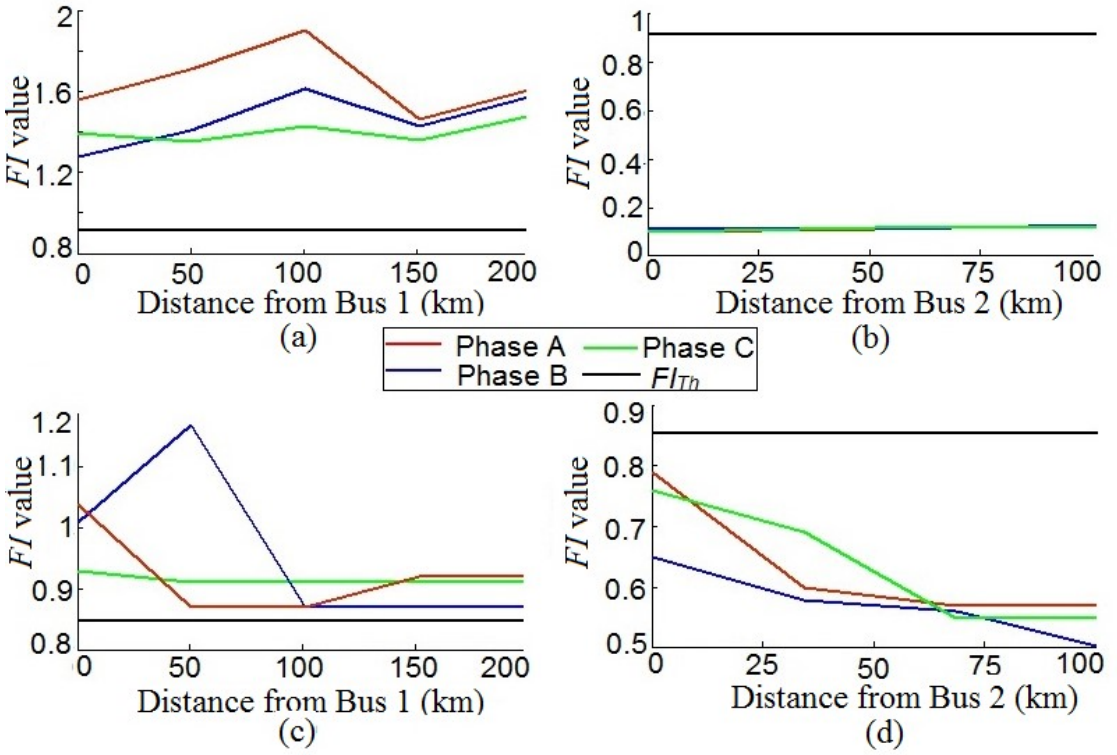

Fig. 5.15. Effectof series compensation
LLL fault with FR = 300 Ω and compensation level 30%:
(a) Internal fault (b) External fault.

LLL fault with FR = 0 Ω and compensation level 70%:
(c) Internal fault (d) External fault.

5.4.3.10. Effect of Variation of Power Transfer Angle

This section examines the impact of the change of the power transfer angle on the proposed algorithm. The power transfer angle has a significant impact on the threshold value of *FI*. The proposed method has been carried out with a power transfer angle of 20°. To verify the reliability of the proposed technique under the variation of power transfer angle, Fig. 5.3 has been simulated with six different power transfer angles viz. -10°,10°, -20°, 20°, -30° and 30°.

From this study, it is revealed that adaptive threshold values for different power transfer angles are required to detect the fault in the protective zone. For 10° and -10° power transfer angles, the threshold value FI_{Th} is the same as the *FI* value under no-fault condition, whereas for 20° and -20°, FI_{Th} is twice the no-fault *FI* value and for 30° and -30°, power transfer angle FI_{Th} is three times of the no-fault *FI* value. Table 5.3 shows the *FI* value at no-fault conditions with the corresponding FI_{Th} value at different power transfer angles. It has been observed that for power transfer angle of 10°, *FI* values calculated using Eq. (5.10) remain below the calculated no-fault *FI* under all no-fault dynamic and stressed conditions viz. power swing, CT or CVT transient, synchronization delay and external fault beyond the protective zone. Hence, FI_{Th} has been considered same as the calculated *FI* under no-fault condition. For 20° power transfer angle,

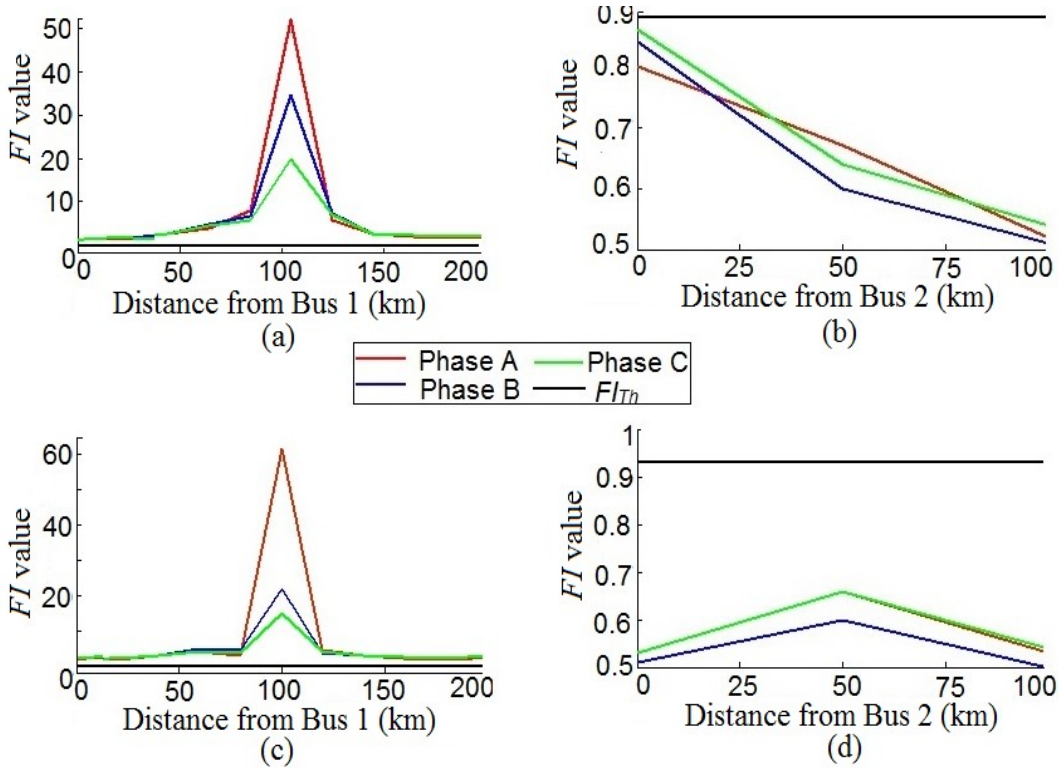

Fig. 5.16. Effect of variation power transfer angle
LLL fault when power transfer angle 10°: (a) Internal fault (b) External fault
LLL fault when Power transfer angle 30°: (c) Internal fault (d) External fault

some *FI* values exceed the calculated no-fault *FI*, but always remain less than twice that of *FI* in case of no-fault in the protective zone and it is always above twice that *FI* when fault occurs in the protective zone. For 30° power transfer angle it has been observed that *FI* values under no-fault condition may be above the calculated no-fault *FI*, but always remain below thrice that value and it is always above thrice the calculated no-fault *FI* when fault occurs in the protective zone. Fig. 5.16 shows the trajectories of *FI* with FR of 0 Ω and FIA of 0° for internal and external faults with variation of power transfer angle.

5.4.3.11. Effect of Power Swing

Swing in a power system network occurs when a fault is removed or the load is suddenly increased to fulfill the extra power demand of the system. Hence, power swing is an integral part of the system and the proposed logic must be validated under power swing conditions. In this case study, two swing conditions have been considered. A 150 MW load is connected to bus 1 at 0.1s to simulate the load swing in the line. *FI* values continue to change for some time and then becomes steady. But *FI* never exceeds the threshold value as shown in Fig. 5.17(a). The first row in Table 5.4 represents the steady state values of *FI* under load swing condition. Another swing condition, by sudden removal of a fault is simulated creating SLGA fault at 0.02s at a distance of 5 km from bus 1 with FR of 0 Ω and FIA 0°. The fault is removed at 0.1s. From Fig. 5.17(b) it is observed that after the occurrence of fault *FI* value of phase A crosses the FI_{Th} line at 0.025s and remains above the FI_{Th} line until the fault is cleared. At 0.1s fault is cleared and it is observed that *FI* value of phase A decreases and crosses the FI_{Th} line at 0.118s and remains below the threshold value. The second row of Table 5.4 shows the *FI* values at 0.12s for the sudden removal of fault. It is seen that *FI* is less than the pre-defined threshold value in both cases. After investigating these two swing conditions it is observed that this algorithm is not influenced by power swing.

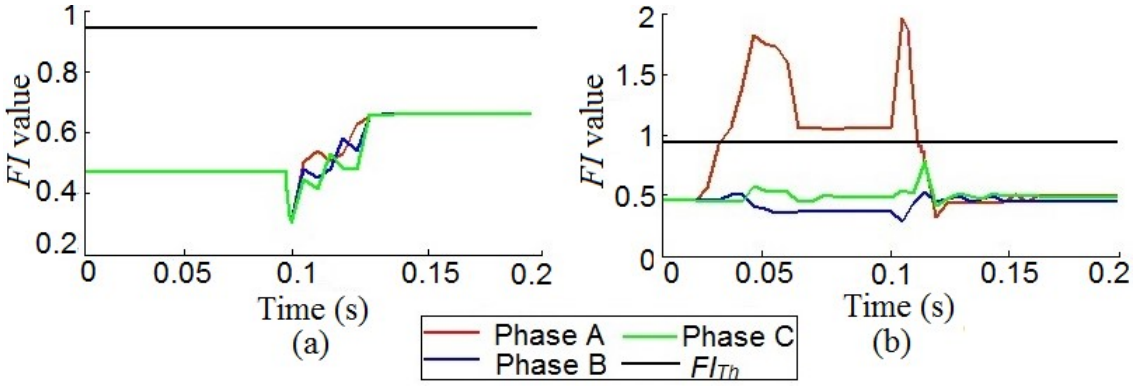

Fig. 5.17. Effect of power swing
(a) Swing due to connection of sudden load
(b) Swing due to clearance of fault

Table 5.4. Performance of proposed method during power swing

	FI_{Th}	*FI*		
		A Phase	B Phase	C Phase
Load is connected	0.94	0.65	0.65	0.65
Sudden removal of SLG fault	0.94	0.34	0.47	0.40

5.4.3.12. Effect of Non-Linear HIF

As already stated before, HIFs are very complicated phenomenon that produce unforeseeable and stochastic non-linear currents. The arcing effect is an important feature of HIFs, and it produces heat which may change the resistance in the fault path. As a result, the magnitude of the fault current varies unpredictably. Due to these dynamic characteristics, V-I curve during HIF is non-linear. This non-linear behavior of current signals makes it difficult to detect fault. Hence, HIF may exist for long period without tripping the protecting devices causing risk of public safety.

In this chapter, two-diode Emanuel's arc model has been considered [60]. Emanuel's arc model consists of two sets of diodes connected in anti-parallel, DC voltage sources, and variable resistors. Current during HIF is influenced by many factors such as type of conductor, short-circuit rate, condition of ground material (i.e. wet or dry), and also type of material. Therefore, the model should be such that, it complies with all the probable conditions. The two DC voltage sources are set in the range of 900 V-1100 V and 450 V-1100 V [60]. The resistances are in the range of 100 Ω-150 Ω. To examine the applicability of the proposed technique during non-linear

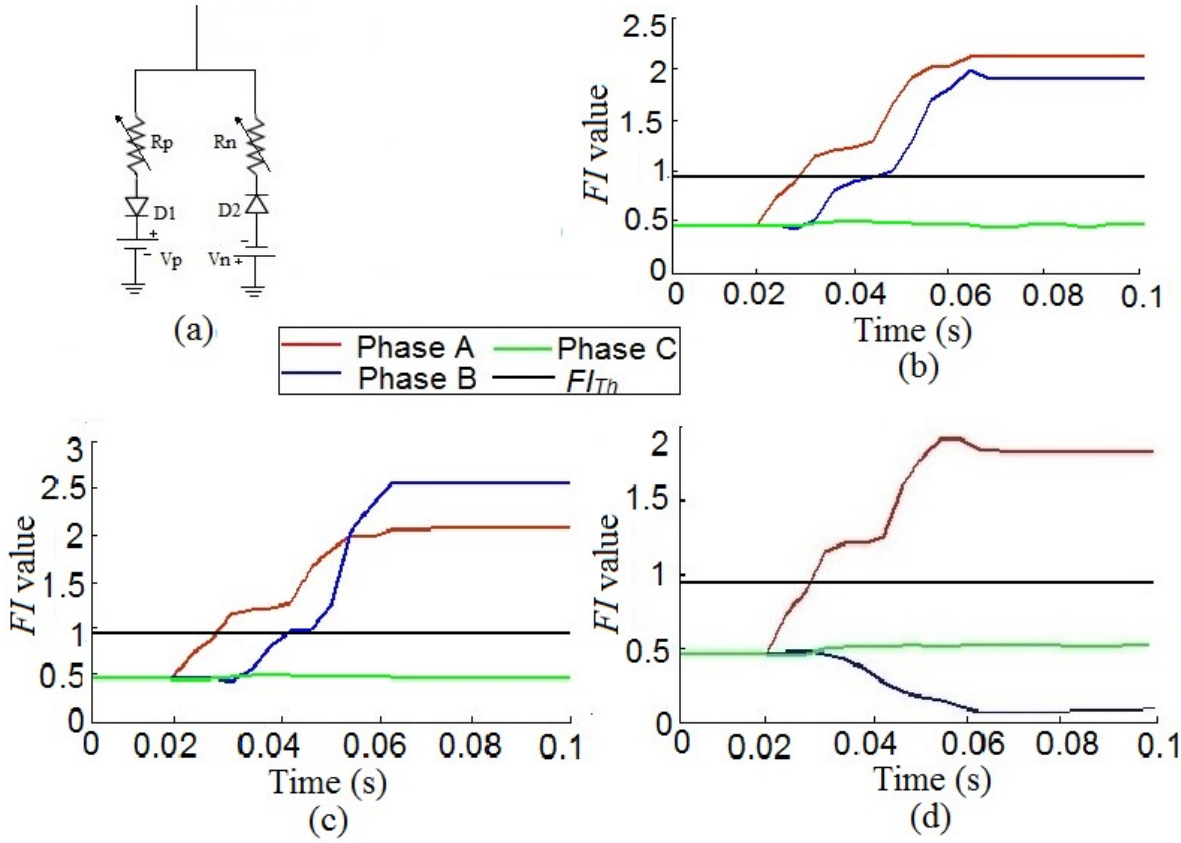

Fig. 5.18. Effect of non-linear HIF
(a) HIF model (b) Evolving fault
(c) Cross-country fault (d) Complex cross-country fault

HIF, all ten types of faults at different FIA and various fault locations have been simulated using this HIF model. The simulation results show that the *FI* values of the faulty phase/s are well above the FI_{Th} value in the main protection zone and the same are below FI_{Th} during external fault conditions. Fig. 5.18 shows the *FI* trajectory during evolving, cross-country, and complex cross-country faults under non-linear HIF conditions. To investigate the efficacy of the proposed algorithm during evolving faults, HIF in phase A has been simulated at 50 km from bus 1 at t = 0.02s and then another HIF has been generated at t = 0.03s in phase B at the same location. In case of cross-country fault, HIF in phase A has been generated at 50 km from bus 1 at t = 0.02s and then the second HIF has been generated at t = 0.03s in phase B at 100 km from bus 1. During complex cross-country fault, HIF at phase A has been generated at 50 km from bus 1 at 0.02s in the protection zone while HIF at phase B has been generated at 250 km from bus 1 at 0.03s. Fig. 5.18(a) represents the HIF model. Figs. 5.18(b), 5.18(c), and 5.18(d) depict the response of the proposed algorithm when both the resistances (R_p and R_n) are 150 Ω and V_p and V_n are 900 V and 1100 V respectively. Hence this proposed algorithm can detect fault in the protective zone during non-linear HIFs.

In Figs. 5.18(b), 5.18(c) and 5.18(d) faults in phase A occur at 0.02s and fault in phase B occur at 0.03s at different locations. *FI* values of phase A and phase B cross FI_{Th} at 0.03s and 0.044s, respectively in Fig. 5.18(b) and *FI* values of phase A and phase B cross FI_{Th} at 0.03s and 0.04s in Fig. 5.18(c). In Fig. 5.18(d) *FI* value of phase A crosses FI_{Th} at 0.03s.

5.5. Performance of the Proposed Algorithm on IEEE 9-Bus System

To check its usefulness in power network, the proposed algorithm has been verified on an IEEE 9-bus system. Fig. 5.19 shows the single line diagram of the IEEE 9-bus system. This system consists of three transformers, three generators, three loads, and six transmission lines which are connected between 9 buses.

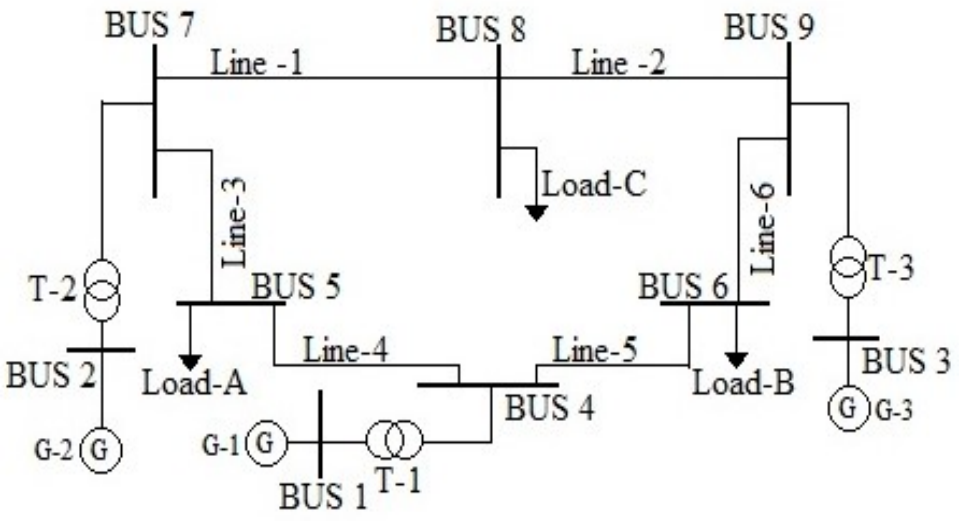

Fig. 5.19. IEEE 9-bus system

To study the performance of this threshold-based algorithm on the IEEE 9-bus system, various types of faults have been simulated with various FR and FIA. Voltage and current samples are acquired from bus 4 and bus 6. Faults that occur in line 5 are considered as internal faults, whereas faults created in other lines are external faults. Table 5.5 depicts the results of internal and external faults with FR= 0Ω. The same criterion (i.e. two times of *FI* at no-fault condition) is applied to determine the FI_{Th}. Hence, in the IEEE 9-bus system FI_{Th} is 1.58 because *FI* at no-fault condition is 0.79.

Table 5.5 shows that during internal faults *FI* value of faulty phase/s is well above the FI_{Th} and during external faults, the same value is less than FI_{Th}. Therefore, it reveals that this algorithm can accurately discriminate internal and external faults and also can classify internal faults.

Table 5.5. Results of internal and external fault with FR = 0 Ω in IEEE 9-bus system

	Fault Location	Types of faults	FI_{Th}	FI_A	FI_B	FI_C
Internal Fault	Line -5	BG	1.58	0.79	**3.39**	0.91
		ABG		**1.63**	**1.76**	0.88
		AB		**2.30**	**40.13**	0.79
		ABC		**10.15**	**9.41**	**22.18**
External fault	Line -6	CG		0.89	0.76	0.57
		ABG		0.67	0.70	0.88
		AB		0.23	0.35	0.79
		ABC		0.44	0.38	0.38
	Line -2	CG		0.80	0.77	0.75
		ABG		0.28	0.89	0.88
		AB		0.18	1.05	0.79
		ABC		0.55	0.30	0.35
	Line -4	AG		0.47	0.78	0.79
		BCG		0.80	0.41	0.02
		BC		0.79	0.25	0.50
		ABC		0.94	0.42	0.40

5.5.1. Effect of Evolving and Cross-Country Faults on IEEE 9-Bus System

Cross-country and evolving faults have been generated in different lines to study their effects on the proposed algorithm. Fig. 5.20(a) and Fig. 5.20(b) depict the responses of *FI* during evolving faults with FR 0 Ω and 300 Ω respectively. In both the cases initially, SLGA fault

occurs at 150 km from bus 6 in Line 5 at 0.02s and converted into LLGAB fault at 0.025s. Fig. 5.20(c) and Fig. 5.20(d) illustrate the results of cross-country faults. During cross-country fault SLGA fault occurs at 150 km from bus 6 in Line 5 at 0.02s and SLGB fault at 200km from bus 6 in Line 5 at 0.025s. Hence, it is noticed that *FI* trajectories of phase A and phase B (i.e. faulty phases) are well above the threshold line after the inception of fault. It reveals that the proposed threshold-based algorithm can protect IEEE 9-bus system from cross country and evolving faults. In Fig. 5.20(a) and Fig. 5.20(b), SLGA fault occurs at0.02 s and converted into LLGAB fault at 0.025s. *FI* of phase A and phase B crosses the FI_{Th} line at 0.028s and 0.03s respectively in Fig. 5.20(a) and the same crosses FI_{Th} line at 0.038s and 0.04s respectively as shown in Fig. 5.20(b). In Fig. 5.20(c) and Fig. 5.20(d) SLGA occurs at 0.02s and another fault in phase B occurs at 0.025s. *FI* of phase A and phase B cross FI_{Th} at 0.025s and 0.028s respectively, as shown in Fig 5.20(c) and in Fig. 5.20(d) *FI* of phase A and phase B cross FI_{Th} at 0.035s and 0.042s respectively.

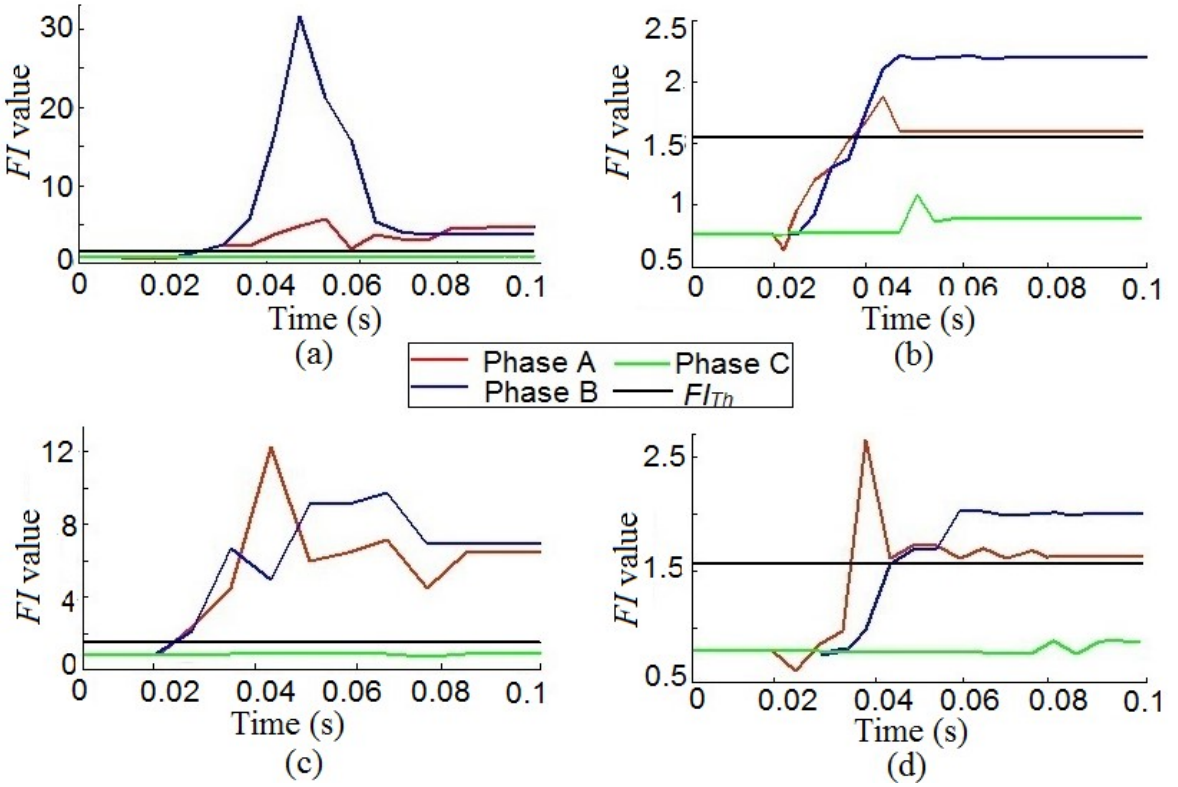

Fig. 5.20. Effect of Evolving fault and Cross-country faults in IEEE-9 bus system
Evolving fault: (a) With FR 0 Ω (b) With FR 300 Ω
Cross-country fault: (c) With FR 0 Ω (d) With FR 300 Ω

5.5.2. Effect of Complex Cross-Country Faults on IEEE 9-Bus System

Fig. 5.21 depicts the nature of *FI* during complex cross-country faults. To simulate the complex cross-country fault in the IEEE 9-bus system, SLGA fault has been generated at 150 km from bus 6 in Line 5 (internal fault) at 0.02s and another fault i.e. SLGB fault has been generated at 200 km from bus 9 in Line 2 (external fault) at 0.03s. From Fig. 5.21, it is seen that the *FI* trajectory of phase A is well above FI_{Th} after the occurrence of fault. On the other hand, the *FI* trajectory of phase B is below FI_{Th} before and after the inception of fault. Hence, it is ascertained that the proposed line admittance-based schemecan efficiently protect the IEEE 9-bus system from complex cross-country faults. In Fig. 5.21(a) and Fig. 5.21(b) internal fault occurs in phase A at 0.02s and the *FI* crosses FI_{Th} line at 0.035s in both cases. Hence, the fault is detected at 0.015s i.e. within one cycle after the occurrence of fault.

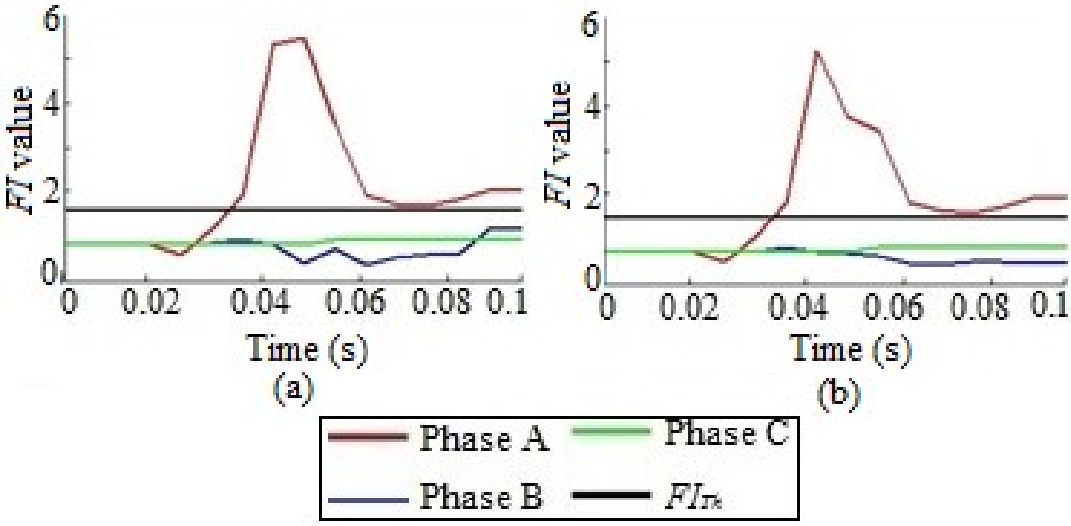

Fig. 5.21. Effect of Complex cross-country faults in IEEE 9-bus system
(a) With FR 0 Ω (b) With FR 300 Ω

5. 6. Comparative Assessment

The proposed algorithm has been compared with the previously published fault detection techniques [92, 109, 110, 112, 113 and 114] which considered cross-country faults. This algorithm gives accurate results at low resistance as well as high resistance up to 300 Ω whereas references [109, 110 and 113] considered resistances up to 150 Ω. Moreover, none of these references observed the performance of their scheme during non-linear HIF. The proposed algorithm does not require any artificial intelligent based technique to classify the faults unlike [114] which used ANN and ELM. This scheme correctly detects and classifies faults in the protective zone in presence of series compensator whereas references [109, 110, 112, 113 and 114] did not validate their algorithm in compensated lines. Faulty phase identification has not been performed in [92 and 112]. The impact of synchronization delay has not been studied in

[110] and [114] though these schemes used signals from both ends of the transmission line. Unlike [110, 112, and 113], the authors have observed the performance of the proposed scheme with source strength variation and under power swing condition.

The comparative assessment of the proposed scheme with other existing literature confirms the following salient features of the proposed scheme:

- Though HIF protection schemes have been developed by many researchers, but evolving, cross country and complex cross country faults under non-linear HIF have not been considered.
- The proposed scheme does not use any complex transform based technique that requires rigorous mathematical computation. It uses sequence component analysis which involves low computation burden.
- The proposed scheme can replace existing relaying schemes that essentially require pre-fault and post-fault data and training of available dataset. Hence, the scheme is suitable for real time application.
- The performance of the proposed scheme has been tested in the presence of series compensation and power swing and under different dynamic situations that generally prevail in a transmission line.
- The sampling frequency used in this scheme is 12.5 kHz, which is not very high as considered in many other fault protection schemes.
- The time of detection of fault is always less than one cycle.

The proposed algorithm has been applied in IEEE 9-bus system and the accurate results prove the applicability of the scheme in real time transmission and distribution network under complicated faulty situations of evolving and cross country faults. The proposed scheme is also applicable for SCTLs.

5.7. Conclusion

This chapter proposes the use of an admittance-based technique for HIF detection and faulty phase/s selection in transmission lines. This research mainly focuses on the detection and classification of internal fault with wide variation of fault parameters including cross-country and evolving faults. The proposed technique is simple and has low computational burden as it is a threshold-based technique and does not utilize any artificial intelligent based technique. It has been observed that the proposed technique has the ability to perform satisfactorily under major challenges imposed by the dynamic changes in the transmission system. It is independent of fault inception angle, fault location, fault impedance, series compensation, source strength, and synchronization delay and is unaffected under power swing condition. Moreover, the operation time of the proposed scheme is from half-cycle to maximum one cycle. Comparison of the proposed algorithm with recent power system protection methods, which considered evolving and cross-country faults, confirms the reliability and robustness of this algorithm.

CHAPTER 6

Back-up Protection Scheme for Series Compensated Transmission Line Connected to Wind farm

6.1. Introduction

Due to the urban growth, scarcity of land and various environmental problems, increase of the power transfer capability as well as enhancement of power system stability have become essential. To enhance the loadability and transient stability of the power networks, SCTLs are widely used nowadays. Significant penetration of DG, especially wind power into the grid is a common practice to improve the reliability of the power system network. Power system is facing serious challenges due to the stochastic behaviour of wind energy. Incorporation of DG units changes the behaviour of protective devices. In this context, accurate, efficient and fast response protection scheme is necessary to detect any abnormal or faulty condition in the power network.

In the fault diagnosis approach, WT is one of the most common and efficient tools. A wavelet-alienation-based algorithm has been used in [8] to identify, classify, and estimate the location of faults in uncompensated transmission line. Alienation coefficients of both end current signals (quarter-cycle) have been utilized to detect and classify faults in the transmission lines. In addition, to estimate the fault locations, approximation coefficients of voltage and current samples have been fed to ANN. To estimate the fault position for ground and non-ground faults, two distinct ANNs have been employed, which increases the computation complexity. The performance of the differential protection schemes is affected by distributed capacitance current and CT saturation [99]. Differential protection method that depends on the equivalent travelling waves and WT can be applied to differentiate internal and external faults in transmission lines.

HIF in transmission line causes safety hazards for human being and also leads to the risk of fire hazards. Thus fast detection and classification of HIF are very important. Methods like Mathematical morphology, Evidential reasoning, DWT and DWT combined with FIS have been widely used for HIF identification and classification in DS [63, 52, 54, and 56]. CT saturation and CVT transient effects have not been addressed in the MM-based HIF detection and classification method in [63], despite the fact that it employed both current and voltage signals in the protection technique. The authors in [52 and 54] only detected HIF in DS, but not identified the faulty phase/s. The authors in [106] proposed a PMU-based backup protection technique that utilizes only the voltage magnitudes as input. This protection technique detects faults, faulted feeder and also analyzes the protection performance of the circuit breakers. Though the performance of this scheme has been validated on the IEEE 14-bus system, this technique has not addressed close-in faults as it used only magnitudes of voltage signals. In [62], a fault zone

detection and fault position estimation algorithm for three-terminal transmission lines has been proposed, which used time-synchronized current and voltage samples.

To eliminate errors caused by synchronized measurement, a method has been developed in [43] to detect the fault location utilizing fault current and pre-fault voltage phasors from one end of the line. Though this approach performs satisfactorily on the IEEE 118-bus system, the main issue is that it requires pre-fault data to estimate the fault position. The authors in [38] developed a method for fault location in multi-terminal DCTL that makes the use of the negative sequence component of current signals. Signals have been recorded at the relay point in this proposed approach. The fundamental issue with DCTL is the effect of mutual coupling between neighboring circuits of the line. To mitigate this issue, Nemati et al. proposed a fault location scheme based on negative-sequence current and voltage components in [85]. Even though this approach employs voltage components, its efficiency has not been examined during close-in fault conditions and it only considered LIF.

In recent years, SCTLs have been used to maximize power transmission capacity, minimize voltage drop, and improve the flexibility of power flow management. The authors in [69] have proposed a WT and ANFIS based algorithm for identifying, classifying, and determining the fault position in SCTLs. In [73], the authors suggested a DWT and DNN based approach for SCTLs to estimate the fault position. Four different methods for faulty zone detection in SCTLs have been described in [66]. This scheme utilized the dc components of current and voltage, instantaneous current and instantaneous power to identify the fault zone. Undecimated WT and Chebyshev neural network-based scheme to identify fault zones in SCTLs has been introduced in [70]. A protection technique using DWT and ANN has been developed to estimate the location of multi-location faults without classifying the faults in [72]. Sometimes, sudden changes in load cause power swing in the power network resulting in mal-operation of protection devices in the system. To ensure better performance of the protecting devices, a sequence-spaced-aided SVM classifier has been utilized in [95] for disturbance detection in SCTL.

The authors in [81] presented a fault classification technique for SCTL based on DT and FDOST. In this approach, FDOST coefficients have been derived from both voltage and current data and then fed into DT for classifying the faults. The WSCC-9 bus test system has been used to validate this approach. But the accuracy of fault localization in the presence of DG has not been investigated. Also, the use of DT increases the execution effort and time. More computationally intensive tools are necessary as the complexities of the interactions between the input and output features of the protection techniques increase. DNNs have intelligent architecture that outperform traditional neural networks when it comes to dealing with complex input-output relationships. The authors of [74] utilized DWT and DNN to develop a transmission line protection approach for shunt compensated transmission line in the presence of STATCOM. The authors in [8 and 85, 56, 62, 43 and 74, 69, 73, 81] employed ANN, fuzzy-based methodology, ANFIS, DNN, Chebyshev neural network, SVM classifier, and DT respectively, for power system protection which take much time for training and testing process and hence

may not yield satisfactory results in real-time operations that demand rapid response for digital relay operations.

A communication-aided technique for detecting and locating faults in a TCSC compensated transmission lines has been developed in [87]. Although this approach used synchronized measurements of current signals, it did not address the issue of CT saturation. Another technique for estimating fault position using the FDOST and Gaussian Process Regression for UPFC compensated long transmission line has been described in [82]. In this case, Gaussian process regression is employed to reduce the dimension of the FDOST-extracted voltage signal characteristics. Although it uses voltage signals, this technique did not address the close-in fault state, and its reliability has not been assessed in the presence of DG system.

One of the major drawbacks of the SCTL is that the positive-sequence line-impedance of the fault path gets changed due to the presence of a compensator, causing the directional relay to malfunction. To address this issue, the authors in [93] reported a mutual impedance-based protection scheme. In this scheme, the impedance between the fault position and the relay point of the transmission line phases is determined using the currents and voltages of both terminals of transmission line. Only single-phase to-ground and double-phase-to-ground faults are reliably protected by the proposed approach. A new positive-sequence-based directional relaying algorithm has been proposed in [85] to solve the inversion problems of voltage and current in SCTLs. However, system oscillations influence the positive-sequence components in directional relaying techniques. The authors in [75] have developed a time–frequency-based real-time differential protection technique for shunt compensated transmission line where Hilbert Huang transform algorithm has been employed. To detect and identify the faulty phase in transmission line, the integrated moving sum approach has been used in [102]. This approach is equally useful in SCTL, but some misclassification occurs during CT saturation.

A sequence-component-based protection technique for UPFC compensated transmission line has been presented in [84]. Complex power has been used to differentiate internal and external faults. This approach determines the fault location using both the positive and negative-sequence components of the signals. In [96], a negative-sequence current component-based protection approach for UPFC compensated DCTL has been described. However, both these techniques [84 and 96] cannot estimate fault location in the case of symmetrical faults. To circumvent the disadvantages of impedance-based systems, the authors in [86] developed a fault location technique for SCDCTL using KVL in the negative sequence circuit of SCDCTL. Despite its high accuracy, this technique fails to account for the HIF in the system. The authors in [88] developed a method for detecting, classifying, and identifying the fault location in series compensated transmission line. Only current data at the relay point is required for this method. The reverse synchronous reference frame approach has been used to identify and classify faults. The symmetrical components of current signals have been used to pinpoint the location of the fault. But the effect of the existence of DG in the system has not been considered. Because of its long life, low cost, and ease of maintenance, series capacitor banks are used in transmission line for compensating the line. For single circuit SCTL and SCDCTL, a new fault location technique based on sequence network modeling has been proposed in [89].

The operational behavior of the power system network changes when DG is connected with the network. Therefore, traditional protection schemes are unable to identify and classify the faults in the DG-connected systems. A novel adaptive wind farm collector line protection technique employing the phase angle difference between the zero-sequence current and the fault current at the relaying point has been developed in [119]. This scheme is applicable for low fault resistance up to 30 Ω only. In presence of DGs, the authors in [118] described a new approach for identifying, classifying, and locating faults in distribution lines. For this purpose, the proposed scheme made use of fuzzy logic and wavelet singular entropy. WT-ANN-based algorithm has been proposed in [120] for detecting single phasing condition in the transmission line connected to wind farm. The main disadvantage of power system protection methods based on fuzzy logic and ANN [118 and 120] is that they involve a large amount of training data, which increases the computation complexity and time. In [117], a new method has been developed for TCSC compensated transmission line in presence of wind farm to detect and locate faults. This proposed technique used travelling wave and FDST. But the error caused by synchronization delay has not been addressed. Power differential scheme has been described in [101] to detect and classify HIF in UPFC compensated transmission line under dynamic situations. Though the power differential concept gives accurate results for compensated transmission line, it fails to segregate internal and external faults in presence of DG.

This chapter aims to develop an efficient and reliable back up protection technique for SCTL connected with wind farm. Internal faults are separated from external ones using the positive-sequence component of current, whereas DP is considered for classifying the faults. Time-synchronized current and voltage samples from both ends of the transmission lineare used to classify faults. The key advantage of this algorithm is minimal calculation involved and nominal computational burden as no transform based technique is used. Moreover, the proposed scheme can detect close-in faults correctly as it does not require any voltage signal to detect fault and the voltage signal falsely collapses to zero value for close-in faults. As this scheme uses the phase angle difference between positive-sequence current only, it can detect all types of faults. Its performance is satisfactory under different dynamic and stressed situations such as change in compensation level and compensator position, non-linear HIF, source strength and load angle variation and also change in the direction of power flow. It has been shown that this scheme can efficiently detect and classify faults in islanded mode of operation of the transmission line. The proposed backup protection scheme is accurate under varying FR, fault location, FIA, compensation level, pre-fault transfer angle, source capacity and also wind-speed.

6.2. Proposed Algorithm

SCTL creates several problems to fault protection techniques due to the non-linear behaviour of the inserted capacitor into the line. Many efforts have been attempted to propose protective schemes for SCTL using voltage-current phasors. But these techniques find limitations when the line incorporates DG units to increase the stability and reliability of power transmission system. A series compensated long transmission line fed at both ends by sources E_1 and E_2 as shown in Fig. 6.1 has been considered to develop the protective scheme in this chapter.

R_1 and R_2 relays are mounted on buses S and R respectively. If a fault occurs in section L_1, it is considered as an internal fault (F_x), otherwise external fault (F_y). Section L_1 contains the series compensation unit whose position may be altered within the section.

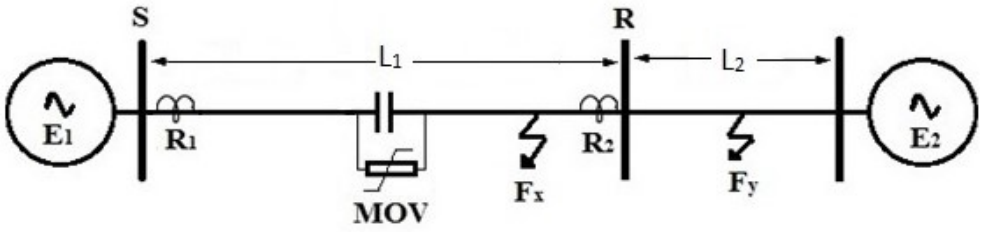

Fig. 6.1. Transmission line system model

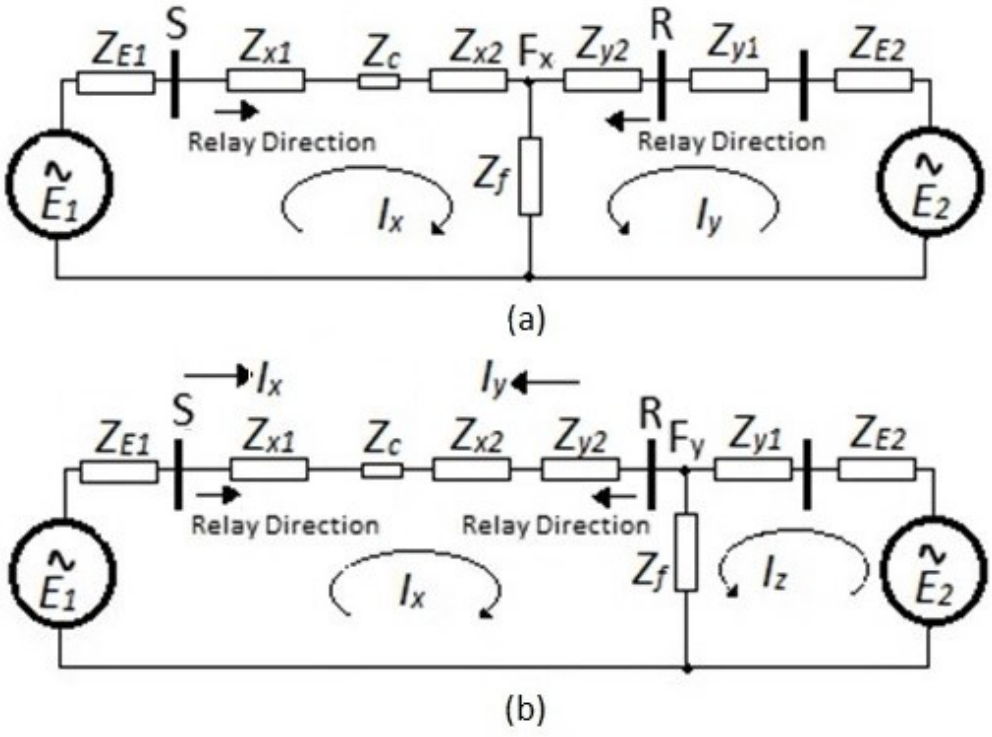

Fig. 6.2. Sequence circuit diagram
(a) For internal fault (b) For external fault

Fig. 6.2 shows the sequence diagram when fault occurs at F_x (internal fault) and F_y (external fault). I_x, I_y and I_z are the positive-sequence components of the currents flowing in the different sections of the line during internal and external fault.

From Fig. 6.2(a), the voltage-current relationship for an internal fault can be expressed as

$$E_1 - I_x(Z_x + Z_f) - I_y Z_f = 0 \tag{6.1}$$

$$E_1 - I_x Z'_{E1} - I_y Z_f = 0 \tag{6.2}$$

$$E_2 - I_y(Z_y + Z_f) - I_x Z_f = 0 \tag{6.3}$$

or,

$$E_2 - I_y Z'_{E2} - I_x Z_f = 0 \tag{6.4}$$

where,

$Z_x = Z_{E1} + Z_{x1} + Z_{x2} + Z_c$, $Z_y = Z_{E2} + Z_{y1} + Z_{y2}$, $Z'_{E1} = Z_x + Z_f$ and $Z'_{E2} = Z_y + Z_f$

Solving Eq. 6.2 and Eq. 6.4

$$I_x = \frac{E_1 Z'_{E2}}{Z'_{E1} Z'_{E2} - Z_f^2} - \frac{E_2 Z_f}{Z'_{E1} Z'_{E2} - Z_f^2} \tag{6.5}$$

$$I_y = \frac{E_2 Z'_{E1}}{Z'_{E1} Z'_{E2} - Z_f^2} - \frac{E_1 Z_f}{Z'_{E1} Z'_{E2} - Z_f^2} \tag{6.6}$$

or,

$$I_x = \frac{E_1}{K_1} - \frac{E_2}{K_2} = I_1 - I_2 \tag{6.7}$$

$$I_y = \frac{E_2}{K'_2} - \frac{E_1}{K'_1} = I'_2 - I'_1 \tag{6.8}$$

where,

$$K_1 = \frac{Z'_{E1} Z'_{E2} - Z_f^2}{Z'_{E2}}, K_2 = \frac{Z'_{E1} Z'_{E2} - Z_f^2}{Z_f}, K'_1 = \frac{Z'_{E1} Z'_{E2} - Z_f^2}{Z_f} \text{ and } K'_2 = \frac{Z'_{E1} Z'_{E2} - Z_f^2}{Z'_{E1}}$$

Hence,

$$\frac{K_1}{K_2} = \frac{Z_f}{Z'_{E2}} \tag{6.9}$$

and

$$\frac{K'_1}{K'_2} = \frac{Z'_{E1}}{Z_f} \tag{6.10}$$

Therefore, for internal fault, as $Z'_{E2} > Z_f$, hence, $K_2 > K_1$ and $I_1 > I_2$. Again, as $Z'_{E1} > Z_f$, hence, $K'_1 > K'_2$ and $I'_2 > I'_1$.

Fig. 6.3(a) shows the different positive-sequence phasor positions of current I_x and I_y during fault at F_x. The voltage phasors E_1 and E_2 represent source voltages at the two ends. The phasor diagram illustrates that $\Delta\theta$, which is the ratio of angles θ_x and θ_y, is positive.

In the occurrence of an external fault, i.e. when the fault is detected at F_y, the positive-sequence fault currents measured by relays R_1 and R_2 are I_x and $-I_x$ respectively, and Fig. 6.2(b) is considered for obtaining the current I_x during an external fault.

$$E_1 - I_x\left(Z'_x\right) - I_z Z_f = 0 \tag{6.11}$$

$$E_2 - I_z\left(Z'_z\right) - I_x Z_f = 0 \tag{6.12}$$

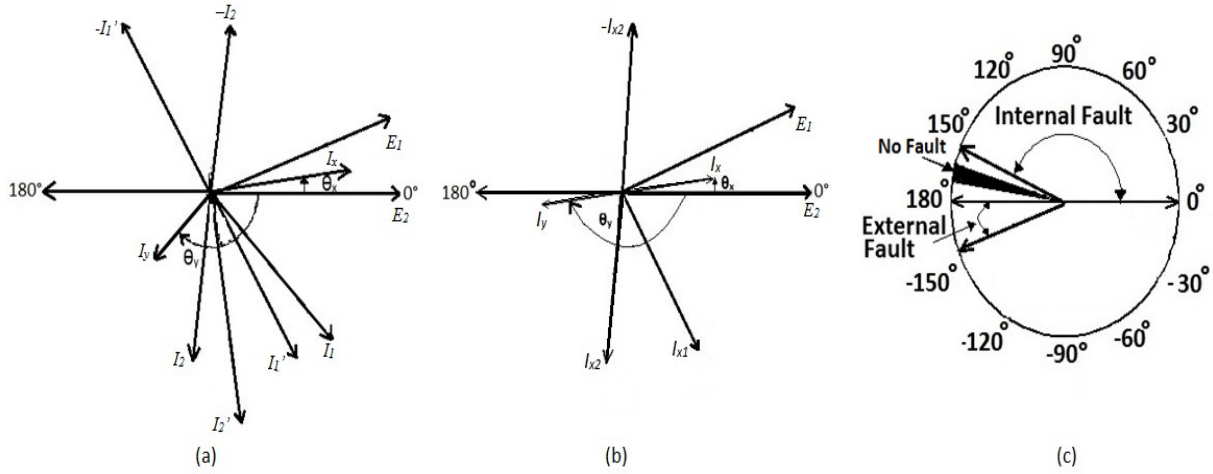

Fig. 6.3. Phasor diagram and variation of Δθ
(a) Phasor diagram of +ve sequence voltage and current during internal fault
(b) Phasor diagram of+ve sequence voltage and current during external fault
(c) Variation of Δθof +ve sequence currents for faultand no-fault conditions

where,

$$Z'_x = Z_{E1} + Z_{x1} + Z_{x2} + Z_{y2} + Z_c + Z_f \,,\; Z'_z = Z_{E2} + Z_{y1} + Z_f$$

From Eq. 11 and Eq. 12, it is found that

$$I_x = \frac{E_1 Z'_z}{Z'_x Z'_z - Z_f^2} - \frac{E_2 Z_f}{Z'_x Z'_z - Z_f^2} = \frac{E_1}{K_{x1}} - \frac{E_2}{K_{x2}} = I_{x1} - I_{x2} \tag{6.13}$$

where,

$$K_{x1} = \frac{Z'_x Z'_z - Z_f^2}{Z'_z} \text{ and } K_{x2} = \frac{Z'_x Z'_z - Z_f^2}{Z_f}.$$

Therefore, $\frac{K_{x1}}{K_{x2}} = \frac{Z_f}{Z_z}$

As $Z'_z > Z_f$, hence, $K_{x2} > K_{x1}$. Therefore, for this system it is seen that during external fault $I_{x1} > I_{x2}$. As seen in Fig. 6.2(b), the current I_y is almost 180° out of phase with the current I_x. The current phasors during an external fault are shown in Fig. 6.3(b), where it is seen that the phase angle ratio of θ_x and θ_y i.e. $\Delta\theta$ is close to 180º and lies in the third quadrant.

As a consequence, it is possible to say that during an internal fault $\Delta\theta$ is positive, and for an external fault, $\Delta\theta$ becomes negative. Fig. 6.3(c) shows the angular positions of $\Delta\theta$ for both internal and external faults along with the no-fault condition. The phase angle ratio of the positive-sequence fault currents I_x and I_y can be applied conveniently to segregate the internal and external faults.

The primary goal of this study is to differentiate internal faults from external ones utilizing the phase angle of positive-sequence phasor of fault currents. The positive-sequence component has the advantage that it reduces the effects of mutual coupling between two transmission lines. The ratio of the positive-sequence currents at the two ends of the transmission line is $A(\angle\theta_x - \angle\theta_y)$or $A\angle\Delta\theta$, where θ_x and θ_y are the positive-sequence phase angle of I_x and I_y and A is the ratio of the absolute values of I_x and I_y. The positive value of $\Delta\theta$ denotes an internal fault and negative value denotes an external fault and the shaded region in Fig. 6.3(c) represents the no-fault condition. The information from the positive-sequence component of the fault current signal alone is sufficient to detect the fault and fault zone in this scheme. The flowchart of the developed fault zone identification scheme is demonstrated in Fig. 6.4.

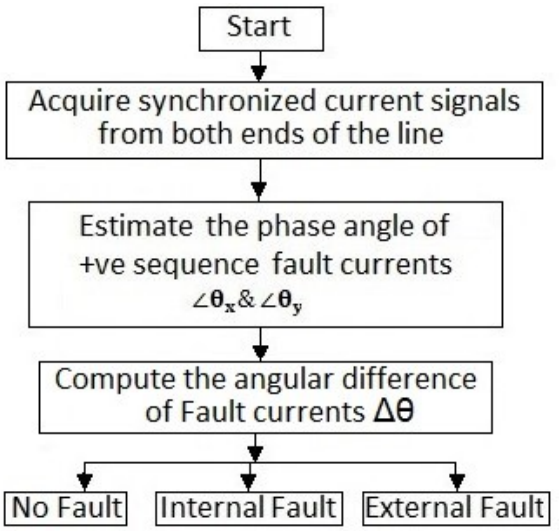

Fig. 6.4. Flowchart for fault-zone identification

After identification of faulty zone, the faulty phase detection has been done in next step considering the time-synchronized measurement of voltage and current samples from both the line terminals. The complex power for all phases are calculated individually at both ends of the

transmission line. The magnitude of DP as given in Eq. 6.14 is then used to classify faults by calculating the difference in complex power of two ends of the transmission line.

$$DP = \left| S_S - S_R \right| \tag{6.14}$$

where, the apparent powers at buses S and R are S_S and S_R respectively.

The phase with the highest DP is always faulty. The involvement of other phases in fault has been detected considering some threshold values. If the magnitude of the DP of all the phases is greater than ε_1, then the fault is three phase (LLL) fault. In the event of an unsymmetrical fault, the difference of the DP of the lower two values is calculated and if it is less than the predefined threshold value ε_2, then fault is SLG, otherwise LLG or LL fault. To discriminate between LLG and LL fault, zero sequence current may be calculated by adding three line currents at one end of the transmission line. If this zero-sequence current is large then it is LLG fault, otherwise LL fault. Fig. 6.5 depicts a fault classification flowchart for internal faults, where threshold ε_1 is twice the magnitude of DP of each phase under no-fault condition and ε_2 is same as the magnitude of DP of each phase under no-fault condition.

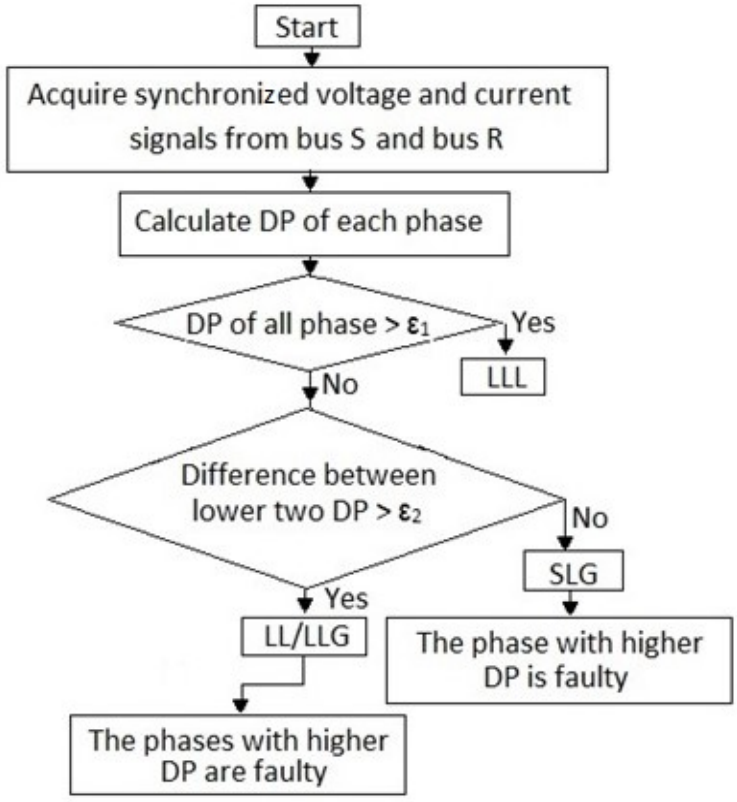

Fig. 6.5. Flowchart for fault classification

6.3. Power System Model

In this research work, the proposed scheme has been implemented using a system, modelled in Simpower system in Matlab environment. The test system model made up of two substations connected by three-phase 400 kV-50 Hz, 300 km multi-section transmission line is shown in Fig. 6.6.

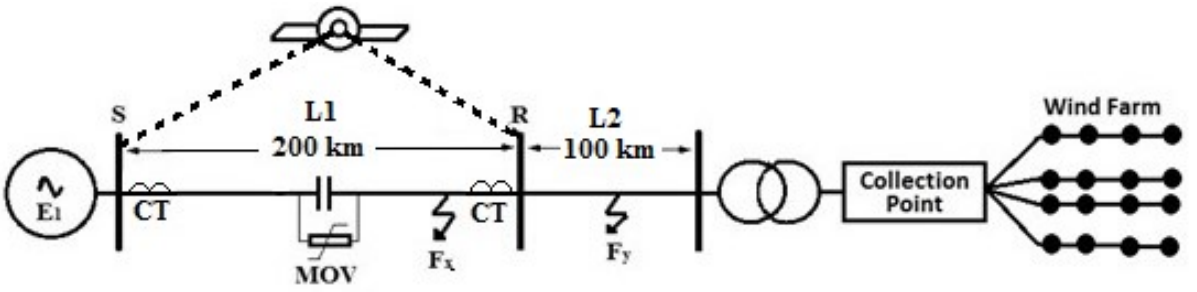

Fig. 6. 6. Series-compensated transmission line connected to wind farm

A three-phase capacitor bank with MOV compensator is placed at the middle section of the transmission line. The transmission line parameters are as follows:

Z_1=0.01273 + j 0.29318 (Ω/km): Positive-sequence impedance

Z_0=0.3864 + j 1.2956(Ω/km): Zero-sequence impedance

C_1=12.74×10^{-9} (F/km): Positive-sequence capacitance

C_0=7.751×10^{-9} (F/km): Zero-sequence capacitance

The source impedance of E_1, which is connected at substation 1, is 0.5333+ j5.333 Ω. Substation 2 is connected with the wind farm through a transformer. The wind farm is made up of 40 numbers of DFIG type wind turbines, each with a capacity of 1.5 MW. A total of 65,370 test cases have been created for analyzing the proposed methodology thoroughly.

6.4. Performance of the Proposed Technique

The system model as depicted in Fig. 6.6 is used to assess the proposed technique. The various kinds of faults viz. SLG, LLG, LL, and LLL have been simulated to investigate the efficiency of the developed scheme. In this chapter, faults have been simulated at various fault resistances (0 Ω to 200 Ω) at a wide range of fault inception angle (0° to 90°) at an interval of 10 km. The fault current data are acquired at a sampling frequency of 12.5 kHz (i.e. 250 samples/cycle) at 50 Hz supply frequency. In this scheme only post fault one cycle data samples are sufficient to segregate the external and internal faults and also to determine the faulty phase. To determine the robustness of this technique, compensation level of the transmission line has been varied from 30% to 70%. The angular position of Δθ is shown in Fig. 6.7, where Δθ is the

phase angle difference between positive-sequence fault currents I_x and I_y. From Fig. 6.7, it can be observed that in this test system, for internal fault Δθ varies from -15° to 165° and for external fault its value lies between -95° to -180°. For no fault condition Δθ varies from 174° to 177°.

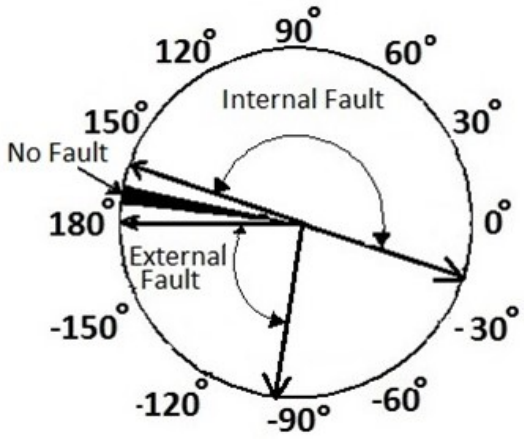

Fig. 6.7. Angular position of Δθ to distinguish the internal and external faults

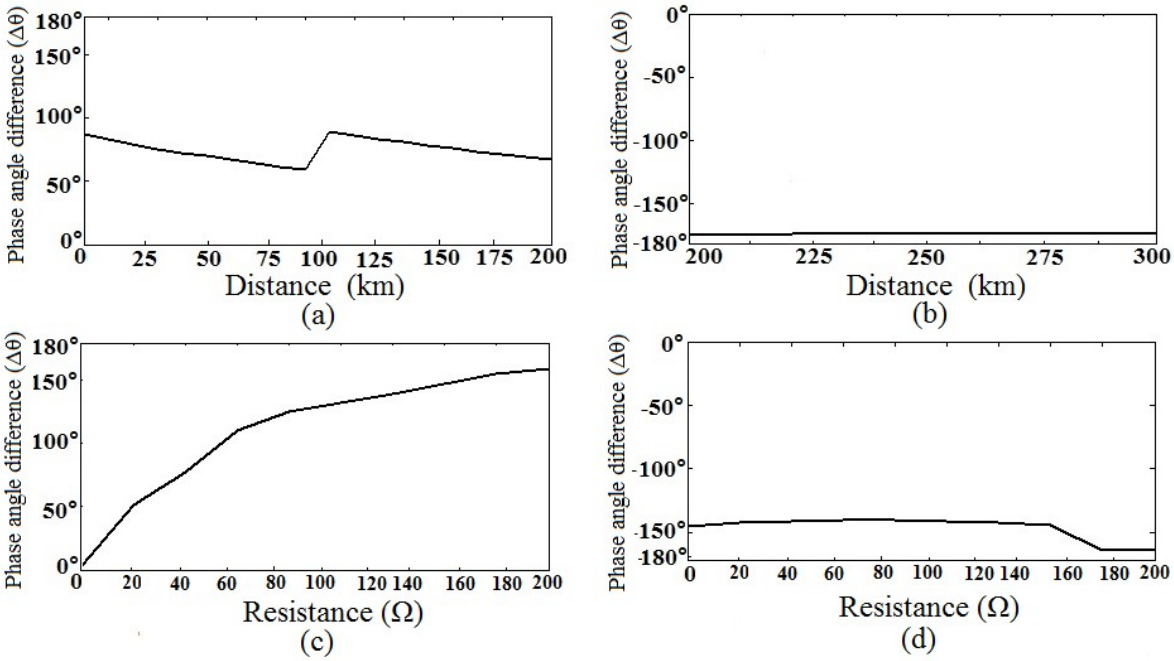

Fig. 6. 8. Variation of (Δθ) with fault location and FR
(a) Variation of (Δθ) with fault location during internal fault
(b) Variation of (Δθ) with fault location during external fault
(c) Variation of (Δθ) with fault resistance during internal fault (at 50 km)
(d) Variation of (Δθ) with fault resistance during external fault (at 250 km)

To assess the authenticity of the proposed method, faults are simulated at different positions in the transmission line. Figs. 6.8(a) and (b) demonstrate the results of the developed scheme at various fault locations along L_1 and L_2 when LLAB fault occurs with FR of 50 Ω and FIA of 0°. In this case, simulation is done considering that the line is 30% compensated. It is found that $\Delta\theta$ is positive when a fault is detected in line L_1 up to 200 km i.e. internal fault and $\Delta\theta$ is negative when the fault is detected in line L_2 between 200 km and 300 km i.e. external fault.

Table 6.1. Performance of proposed method during different fault type

Fault position	Fault type	FIA (°)	FR (Ω)	θ_x (°)	θ_y (°)	$\Delta\theta$ (°)	Differential power (VA)×10^8		
							Phase A	Phase B	Phase C
Internal fault (10 km)	AG	90	200	59.2	-67.34	126.54	4.31	0.818	0.870
	ABG	90	200	37.9	-67.21	105.11	4.27	4.88	0.837
	AB	90	200	49.2	-64.4	113.6	4.89	3.26	0.862
	ABC	90	200	30.53	-67.34	97.87	4.66	4.83	4.68
Internal fault (70 km)	AG	0	0	-42.4	-65.86	23.46	19.8	0.686	0.634
	ABG	0	0	-62.65	-62.15	-0.5	32.7	29.6	0.692
	AB	0	0	-64.6	-62.9	-1.7	314	31.2	0.858
	ABC	0	0	-64.14	-60.65	-3.49	33.7	32.7	31.1
Internal fault (110 km)	AG	0	200	58.12	-69	127.12	4.17	0.783	0.925
	ABG	0	200	40	-68.9	108.9	4.29	4.52	0.802
	AB	0	200	47.5	-68.6	116.1	4.75	3.16	0.816
	ABC	0	200	33.8	-69.6	103.4	4.72	4.56	4.63
Internal fault (190 km)	AG	45	0	-28	-66.07	38.07	9.64	0.557	0.584
	ABG	45	0	-39.18	-57.45	18.27	18.3	15.7	0.667
	AB	45	0	-40.125	-58.25	18.125	17.3	15.8	0.863
	ABC	45	0	-33.19	-58.9	25.71	21.6	15.8	22.2
External fault (220 km)	AG	0	0	-9	157.5	-166.5	-	-	-
	ABG	0	0	37.83	140.72	-102.89	-	-	-
	AB	0	0	-38.07	140.5	-178.57	-	-	-
	ABC	0	0	-35.05	144.35	-179.4	-	-	-
External Fault (270 km)	AG	45	200	65	-156.28	-138.72	-	-	-
	ABG	45	200	34.1	-163.74	-162.16	-		-
	AB	45	200	-38.73	140	-178.73	-	-	-
	ABC	45	200	22.72	-167	-170.28	-	-	-

Fault resistance, which modulates the phase angle of the fault current, has an impact on the performance of the developed method. Therefore, the effect of FR is investigated to validate the developed method. Figs. 6.8(c) and (d) show the variation of $\Delta\theta$ of positive-sequence fault currents with the variation of FR for both internal and external faults. Figs. 6.8(c) and (d) are obtained by variation of FR from 0 Ω to 200 Ω when LLGAB fault occurs at FIA of 90° and the transmission line is 30% compensated. Figs. 6.8(c) and (d) demonstrate that in both situations

i.e. for internal and external fault, with the change in FR, the variation of Δθ is within the limit as described earlier. It is noticed that Δθ can clearly distinguish the internal and external faults. For other types of faults also, similar results can be achieved. As a result, the developed technique is immune to FR.

As mentioned earlier, the developed method has been simulated for all types of faults. Therefore, to verify the applicability of the designed algorithm, all ten types of faults have been generated under variable conditions. Table 6.1 provides the simulated results of this proposed technique for various types of faults when the transmission line is 30% compensated. It has been shown that internal faults have a positive phase angle difference (Δθ) of positive-sequence fault currents, while external faults have a negative phase angle difference (Δθ) of the same. The DPs for the three phases are also presented which reveal that the type of fault can easily be identified from these values. The threshold value for ε_2 has been considered as 0.9×10^8 for this system.

6.5. Evaluation of Proposed Technique

6.5.1. Close-in-Fault

Close-in fault is complicated to detect using the voltage signal as the voltage falsely collapses to zero value near the relay bus. The directional relaying algorithm is also affected by the presence of transients in the CCVTs. The voltage signal does not influence the fault zone

Table 6.2. Result for close in fault

	Fault location (km)	FR (Ω)	FIA (°)	Compensation level	Δθ(°)	Differential power		
						Phase A	Phase B	Phase C
Internal Fault	5	0	0	30%	3.14	35.1	33.7	31.2
	5	200	0	30%	102.27	4.83	4.76	4.81
	195	0	0	30%	30.05	23.2	19.7	16.3
	195	200	0	30%	96.6	4.61	4.25	4.51
	5	0	0	70%	25.2	35.1	33.9	31.1
	5	200	0	70%	103.77	5.33	5.18	5.11
	195	0	0	70%	58.58	19.5	15.8	21.8
	195	200	0	70%	115.2	4.67	4.69	4.84
External Fault	205	0	0	30%	-179	-	-	-
	205	200	0	30%	-170.7	-	-	-
	295	0	0	30%	-178.4	-	-	-
	295	200	0	30%	-170.84	-		-
	205	0	0	70%	-179.55	-	-	-
	205	200	0	70%	-170.8	-	-	-
	295	0	0	70%	-179.23	-	-	-
	295	200	0	70%	-170.03	-	-	-

identification algorithm in this research work. As a consequence, the accuracy of the developed protection system is unaffected during close-in faults. To demonstrate the efficacy of the developed method during close-in fault, a LLL fault has been generated in the lines $L_1$and L_2 as shown in Fig. 6.6, near the relay buses S and R and also close to the wind farm. Fig. 6.7 shows the angular position of θ_x and θ_y for internal and external faults. It is clear from Table 6.2 that this approach can accurately distinguish the internal and external faults under close-in fault situation. Table 6.2 shows the results when faults occur at inception angle of 0° with FR of 0 Ω and 200 Ω only. This method identifies the fault zone efficiently at all FIA and FR. The DP of each phase is also presented which shows the fault classification capability of the proposed scheme in close-in fault conditions.

6.5.2. Change in Compensation Level

Table 6.3. Performance of the proposed method for different compensator location and percentage of compensation level

	Compensator position	% compensation level	Δθ(°)	Differential power (VA)×10^8		
				Phase A	Phase B	Phase C
Internal fault (110 km)	Front End	30	127.32	3.75	0.75	0.87
		50	130.9	3.73	0.76	0.87
		70	134.3	4.04	0.81	0.82
	Middle	30	127.6	3.83	0.75	0.88
		50	131.35	3.9	0.78	0.89
		70	114.25	4.33	0.87	0.85
	Rear End	30	123.5	3.7	0.74	0.97
		50	125	3.72	0.75	0.89
		70	71	4.1	0.82	0.82
External fault (270km)	Front End	30	-138.62	-	-	-
		50	-141.71	-	-	-
		70	-137.46	-	-	-
	Middle	30	-138.73	-	-	-
		50	-141.92	-	-	-
		70	-134.3	-	-	-
	Rear End	30	-139.04	-	-	-
		50	-142.62	-	-	-
		70	-130.6	-	-	-

Degree of compensation is an important factor that may influence the performance of the protection schemes. Due to this reason, the proposed method is assessed under various levels of compensation of the compensator. In this chapter, the degree of compensation isvaried from 30% to 70% and some results of SLGA fault at various distances are given in Table 6.3. In this

case, simulation is done by considering FR of 200 Ω and FIA of 45°. The obtained results validate the proposed logic and can accurately distinguish internal and external faults with varying compensation levels and from the magnitudes of DP the type of fault can be identified.

6.5.3. Effect of Compensator Position

To verify the authenticity and efficiency of the developed protection algorithm, investigations have been made on the effects of the compensator position. Initially, simulations have been done considering the mid-point position of the compensator. The effect of the proposed method with the change in compensator position has been studied by positioning the compensator at the front-end and rear-end of the line. For this purpose, SLGA faults with FR of 200 Ω and FIA of 45° are considered and Table 6.3 displays the results.

6.5.4. Effect of Wind Speed Variation

Table 6.4. Performance of the developed method with variation of wind speed

	Fault location (km)	Wind speed (km/hr)	Δθ(°)	Differential power (VA)×10^8		
				Phase A	Phase B	Phase C
Internal Fault	10	5	127.7	4.68	0.82	0.79
	10	10	109.8	4.56	0.79	0.85
	10	15	88.98	4.53	0.75	0.79
	10	20	87.93	4.36	0.75	0.76
	180	5	127.7	3.2	0.66	0.87
	180	10	109.0	3.12	0.67	0.84
	180	15	87.45	3.08	0.67	0.79
	180	20	86.21	2.89	0.66	0.76
External Fault	270	5	-177.8	-	-	-
	270	10	-176.1	-	-	-
	270	15	-175	-	-	-
	270	20	-174	-		-

The amount of electricity produced by a wind turbine is primarily determined by the wind speed. The proposed technique has also been tested to verify the effects of variation of wind speed. Table 6.4 shows the impact of varying wind speeds ranging from 5 km/hr to 20 km/hr. In this case, again SLGA faults with FR of 200 Ω at FIA of 45° are considered for simulation purpose when transmission line is 30% compensated. From Table 6.4, it is found that the values

of Δθ for different wind speeds lie within the pre-established limit which can accurately identify the internal and external faults. Also, the magnitudes of DP can identify the type of fault.

6.5.5. Effect of Non-Linear HIF

HIF develops when energized electrical conductor makes contact with the ground substance or third-party objects, HIF model shown in Fig. 6.9 is used in this research work. R_p and R_n are the two fault resistances in this HIF model. Unequal fault resistances can be used to model the asymmetric fault currents. The inception voltage between the transmission line and third-party objects is represented by two DC voltage sources, V_p and V_n. As V_p is less than phase voltage, fault current flows towards the ground and current flows in the reverse direction when V_n is higher than phase voltage.

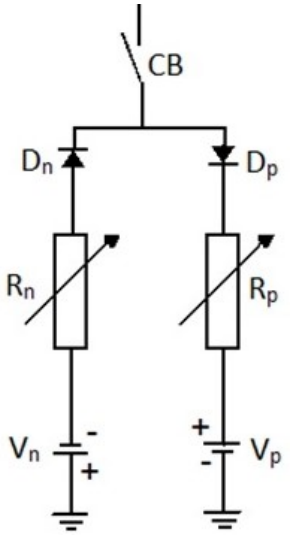

Fig. 6.9. Single line diagram of HIF model

Fig. 6.10(a) and Fig. 6.10(b) show the variation of phase angle difference (Δθ) with different fault locations for two different HIF model parameters. The figures prove that when HIF occurs, the proposed technique correctly identifies the internal and external faults. To validate the efficacy of the developed algorithm during HIF (R_n = 212 Ω, R_p = 208 Ω, V_n = 3847 V, and V_p = 3588V), SLGA has been generated with FIA 90° when the transmission line is 30% compensated and the results are shown in Table 6.5. Thus it is seen that this technique is able to identify the fault zone and faulty phase when non-linear HIF occurs in the transmission line.

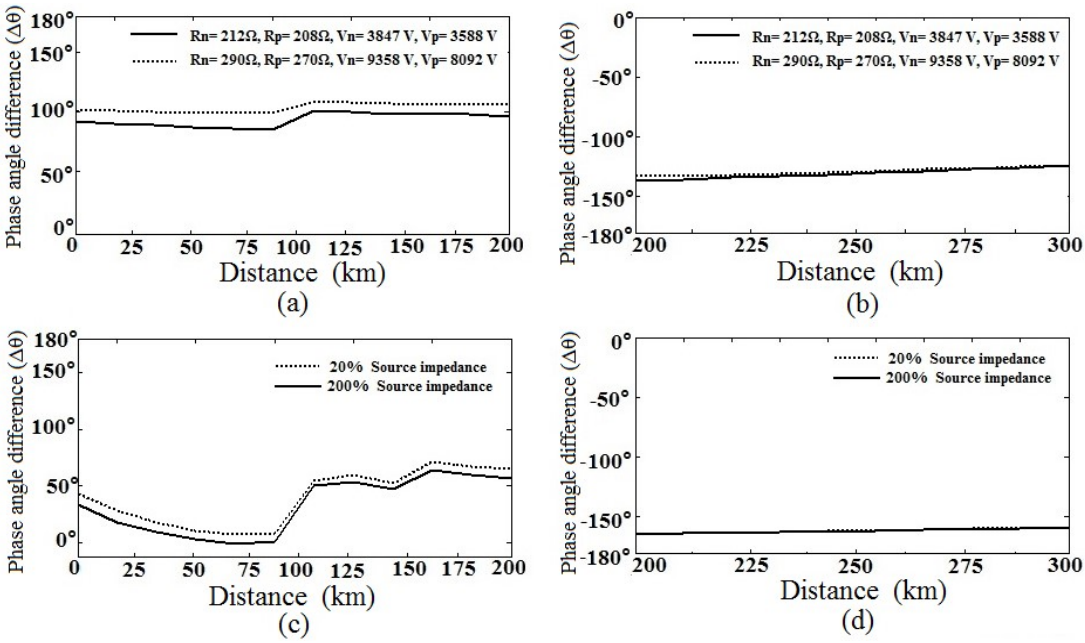

Fig. 6.10. Phase difference Δθ for SLGA fault under HIF and variation of source impedance at different locations for FIA 45° when the line is 70% compensated

(a) Internal fault during HIF (b) External fault during HIF (c) Internal fault with variation of source impedances (d) External fault with variation of source impedances

Table 6.5. Fault classification in case of non-linear HIF and varying source strength

Condition		Fault location (km)	Δθ(°)	Differential power (VA)×10^8		
				Phase A	Phase B	Phase C
HIF		Internal fault (10 km)	130.23	4.43	0.85	0.87
		Internal fault (190 km)	130.4	3.01	0.68	0.87
		External fault (280 km)	-146.34	-	-	-
Source strength	20%	Internal fault (90 km)	121.2	3.59	0.73	0.78
		External fault (280 km)	-137.92	-	-	-
	100%	Internal fault (90 km)	123.22	3.6	0.74	0.78
		External fault (280 km)	-137.97	-	-	-
	200%	Internal fault (90 km)	123.62	3.58	0.74	0.78
		External fault (280 km)	-137.9	-	-	-

6.5.6. Effect of Change in Source Capacity

Fault currents are also affected by the power system generation capacity. Hence, the authors have considered the effects of change in source impedance by adjusting the source impedance of the source E_1 from 20% to 200% to test the reliability of this method. Under this condition, SLGA fault has been simulated with FR of 200 Ω and FIA of 45°, and the graphical results are shown in Fig. 6.10(c) and Fig. 6.10(d). It is seen that the proposed technique is efficient in distinguishing the internal and external faults under varying source capacity. Table 6.5 also shows the fault classification capability of the proposed method for change in source capacity when SLGA fault occurs at 90 km and 280 km.

6.5.7. Effect of Time Synchronization Error

Any delay in obtaining data samples (voltage and current) from buses S and R would reduce the precision of the proposed algorithm. Hence, the impact of various time synchronizing delays have been evaluated. In this case, the authors have applied a delay in receiving the remote end data samples. To validate the proposed method, 2, 4, 6, 8 and 10 ms synchronizing time delay has been applied to the system. To study the impact of synchronization delay on the developed protection scheme, an SLGA fault has been generated at 90 km (internal fault) and 280 km (external fault) with FR of 200 Ω and FIA of 45°. Table 6.6 shows the results of the effect of time delay on this method. This technique is unaffected by the time synchronizing delay/ error, as seen in Table 6.6.

Table 6.6. Performance of the proposed method with synchronizing time delay and variation of pre-fault transfer angle

		Time synchronizing error (ms)					Pre-fault loading angle		
		2	4	6	8	10	10°	20°	30°
Δθ(°)	Internal Fault	124.3	122.8	123.7	123.9	123.2	122.5	123.2	124.15
	External Fault	-138.3	-136.3	-134.5	-134.4	-133.8	-138.4	-138.04	-138.4
DP (VA) $\times 10^8$	Phase A	4.02	3.38	4.02	3.82	3.85	3.97	3.91	3.83
	Phase B	0.97	0.72	1.02	0.79	0.76	0.77	0.76	0.77
	Phase C	1.19	0.96	1.10	0.89	0.91	0.89	0.88	0.88

6.5.8. Effect of variation of Pre-Fault Power Transfer Angle

The pre-fault loading conditions have been altered by changing the pre-fault loading angle from 10° to 30° to examine the efficiency of the developed algorithm. Table 6.6 represents the

test results. All kinds of faults have been simulated at various pre-fault conditions and it has been noticed that the developed approach distinguishes between internal and external faults correctly. Simulation results of SLGA fault at FR 200 Ω and FIA of 45° are illustrated in Table 6.6.

6.5.9. Capacitor Self-Protection with MOV

Over voltage protection is a major factor in the design and use of series capacitors. MOV replaces the typical gap type design in modern power systems, which bypasses the series capacitor to prevent over voltage. In normal situations, the MOV provides high resistance and current flows through the capacitor; but, when high voltages appear across the capacitor during faults, the MOV provides a low resistance path to divert a part of the fault current away from the capacitor. The protection level of the MOV is normally set higher than the highest voltage predicted during power swing or overload scenario, so it only conducts when there is a fault.

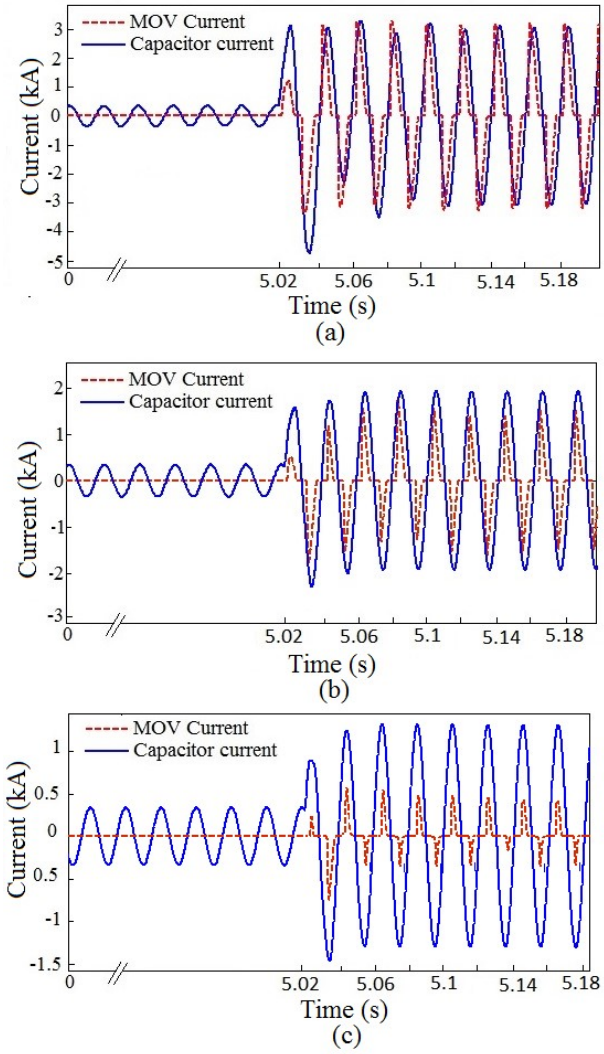

Fig. 6.11. Currents in capacitor and MOV when the capacitor is self protected with MOV (a) High fault current (b) Moderate fault current (c) Low value of fault current.

There are three possible ways for current to pass through the MOV and capacitor depending upon the severity of the fault. Fig. 6.11 depicts these three scenarios when SLGA fault occurs at 180 km from bus 1 with FIA 0° and when the transmission line is 30% compensated. As illustrated in Fig. 6.11(a), when the fault current is significantly high with FR of 0 Ω, the MOV begins conducting a maximum amount of fault current after the occurrence of fault. Both the MOV and the capacitor carry fault current for a moderate fault current with FR of 100 Ω until the MOV absorbed energy reaches its limit, as illustrated in Fig. 6.11(b). As seen in Fig.6.11(c), the MOV conducts very less amount of fault with FR of 200 Ω, and the fault current passes mainly through the capacitor. Table 6.7 shows the performance results of the proposed scheme when the capacitor is self-protected with MOV and it is observed that this algorithm can detect the internal and external fault and also identify the faulty phase/s.

Table 6.7. Performance results when the capacitor is self protected with MOV

	Fault location (km)	Type of fault	FR (Ω)	FIA (°)	Compensation level	Δθ(°)	Differential power		
							Phase A	Phase B	Phase C
Internal Fault	50	AG	0	45	30%	10.75	24.9	0.69	0.72
	50	ABG	0	45	30%	-3	38.5	33.4	0.71
	50	AB	0	45	30%	-4.98	36.2	36.5	0.86
	50	ABC	0	45	30%	-2.2	40.3	37.2	39.4
	180	AG	200	0	70%	124.1	4.04	0.90	0.83
	180	ABG	200	0	70%	115.8	4.11	4.67	0.83
	180	AB	200	0	70%	118.75	4.6	3.47	0.85
	180	ABC	200	0	70%	116	4.79	4.75	4.88
External Fault	230	AG	200	90	30%	-165.94	-	-	-
	230	ABG	200	90	30%	-178.87	-	-	-
	230	AB	200	90	30%	-178.8	-	-	-
	230	ABC	200	90	30%	-179	-	-	-
	290	AG	0	0	70%	-139.86	-	-	-
	290	ABG	0	0	70%	-162.36	-	-	-
	290	AB	0	0	70%	-159.24	-	-	-
	290	ABC	0	0	70%	-170.8	-	-	-

6.5.10. Effect of Change in Direction of Power Flow

To ascertain the applicability of the proposed scheme under change in direction of power flow, the number of wind turbines has been decreased to 30. SLGA faults have been created at different locations on the transmission line at various FR, FIA, and different compensation levels

to evaluate the efficacy of the proposed technique under the reverse direction of power flow. Table 6.8 shows the performance of the proposed scheme for change in direction of power flow in the system. It can be observed that the proposed technique remains unaffected by the reverse power flow and it can efficiently discriminate the internal and external faults with proper fault classification.

Table 6.8. Performance of the proposed method for reverse direction of power flow and islanding mode of operation

Condition	Fault location (km)	FR (Ω)	FIA (°)	Compensation level	Δθ(°)	Differential power (VA)×10^8		
						Phase A	Phase B	Phase C
Reverse direction of power flow	Internal fault (10)	0	45°	30%	-2.95	52.2	0.762	0.76
	Internal fault (160)	0	45°	30%	27.5	11.6	0.576	0.632
	Internal fault (70)	100	0°	70%	66.95	8.2	0.82	0.89
	Internal fault (190)	100	0°	70%	81.8	5.91	0.77	0.89
	External fault (220)	0	45°	30%	-177.39	-	-	-
	External fault (270)	100	0°	70%	-158	-	-	-
Islanding mode	Internal fault (10)	0	45°	30%	97.4	5.05	0.19	0.0629
	Internal fault (160)	0	45°	30%	-12.27	0.91	0.087	0.16
	Internal fault (70)	100	0°	70%	100	0.69	0.119	0.29
	Internal fault (190)	100	0°	70%	81.64	0.35	0.11	0.07
	External fault (220)	0	45°	30%	-100.09	-	-	-
	External fault (270)	100	0°	70%	-102.31	-	-	-

6.5.11. Effect of Islanding Mode of Operation

Islanding occurs when the load of a large distribution system loses grid power and is exclusively fed by the DG system i.e. the load is electrically secluded from the grid. When this happens, the system voltage and frequency are no longer within control, which implies that they

may be over their normal limits, inflicting substantial and catastrophic damage to the equipment, devices, and gadgets linked to the system. The proposed scheme has been implemented for faults at various positions of the transmission line under varying FR, FIA, and compensation levels in islanding mode of operation. The results of SLGA faults have been presented in Table 6.8, which demonstrate the satisfactory performance of the proposed scheme under islanding mode of operation.

6.5.12. Effect of CT Saturation

To investigate the effect of CT saturation, the current in bus S and bus R is measured using CTs rated 2000A/5A, 30VA. The CT parameters have been considered to be same as provided in Ref. [101]. Fig. 6.12 shows the three-phase current waveform with CT saturation for the test system shown in Fig. 6.6 when the transmission line is 70% compensated. Results of SLGA fault at various distances are given in Table 6.9 and it reveals that the proposed logic remains unaffected by CT saturation.

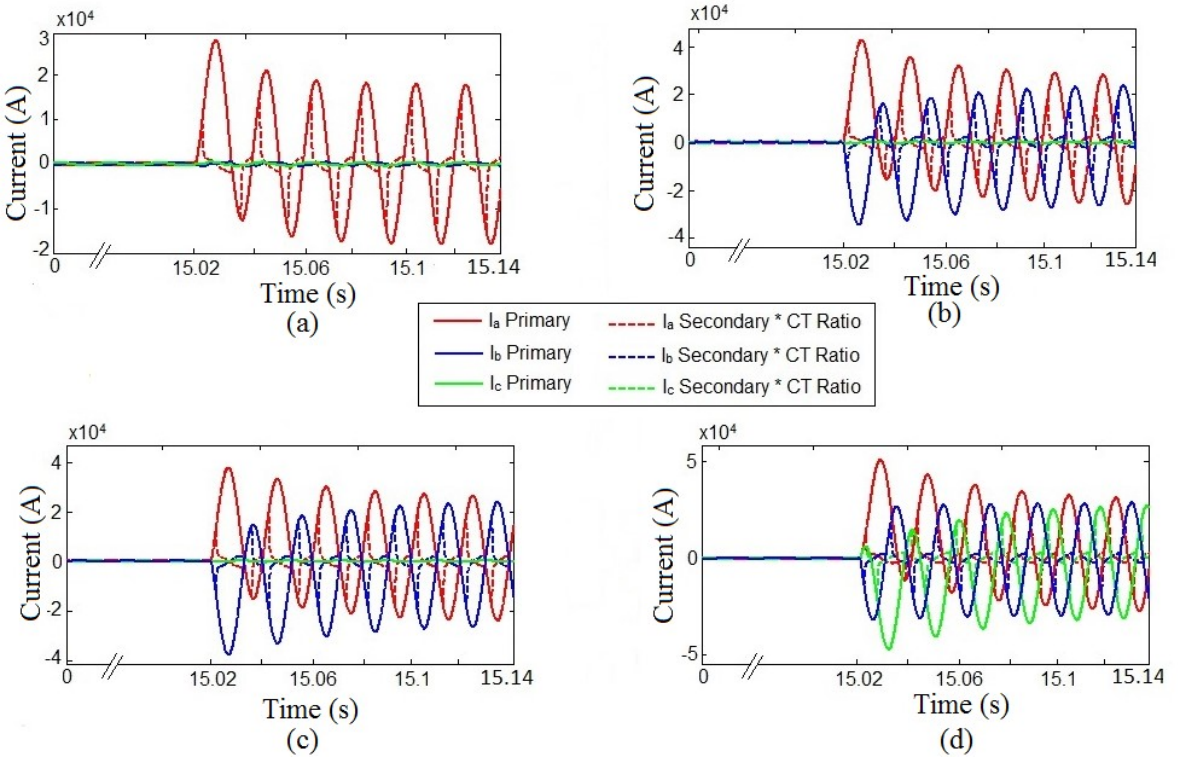

Fig. 6.12. Three phase current waveform under CT saturation with fault at 20 km from bus 1 at FR 0 Ω and FIA 0°
(a) SLGA (b) LLGAB (c) LLAB (d) LLL

Table 6.9. Effect of CT saturation

	Fault location (km)	Type of fault	FR (Ω)	FIA (°)	Compensation level	Δθ(°)	Differential power		
							Phase A	Phase B	Phase C
Internal Fault	50	AG	100	0	70%	49	8.97	0.89	0.76
	50	ABG	100	0	70%	36	8.96	9.54	0.78
	50	AB	100	0	70%	41.8	9.46	7.99	0.79
	50	ABC	100	0	70%	28	10.1	9.45	9.85
	180	AG	0	45	30%	40.94	10.2	0.66	0.72
	180	ABG	0	45	30%	15.78	19.4	16.2	0.77
	180	AB	0	45	30%	13.01	18.3	16.9	0.96
	180	ABC	0	45	30%	24	19.01	14.7	22.7
External Fault	220	AG	0	90	30%	-142.85	-	-	-
	220	ABG	0	90	30%	-176.88	-	-	-
	220	AB	0	90	30%	-175.6	-	-	-
	220	ABC	0	90	30%	-179.44	-	-	-
	280	AG	200	90	70%	-178.2	-	-	-
	280	ABG	200	90	70%	-159.36	-	-	-
	280	AB	200	90	70%	-157.23	-	-	-
	280	ABC	200	90	70%	-168.43	-	-	-

6.5.13. Validation of the Proposed Scheme on RTDS Platform

The proposed technique has been validated in Opal-RT with RTS OP5600 chassis and RT lab version 19.3.0.228, which uses parallel processing techniques to record continuous real-time digital simulation in power system operation. The current phasors have been collected from bus S and bus R in Opal-RT real-time simulator and transferred to IO cards ML605 to obtain the necessary data. The data has been recorded at different fault locations for different types of faults. Using the extracted current phasors from both the buses, internal faults have been detected and classified. The RTDS platform results of the designed system, when SLGA fault occurs on 30% compensated line with an FR of 10 Ω and an FIA of 90°, have been collected and plotted as shown in Figs. 6.13 (a) and (b). The DSO output waveforms of θx and θy when SLGA fault occurs at 10 km with FR 10 Ω and FIA 45° have been shown in Figs. 6.14(a) and (b). The RTDS results of this proposed technique when the transmission line is 70% compensated, are shown in Table 6.10. The DP of each phase is also shown in the table, revealing the efficacy of the proposed scheme in RTDS platform.

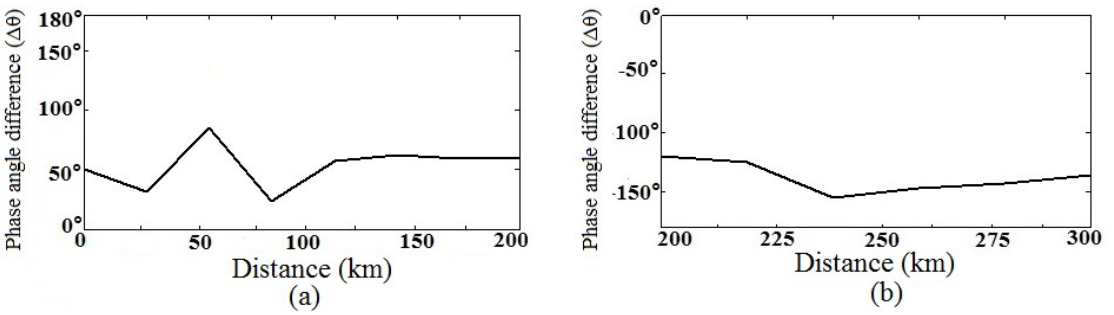

Fig. 6.13. Variation of (Δθ) with fault location
(a) Variation of (Δθ) with fault location during internal fault
(b) Variation of (Δθ) with fault location during external fault

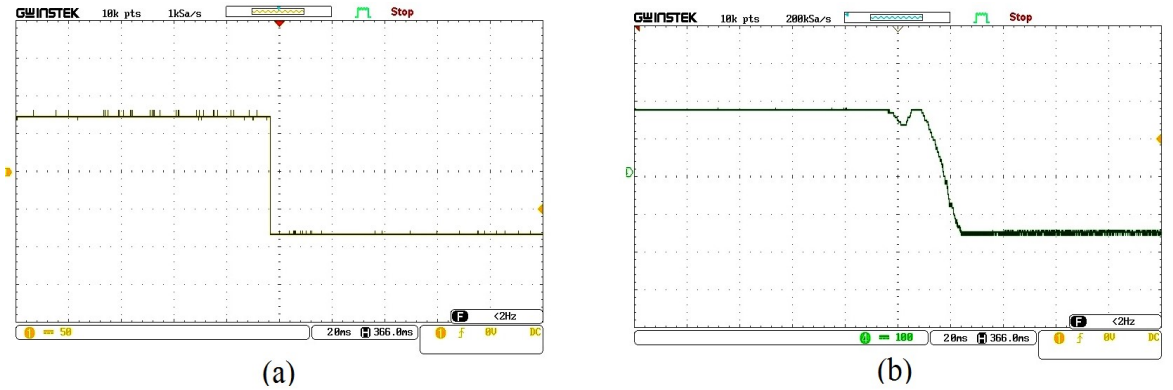

(a) (b)

Fig. 6.14. Variation of phase angle obtained from DSO
(a) Variation of θ_x obtained from DSO (b) Variation of θ_y obtained from DSO

Table 6.10. Performance of the proposed method in RTDS platform

Fault position	Fault type	FIA (°)	FR (Ω)	θ_x (°)	θ_y (°)	Δθ (°)	Differential power (VA)×10^8		
							Phase A	Phase B	Phase C
Internal fault (50 km)	AG	0	0	4	-32	36	12.9	0.797	0.801
	ABG	0	0	1.52	-24.7	26.22	14.6	15.8	1.38
	AB	0	0	5	-25.2	30.2	14.9	12.9	0.804
	ABC	0	0	2.5	-24.9	27.4	16.9	16.4	18.4
External fault (250 km)	AG	45	50	8.85	158.3	-149.45	-	-	-
	ABG	45	50	15.3	-171.5	-173.2	-	-	-
	AB	45	50	19	-165.4	-175.6	-	-	-
	ABC	45	50	13.2	-170	-176.8	-	-	-

6.6. Comparison with Existing Schemes

Table 6.11. Proposed scheme compared with other schemes

References Criterion	[85]	[69]	[70]	[72]	[81]	[87]	[93]	[86]	[117]	[101]	Proposed scheme
Technique used	Ve-sequence comp.	WT & ANFIS	DWT & ANN	UDWT & ChNN	FDOST & DT	Sequence comp	+Ve sequence impedance	-Ve sequence phasors & KVL	TW & FDST	DP	DP
Data collection	One end	One end	One end	One end		Both end	Both end	One end	Both end	Both end	Both end
Fault resistance (Ω)	300	50	100	50	200	500 (SLG & LLG) 100 (LL & LLL)	50	300	200	600	200
DG	x	x	x	x	x	x	x	x	√	x	√
Line length	200 km	300 km	400 km	300 km	400 kV, 50 Hz TL Chhattisgarh, India	300 km	-	300 km	200 km	80 km	300 km
Task performed	L	C, L, Z	L	Z	C	D, L	C, Z	L	D ,L	C, D, Z	C,D,Z
Signal used	V,I	V,I	V,I	I	V,I	V,I	V,I	V,I	I	V,I	V,I
Reverse direction of power flow	-	**x**	**x**	-	√	√	√	-	**x**	-	√
Pre-fault power transfer angle	√	√	**x**	√	-	√	**x**	**x**	**x**	√	√
CT saturation	√	**x**	**x**	**x**	√	**x**	**x**	√	**x**	√	√
Source strength variation	√	√	**x**	√	√	**x**	**x**	√	**x**	**x**	√
Islanding mode of operation	-	-	-	-	-	-	-	-	**x**	-	√
Operating time (cycle)	-	1cycle	1 pre fault and 2-post fault	½ cycle	½ cycle	-	1cycle	1cycle	-	1cycle	1cycle
HIF modeling	**x**	**x**	**x**	**x**		**x**	**x**	**x**	**x**	**√**	**√**

V= voltage signal, I= current signal, D= fault detection, C= fault classification, L= fault location, Z= discrimination of internal and external fault zone, DP= Differential power,

The proposed method has been compared with recently published SCTL protection schemes. Table 6.11 presents a comparative assessment of the proposed scheme with other existing schemes, the first column listing different comparative criteria. The authors in [93] developed a backup protection technique for SCTLs against ground faults only. As their scheme uses zero-sequence network, the proposed relay remains ineffective during double line and triple line faults. Furthermore, supervisory control of single pole tripping is ineffective since they are unable to detect the faulty phase.

For fault classification and fault zone identification in SCTL, the proposed scheme does not involve any complicated transform-based approaches [69, 70, 81 and 117] or machine learning tools [72 and 74]. Transform-based approaches [69, 70, 81 and 117] impose a significant computational burden, which is significantly reduced by the proposed approach. Also, the proposed method does not require any training resulting in less computational complexity and less response time. The authors in [69] used DWT for feature extraction and three different ANFIS for faulty section detection, fault classification and location estimation which imposes huge computational burden and generation of huge dataset for training the expert system. The authors in [70] only identified fault location using WT and neural network. Fault classification is not done. The authors in [117] detected fault and identified faulty section using S-transform based analysis. They have not considered dynamic conditions viz. effect of time synchronization error, change of pre-fault power transfer angle and change in source capacity. The authors in [95] have used the FDOST-DT based technique to identify the type of fault and detected the faulty phase. The researchers reported a fault zone detection method for SCTL based on undecimated WT and Chebyshev Neural Network in [72], which increased computation complexity. For detecting the faulty section and estimating the location of the fault, the author in [74] applied DWT and DNN, whereas this proposed system can successfully determine the fault zone without using any artificial intelligent techniques, hence reducing computing time and effort. Most of the investigations considered either the SCTL [69, 73, 66, 70, 72, 95, 81, 74, 87, 93, 85, 75, 84, 88, 89 and 101] or the transmission line linked with DG system [119 and 118], while very few researchers considered SCTL connected with DG system [117 and 101]. Although the authors in [119, 118, 117 and 101] discussed transmission line in conjunction with the DG system, they did not address the performance of their schemes for the islanding mode of operation. HIF features are very unpredictable and non-linear, which makes HIF detection and classification more difficult. Despite the fact that the authors in [69, 73, 66, 70, 72, 95, 81, 74, 87, 84, 88 and 89] examined SCTL, they did not address the effect of non-linear HIF on their schemes. During a HIF scenario, this proposed method is able to detect, classify, and locate the fault zone.

DP has been used to distinguish internal faults from external faults as well as to classify the faults in [101]. The DP values for external fault are always less than the threshold value and for internal fault; they are always above the threshold level. Though this method presented in [101] correctly classified faults in UPFC compensated line, it failed to distinguish internal and external faults in presence of wind farm. Table 6.12 shows the DP values when SLGA fault occurs at 190 km (internal fault) and 290 km (external fault) with FR of 200 Ω and FIA of 45°. It can be seen that the values of DP can be more in case of external fault when compared with

internal fault, in presence of wind farm. Hence, fault zone cannot be identified from the DP values as developed in [101] in presence of DG.

Table 6.12. DP values for internal and external faults

Compensation level	Fault zone	DP(VA)×10^8		
		Phase A	Phase B	Phase C
30%	Internal	1.1	0.77	0.88
	External	1.3	0.65	0.64
70%	Internal	1.4	0.84	0.87
	External	1.45	0.85	0.86

6.7. Conclusion

This chapter presents a new and reliable backup protection method for a SCTL. To detect the fault and distinguish the internal and external faults, phase angle difference of the positive sequence current signals from both ends of the transmission line have been used. In case of internal fault, the faulty phase is identified from the differential apparent power obtained from the two ends of the line. The efficiency and robustness of the proposed method has been validated through several case studies under different dynamic conditions. The performance comparison demonstrates the superiority of this scheme compared to existing distance protection methods for SCTL.

CHAPTER 7

A New PSD based Ground Fault Protection Scheme for Series Compensated Transmission Line

7.1. Introduction

Rapid technological progress necessitates continuous power supply to reduce the cascading outages and to enhance the reliability of the power supply. Rapid and precise fault identification, classification, and localization are essential for quick repair and restoration of the electric supply. SCTLs are commonly employed in the power system network to improve its stability, reliability, and loadability.

In transmission line protection scheme, WT is a well established tool as it can analyze the transient frequency component of current signals, which occur during faults [13]. In this research work, the maximum singular value energy of current signal has been extracted from the wavelet matrix because it has sufficient information to identify and classify faults in transmission line correctly. The authors in [3] proposed a protection technique for multi-generator-connected transmission lines using wavelet-multiresolution analysis. RTUs and GPS have been used to collect synchronized currents in this fault classification method. The developed algorithm has been tested for real-time smart grid operation, but the influence of synchronization delay has not been discussed. The effect of CT saturation was not explored in [13 and 3], though they employed current signals. A relaying technique based on DSP has been developed in [20] for analyzing the faults in transmission lines. A wavelet-alienation-based high-speed protection method for transmission line has been proposed by Rathore et al. in [8]. In this research work, faults in transmission lines were detected and classified using alienation coefficients of post-fault (quarter-cycle) current signals. DWT-along with ANN [1], has been used to identify, classify, and localize the faults in transmission lines. However, two different ANNs are required to determine the fault location, one for ground faults and the other for non-ground faults. A frequency-domain-based digital relaying algorithm for transmission line has been proposed in [5]. In this study, FIS and ANFIS have been used for estimating the fault distance. A fault classification scheme [81] based on DT and FDOST for SCTL has been reported. FDOST coefficients have been generated from both voltage and current signals and then supplied to DT for fault classification.

Due to the low amplitude of fault current, identification of HIF in the power network is a very difficult task. Most of the traditional techniques fail to identify the HIF. To overcome this issue, methods such as evidential reasoning [52], DWT [54], difference in voltage phasor, and DWT–ANN algorithm [10] have been utilized to identify and classify HIFs in the DN. The main drawback of different transmission line protection schemes based on ANN, WT/DWT aided ANN, DT [8, 1, 5, 81 and 55] is that they demand a lot of training data, which adds to the

computational burden. Most of the conventional techniques fail to detect HIF when it occurs close to the relay point. To deal with this problem, [62] describes a protection method that uses time-synchronized measurements of current and voltage samples from all three line terminals to detect faults and faulty segments, and finally estimate fault position during HIF in transmission line. Though the scheme gives good results with FR of 200 Ω, but the effect of non-linear HIF has not been discussed.

The main aim of the fault diagnosis system is to detect and classify the fault as fast as possible. Spectral analysis methods have been used in power networks for fault diagnosis as they require minimal time for detecting and classifying faults in transmission line. Due to the increasing use of power electronics devices, different types of harmonics develop in the network and create problems in the proper operation of relays. Four different parametric spectral estimation techniques for the identification of harmonics have been described in [25]. The authors in [26] utilized a PSD-based technique to identify and classify faults in transmission lines. Though this scheme is tested in the New England power grid, this scheme has not been investigated under varying source strength, power transfer angle, and in the presence of a series compensator. The wavelet-based PSD method has been described in [27] for detecting and classifying HIFs in a DS. Despite the fact that this protection method has been evaluated under various fault circumstances, the error caused by CT saturation has not been considered, although the technique only used current signals. The authors in [30] described an impedance-based fault location technique in radial DS. But the accuracy of this technique is not very high. A fault localization algorithm for single-circuit untransposed overhead transmission lines has been presented in [42]. Despite the fact that the algorithm delivers good results, the influence of measurement error owing to synchronization delay has not been explored in this study. Apostolopoulos et al. presented a fault location estimation methodology in [44] for both transposed and untransposed DCTLs. Positive-sequence current phasors of two-end unsynchronized current signals were utilized to locate the fault position in this methodology. However, the influence of non-linear HIF has not been considered.

To overcome the shortfall of impedance-based techniques, a remote telemetry unit and an intelligent computational technique-based smart fault location scheme for the smart grid has been described in [2]. Using detail coefficients of current samples measured from both ends of the transmission line, this method estimates the location of faults. A microcontroller-based transmission line protection technique has been developed in [12] to detect, classify, and locate faults using WT-ANN technique. A scheme for identifying and classifying faults in transmission lines during power swing has been presented in [103]. In this algorithm covariance index computed from synchronized current signals, was compared with the threshold value to identify and classify faults. The proposed approaches [2, 12 and 103] did not address the synchronization issue though they employed signals from both ends of the transmission lines. A PMU-based transmission line protection method that uses the minimum number of PMU for detection and localization of faults has been developed in [105]. Despite the fact that the developed method is fast and simple to implement, the evaluation of the method under the variation of system characteristics and load situations has not been performed.

A filter-based ANN approach has been developed in [108] to identify, classify and locate faults in transmission lines. This method is suitable only for short transmission lines and not for long ones. In [104], Das et al. developed a fault location estimation technique using WAMS and the bus admittance matrix. However, the performance of this scheme under close-in fault conditions remains unaddressed though it utilizes the voltage signals. Chatterjee et al. [92] used the positive-sequence component of voltage and current phasor to develop a fault-zone detection and location estimation technique for transmission line. This protection method takes into account all dynamic situations; however, the classification and fault localization accuracy under multi location fault scenarios have not been addressed. For series compensated DCTL, the authors in [116] proposed a directional relaying technique based on FIS. To detect the direction of faults, FIS is supplied with four separate features of positive-sequence components of current and voltage samples. Reddy et al. presented a real-time wavelet-fuzzy combined scheme for transmission line to classify and locate faults in [4]. For fault classification and localization, this method employs post-fault current signals (one-cycle). However, owing to the employment of WT-Fuzzy technology, the schemes proposed in [116 and 4] are sensitive to multilevel filtering.

SCTLs are used in power supply systems to maintain voltage profiles, improve the system stability (both steady-state and transient), and also enhance the power transmission capability. Four new methods have been suggested [66] only for identification of the fault zone in SCTL based on the DC component of current and voltage samples from both the line ends, instantaneous current, and instantaneous power waveform behaviour. UPFC is one of the modern FACTs devices that is extensively utilized nowadays. In [67], a fuzzy-based protection method for identifying faults and estimating fault location in a DCTL has been developed by Goli et al. This approach is suitable for both UPFC compensated and uncompensated transmission lines. However, the impacts of changes in line parameters owing to loading, aging, and environmental conditions were not discussed. Akmaz et al. [98] developed a fault location estimation technique for SCTLs based on travelling waves. However, the influence of power swing and load switching on the efficiency of the developed scheme has not been discussed. A sequence-component-based protection algorithm for UPFC compensated transmission line has been reported in [84]. Internal and external faults were separated by using complex power. The authors in [96] presented a negative-sequence current component-based DCTL protection technique that is compensated by a UPFC compensator.

Mal-functioning of conventional distance relay occurs under some conditions like load encroachment, power swing, etc. To overcome these issues, a power-differential based back-up protection scheme has been described in [101] to identify external and internal faults as well as to classify the various types of faults in UPFC compensated transmission line. This backup protection approach, however, does not address close-in and far-end fault situations. Some of the authors have used neuro-fuzzy inference system [69], Undecimated WT and Chebyshev neural network [72], Sequence–space–aided–SVM classifier [95], and deep neural network combined with DWT [73] in SCTL for faulty state identification, classification, and fault location purpose. The above schemes have made a significant contribution to the protection of SCTLs; however, as the performance of these techniques proposed in [69, 72, 95 and 73] is determined by a predefined structure, which necessitates a training process, relay response time remains a

concern. In [102], a study has been done by using an integrated moving sum technique to identify and classify the faults in transmission lines. However, CT saturation and weak infeed circumstances reduce the effectiveness of this method, resulting in some misclassifications. The authors in [75] developed a scheme based on real-time fault analysis using Hilbert Huang Transform for shunt-compensated transmission line. The effectiveness of this method has not been examined for non-linear HIF and swing conditions, although it exhibits good results under different dynamic circumstances and resistance up to 500 Ω.

In SCTL, due to the change in positive-sequence impedance, distance relays cannot operate accurately. For the protection of SCTLs, a mutual impedance-based protection technique has been developed in [93] to overcome this issue. Instead of using positive-sequence impedance, the developed system protects against ground faults only using mutual impedance between phases. An ANN-based fault distance determination approach for multi-location faults in TCSC connected transmission line has been presented in [70]. Though this scheme does not need fault classification to estimate the distance of multi-location fault, it requires a large quantity of data (SD of 3^{rd} level cAs of one pre-fault and two post-fault currents and voltages) as input to ANN for training a DWT-ANN-based fault locator, which increases the computational burden and execution time.

The novelty of this chapter lies in the potential application of the PSD algorithm for ground fault detection, classification, and location estimation with minimal features in SCTL. No synchronization is necessary as one end current signal is sufficient to accomplish all the objectives. This technique decouples time and frequency information and this knowledge can be applied to ground fault detection and classification. As revealed from the literature survey, PSD technique has not been used previously to locate faults in SCTL. Though the authors in the present paper have demonstrated the potentiality of PSD technique in the time domain, the PSD values in the frequency domain are equally effective for identifying and classifying ground faults in SCTL.

7.2. Proposed Scheme for Fault Classification

Series compensation is used in transmission lines to enhance the power system stability by improving the system voltage and reducing transmission losses. MOVs are commonly used to protect the capacitor used for compensation from transient over-voltage. The non-linear characteristics of the series capacitor create difficulties in classification of faults and estimation of the fault location in SCTLs. In this chapter, an attempt has been made to propose a new protection scheme for SCTLs against ground faults using the PSD based on WT.

7.2.1. Feature extraction

The detection of faults and identifying the types of faults are essential for the protection of transmission lines. In this chapter, the authors consider the protection against ground faults only.

The current samples in the time domain have been measured at an f_s of 12.5 kHz [3, 20, 5 and 4]. To obtain the unique features from the fault signal, one cycle data immediately after the occurrence of the fault has been analyzed by DWT. The db4 mother wavelet has been chosen for this study because of its excellent performance in the domain of power system fault analysis. During the MRA process, different sub-band frequency components are generated, which represent the different characteristics such as fundamental frequency, harmonic frequency, and transient frequency. Among the different types of frequency bands, only transient frequency components are considered in this chapter. 1st level, 2nd level, and 3rd level of detail coefficients having frequency bands 3.125 kHz–6.25 kHz, 1.562 kHz–3.125 kHz, and 0.781 kHz–1.562 kHz respectively represent the transient characteristics. In the proposed scheme, a threshold

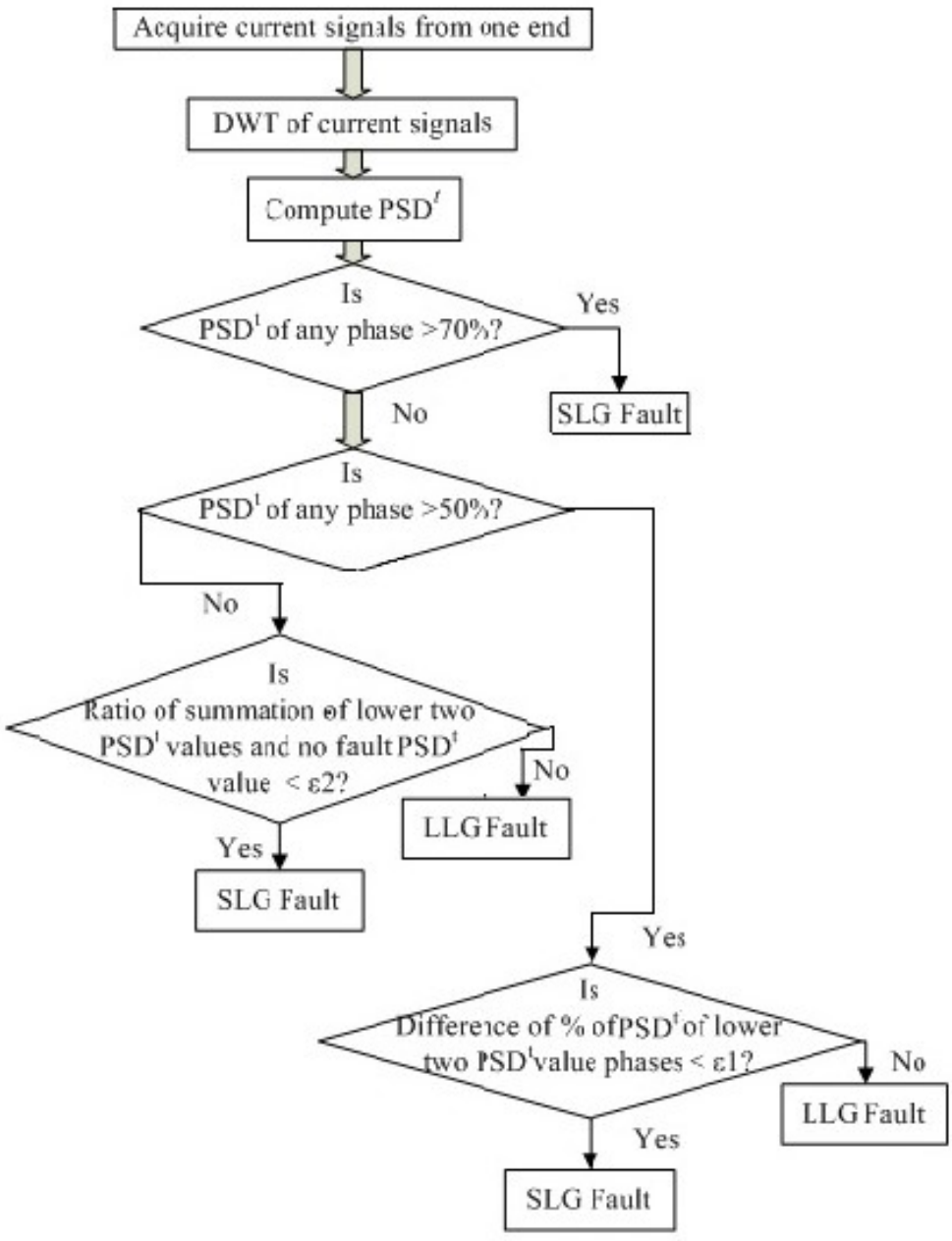

Fig. 7.1. Flowchart for fault classification

value of PSD^t has been considered to detect fault conditions and approximate coefficients (a_1) of current signals are considered to distinguish the ground and non-ground faults. If the PSD^t value of any phase is above the threshold value, then the fault is detected. If the sum of 1st level a_1 of three-phase currents is greater than zero, then it denotes ground fault, else non-ground fault.

After the detection of ground fault, the covariance matrix in the time domain is calculated applying Eq. (1.14), containing 1st (d_1), 2nd (d_2), and 3rd (d_3) level detail coefficients and 3rd level of approximation (a_3) coefficients. *PSD* value obtained from Eq. (1.16) is used for fault classification purposes. *PSD* values of three phases are used to discriminate between SLG and LLG faults. The flowchart shown in Fig. 7.1 describes the classification process of the proposed method. According to the flowchart in Fig. 7.1, if the PSD^t value of any one phase is higher than 70% of the total of all the PSD^t values of the three phases, the fault is SLG. The remaining fault cases can be discriminated using two threshold values ε_1 and ε_2. ε_1 is used to discriminate the SLG and LLG fault if PSD^t of any phase is greater than 50% and ε_2 is considered if PSD^t of all the phases is less than 50%. The faulty phase/s can be easily identified as the phase with the highest PSD^t in SLG fault indicates the faulty phase and the two phases with higher PSD^t values indicate the faulty phases in LLG fault.

7.3. Proposed Scheme for Fault Location Estimation

After subsequent fault identification and classification, the next step of the proposed backup protection algorithm is to estimate the fault distance utilizing ANN. The proposed fault localization approach is divided into two parts: one for identifying the faulty zone and the other for precisely measuring the fault distance.

7.3.1. Fault Zone Identification

After the classification of faults, faulty zone needs to be identified. In the case of LLG fault, there is one healthy phase which is considered as *H1*. In SLG fault, *H1* is considered as the healthy phase which is lagging the faulty phase under normal condition. For example, if SLG fault occurs in phase A, then *H1* is B phase and if a fault occurs in phase B, then *H1* is phase C. Similarly, if the C phase is the faulty phase, then *H1* is assigned to phase A. The criterion used to identify the fault zone is shown in Table 7.1 and it depicts that, if the PSD^t value of *H1* phase is less than the no-fault PSD^t value, then fault occurs before the compensator, whereas if the PSD^t value of *H1* phase is greater than PSD^t value at no-fault condition, then fault occurs after the compensator.

Table 7.1. Fault zone identification criterion

Faulty zone	Criterion
Before compensator	PSD^t of *H1* phase $<PSD^t$ at no fault condition
After compensator	PSD^t of *H1* phase $>PSD^t$ at no fault condition

7.3.2. Fault Location

After identifying the faulty zone, accurate fault distance calculation is carried out using ANN. The fault position estimation scheme is shown in Fig. 7.2. For this purpose, three-phase current samples from the local end are decomposed with db4 wavelet and PSD^t is obtained from Eq. (1.16).

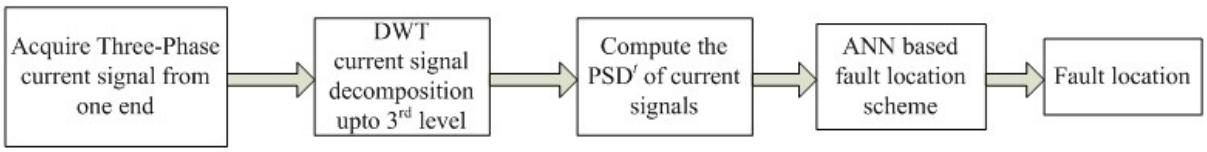

Fig. 7.2. Frame work of the proposed fault location scheme of SCTL

In the proposed scheme, two separate ANNs are employed, one for before and one for after the compensator. ANN is a computational model, based on the structure and operations of biological neural networks. ANN consists of a large number of connected units or nodes known as artificial neurons. ANNs are extensively employed to estimate the location of faults in transmission line, due to their ability to handle large data sets and high computing capabilities. The PSD^t value obtained from three-phase current signals is fed into ANN as an input vector to estimate the fault location. All six types of ground faults (AG, BG, CG, ABG, ACG and BCG) have been simulated at various positions throughout the transmission line, under various FIAs and FRs. The fault cases thus generated are fed to the ANN for training purposes. In the proposed scheme, only one cycle of current signal, immediately after the fault inception is enough to determine the location of the fault. Since single end data is adequate to precisely compute the fault distance, the computational complexity is reduced.

A four-layer feed-forward back propagation ANN is chosen for this study. The ANN architecture consists of one input layer with four neurons for inputs PSD^t A, PSD^t B, PSD^t C and type of fault. The output layer with one neuron provides fault location as the output. Four hidden layers having thirty-five neurons in each layer have been considered. Performance of the ANN is greatly influenced by the training process and it depends on the neurons per hidden layer. Number of neurons control over fitting and under fitting of data. Therefore, the proper selection of neurons and hidden layers is very important for obtaining better results. The transfer function

used in this ANN is a log-sigmoid type for all layers. Owing to its fast convergence capabilities, the Levenberg-Marquardt method is employed to train the ANN to estimate the location of faults. In this ANN architecture, we have chosen 800 epochs, a mean squared error of 0.002, and 450 maximum number of fails to obtain a good set of output.

7.4. Test System

A 400 kV, 50 Hz transmission line model, with the MOV linked at the midpoint of the transmission line as shown in Fig. 7.3, has been considered for this study. The test system model designed here consists of two substations connected through 300 km long transmission line and simulated in Matlab environment. Both sources (E_1 and E_2) have internal impedances of 0.5333+j5.333 Ω. The load angle of E_1 is 20° whereas the load angle of E_2 is 0°. The transmission line parameters considered for this study are given below:

Positive-sequence resistance (R_1) =0.01273 Ω/km
Zero-sequence resistance (R_0) =0.3864 Ω/km
Positive-sequence inductance (L_1) =0.9337×10^{-3} H/km
Zero-sequence inductance (L_0) =4.1264×10^{-3} H/km
Positive-sequence capacitance (C_1) =12.74×10^{-9} F/km
Zero-sequence capacitance (C_0) =7.751×10^{-9} F/km

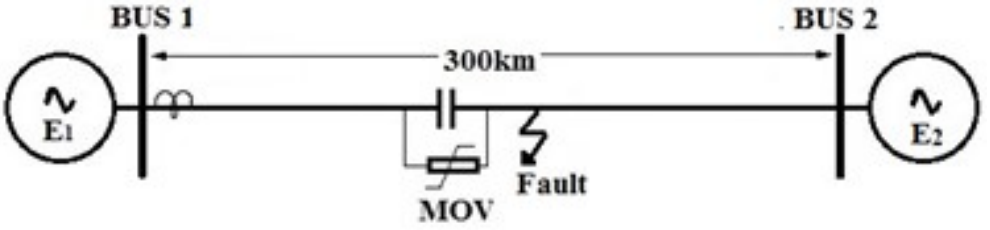

Fig. 7.3. Simulation model

7.5. Simulation Results

To check the authenticity, robustness, and accuracy of the designed backup protection technique for SCTL, all types of ground faults (SLG and LLG) with varying FR (0 Ω to 100 Ω), FIA (0° to 90°) and fault position (before and after compensator at an interval of 5 km) have been simulated on a 300 km long transmission line. The proposed scheme classifies the faults and also estimates the location of fault utilizing the PSD^t value of the current signals. To evaluate the proposed technique, one cycle data (current signal) has been collected from the local end (bus 1) at f_s of 12.5 kHz from the time instant after the occurrence of the fault. To evaluate the algorithm, the compensation level of the transmission line has been varied from 30% to 70%.

In the proposed scheme, a proper PSD^t value has been chosen as threshold to distinguish between the fault states and the no-fault condition. The current samples have been acquired from bus1 and the PSD^t values of all the phases have been computed. In this chapter, the threshold value has been considered as 1.2 times the no-fault PSD^t value. Hence, a fault is detected if PSD^t value of any phase is greater than this threshold value. Fig. 7.4(a) shows the PSD^t values of all the phases under 70% compensation when SLG fault occurs at 0.02s before the compensator and the PSD^t of *H1* phase is less than the PSD^t at no fault condition. Fig. 7.4(b) depicts the PSD^t values when the same fault occurs after the compensator at 0.02s under 30% compensation. According to Fig. 7.4(b), it is seen that for fault after compensator PSD^t of *H1* phase is greater than the PSD^t at no fault condition. Once the fault is detected, the next step is to identify whether it is a ground or non-ground fault. The summation of the first level a_1 of all the three phases is computed to distinguish between ground and non-ground faults. If this value is close to zero, the fault is non-ground, i.e. LL or LLL fault. If it is greater than zero, the fault is considered a ground fault, i.e., SLG or LLG fault.

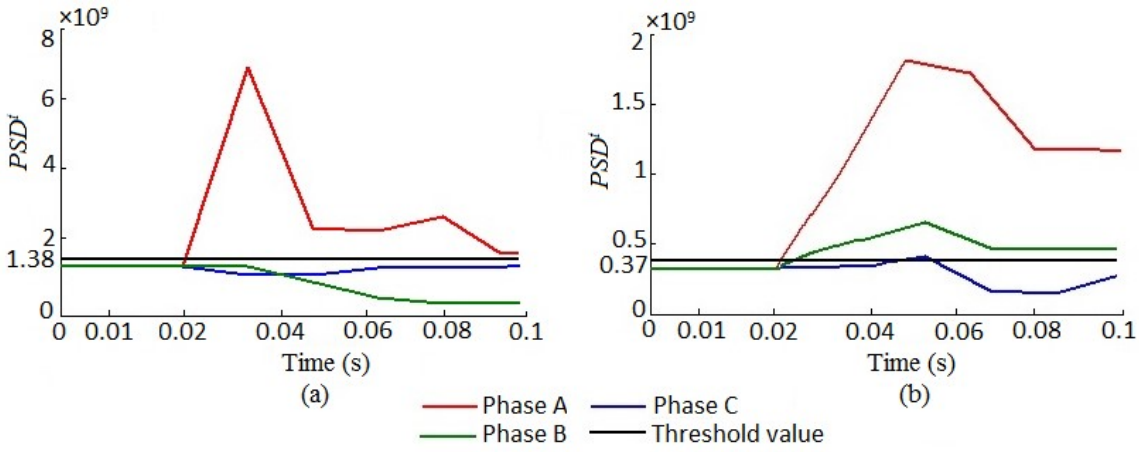

Fig. 7.4.Variation of PSD^t for SLGA fault with FR 0Ω and FIA 0°
(a) Fault at 100 km when line is 70% compensated (before the compensator)
(b) Fault at 265 km when line is 30% compensated (after the compensator)

Table 7.2 describes the results of the ground fault classification when the line is 70% compensated. According to the proposed fault classification scheme shown in Fig.7.1, it appears that if the PSD^t value of any one phase is greater than 70% of the total PSD^t value ($\sum PSD^t$ A + PSD^t B + PSD^t C), then it indicates SLG fault as depicted in rows 1 to 3 in Table 7.2. From Table 7.2 and Table 7.3, it is evident that some of the cases do not satisfy the condition stated above. If the % PSD^t value of one phase is greater than 50% but less than 70%, then ε_1 is calculated, which is the difference of lower two % PSD^t values. If it is less than the threshold value, which is considered as 12, then it indicates SLG fault, else the fault is LLG. Rows 4 to 6 in Table 7.2 and rows 1 to 6 in Table 7.3 satisfy this condition.

Table 7.2. Results for SLGA faults at various FRs, FIAs, and fault locations

Sl. no	Fault position (km)	FR (Ω)	FIA (°)	% of PSD^t			Fault PSD^t / No-fault			ε_1	ε_2
				Phase A	Phase B	Phase C	Phase A	Phase B	Phase C		
1	10	0	0	98.9	0.7	0.5	152.8	0.99	0.701	-	-
2	30	0	0	95.4	2.3	2.3	36.17	0.88	0.87	-	-
3	50	0	0	84.9	7.0	8.1	16.78	0.84	0.93	-	-
4	70	50	45	66.9	14.4	18.7	3.31	0.79	0.21	4.3	-
5	90	50	45	62.4	16.1	21.5	2.69	0.76	1.09	5.4	-
6	110	50	45	58.2	17.5	24.2	2.38	0.73	1.11	6.7	-
7	110	100	90	45.9	24.6	29.5	1.58	0.83	1.03	-	1.86
8	130	100	90	42.5	25.7	31.8	1.37	0.82	1.02	-	1.84
9	270	100	90	40.7	30.8	28.5	1.43	1.08	1.01	-	2.09
10	290	100	90	37.7	31.8	30.5	1.25	1.06	1.02	-	2.08

Table 7.3. Results for LLGAB fault at various FRs, FIAs, and fault locations

Sl. no	Fault position (km)	FR (Ω)	FIA (°)	% of PSD^t			Fault PSD^t / No-fault PSD^t			ε_1	ε_2
				Phase A	Phase B	Phase C	Phase A	Phase B	Phase C		
1	10	0	0	63.9	36.0	0.2	277.4	156.7	0.66	35.8	-
2	30	0	0	62.2	37.3	0.5	97.22	58.23	0.77	36.8	-
3	50	0	0	61.9	37.1	1.0	51.47	30.87	0.8	36.1	-
4	110	50	45	50.6	33.9	15.6	2.93	1.97	0.90	18.3	-
5	170	50	90	34.1	51.8	14.0	2.93	1.97	1.04	20.1	
6	190	50	90	34.8	50.2	15.0	2.8	4.26	1.15	19.8	-
7	250	50	45	36.0	46.1	17.9	2.17	2.79	1.08	-	3.26
8	270	50	45	35.9	43.3	20.9	1.86	2.24	1.07	-	2.94
9	290	50	45	35.6	39.2	25.1	1.53	1.67	1.07	-	2.61
10	250	10	0	33.3	42.3	24.4	1.46	1.85	1.06	-	2.52
11	270	10	0	33.5	39.9	26.7	1.33	1.58	1.06	-	2.39
12	280	10	0	33.4	38.5	28.0	1.26	1.45	1.06	-	2.32

To distinguish the SLG and LLG fault, when PSD^t values of all the phases is less than 50%, ε_2 is calculated. ε_2 is the ratio of summation of lower two PSD^t values and no-fault PSD^t value (1.15×10^9). If it is less than the threshold value, then the fault is SLG fault, else LLG fault. In this chapter the threshold value for ε_2 has been considered as 2.2. Rows 7 to 10 in Table 7.2 and rows 7 to 12 in Table 7.3 reveal this condition. Similar results are obtained for faults in other phases also and the proposed algorithm is verified.

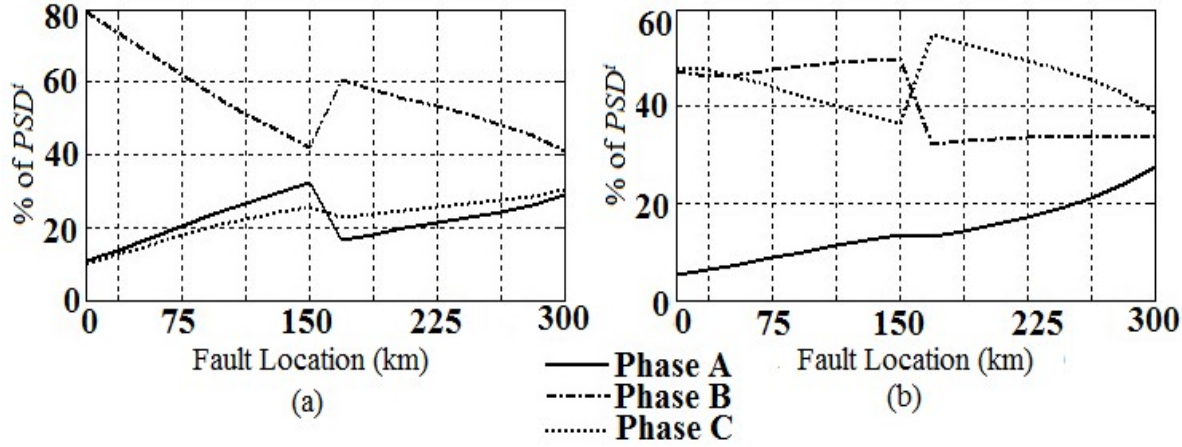

Fig. 7.5. Variation of % PSD^t value for SLG and LLG fault
(a) SLGB (b) LLGBC

Fig. 7.5 shows the percentage PSD^t for SLG and LLG faults. Fig. 7.5(a) represents SLGB fault at FR of 50 Ω when FIA is 45° whereas Fig. 7.5(b) shows the LLGBC fault at FR of 50 Ω and FIA of 90°. From Fig. 7.5(a), it is seen that in the event of SLG fault, the PSD^t value of the faulty phase decreases as the fault distance before the compensator increases. Its value increases immediately after the compensator and then progressively drops as the fault distance increases after the compensator. Healthy phases show just opposite nature i.e. before the compensator PSD^t value increases and just after the compensator, it decreases and then again gradually increases. In the case of LLG fault, shown in Fig. 7.5(b), PSD^t value of faulty phases shows opposite nature to each other, when PSD^t of one phase is decreasing another phase is increasing and vice versa. The PSD^t value of the healthy phase is always increasing in nature. The proposed scheme compares the PSD^t value of the *H1* phase (healthy phase 1) with the PSD^t value in the no-fault condition to identify faulty sections. If the PSD^t value of *H1* phase is less than the no-fault condition PSD^t value, then the fault is before the compensator, else after the compensator. Fig. 7.6 presents the results of the proposed faulty section identification technique at various locations when the transmission line is 70% compensated. Fig. 7.6(a) shows the SLGC fault at FR of 0 Ω and FIA of 0°, whereas Fig. 7.6(b) represents the LLGAB fault at FIA of 90° when FR is 100 Ω. In both cases, it is seen that when a fault occurs after the compensator, PSD^t of the *H1* phase is greater than the no-fault PSD^t value. Similar types of results are obtained for other types of faults also. Therefore, these results agree with the proposed algorithm and identify the fault zone correctly. After locating the fault zone, the next step is to determine the fault distance. In this proposed scheme, an ANN-based technique is applied to locate the fault accurately. The accuracy of the fault location estimation technique is evaluated by computing the % error, which is represented as

$$Error(\%) = \frac{Fault\ location_{actual} - Fult\ location\ _{estimated}}{Total\ lengt\quad of\ the\ line} \times 100 \qquad (7.1)$$

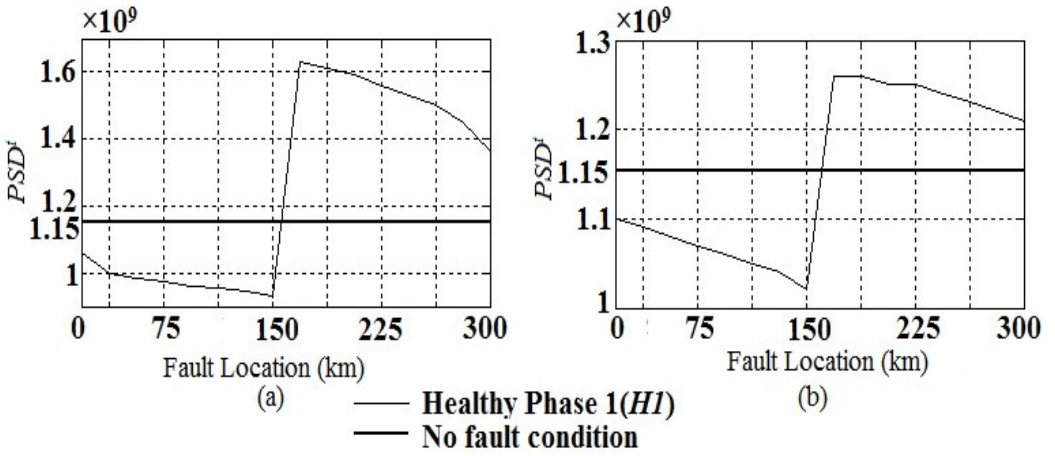

Fig. 7.6. PSD^t value of *H1* phase with respect to the fault location
(a) Variation of PSD^t value of *H1* phase (phase A) during SLGC fault
(b) Variation of PSD^t value of *H1* phase (phase C) during LLGAB fault

In the proposed technique, two separate ANNs have been constructed, one for fault before the compensator and another for fault after the compensator; hence the total distance of the transmission line is considered as 150 km. Table 7.4 and Table 7.5 present the errors obtained from SLG and LLG faults before and after the compensator at various locations with variable FR and FIA when the transmission line is 70% compensated. Fig. 7.7 shows the % error for various locations in case SLG and LLG fault at FR of 0 Ω and FIA of 0° for before compensator and after compensator. The mean percentage error for SLG fault is 1.5% and for LLG fault it is 0.7% before the compensator, whereas for beyond the compensator, the mean percentage errors for SLG and LLG fault are 1.5% and 1.2% respectively.

Table 7.4. Fault location estimation error for different FR and FIA before compensator

Fault Type		FR (Ω)	FIA (°)	Fault location (km)	ANN location (km)	% error
SLG	AG	0	0	11	11.59	0.39
	BG	0	0	33	32.46	0.35
	CG	50	45	40	40.45	0.31
	AG	100	45	80	79.72	0.18
	BG	100	90	105	105.6	0.4
	BG	0	90	136	137.52	1. 01
	CG	50	0	149	149.22	0.15
LLG	BCG	50	45	36	36.39	0.26
	BCG	0	0	82	83	0.6
	ACG	100	0	86	85.12	0.58
	ABG	0	90	99	99.67	0.45
	ACG	0	45	114	114.59	0.39
	ABG	100	45	136	135.34	0.43
	BCG	100	90	148	148.84	0.56

Table 7.5. Fault location estimated error for different FR and FIA after compensator

Fault Type		FR (Ω)	FIA (°)	Fault location (km)	ANN location (km)	% error
SLG	AG	50	90	176	175.72	0.12
	BG	0	90	188	187.48	0.34
	CG	0	45	196	195.25	0.5
	AG	100	45	221	222.21	0.8
	BG	50	45	232	231.69	0.2
	CG	50	0	271	272.77	1.1
	AG	100	0	296	295.94	0.03
LLG	ABG	50	0	162	161.31	0.46
	BCG	100	45	170	171.9	1.2
	CAG	0	0	194	193.71	0.19
	ABG	100	0	226	225.37	0.42
	BCG	0	45	247	245.17	1.2
	CAG	0	90	272	271.78	0.14
	ABG	50	90	294	293.49	0.33

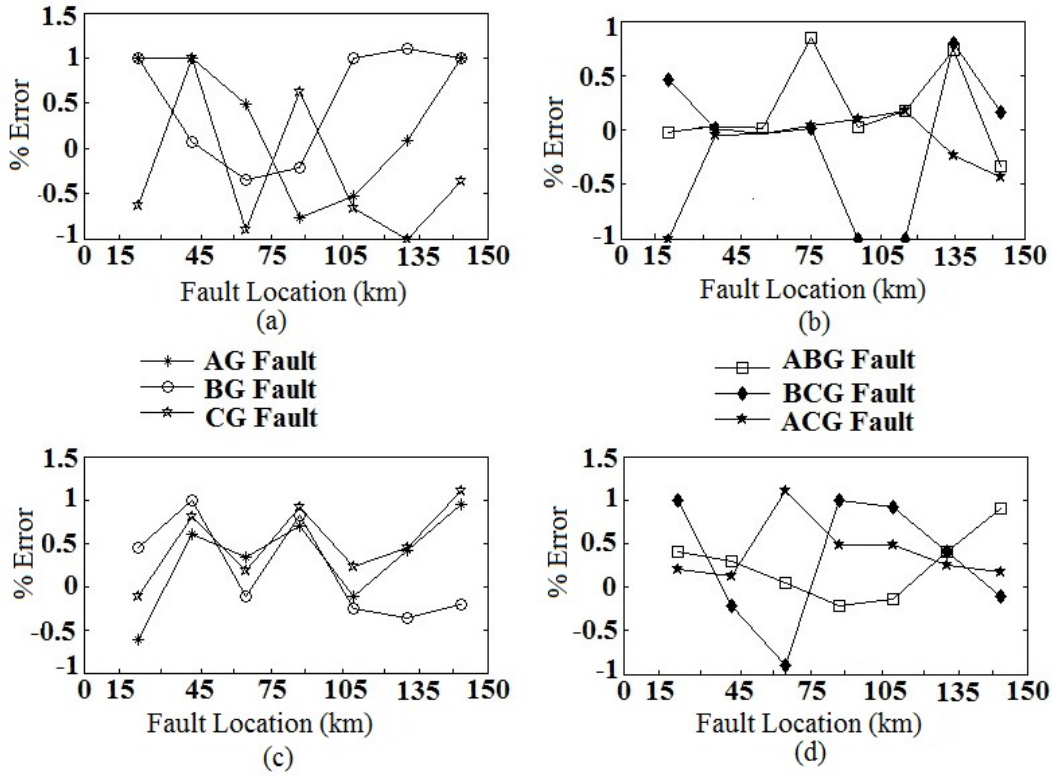

Fig. 7.7. % Error at different locations of fault
(a) SLG fault before compensator (b) LLG fault before compensator
(c) SLG fault after compensator (d) LLG fault after compensator

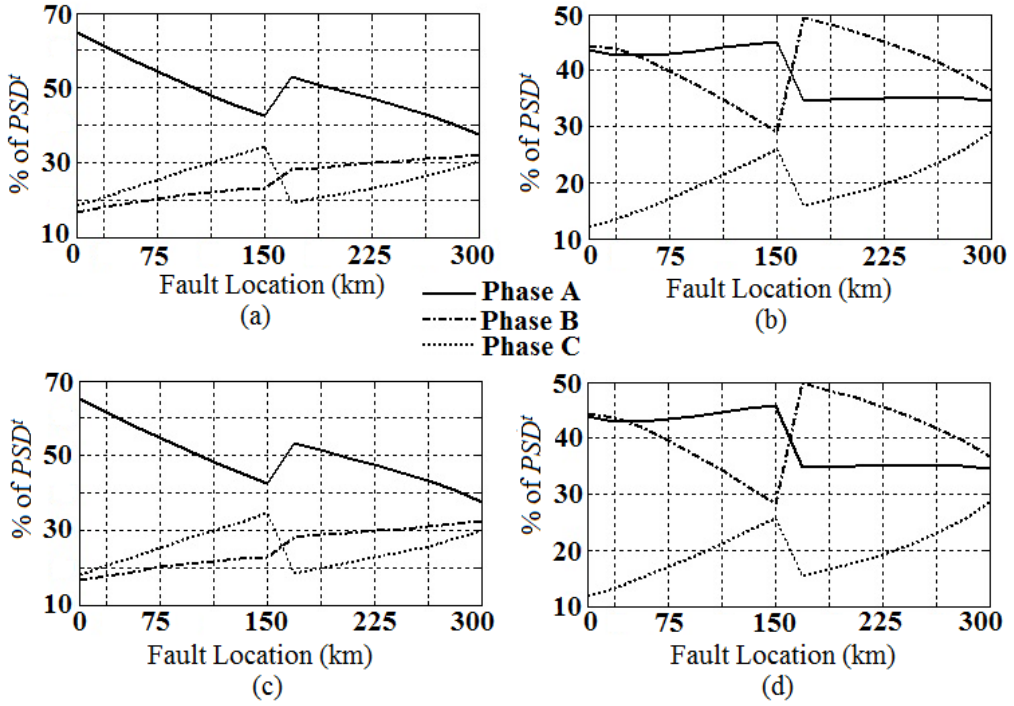

Fig. 7.8. % *PSD*^{t} for SLG and LLG fault at different sampling frequencies
(a) SLGA fault at f_s of 4 kHz (b) LLGAB fault at f_s of 4 kHz

7.6. Evaluation of the Proposed Technique

To assess the effectiveness and reliability of the proposed technique, the system is tested at various sampling frequencies (f_s) and different compensation levels of the compensator. In transient-based fault analysis techniques, sampling frequency plays an important role during analog to digital conversion of the signal. The test system has been simulated at 4 kHz and 60 kHz in addition to 12.5 kHz to observe the influence of the sampling frequency on the proposed approach.

It is seen that the designed technique shows satisfactory results for classifying the faults and also identifying the fault zone accurately. Fig. 7.8 shows the fault classification results, whereas Fig. 7.9 shows the fault zone identification results at 4 kHz and 60 kHz sampling frequency when FIA is 45° and FR is 100 Ω. Throughout this study, 12.5 kHz sampling frequency has been chosen [3, 20, 5 and 4], because most of the commercial devices are available with this sampling frequency.

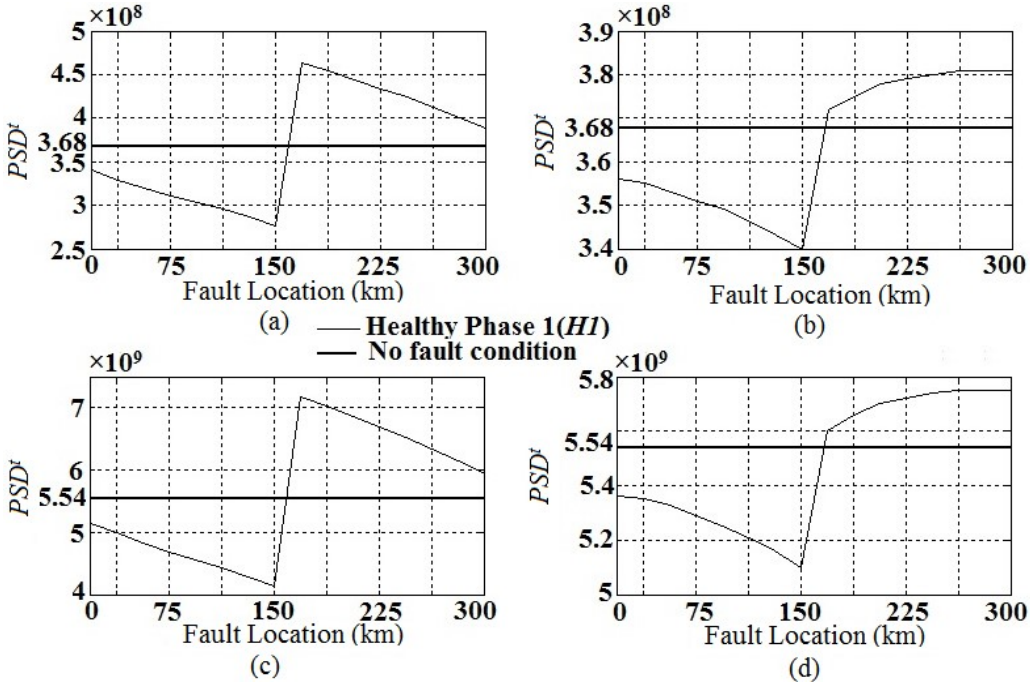

Fig. 7.9. Variation of PSD^t value of *H1* phase with respect to fault location at different f_s

(a) *H1* phase (phase B) during SLGA fault at f_s of 4 kHz

(b) *H1* phase (phase C) during SLGAB fault at f_s of 4 kHz

(c) *H1* phase (phase B) during SLGA fault at f_s of 60 kHz

(d) *H1* phase (phase C) during SLGAB fault at f_s of 60 kHz

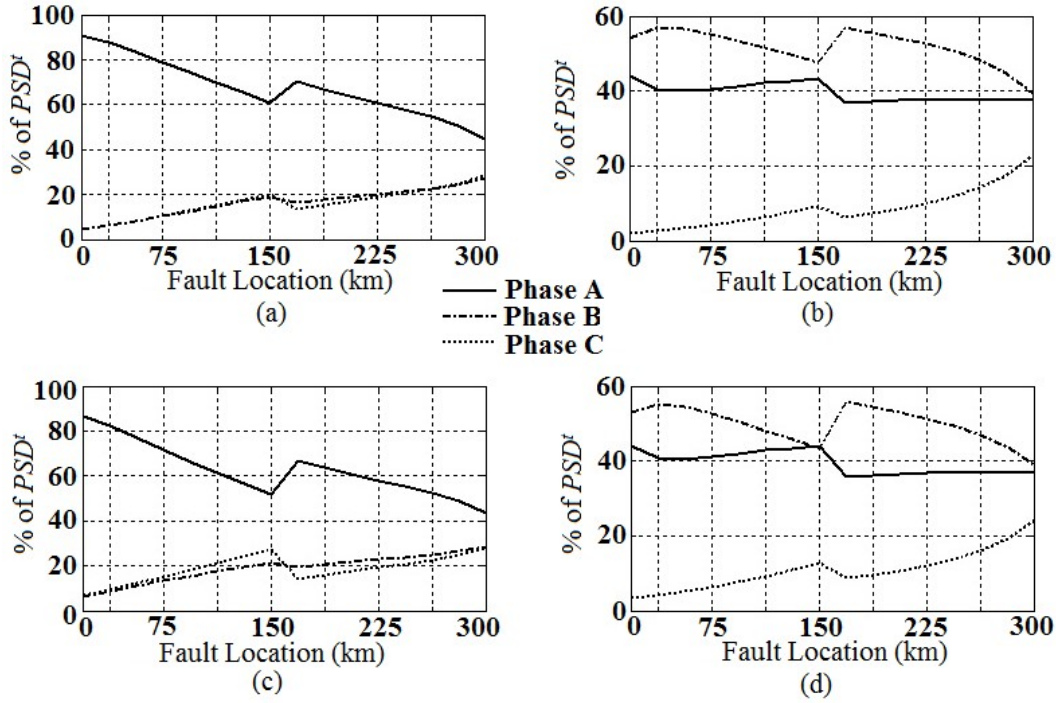

Fig. 7.10. PSD^t for SLG and LLG fault at different compensation level

(a) SLGA fault at 30% compensation level (b) LLGAB fault at 30% compensation level

(c) SLGA fault at 50% compensation level (d) LLGAB fault at 50% compensation level

To evaluate the efficiency and reliability of the method, the system is examined under three different levels (30%, 50%, and 70%) of compensation of the compensator. The results are presented in Fig. 7.10 and Fig. 7.11 with FR of 50 Ω and FIA of 90°, respectively, and it is found that the proposed logic can efficiently classify the faults and at the same time, it can also identify the faulty section.

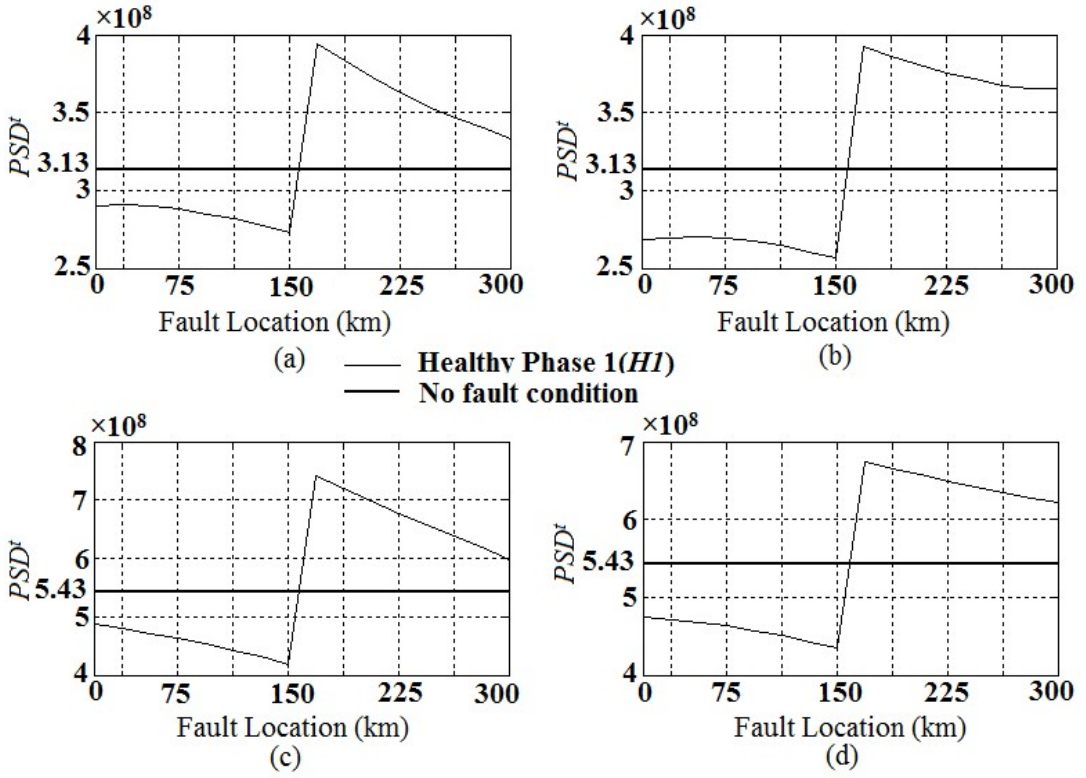

Fig. 7.11. ***PSD*^{t} value of *H1* phase with respect to fault location at different compensation level**
(a) *H1* phase (phase B) during SLGA fault at 30% compensation level,
(b) *H1* phase (phase C) during SLGAB fault 30% compensation level
(c) *H1* phase (phase B) during SLGA fault at 50% compensation level,
(d) *H1* phase (phase C) during SLGAB fault at 50% compensation level

The power generation capacity also affects the fault current. Therefore, PSD^t value of the fault currents is also changed. The authors have considered the effects of change in source impedances by changing the equivalent impedance of the source E_1 from 50% to 200% to ensure the reliability of this proposed method. In this situation, SLGA and LLGBC faults were simulated at FR 0 Ω and FIA 0°. Fig. 7.12 and Fig. 7.13 show the fault classification and fault zone identification results respectively. It is observed from Fig. 7.12 and Fig. 7.13, that the algorithm is efficient to detect the faulty zone and classify the faults accurately.

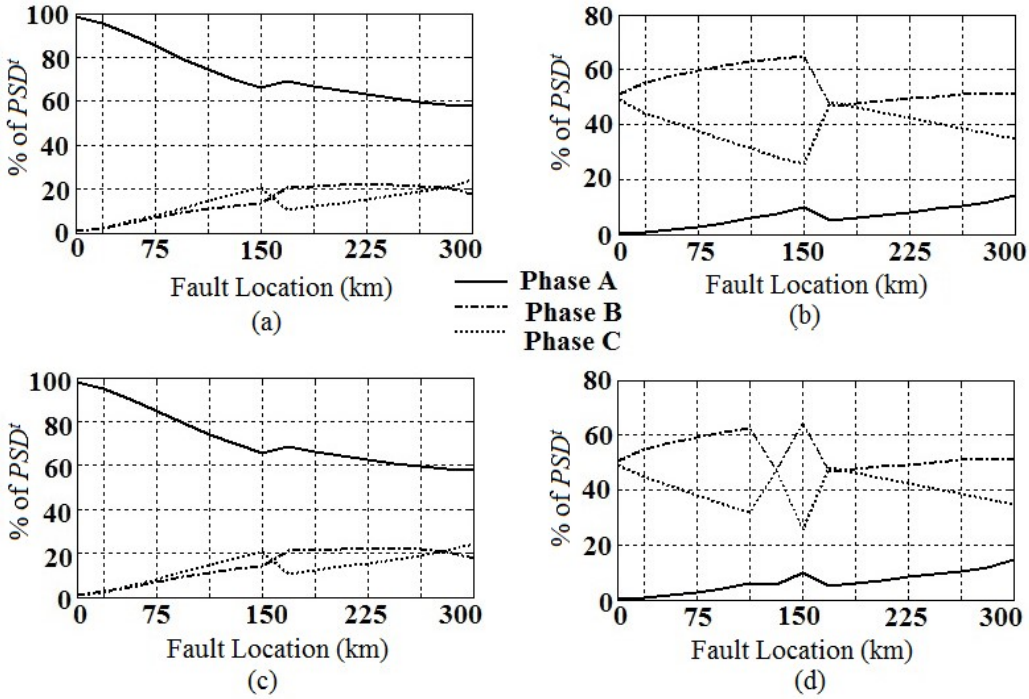

Fig. 7.12. ***PSD*^{t} for SLG and LLG fault at different source impedance**
(a) SLGA fault at 50% source impedance (b) LLBCG fault at 50% source impedance
(c) SLGA fault at 200% source impedance (d) LLBCG fault at 200% source impedance

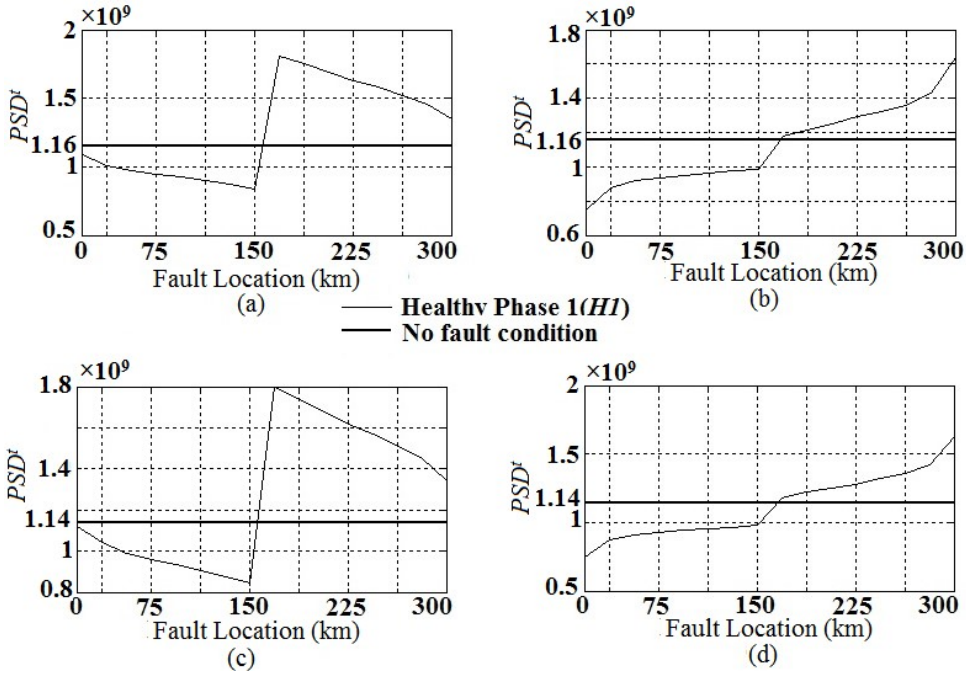

Fig. 7.13. *PSD*^{t} value of *H1* phase with respect to fault location at different source impedances
(a) *H1* phase (i.e phase B) during SLGA fault at 50% source impedance,
(b) *H1* phase (i.e phase A) during SLGBC fault 50% source impedances
(c) *H1* phase (i.e phase B) during LLGA fault at 200% source impedance,
(d) *H1* phase (i.e phase A) during LLGBC fault at 200% source impedance

To establish the superiority of this PSD^t based fault classification and location strategy, it has been compared with other published protection schemes available in the literature for SCTLs. The authors in [66] only identified fault zone applying four different methods. Neither they have classified the faults, nor estimated the fault location. The authors in [93] proposed a backup protection algorithm for SCTLs against ground faults. They have considered the voltage and currents of both terminals of the line which may be considered as a drawback from the economic aspect as it requires communication channel for data transfer and more measurement devices as compared to the proposed scheme which uses only local end current signal. Moreover, fault location estimation has not been performed.

Compared to other published methods, this scheme does not require a large number of features such as SD of approximate coefficients of current and voltage samples [70], entropy, detail coefficients (maximum and minimum value) of current signals [73], norm entropy of fundamental frequency coefficients, harmonic frequency coefficients, and transient frequency coefficients of current and voltage samples [69] for estimating the location of fault. Therefore, using only one feature from single end current signal, the proposed algorithm reduces computational complexity.

7.7. Conclusion

This research work proposed an enhanced and robust ground fault classification and fault position estimation scheme for SCTL. The concept of the proposed technique is associated with the energy distribution of current samples measured from one end of the transmission line. The energy distributions of the faulty and healthy phases are used to discriminate between the SLG and LLG faults. At the same time, comparing the PSD^t values under fault conditions with the normal operating condition, fault zone is identified with 100% accuracy. For SLG and LLG fault classification and location estimation, this technology utilizes one cycle of data immediately after the occurrence of the fault. The reliability and efficiency of the suggested method has been examined under various dynamic situations and the results ascertain that the scheme is immune against the degree of compensation level, sampling frequency, fault location, FR and FIA. The significant advantage of this proposed strategy is that only one feature is sufficient for accurate classification of faults, identification of fault zone and also estimation of the location of faults. This method also has no synchronization issues and requires less measuring equipment as it uses only current samples from one end of the line.

CHAPTER 8

Conclusions

8.1. Conclusions

Continuous expansion in electrical power networks is the direct consequence of industrialization and modernization in all sectors and also urban growth. As a result of these factors, developing unique, accurate and rapid action protection techniques and protective equipment for electrical power systems have become the highest priority. High voltage transmission lines are the main linkage of the power networks since they transmit a large amount of electric power over long distances at near the velocity of light. Since transmission lines traverse through tough terrain and are subjected to intense environmental stress, the occurrence of faults in transmission lines is higher than in other power system equipment. Such failures endanger the safe operation of advanced grid-connected power networks, necessitating the use of high-speed fault clearing protective systems for better stability. To address such issues, researchers are always developing new measures to enhance the immunity of transmission line protection, which should be prompt, accurate, and trustworthy, allowing for quick restoration of power after faults occur. The aim of this thesis is to propose transmission line protection technologies that can be used in real-world power networks.

HIF detection in power networks is essential, and it is also challenging owing to the low magnitude of the fault current. Failure to identify HIF increases the risk of fire and poses safety risk to persons. The energy spectrum of wavelet coefficients is used in this study to detect, differentiate and classify LIFs and HIFs. The wavelet coefficients are derived from one end current signals using DWT.

The constant growth of the transmission network necessitates the utilization of renewable energy in the main power grid. Fuzzy logic has been used to propose a novel impedance-based fault classification approach for long transmission lines combined with DG. Using one end voltage and current signals of the transmission line, the presented technique computes line impedance from the ratio of the cAs of voltage and current signals. The fault state is detected using cDs, and the faults are classified using a fuzzy-based fault classifier employing line impedance. Line impedance has also been utilized as input to an ANFIS-based fault locator to determine the location of an SLG fault in transmission lines.

Subsequently, an admittance-based fault index was calculated to propose a novel transmission line protection method. This method makes a substantial contribution by detecting and classifying non-linear HIF in transmission networks, including evolving and cross-country faults. This method has also been tested on an IEEE 9-bus test system, confirming that it can be implemented in real-world power networks.

Series compensation provides various benefits, including increased transmission capacity, improved system stability, voltage regulation management, and optimal load distribution across parallel feeders. As a result, an innovative and efficient backup protection method for series compensated transmission lines linked to wind farms has been developed.This work identifies the fault and differentiates between internal and external faults using phase angle differences of positive sequence current signals collected from both ends of the line segment. Moreover, DP has been used to classify internal faults.

Finally, a PSD-based ground fault protection scheme for series compensated transmission lines has been developed. PSD has been computed from the wavelet covariance matrix to classify the faults and has been fed into ANN to determine the fault position.

8.2. Comparison of the Methods used in this Research Work

This section includes a comprehensive evaluation to emphasize the advantages and disadvantages of the methodologies/ techniques used in this research.

WT has been employed in most of the schemes developed in this research work due to its superior capacity to analyze non-stationary signals in both the time and frequency domain. In chapter 2, single-level wavelet decomposition is used to compute the energy spectrum of wavelet coefficients, which reduces computational burden and time as compared to most existing wavelet-based algorithms that have used multilevel decomposition.

In chapters 3 and 4, a WT-based technique for classifying faults and locating ground faults in long transmission lines has been described. In Chapter 3, line impedance was employed to apply fuzzy logic to classify faults in wind farm-connected transmission lines, and in Chapter 4, an ANFIS-based fault locator was used to estimate the location of SLG fault. Despite the fact that WT has a higher processing overhead than sequence-based techniques, the sequence component approach is incapable of fault classification since phase data is lost during the conversion process.

In chapter 5, DFT was used efficiently to detect and classify evolving and cross-country faults by extracting the fundamental frequency component of current and voltage signals. Although the DFT process is simple and the calculation time is less, the existence of ddc components in current signals employs complicated computation for the elimination of ddc components.

Chapter 6 proposes an effective and reliable backup protection methodology for series compensated transmission lines linked to wind farms. Internal faults are distinguished from external ones in this study by using the positive sequence component of the current signal, while the faults are classified using DP. The main benefits of sequence-based algorithms are that they have a lower computing burden and can avoid the problem of voltage inversion and current inversion that happens in series compensated transmission lines.

In Chapter 7, a wavelet covariance matrix has been utilized to compute the PSD of fault signals to identify faults and estimate the location of ground faults in SCTLs. The covariance matrix approach has an advantage over other parametric methods as it does not require data zeroing. It makes use of all the data points to estimate power and prediction error calculation.

This research also employs some AI algorithms for fault classification and location. FIS, ANN, and ANFIS are employed in this study for the aforementioned purposes. As compared to other AI approaches, the fuzzy method takes less computing time. It is both robust and versatile, accepting imprecise input and employing extremely simple mathematical concepts with fuzzy reasoning. The fundamental advantage of a fuzzy based method is that it does not require any training data; hence the computing time is significantly lower than that of other training-based approaches like ANN, ANFIS, DNN, etc. ANN and ANFIS, on the other hand, require enormous amount of information for training, which increase the computing time and burden and is unsuitable for real-time analysis. Furthermore, the performance of ANN and ANFIS is strongly impacted by the training process, which is dependent on some aspects such as architecture, selection of neurons and hidden layers, selection of proper transfer function, membership functions, etc.

8.3. Future Scope of the Work

Traditionally, electrical power transmission lines have been intended to transmit power at high-voltage levels and distribute it to reduced voltage-level power system networks. Large number of power generation units are linked to transmission networks. However, in the near future, there will be a greater number of small generators connected to distribution networks to meet the growing electricity demand. The effective integration of DG necessitates network advancements. Microgrids are an evolution of such concept. Fault detection and classification are extremely challenging in microgrids since inverter-interfaced DG restricts the fault current to around two times the rated current due to the low thermal overload capability of the inverter. As a result, conventional protective relays are incapable of providing precise responses. Despite the fact that this research work provided a protection method for DG-connected power networks, it cannot estimate the fault location in transmission lines connected to DGs. A robust technique for determining the exact location of faults in microgrids will be developed as the future scope of this research work. Also, reliable protection schemes for microgrids will be developed. Another future goal of this study is to provide a protection scheme for double-circuit series compensated transmission lines, which is essential for transmitting stable and reliable power with a better voltage profile.

REFERENCES

1. A. G. Shaik and R. R.V. Pulipaka, "A new wavelet based fault detection, classification and location in transmission lines," *Electrical Power and Energy Systems*, vol. 64, pp. 35-40, 2015.

2. M. J. B. Reddy, D. V. Rajesh and P. Gopakumar and D. K. Mohanta, "Smart fault location for smart grid operation using RTUs and computational intelligence techniques," *IEEE Systems Journal*, vol. 8, no. 4, pp. 1260-1271, 2014.

3. M. J. B. Reddy, D. V. Rajesh and D. K. Mohanta, "Robust transmission line fault classification using wavelet multi-resolution analysis," *Computers and Electrical Engineering*, vol. 39, no. 4, pp. 1219-1247, 2013.

4. M. J. B. Reddy, and D.K. Mohanta, "A wavelet-fuzzy combined approach for classification and loc ation of transmission line faults," *Electrical Power and Energy Systems*, vol. 29, pp. 669–678, 2007.

5. M. J. B. Reddy and D. K. Mohanta, "Adaptiveneuro-fuzzy inference system approach for transmission line fault classification and location incorporating effects of power swings," *IET Generation Transmission & Distribution*, vol. 2, no. 2, pp. 235-244, 2008.

6. A. Yadav and A. Swetapadma, "A single ended directional fault section identifier and fault locator for double circuit transmission lines using combined wavelet and ANN approach," *Electrical Power and Energy Systems*, vol. 69, pp. 27-33, 2015.

7. W. Li, A. Monti and F. Ponci, "Fault detection and classification in medium voltage DC shipboard power systems with wavelets and artificial neural networks," *IEEE Transactions on Instrumentation and Measurement*, vol. 63, no. 11, pp. 2651-2665, 2014.

8. B. Rathore and A.G. Shaik, "Wavelet-alienation based transmission line protection scheme," *IET Generation Transmission & Distribution*, vol. 11, no. 4, pp. 995–1003, 2017.

9. B. Rathore and A.G. Shaik, "Wavelet-alienation based protection scheme for multi-terminal transmission line," *Electric Power Systems Research*, vol. 161, pp. 8–16, 2018.

10. Y. Usama, L. Xiaomin, H. Imam, C. Sen, and N. C. Kar, "Design and implementation of a wavelet analysis-based shunt fault detection and identification module for transmission lines application," *IET Generation Transmission & Distribution,* vol. 8, no. 3, pp. 431-441, 2014.

11. S. Zarbita, A. Lachouri, and H. Boukadoum, "A new approach of fast fault detection in HV-B transmission lines based on Detail Spectrum Energy analysis using oscillographic

data," *International Journal of Electrical Power and Energy Systems,* vol. 73, pp. 568-575, 2015.

12. E. Koley, R. Kumar and S. Ghosh, "Low cost microcontroller based fault detector, classifier, zone identifier and locator for transmission lines using wavelet transform and artificial neural network: A hardware co-simulation approach," *International Journal of Electrical Power and Energy Systems*, vol. 81, pp. 346–360, 2016.

13. D. Guillen, M. R. A. Paternina, A. Zamora, J. M. Ramirez and G. Idarraga, "Detection and classification of faults in transmission lines using the maximum wavelet singular value and Euclidean norm," *IET Generation Transmission & Distribution*, vol. 9, no. 15, pp. 2294–2302, 2015.

14. R. Dubey and S. R. Samantaray, "Wavelet singular entropy-based symmetrical fault-detection and out-of-step protection during power swing," *IET Generation Transmission & Distribution*, vol. 7, no. 10, pp. 1123–1134, 2013.

15. F. B. Costa, "Fault-induced transient detection based on real-time analysis of the wavelet coefficient energy," *IEEE Transactions on Power Delivery*, vol. 29, no. 1, 2014.

16. S. Ekici, "Support vector machines for classification and locating faults on transmission lines," *Applied Soft Computing*, *Elsevie*r, vol.12, pp. 1650–1658, 2012.

17. A. Dasgupta , S. Nath and A. Das, "Transmission line fault classification and location using wavelet entropy and neural network," *Electric Power Components and Systems, Taylor & Francis*, vol. 40, no. 15, pp. 1676-1689, 2012.

18. Z. He, S. Lin, Y. Deng, X. Li and Q. Qian, "A rough membership neural network approach for fault classification in transmission lines,"*Electrical Power and Energy Systems*, vol.61, pp. 429-439, 2014.

19. J. Zhang, Z.Y. He, S. Lin, Y.B. Zhang and Q. Qian, "An ANFIS-based fault classification approach in power distribution system," *International Journal of Electrical Power and Energy Systems*, vol. 49, pp. 243-252, 2012.

20. M. J. Reddy and D.K. Mohanta, "A DSP based frequency domain approach for classification of transmission line faults," *Digital Signal Processing, Elsevier*, vol.18, pp. 751–761, 2008.

21. S. N. Ananthan, R. Padmanabhan, R. Meyur, B. Mallikarjuna, M. J. B. Reddy and D. K. Mohanta, "Real-time fault analysis of transmission lines using wavelet multi-resolution analysis based frequency-domain approach," *IET Science Measurement & Technology,* vol. 10, no. 7, pp. 693–703, 2016.

22. B. Patel, "A new FDOST entropy based intelligent digital relaying for detection, classification and localization of faults on the hybrid transmission line," *Electric Power Systems Research*, vol.157, pp. 39–47, 2018.

23. M. J. B. Reddy, P. Gopakumar and D.K. Mohanta, "A novel transmission line protection using DOST and SVM," *Engineering Science and Technology an International Journal*, *Elsevier*, vol. 19, no. 2, pp. 1027-1039, 2016.

24. S. R. Samantaray, "Fast S-transform based distance relaying in transmission line," *Electric Power Systems Research*, vol. 95, pp. 268-274, 2013.

25. A. S. Yilmaza, A .Alkan and M.H. Asyali, "Applications of parametric spectral estimation methods on detection of power system harmonics," *Electric Power Systems Research,* vol.78, pp. 683-693, 2008.

26. D. Guillen, M.R.A. Paternina, J. Ortiz-Bejar, R.K. Tripathy, A. Zamora-Mendez, R. Tapia-Olvera and E.S. Tellez, "Fault detection and classification in transmission lines based on a PSD index," *IET Generation Transmission & Distribution*, vol.12, no. 18, pp. 4070–4078, 2018.

27. S. Roy, and S. Debnath, "PSD based high impedance fault detection and classification in distribution system," Measurement, doi: org/10.1016/j.measurement.2020.108366, vol.169, 2020.

28. M. R. D. Zadeh, and Z. Zhang, "New DFT-Based current phasor estimation for numerical protective relaying," *IEEE Transactions on Power Delivery*, vol. 28, no. 4, 2013.

29. J. C. Gu and S.L. Yu, "Removal of DC offset in current and voltage signals using a novel Fourier filter algorithm," *IEEE Transactions on Power Delivery,* Vol. 15, no. 1, pp. 73-79, 2000.

30. M. A. Gabr, D. A. Ibrahim, E.S. Ahmed and M. I. Gilany, "A new impedance-based fault location scheme for overhead unbalanced radial distribution networks," *Electric Power Systems Research*, vol.142, pp. 153–162, 2017.

31. M. Farshad and J. Sadeh, "Accurate single-phase fault-locaton method for transmission lines based on K-nearest neighbor algorithm using one-end voltage', *IEEE Transaction on Power Delivery*, vol. 27, pp. 2360-2367, 2017.

32. P. Gopakumar, M. J. B. Reddy and D. K. Mohanta, "Transmission line fault detection and localisation methodology using PMU measurements," *IET Generation Transmission & Distribution*, vol. 9, no. 11, pp. 1033–1042, 2015.

33. S. R. Nam, S.H. Kang, and J.K. Park, "An analytic method for measuring accurate fundamental frequency components," *IEEE Transactions on Power Delivery*, vol.17, no. 2, pp. 405-411, 2002.

34. B. Jafarpisheh, S. M. Madani, and S. M. Shahrtash, "A new DFT-based phasor estimation algorithm using high-frequency modulation," *IEEE Transactions on Power Delivery*, vol. 32, no. 6, pp. 2416 – 2423, 2017.

35. R. L. A. Reis, W. L. A. Neves, F. V. Lopes and D. Fernandes, "Coupling capacitor voltage transformers models and impacts on electric power systems: a review," *IEEE Transactions on Power Delivery*, vol. 34, no. 5, pp. 1874 – 1884, 2019.

36. A. Swetapadma, and A.Yadav, "Data-mining-based fault during power swing identification in power transmission system," *IET Science Measurement & Technology,* vol. 10, no. 2, pp. 130-139, 2015.

37. B. Chatterjee and S. Debnath, "Fuzzy-based relaying scheme for transmission line based on unsynchronized voltage measurement, *IETE Journal of Research,* doi.org/10.1080/ 03772063.2020.1754934, 2020.

38. A. Ghorbani and H. Mehrjerdi, "Negative-sequence network based fault location scheme for double circuit multi terminal transmission lines," *IEEE Transaction on Power Delivery,* vol. 34, no. 3, doi:10.1109/TPWRD.2019.2906056, 2019.

39. J. Ma, X. Yan, B. Fan, C. Liu and J. S. Thorp, "A novel line protection scheme for a single phase-to-ground fault based on voltage phase comparison. *IEEE Trans. on Power Delivery*, doi: 10.1109/TPWRD.2015.2507600, vol. 31, no. 5, 2016.

40. S. Huang, L. Luo, and K. Cao, "A novel method of ground fault phase selection in weak-infeed side. *IEEE Transactions on Power Delivery*, vol. 29, no. 5, pp. 2215-2222. 2013.

41. A. Yadav, and A. Swetapadma, "Enhancing the performance of transmission line directional relaying, fault classification and fault location schemes using fuzzy inference system," *IET Generation Transmission & Distribution*, vol. 9, no. 6, pp. 580–591, 2015.

42. A. S Dobakhshari, "Noniterative parameter free fault location on un transposed single-circuit transmission lines," *IEEE Transactions on Power Delivery*, Vol. 32, no. 3, pp.1636-1644, 2017.

43. S. Didehvar and R. M. Chabanloo, "Accurate estimating remote end equivalent impedance for adaptive one ended fault location," *Electric Power Systems Research*, doi:10.1016/j.epsr.2019.01.011 vol. 170, pp. 194-204, 2019.

44. C. A. Apostolopoulos and G. N. Korres, "A novel fault-location algorithm for double-circuit transmission lines without utilizing line parameters. *IEEE Transactions on Power Delivery,* vol. 26, no. 3, pp.1467-1478, 2011.

45. A. Swetapadma and A. Yadav, "An innovative finite state automata based approach for fault direction estimation in transmission lines," *Measurement*, doi:10.1016/j.measurement.2016.09.046, vol. 99, pp. 13-22, 2017.

46. H. Seyedi, S. Teimourzadeh and P. S. Nezhad, "Adaptive zero sequence compensation algorithm for double-circuit transmission line protection," *IET Generation Transmission & Distribution*, vol. 8, no. 6, pp. 1107–1116, 2014.

47. Y. Zhong, X. Kang, Z. Jiao, Z. Wang and J. Suonan, "A novel distance protection algorithm for the phase-ground fault," *IEEE Transactions on Power Delivery*, vol: 29, no. 4, pp. 1718 – 1725, 2014.

48. B. Mahamedi and J. G. Zhu, "Unsynchronized fault location based on the negative-sequence voltage magnitude for double-circuit transmission lines," *IEEE Transactions on Power Delivery*, vol. 29, no. 4, pp. 1901-1908, 2014.

49. A. R. Adly, R.A. El Sehiemy, A. Y. Abdelazizand, and N. M.A. Ayad, "Critical aspects on wavelet transforms based fault identification procedures in HV transmission line," *IET Generation Transmission & Distribution*, vol. 10, no. 2, pp. 508–517, 2016.

50. M. Paul, and S. Debnath, "Wavelet Based Single Ended Scheme for High Impedance Fault Classification in Transmission Lines," *IEEE. International Conference on Smart Technologies in Computing, Electrical and Electronics,* pp. 157-162, 2020.

51. I. Baqui, Zamora, J. Mazón, and G. Buigues, "High impedance fault detection methodology using wavelet transform and artificial neural networks," *Electric Power Systems Research*, vol. 81, pp.1325–1333, 2011.

52. A.Soheili, and J.Sadeh, "Evidential reasoning based approach to high impedance fault detection in power distribution systems," *IET Generation Transmission & Distribution*, vol. 11, no. 5, pp. 1325-1336, 2017.

53. T. M. Lai, L. A. Snider, E. Lo, and D. Sutanto, "High-impedance fault detection using discrete wavelet transform and frequency range and RMS conversion", *IEEE Transactions on Power Delivery*, vol. 20, no. 1, pp. 397-407, 2005.

54. W. C. Santos, F. V. Lopes, N. S. D. Brito, and B. A. Souza, "High-impedance fault identification on distribution networks," *IEEE Transactions on Power Delivery,* vol. 32, no. 1, pp. 23-32, 2017.

55. T. Hubana, M. Saric, and S. Avdakovic, "Approach for identification and classification of HIFs in medium voltage distribution networks," *IET Generation Transmission & Distribution*, vol. 12, no. 5, pp. 1145-1152, 2018.

56. M. S. Tonelli-Neto, J.G.M.S. Decanini, A.D.P. Lotufo and C.R. Minussi, "Fuzzy based methodologies comparison for high-impedance fault diagnosis in radial distribution feeders," *IET Generation Transmission & Distribution*, vol. 11, no.. 6, pp. 1557-1565, 2017.

57. P. Qi, S. Jovanovic, J. Lezama, and P. Schweitzer, "Discrete wavelet transform optimal parameters estimation forarc fault detection in low-voltage residential power networks," *Electric Power Systems Research*. vol. 143 pp. 130–139, 2017.

58. A. H. A. Bakar, M.S. Ali, C. K. Tan, H. Mokhlis, H. Arof and H.A. Illias, "High impedance fault location in 11kV underground distribution system using wavelet transforms," *Electrical Power and Energy Systems,* vol. 55, pp. 723–730, 2014.

59. M. Michalik, W. Rebizant, M. Lukowicz, S.J. Lee and S.H. Kang, "High-impedance fault detection in distribution networks with use of wavelet-based algorithm," *IEEE Transactions on Power Delivery*, vol. 21, no. 4, pp. 1793-1802, 2006.

60. A. Soheili, J. Sadeh and R. Bakhshi, "Modified FFT based high impedance fault detection technique considering distribution non-linear loads: simulation and experimental data analysis," *International Journal of Electrical Power and Energy Systems* , vol. 94, pp. 124–140, 2018.

61. V. Torres, J. L. Guardado, H. F. Ruiz and S. Maximov, "Modelling and detection of high impedance faults," *International Journal of Electrical Power and Energy Systems*, vol. 61, pp. 163–172, 2014.

62. V. K. Gaur and B. Bhalja, "A new faulty section identification and fault localization technique for three-terminal transmission line," *Electrical Power and Energy Systems*, vol. 93, pp. 216-227, 2017.

63. M. Kavi, Y. Mishra, and M. D. Vilathgamuwa, "High -impedance fault detection and classification in power system distribution networks using morphological fault detector algorithm," *IET Generation Transmission & Distribution*, vol. 12, no. 15, pp. 3699-3710, 2018.

64. S. Gautam and S.M. Brahma, "Detection of high impedance fault in power distribution systems using mathematical morphology," *IEEE Transactions on Power Systems,* vol. 28, no. 2, pp. 1226-1234, 2013.

65. M. Sarlak and S.M. Shahrtash, "High impedance fault detection using combination of multi-layer perception neural networks based on multi-resolution morphological gradient features of current waveform," *IET Generation Transmission & Distribution,* vol. 5, no. 5, pp. 588–595, 2011.

66. A. A. Razavi and G. Samet, "Algorithms for fault zone detection in series-compensated transmission lines. *IET Generation Transmission & Distribution,* vol. 9, no. 4, pp. 386–394, 2015.

67. R. K. Goli, A. G. Shaik and S.S.T.Ram, "A transient current based double line transmission system protection using fuzzy-wavelet approach in the presence of UPFC. *International journal of Electrical Power and Energy Systems,* vol. 70, pp. 91–98, 2015.

68. A. K. Pradhan, A. Routray, S. Pati, and D. K. Pradhan, "Wavelet fuzzy combined approach for fault classification of a series-compensated transmission line," *IEEE Transactions on Power Delivery*, vol. 19, no. 4, pp. 1612-1618, 2004.

69. H. Erist, "Fault diagnosis system for series compensated transmission line based on wavelet transform and adaptive neuro-fuzzy inference system," *Measurement*, vol. 46, no. 1, pp. 393-401, 2013.

70. A. Swetapadma and A. Yadav, "Improved fault location algorithm for multi-location faults, transforming faults and shunt faults in thyristor controlled series capacitor compensated transmission line," *IET Generation Transmission & Distribution*, vol. 9, no. 13, pp. 1597–1607, 2015.

71. A. Swetapadma and A. Yadav, "An artificial neural network-based solution to locate the multilocation faults in double circuit series capacitor compensated transmission lines, *International Transactions on Electrical Energy Syst*ems, doi.org/10.1002/etep.2517, vol. 28, no. 4, 2017.

72. B. Vyas, B. Das and R.P. Maheshwari, "An improved scheme for identifying fault zone in a series compensated transmission line using undecimated wavelet transform and Chebyshev Neural Network. *International journal of Electrical Power and Energy Systems,* vol. 63, pp. 760–768, 2014.

73. M. Mirzaei, B. Vahidi and S.H. Hosseinian, "Fault location on a series-compensated three-terminal transmission line using deep neural networks," *IET Science Measurement & Technology*, vol. 12, no. 6, pp. 746-754, 2018.

74. M. Mirzaei, B. Vahidi, and S. H. Hosseinian, "Accurate fault location and faulted section determination based on deep learning for a parallelcompensated three-terminal transmission line," *IET Generation Transmission & Distribution,* vol. 13, no.13, pp. 2770 – 2778, 2019.

75. S. Biswal, M. Biswal and O.P. Malik, "Hilbert Huang transform based online differential relay algorithm for a shunt-compensated transmission line," *IEEE Transactions on Power Delivery,* vol. 33, no. 6, pp. 2803-2811, 2018.

76. A. Swetapadmaa and A. Yadav, "A hybrid method for fault location estimation in a fixed series compensated lines," *Measurement*, doi:org/10.1002/etep.2517, vol.123, pp. 8-18, 2018.

77. L. N. Tripathy, S.R. Samantaray and P.K. Dash, "A fast time–frequency transform based differential relaying scheme for UPFC based double-circuit transmission line," *Electrical Power and Energy Systems,* vol. 77, pp. 404–417, 2016.

78. L. N. Tripathy, P. K. Dash, and S. R. Samantaray, "A New Cross-Differential Protection Scheme for Parallel Transmission Lines Including UPFC. *IEEE Transactions On Power Delivery,* vol. 29, pp.1822-1830, 2014.

79. K. R. Krishnanand and P. K. Dash, "A new real-time fast discrete s-transform for cross-differential protection of shunt-compensated power systems," *IEEE Transactions on Power Delivery*, vol. 28, no. 1, 2013.

80. Z. Moravej, M. Pazoki and M. Khederzadeh, "New pattern-recognition method for fault analysis in transmission line with UPFC," *IEEE Transactions on Power Delivery*, vol. 30, no. 3, pp. 1231-1242, 2015.

81. P. K. Mishra, A. Yadav and K. Pazoki, "FDOST based fault classification scheme for fixed series compensated transmission system," *IEEE Systems Journal*. vol. 13, no. 3, pp. 3316-3325, 2019.

82. H.R. S. Khoramabadi, A. Keshavarz and R.Dashti, "A novel fault location method for compensated transmission line including UPFC using one-ended voltage and FDOST transform," *International journal of Electrical Power and Energy Systems,* doi: org/10.1002/2050-7038.12357, 2020.

83. P. Jena, and A.K. Pradhan, "A Positive-Sequence Directional Relaying Algorithm for Series-Compensated Line '. *IEEE Transactions on Power Delivery,* vol. 25, no. 4, pp. 2288 – 2298, 2010.

84. B. Chatterjee and S. Debnath, "Sequence component based approach for fault discrimination and fault location estimation in UPFC compensated transmission line," *Electric Power Systems Research*, doi:10.1016/j.epsr.2019.106155, vol. 180, 2020

85. M. Nemati, M. Bigdeli and A. Ghorbani, "Impedance-based fault location algorithm for double-circuit transmission lines using single-end data," *Journal of Control*, *Automation and Electrical Systems*,vol. 31, no.5, pp. 1267-1277, 2020.

86. M. Nemati, M. Bigdeli, A. Ghorbani and H. Mehrjerdi, "Accurate fault location element for series compensated double-circuit transmission lines utilizing negative-sequence phasors,"*Electric Power Systems Research,* doi.org/10.1016/j.epsr.2021.107064, vol. 194, 2021.

87. H. Mehrjerdib, H. Heydaria, S. Ghanimati and A. Ghorbania, "A pilot protection algorithm for TCSC compensated transmission line with accurate fault location capability,"*Electrical Power and Energy Systems*, doi:org/10.1016/j.ijepes.20 20.106191, vol .122, 2020

88. A. Elmitwally and A. Ghanem, "Local current-based method for fault identification and location on series capacitor-compensated transmission line with different configurations," *International Journal of Electrical Power and Energy Systems*, doi:org/10.1016/j.ijepes.2021.107283, vol. 194, 2021.

89. A. Elmitwally, M. Elgamal and A. Al-Zyoud, "A linearized MOV model-based method for fault location on off-terminal series capacitor bankcompensated transmission line using one-end current," *Electric Power Systems Research*, doi:org/10.1016/j.epsr.2021.107400, vol. 199, 2021.

90. P. K. Nayak, A. K. Pradhan and P. Bajpai, "A fault detection technique for the series-compensated line during power swing," *IEEE Transactions on Power Delivery*, vol. 28, no. 2, 2013.

91. V. H. Makwana and B. R. Bhalja, "A new adaptive distance relaying scheme for mutually coupled series-compensated parallel transmission lines during intercircuit faults," *IEEE Transactions on Power Delivery*, vol. 26, no. 4, pp. 2726-2734, 2011.

92. B. Chatterjee and S. Debnath, "A new protection scheme for transmission lines utilizing positive sequence fault components," *Electric Power Systems Research,* doi:org/10.1016/j.epsr.2020.106847, vol.190, 2021.

93. S. M. Hashemi, M. T. Hagh and H. Seyedi, "A novel backup distance protection scheme for series-compensated transmission lines," *IEEE Transactions on Power Delivery*, vol. 29, no. 2 , pp. 699 –707, 2014.

94. M. M. Taheri, H. Seyedi, M. Nojavan, M. Khoshbouy and B. Mohammadi-ivatloo, "High speed decision tree- based series compensated transmission lines protection using differential phase angle of superimposed current," *IEEE Transactions on Power Delivery*, vol.33, no. 6, pp. 3130-3138, 2018.

95. U. J. Patel, N. G. Chothani and P. J Bhatt, "Sequence-space-aided SVM classifier for disturbance detection in series compensated transmission line," *IET Science Measurement & Technology*, vol. 12, no. 8, pp. 983-993, 2018.

96. M. Kundu, & S. Debnath, "Fault location in UPFC compensated double circuit transmission line using negative sequence current phasors," *Electric Power Systems Research,* doi:10.1016/j.epsr.2020.106347, vol.184, 2020.

97. F. Den, X. Li and X. Zeng, " Single-ended travelling wave protection algorithm based on full waveform in the time and frequency domains," *IET Generation Transmission & Distribution*, vol. 12, no. 15, pp. 3680–3691, 2018.

98. D. Akmaz, M.S. Mamiş, M. Arkan, nd M.E. Tağluk, "Fault location determination for transmission lines with different series-compensation levels using transient frequencie," *Turkish Journal of Electrical Engineering & Computer Sciences*, vol. 25, no. 5, pp. 3764-3775, 2017.

99. L. Tang, X. Dong, S. Luo, S. Shi and B. Wang, "A new differential protection of transmission line based on equivalent travelling wave," *IEEE Transactions on Power Delivery* , vol. 32, no.3, pp. 1359–1369, 2017.

100. M. M. Taheri, H. Seyedi, and B. Mohammadi-ivatloo, "DT-based relaying scheme for fault classification in transmission line using MODP," *IET Generation Transmission & Distribution*, vol.11, no. 11, pp. 2796-2804, 2017.

101. B. Kumar and A. Yadav, "Backup protection scheme for transmission line compensated with UPFC during high impedance faults and dynamic situations," *IET Science Measurement & Technology,* vol.11, no. 6, pp. 703-712, 2017.

102. M. Biswal, "Faulty phase selection for transmission line using integrated moving sum approach," *IET Science Measurement & Technology,* vol.10, no. 7, pp. 761–767, 2016.

103. M. H. H. Musa, Z. He, L. Fu and Y. Deng, "A covariance indices based method for fault detecti on and classification in a power transmission system during power swing," *International Journal of Electrical Power and Energy Systems*, vol. 105, pp.581-589, 2019.

104. S. Das, S. P, Singh and B. K. Panigrahi, "Transmission line fault detection and location using Wide Area Measurements," *Electric Power Systems Research*, vol. 151, pp. 96–105, 2017.

105. S. Barman, and B. K. S. Roy, "Detection and location of faults in large transmission networks using minimum number of phasor measurement units," *IET Generation Transmission & Distribution*, vol. 12, no. 8, pp. 1941-1950, 2018.

106. F. Yu , C. Booth, A. Dysko, and Q. Hong, "Wide-area backup protection and protection performance analysis scheme using PMU data," *Electrical Power and Energy Systems*, vol. 110, pp. 630-641, 2019.

107. M. Pignati, L. Zanni, P. Romano, R. Cherkaoui and M. Paolone, "Fault detection and faulted line identification in active distribution networks using synchrophasors-based real-time state estimation. *IEEE Transactions on Power Delivery,* vol. 32, no.1, 2017.

108. H. Fathabadi, "Novel filter based ANN approach for short-circuit faults detection, classification and location in power transmission lines," *Electrical Power and Energy Systems*, vol, 74, pp. 374–383, 2016.

109. V. Ashoka, A. Yadava, and A. Y. Abdelazizb, "MODWT-based fault detection and classification scheme for cross-country and evolving faults," *Electric Power Systems Research*, doi:org/10.1016/j.epsr.2019.105897, vol. 175, 2019.

110. S. A. Govar, and H. Seyed, "Adaptive CWT-based transmission line differential protection scheme considering cross-country faults and CT saturation," *IET Generation Transmission & Distribution*, vol.10, no. 9, pp. 2035–2041, 2016.

111. A. Swetapadma, and A.Yadav, "All shunt fault location including cross-country and evolving faults in transmission lines without fault type classification," *Electric Power Systems Research*, doi:org/10.1016/j.epsr.2015.01.014 0378-7796, vol. 123 pp. 1–12. 2015.

112. T. Bi, W. Li, Z. Xu, and Q.Yang, "First-zone distance relaying algorithm of parallel transmission lines for cross-country grounded faults," *IEEE Transactions on Power Delivery*, vol. 27, no. 4, pp. 2185-2192, 2012.

113. Z. Y. Xu, W. Li, T. S. Bi, G. Xu, and Q. X. Yang, "First-zone distance relaying algorithm of parallel transmission lines for cross-country nonearthed faults, *IEEE Transactions on Power Delivery*, vol. 26, no. 4, pp. 2486- 2494, 2011.

114. S. A. Govara, P.Pourghasema, and H.Seyedi, "High impedance fault protection scheme for smart grids based on WPT and ELM considering evolving and cross-country faults," *Electrical Power and Energy Systems*, vol. 107, pp. 412–421, 2019.

115. A. Saber, "Fault location algorithm for multi-terminal mixed lines with shared tower and different voltage levels," *IET Generation Transmission & Distribution*, vol. 2. no. 9, pp. 2029-2037, 2018.

116. P. Jena, and A. K. Pradhan, "An integrated approach for directional relaying of the double-circuit line," *IEEE Transactions on Power Delivery*, vol. 26, no. 3, pp. 1783-1792, 2011.

117. B. Sahoo, and S. R. Samataray, "An enhanced fault detection and location estimation method for TCSC compensated line connecting wind farm," *Electrical Power and Energy Systems,* vol. 96. pp. 432-441, 2018.

118. M. Dehghani, M. H. Khooban, and T. Niknam, " Fast fault detection and classification based on a combination of wavelet singular entropy theory and fuzzy logic in distribution lines in the presence of distributed generations," *Electrical Power and Energy Systems,* vol. 78, pp. 455-462, 2015.

119. J. Ma, W. Zhang, J. Liu, and J. S. Thorp, "A novel adaptive distance protection scheme for DFIG wind farm collector lines," *Electrical Power and Energy Systems,* vol. 94, pp. 234-244, 2018.

120. M. S. ElNozahy, R. A. El-Shatshat, and M. M. A. Salama, "Single-phasing detection and classification in distribution systems with a high penetration of distributed generation," *Electric Power Systems Research*, vol. 131, pp. 41-48, 2016.

121. L. N. Tripathy, M.K. Jena, and S.R. Samantaray, "Differential relaying scheme for tapped transmission line connecting UPFC and wind farm, *Electrical Power and Energy Systems*, vol. 60, pp. 245–257, 2014.

LIST OF FIGURES

LIST OF TABLES

List of publications:

Journal:

1. Monideepa Paul and Sudipta Debnath, "Fault Detection and Classification Scheme for Transmission Lines Connecting Windfarm Using Single end Impedance," *IETE Journal of Research*, doi.org/10.1080/03772063.2020.1754934.

2. Monideepa Paul, Sudipta Debnath and Biswapriya Chatterjee, "Fault Detection and Classification Scheme for Smart Grids considering High Impedance Evolving and Cross Country faults," *Electrical Engineering*, Springer, https://doi.org/10.1007/s00202-022-01490-y.

3. Monideepa Paul and Sudipta Debnath, "Back-up Protection Scheme for Series Compensated Transmission Line Connected to Wind farm, " *IETE Journal of Research*, DOI: 10.1080/03772063.2022.2071772.

Conference:

1. Monideepa Paul and Sudipta Debnath, "ANFIS based single line to ground fault location estimation for transmission lines," Michael Faraday IET International Summit-2020, October 3-4, 2020, Proceedings of MFIIS-2020.

2. Monideepa Paul and Sudipta Debnath, "Wavelet Based Single Ended Scheme for High Impedance Fault Classification in Transmission Lines," IEEE-ICSTCEE 2020, REVA University Bengaluru, October 09th -10th, 2020.

ABBREVIATION

AB	Double Line Fault on Phase A & B
ABC	Triple Line Fault
ABG	Double Line to Ground Fault on Phase A & B
AC	Double Line Fault on Phase A & C
ACG	ACG Double Line to Ground Fault on Phase A & C
AG	Single Line to Ground Fault on Phase-A
AI	Artificial Intelligence
ANFIS	Adaptive-Neuro-Fuzzy Inference System
ANN	Artificial Neural Network
AR	Autoregressive
BC	Double Line Fault on Phase B & C
BCG	Double Line to Ground Fault on Phase B & C
BG	Single Line to Ground Fault on Phase-B
cAs	Approximation Coefficients
CCVT	Capacitor-Coupled Voltage Transformer
cDs	Detail Coefficients
CG	Single Line to Ground Fault on Phase-C
ChNN	Chebyshev Neural Network
CT	Current Transformr
CVT	Capacitive Voltage Transformer
CWT	Continuous Wavelet Transform
DCTL	Double Circuit Transmission Line
ddc	Decaying DC Component
DFIG	Doubly-Fed Induction Generator
DFT	Discrete Fourier Transform
DG	Distributed Generation
DNN	Deep Neural network

DOST	Discrete Orthogonal Stockwell Transform
DP	Differential Power
DPASC	Differential Phase Angle Superimposed Current Signal
DS	Distribution System
DT	Decision Tree
DTE	Discrete Teager Energy
DTR	Decision Tree Regression .
DWT	Discrete Wavelet Transform
EDS	Electrical Distribution Systems
EHV	Extra-High Voltage
ELM	Extreme Learning Machine
FACTS	Flexible Alternating Current Transmission System
FDOST	Fast Discrete Orthogonal S-Transform
FDST	Fast Discrete S-Transform
FFT	Fast Fourier Transform
FI	Fault Index
FIA	Fault Inception Angle
FIS	Fuzzy Inference System
FR	Fault Resistance
FSM	Finite state automata theory
FST	Fast-S-transform
GPS	Global Positioning System
HIF	High Impedance Fault
HVB	High Voltage Class-B
IA	Current at Phase A
IB	Current at Phase B
IC	Current at Phase C
k-NN	k-Nearest Neighbour
KVL	Kirchhoff's Voltage Law
LIF	Low Impedance Fault

LL	Double Line
LLG	Double Line to Ground
LLL	Triple Line
MFCDFT	Modified Full-Cycle DFT
MFs	Membership Functions
MM	Mathematical Morphology
MODP	Magnitude Of Differential Power
MODWT	Maximal-Overlap-DWT
MOV	Metal-Oxide Varistor
MRA	Multi Resolution Analysis
MVDC	Medium-Voltage DC
MWSV	Maximum Wavelet Singular Value
PMUs	Phasor Measuring Units
PNN	Probabilistic Neural Network
PSD	Power Spectral Density
PWM	Pulse Width Modulation
RMNN	Rough Membership Neural Network
RTDS	Real-Time Digital Simulator
RTU	Remote Telemetry Unit
SCB	Series Capacitor Banks
SCDCTL	Series Compensated Double Circuit Transmission Line
SCTL	Series Compensated Transmission Line
SD	Standard Deviation
SE	State Estimator
SLG	Single Line to Ground
ST	Stockwell Transform
STATCOM	Static Synchronous Compensator
STFT	Short Time Fourier Transform
SVD	Singular Value Decomposition
SVM	Support Vector Machine

SVR	Support Vector Regression
TCSC	Thyristor Controlled Series Compensated
TW	Travelling Wave
UDWT	Undecimated Discrete Wavelet Transform
UPFC	Unified Power Flow Controller
VPD	Voltage Phase Difference
WAMS	Wide Area Measurement System
WPT	Wavelet Packet Transform
WSCC	Western System Coordinating Council
WSE	Wavelet Singular Entropy
WT	Wavelet Transform